INFORMATION TO USERS

This manuscript has been reproduced from the microfilm master. UMI films the text directly from the original or copy submitted. Thus, some thesis and dissertation copies are in typewriter face, while others may be from any type of computer printer.

The quality of this reproduction is dependent upon the quality of the copy submitted. Broken or indistinct print, colored or poor quality illustrations and photographs, print bleedthrough, substandard margins, and improper alignment can adversely affect reproduction.

In the unlikely event that the author did not send UMI a complete manuscript and there are missing pages, these will be noted. Also, if unauthorized copyright material had to be removed, a note will indicate the deletion.

Oversize materials (e.g., maps, drawings, charts) are reproduced by sectioning the original, beginning at the upper left-hand corner and continuing from left to right in equal sections with small overlaps. Each original is also photographed in one exposure and is included in reduced form at the back of the book.

Photographs included in the original manuscript have been reproduced xerographically in this copy. Higher quality 6" x 9" black and white photographic prints are available for any photographs or illustrations appearing in this copy for an additional charge. Contact UMI directly to order.

UMI

A Bell & Howell Information Company
300 North Zeeb Road, Ann Arbor MI 48106-1346 USA
313/761-4700 800/521-0600

A

Detailed Dynamic Performance Analysis and Feasibility Assessment of Emerging Optical Switching and its Impact on the Performance of a Fully Reconfigurable WDM Transport Network

by

Dwight Richards

A dissertation submitted to the Graduate Faculty in Engineering in partial fulfillment of the requirements for the degree of Doctor of Philosophy, The City University of New York

1999

UMI
300 North Zeeb Road
Ann Arbor, MI 48103

This manuscript has been read and accepted for the Graduate Faculty in Engineering in satisfaction of the dissertation requirements for the degree of Doctor of Philosophy.

12/11/98 — Date

Chair of Examining Committee

Professor Mohamed A. Ali

12/15/98 — Date

Acting Executive Officer

Professor Mumtaz K. Kassir

Supervisory Committee

Professor S. Ahmed

Professor L. Roytman

Professor B. Gross

Professor F. Moshary

Dr. Janet Jackel (Bellcore)

Dr. Jon Nagel (AT&T Labs Research)

The City University of New York

ABSTRACT

Detailed Dynamic Performance Analysis and Feasibility Assessment of Emerging Optical Switching and its Impact on the Performance of a Fully Reconfigurable WDM Transport Network

by

Dwight Richards

Advisor: Professor Mohamed Ali

This thesis presents a detailed dynamic performance analysis and feasibility assessment of emerging optical switching and its impact on the performance of reconfigurable WDM transport networks. Specifically, this thesis compares and examines the potential of both existing and emerging WDM switching technologies and characterizes a novel prototype liquid crystal crossconnect.

This work examines and identifies EDFA dynamic response to different reconfiguration scenarios (switching) and how this might impact the overall network performance. Each network reconfiguration scenario is shown to cause its own network performance degradation, and requires a different set of EDFA engineering design rules to mitigate this effect. The main objective is to maintain a constant per channel output power in case of a network reconfiguration (adding/ dropping of channels) as well as how to identify and recover from failures in the network.

This thesis will present the first experimental study of an all-optical feedback technique for stabilizing the per-channel output both for single amplifier and cascade of amplifiers. This technique is simple, inexpensive, and robust, requiring neither monitoring of the amplifier output nor any active feedback. One of the great virtues of this technique is that only the first in a chain of amplifiers needs to be modified. Two different all-optical methods of controlling transient power excursions of surviving channels in a chain of EDFAs when switching occurs as a result of the adding or dropping of channels is presented and compared. The focus is on the dynamic effects due to the switching of channels. This study is then extended to look at dynamic effects in self-healing WDM ring networks where fault recovery is achieved through a protection switching mechanism, and how the interaction between the switching dynamics and the dynamics of the EDFAs affects our ability to detect and recover from failures. The ability to detect failures such as fiber cuts is complicated by the amplified spontaneous emission (ASE) noise from the same EDFAs that make WDM possible. We will examine the fundamental difficulties that this ASE imposes on some schemes for detecting failures and propose our novel method that overcomes these difficulties.

ACKNOWLEDGMENTS

This work could not have been done without the guidance and support of my advisor Professor Mohamed Ali, who introduced me to the optical networking group at Bellcore. He is greatly appreciated for his insight and support of my thesis work. Janet Jackel (Bellcore), my co-mentor, made it all possible. She provided the guidance, the teaching and the training that produced research that I am very proud to have been apart of. I thank all the people that I have worked with at Bellcore, some of who have moved on to other places. I thank Jack Tomlinson, Rich Wagner and Bill Anderson for accommodating me in their various research groups. A very big thanks to Ioannis Roudas and Neo Antoniades for the fruitful interactions in my simulation work. Much appreciation to Wei Xin and Jane Baran for their experimental expertise and discussions of real network problems. I also thank Jon Nagel (AT&T Labs Research) and Paul Wysocki (Lucent Technologies) for their tutorials on modeling amplifiers. I thank Ralston Jerimiah (RJ), whose expertise on the "C" programming language was very helpful. I thank Professor Gerard Lowen, whose encouragement and assistance in finding financial support throughout my course of study is the most important reason why I made it to the end.

I thank my friends Michael, Melody, Francine, Paul, Marlene, Mrs. Anderson, Claude, Azed and Carlton for their encouragement from the very beginning. Finally, I thank my parents, my brother and sisters for being such a wonderful family. I know they are all happy to see me accomplish my goal. They kept me going and this work is dedicated to them.

TABLE OF CONTENTS

List of Tables

List of Figures

CHAPTER 1

INTRODUCTION

1.1 Introduction

As the demand for bandwidth increases, it is becoming more and more difficult to meet the increased transport capacity requirements of telecommunication networks by the use of fiber-optics as a single channel point-to-point transmission link with all networking and services functions performed electronically. Electronic switching systems are limited to a capacity of a few tens of Gb/s, orders of magnitude below the requirements of some of the emerging telecommunication applications. To upgrade such an infrastructure, a core transport network is required to handle both narrowband and broadband services together in an efficient manner. Next generation communication networks will be required to handle bandwidth demanding new applications such as desk-top video conferencing, interactive TV, supercomputer interconnections, and tele-medicine applications. The increasing number of users who will use these applications will require ultra-high network throughput ranging from Gb/s to perhaps even several Tb/s. These requirements are being met by the development and deployment of advanced optical communication networks, capable of multiplexing, transmitting, switching, receiving and demultiplexing this tremendous amount of traffic. Wavelength Division Multiplexed (WDM) optical networks using wavelength routing are considered to be the most promising candidates for the next generation of wide-area backbone as well as multi-access networks.

The use of WDM technology has emerged as a powerful tool to overcome the technological bottlenecks of single wavelength systems while preserving their important survivability feature. The transparency and independence of the WDM channels permit vastly dissimilar bit rates to pass between different pairs of nodes, allowing network connectivity and transmission rates to be tailored and upgraded flexibly according to prevailing traffic patterns and evolving service demands. Unlike single-channel TDM systems, WDM systems effectively make better use of the large built-in bandwidth in installed fibers while maintaining the same or greater degrees of system performance, robustness, reliability, survivability, operations, and maintenance as current transport systems.

A WDM system is constituted of several key elements such as: WDM terminals (transmitters and receivers), WDM repeaters, e.g., Erbium-doped fiber amplifiers (EDFAs), wavelength-selective switching elements to perform a number of different routing functions, and Self-Healing optical protection schemes to ensure automatic network survivability.

The prospects for creating such WDM networks that are transparent to signal format and bit rate are being investigated in several consortia activities and research programs around the world. The primary goal for these programs is to create the possibility of a "future proof" network in which some of the optical signals flowing through the network are uninterrupted by electronics from source to destination, and in which the character of the individual signals is determined by the terminal equipment which is attached to the

network at the source and destination. These networks, which provide both switching and transmission in the optical domain, are moving from laboratories around the world to the marketplace, providing several technological advantages over their electronic counterparts. Deployment of such networks is in its infancy but is expected to grow exponentially over the next few years.

The possibility of such WDM networks has arisen because of the realization of optical amplification, particularly with the development of EDFAs. The advent of EDFAs has revolutionized the field of optical communications in two ways. First their large optical gain allows long-haul unregenerated systems with optical repeaters spaced more than 100 km apart. Second, their large bandwidth and slow gain dynamics, which allows them to amplify multiple optical channels simultaneously without significant crosstalk, makes it possible to increase capacity by an order of magnitude using several high bit-rate channels. In conjunction with WDM techniques, EDFAs promise to offer significant economical and performance advantages for a network through improved capacity, reliability, and transparency. Therefore, EDFAs have greatly accelerated the pace at which WDM systems are being developed and deployed.

The deployment of WDM networks will also require reliable high-performance wavelength-selective elements and space switching elements to perform a number of different routing functions.. The dynamic interactions of the space switching elements and the EDFAs are the focus of this thesis. Multiwavelength switching generally requires that the wavelength channels be separated, space switched separately, and then

recombined into the appropriate output fibers. Switching in this context is not intended to switch bits or even packets. Switching is required when channels are dropped and/or added at the network elements (NE), and at the optical cross-connects (OXC) where different wavelengths are dynamically routed to different parts of the network. The transient analysis of this switching is the first focus of this thesis. In addition, the successful implementation and deployment of these WDM networks will require the development of WDM optical protection switching schemes that can provide the survivability for the all-optical layer under the SONET/ATM layers. The dynamics of this protection switching is the second focus of this thesis. Both adding/dropping of channels and protection switching, coupled with the transients of EDFAs perturb the dynamic state of the network causing degradations in the network's performance.

1.2 Thesis Statement

This thesis presents a detailed dynamic performance analysis and feasibility assessment of emerging optical switching and its impact on the performance of reconfigurable WDM transport networks. Specifically, this thesis compares and examines the potential of both existing and emerging WDM switching technologies and characterizes a novel prototype liquid crystal crossconnect. The switching performance of several switching technologies will be assessed and compared based on the following criteria:

- Speed of rearrangement
- Insertion loss
- Optical Isolation (crosstalk)
- Polarization dependence

This work examines and identifies EDFA dynamic response to different reconfiguration scenarios (switching) and how this might impact the overall network performance. Each network reconfiguration scenario is shown to cause its own network performance degradation, and requires a different set of EDFA engineering design rules to mitigate this effect. The main objective is to maintain a constant per channel output power in case of a network reconfiguration (adding/ dropping of channels) as well as how to identify and recover from failures in the network.

This thesis will present the first[1] experimental study of an all-optical feedback technique for stabilizing the per-channel output both for single amplifier and cascade of amplifiers. This technique is simple, inexpensive, and robust, requiring neither monitoring of the amplifier output nor any active feedback. One of the great virtues of this technique is that only the first in a chain of amplifiers needs to be modified. Two different all-optical methods of controlling transient power excursions of surviving channels in a chain of EDFAs when switching occurs as a result of the adding or dropping of channels is presented and compared. The focus is on the dynamic effects due to the switching of channels. It is shown that both can be used successfully but that each imposes different constraints on the EDFAs and on the network. The compatibility of our novel method of stabilizing chains of EDFAs with another method that adjusts the pump power is examined. This study is then extended to look at dynamic effects in self-healing WDM ring networks where fault recovery is achieved through a protection switching mechanism, and how the interaction between the switching dynamics and the dynamics

[1] References of our previous publications of this experimental work are provided in Chapter 4.

of the EDFAs affects our ability to detect and recover from failures. The ability to detect failures such as fiber cuts is complicated by the amplified spontaneous emission (ASE) noise from the same EDFAs that make WDM possible. We will examine the fundamental difficulties that this ASE imposes on some schemes for detecting failures and propose our novel method that overcomes these difficulties. In this scenario a detailed study of the timing requirements necessary in effecting a protection switch as a result of a real failure in the network, and not as a result of a temporary degradation of the performance due to the dynamic interaction of the components in the network, will be specified.

This thesis will identify several optical protection schemes for WDM ring networks. The engineering and implementation considerations for WDM optical layer protection architectures will be presented. We will identify changes to existing SONET Automatic Protection Switching (APS) schemes to WDM optical protection schemes for the 2-fiber uni-directional and 4-fiber bi-directional Self-Healing Rings (SHR). We focus on the WDM optical protection schemes that provide the survivability for the all-optical layer under the SDH/SONET/ATM layer and its potential and limitations.

To model and simulate complex system such as WDM SHR networks with protection switching mechanism to protect the network in case of fiber cuts or equipment failures, a user-friendly application software that uses an input Graphic User Interface (GUI) is developed. Using the developed algorithm, network components are represented by separate modules and thus the simulation program is organized in modular form to satisfy this requirement. Due to the large number of modules, creating the main simulation

program using a text editor is impractical and prone to error. An approach that uses an input Graphic User Interface (GUI) is necessary. Each module is thus associated with a graphical object (icon) which is automatically translated to the main program and unambiguously scheduled for execution. The GUI thus allows for user-friendly simulations requiring little or no programming experience. Signal Processing Workstation (SPW) was found to be most appropriate for this type of modeling. SPW is basically a block diagram based application software where custom coded blocks can be created using the 'C' programming language. These blocks are then used to create complex systems by connecting the custom coded blocks with available standard SPW blocks provided that the interfaces are compatible. Using SPW, network elements (NE) such as wavelength add drop multiplexers (WADM) are modeled. A WADM is a hierarchical block modeled from lower level blocks. The major sub-blocks are EDFAs, demultiplexers (DMUX), multiplexers (MUX), 2×2 switches for dropping and adding of channels, photodetectors to detect power levels, 2×2 protection switches to protect against failures and attenuator blocks.

These systems are used to study dynamic effects by simulating the transition of the switches on realistic time scales and examining the effects at various points of the network. Failure scenarios are simulated; such as fiber cuts on the working and/or protection fiber, to understand the timing requirements to effect consistent protection switching. The constraint on setting threshold levels in detecting fiber cuts in the case where in-line amplifiers are present between the cut and the point at which the failure is detected is studied. In particular, some schemes depend on a loss of total power to effect a

protection switch, but it is shown that because of amplified spontaneous emission (ASE), when in-line amplifiers are present erroneous detection can occur, and thus the wrong action taken. Different means of detecting fiber cuts on the working and protection path, including our novel method that overcomes the constraint that the ASE noise imposes, are also studied. It is shown that because of the transient degradations resulting from switching in these networks, a hold-off time for the protection switches is necessary. It is shown that a protection switch should only take place for degradations that last more than a certain minimum time if these networks are not to display catastrophic behavior, due to the dynamic degradations caused by the perturbations that the switching actions create in reconfigurable survivable all-optical networks.

The main objective is to investigate and analyze, through experiment and computer simulation, the dynamic effects due to the interaction of switching elements and EDFAs transients in a WDM network. It is shown that the desired properties of optical switches can conflict with the requirements for stable EDFA operation. In particular, a fast switch is required for fast rearrangement of the channels in a WDM network, but this fast switching creates dynamic perturbations which in general are more severe for faster switches because of the slow response of the EDFAs. It is also shown that these degradations accumulate in large networks due to fast power transients in long chains of EDFAs.

CHAPTER 2

WDM SWITCHING OPTIONS

2.1 Introduction

Rapid progress in the deployment of wavelength division multiplexed (WDM) communication systems has led to a growing interest in technologies capable of providing switching functions in the optical domain without any optical-to-electronics (O/E) conversion. With the increase in the number of wavelengths and the increased throughput per wavelength, optical switches capable of switching large trunks of data transparently are necessary components for the construction of reconfigurable optical networks. Optical switches are key elements in WDM network elements such as wavelength add-drop multiplexers (WADMs), wavelength selective cross-connects (WSXCs), and wavelength-interchanging cross-connects (WIXCs). Switching in WDM networks normally involves separation of the wavelengths by a demultiplexer, switching the wavelengths in space and finally recombining the outputs by means of a multiplexer. This chapter will concentrate on performance issues that have to do with the space switching aspect. The switches that are deployed in WDM networks will be required to be very reliable, high-performance, and affordable. The required performance of the switches will depend on the application and thus different technologies will be deployed as the technology largely determines the performance. Some of the applications that will require optical switches can be broadly classified as provisioning of lightpath or optical routing switching, protection switching, and packet switching. There are a number of

equally important distinguishing characteristics of optical switches. However, considerable emphasis is placed on the switching time. The provisioning of lightpath and protection switching can tolerate switching times ranging from a few microseconds to several milliseconds. Packet switching at the rates that are been considered for optical transport, require switching times ranging from a few picoseconds to about a nanosecond. Since the power required to switch the device is equal to the switching energy divided by the switching time, a shorter switching time will require more power. These types of tradeoffs are typical of optical switches. This chapter:

- Defines the important parameters used to characterize optical switches.
- Looks at the merits of different switch architectures.
- Examines different optical switching technologies in the context of different performance measures such as switching speeds, crosstalk, polarization effects, ability to support special features and scalability.

The optical switching that is presented here is confined to the so called relational or optically transparent (analog) devices as opposed to the logical (digital) devices [1]. Relational devices establishes a large bandwidth (BW) mapping between inputs and outputs based on a control signal which is independent of the data input. A change in the relationship between the inputs and outputs represents a change in the state of the switch. These devices cannot sense the presence of individual bits passing through them, they can only pass them. The BW transparency of the relational devices allows extremely high-bit-rate channels to be passed which can be either multiple time-multiplexed channels of

differing bit rates, or several dense WDM channels. The inability to sense bits passing through these relational devices means that packet switching cannot be supported by the devices themselves. On the other hand, logical devices are required to respond to the bits in the signals passing through the switch fabric and make routing decisions based on them. They are therefore required to switch as fast as, or faster than the bit rate of the signal. This requirement limits the bit rate that can be supported by the logical devices to considerable lower rates than that which can be supported by the relational devices.

2.2 Switch Definitions

The construction of an optical switch can vary in complexity from the very simple connect-disconnect structure shown in Fig. 2.1a to the more involved M × N constructions, M and N being arbitrary number of inputs and outputs respectively. Many larger switches are constructed from smaller elementary 1 × 2 and 2 × 2 switches shown schematically in Figures 2.1b and 2.1c respectively. The 1 × 2 switch directs optical power from a single input to either of the two output ports. The 2 × 2 switch connects one input port to either of two output ports and the other input port to the other output port. The 2 × 2 switches have two complementary states commonly referred to as the bar and the cross state. Some switches have very distinct loss and crosstalk performance for the different states. An M × N switch can be constructed from M 1 × N switches shown schematically in Fig. 2.1d and N M × 1 switches. Many switch constructions involve a recursive algorithm wherein larger switches are constructed from smaller switches that themselves were constructed from yet smaller elementary 1 × 2 and 2 × 2 switches.

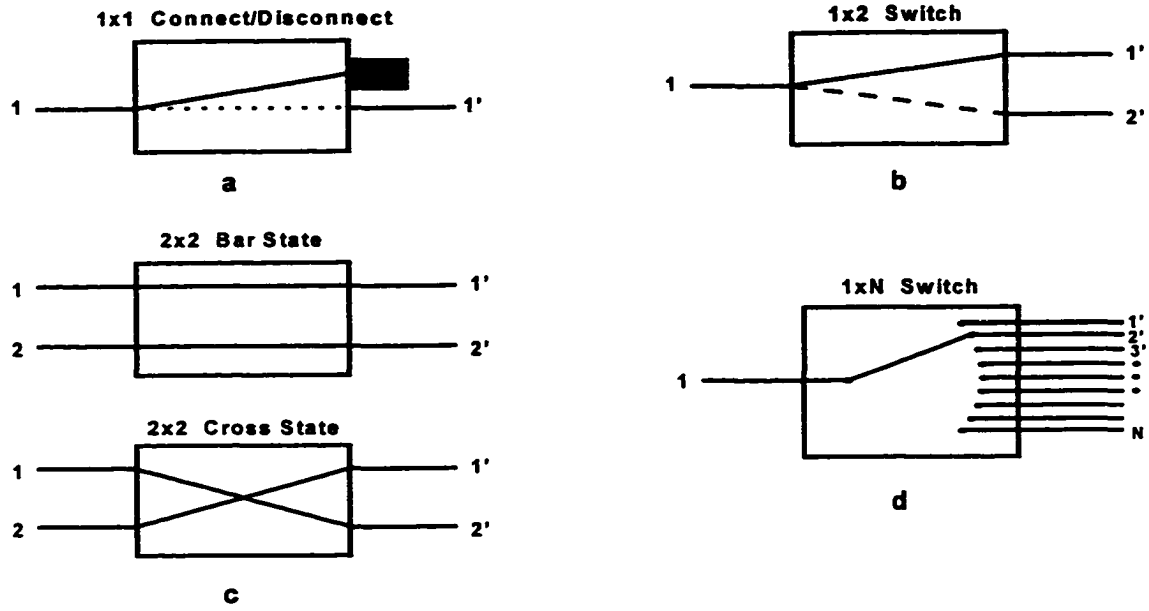

Figure 2.1 Schematic view of the function of switches. Only the connectivity from input to output is indicated. The internal construction of the switch may be very different

2.3 Basic Optical Characteristics and Performance Measures

There are a number of universal needs of optical switching fabrics. Depending on the application one need might become more important than another, but nonetheless they are all important needs of all optical switching fabrics. The following sections describe the established measures of the effectiveness of the switching of the light from the input port to the output port and how the properties of the light such as wavelength and polarization affect the switch performance.

2.3.1 Optical Bandpass

The BW to be supported by the optical switch fabric should be on the order of the BW of the optical amplifiers deployed in the system. For most current applications this is determined by the approximate 35 nm BW of conventional EDFAs. However, laboratory demonstrations have shown that this BW can be expanded to about 40-80 nm through the use of gain flattening techniques [2], split-band configurations [3], through the use of erbium-doped fluoride fiber amplifiers (EDFFA) which are inherently flatter over a wider BW than conventional EDFAs [4], through the use of tellurite-based EDFAs [5], or by incorporating samarium-doped fiber spans with erbium-doped fiber [6]. The switch should be capable of efficient use of the available optical spectrum. Efficient use of the optical spectrum implies that as many channels as possible should be supported. This efficiency is primarily dependent on the wavelength selective components in WDM switches but space switching elements can also play a part.

The switches must give acceptable optical performance over the entire wavelength range of operation. When a number is supplied it should be a worst-case specification over the range of operating wavelengths. Thus, the extinction ratio, insertion loss, crosstalk, reflectance, directivity, polarization mode dispersion (PMD) and polarization dependent loss (PDL) are all defined as the worst-case over the wavelength range of interest. Some switches such as the optomechanical switch are more or less wavelength independent but those that are built based on the interference principle in waveguide devices can show considerable wavelength dependence either as a result of material properties or through deliberate design.

2.3.2 Switching Efficiency

The switching efficiency of the optical switch is a measure of the power transfer from port to port. Ideally, we want all the power to be transferred from a given input port to a desired output port with none transferred to any other port, neither in the forward nor backward directions. The extinction ratio, insertion loss, reflectance, directivity, and crosstalk are measures of the switching efficiency of optical switches [7] and will be defined in the following sections.

2.3.2.1 Extinction Ratio

The extinction ratio is defined for an on-off switch as the ratio of the output power in the on-state to output power in the off-state. The ratio should be as large as possible and is particularly important for external modulators where a small ratio can severely affect the noise performance of the system. The extinction ratio of high-speed modulators can be as little as 10-15 dB causing significant degradation of system performance.

2.3.2.2 Insertion loss

The insertion loss L_{ij} is the worst-case fraction of power that is loss between input port i and output port j as a result of the presence of the switch. It is determined over all wavelengths of interest and for all polarization states when output j is the intended output for a signal entering the switch at input i. Fig. 2.2 shows a simplified diagram of the optical path used to define loss.

$$L_{ij} = 10 \log (Pin_i/Pout_j) \text{ (dB)}$$

The loss may differ for different input-output combinations. This increases the dynamic range of the signals in the network and is therefore an undesirable property. Variable optical attenuators can be used to equalize the loss across different paths but this adds complexity and cost to the network. The acceptable loss of the switch is related to the loss budget of the network and consequently the location and the purpose of the switch is critical. If the switch is part of a larger network element its loss can be absorbed by the loss budget of the network element itself. Optical amplifiers have lessened the effects of loss in amplified optical networks but nonetheless low loss is still a desirable attribute as optical amplifiers add noise and considerable cost.

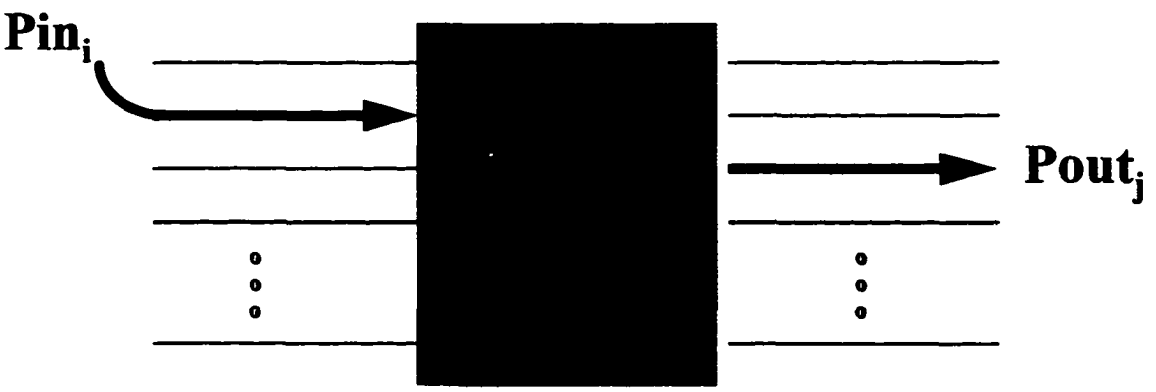

Figure 2.2 Optical path used to define loss. Output j is the intended destination of light entering input i. Loss thus is defined for each path and switch state.

2.3.2.3 Reflectance (Back reflection into the input fiber):

The optical path used to define reflectance is shown in Fig. 2.3. The reflectance R_i is defined as the power transferred from the input port i back into the same input port i.

$$R_i = 10 \log(Pout_i/Pin_i) \text{ (in dB)}$$

The reflectivity R_i of an optical switch must be very small in order to prevent serious impairments in the network. Optical isolators can be placed at critical points in the network to eliminate the overall effect of reflections from different sources.

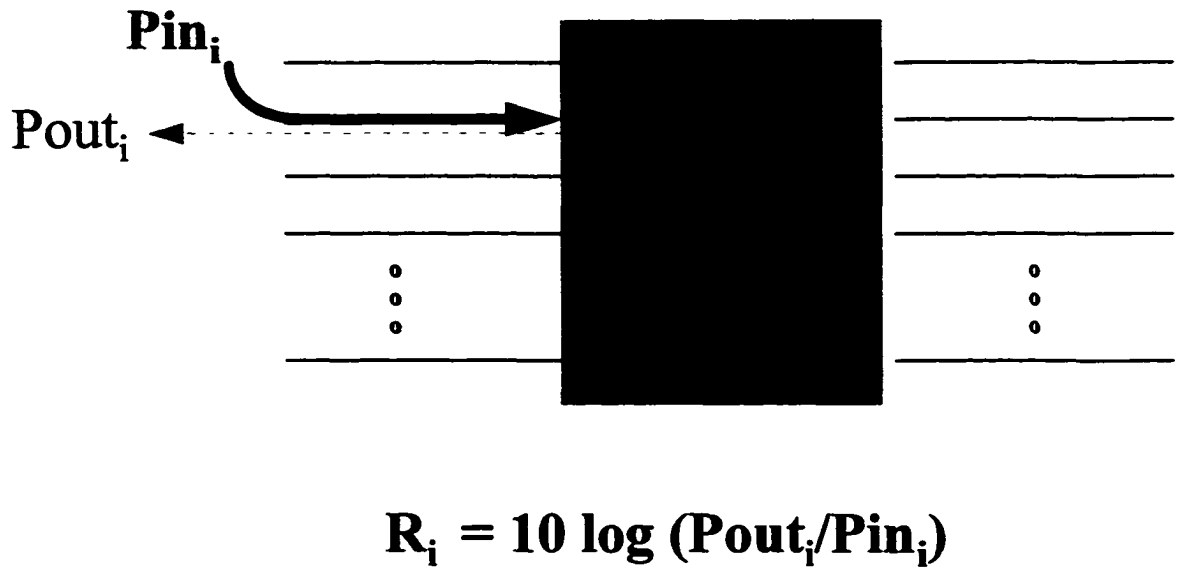

Figure 2.3 Optical path used to define reflectance.

2.3.2.4 Directivity (isolation of input ports from each other):

Fig. 2.4 shows the optical path used to define directivity D_{ij}. It is defined as the power transferred from input port i back into a different input port j.

$$D_{ij} = 10 \log(Pin_i/Pout_j) \text{ (in dB)}$$

In practice directivity is normally not an issue for optical switches because of its insignificant effects in optical networks. Typically greater than 50 dB is achievable.

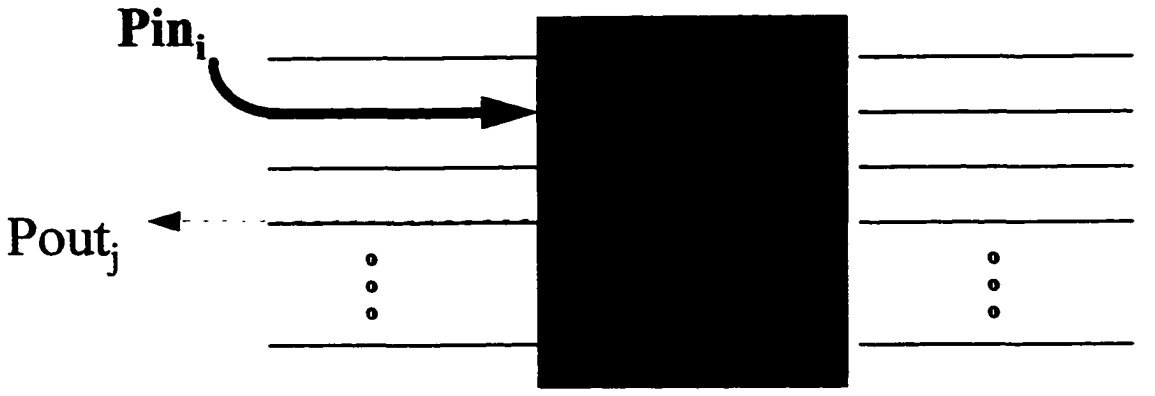

$$D_{ij} = 10 \log (Pin_i / Pout_j)$$

Figure 2.4 Optical path used to define directivity.

2.3.2.5 Linear Crosstalk

For a given switching state or interconnection pattern, and output, the crosstalk is defined as the inverse ratio of the power at that output from the desired input to the power from all other inputs. Crosstalk can lead to serious impairments in optically switched WDM networks and consequently considerable attention will be given to its generation and prevention mechanisms in the following sections. It can limit the number of network elements and therefore the size of the network. The value of crosstalk supplied by vendors is a worst-case number as significant variations occur, depending on the number of active inputs, and the path that is under consideration. Crosstalk is generated by almost all optical components. It is generated by optical filters, wavelength

multiplexers/demultiplexers, optical switches, semiconductor optical amplifiers, and by nonlinearities in the optical fiber itself. In WDM networks two broadly defined types of crosstalk arise, namely, interchannel crosstalk and intrachannel (or common-channel) crosstalk [8-10]. Interchannel crosstalk occurs when the interfering signal is at a wavelength sufficiently different from the desired signal wavelength such that the difference is larger than the receiver's electrical bandwidth. Intrachannel crosstalk occurs when the interferer is at the same wavelength as the desired signal or sufficiently close to it such that the wavelength difference falls within the electrical BW of the receiver. Crosstalk can arise from nonlinear interactions in the fiber medium but here we are concerned with linear crosstalk generated by optical filters and optical switches.

2.3.2.5.1 Intrachannel Crosstalk

Intrachannel crosstalk results in much more severe effects than interchannel crosstalk [10-12]. This type of crosstalk is referred to as coherent [11] and can lead to bit-error rate floors, and imposes severe requirements on the components [10-19]. The exact crosstalk penalty as a result of coherent crosstalk depends on the modulation, relative phase and polarization of the interfering fields. Fig. 2.5 shows two sources of linear intrachannel crosstalk generation mechanism. Fig. 2.5a shows a demultiplexer/multiplexer pair. As a result of the nonideal filters that make up the demultiplexer/multiplexer pair a portion of the signal at λ_1 leaks to the λ_2 path after the demultiplexer and gets combined with λ_1 after the multiplexer. The difference in path length of the signals results in a phase difference which has a worse-case intrachannel crosstalk effect when they are exactly out-

of-phase [12]. The nonideal isolation of one switch port from the other can also lead to intrachannel crosstalk as shown in Fig. 2.5b. Once again the difference in path length through the switch leads to crosstalk even though both signals carry the same modulation. In large networks the analysis of crosstalk can be a very complicated and tedious process because of the increased number of crosstalk sources and the cumulative effect. Computer simulation can provide a more accurate crosstalk estimate [14-15],[19]. The crosstalk penalty is worst when the state of polarization (SOP) of the signal and the interferer are the same. Therefore a worse-case estimate of intrachannel crosstalk assumes that the signal and interferer are out of phase and the SOPs are the same [12-13].

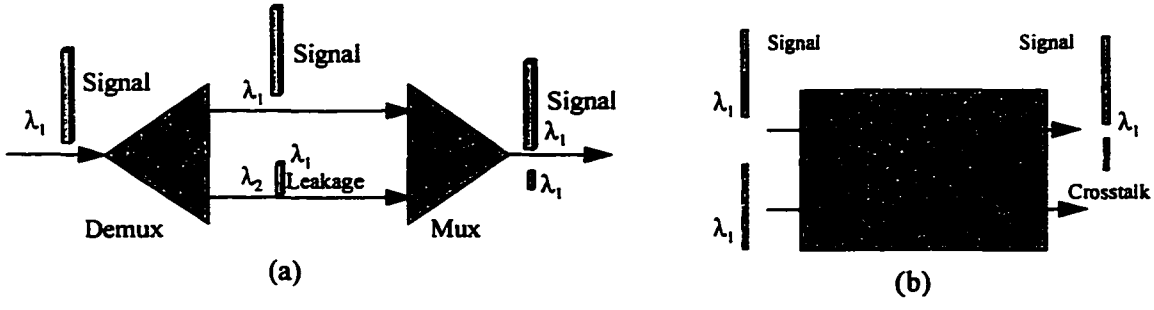

Figure 2.5 Sources of intrachannel crosstalk. (a) Wavelength separation and combining via cascaded wavelength demultiplexer and multiplexer, and (b) incomplete switch port isolation in an optical space switch.

2.3.2.5.2 Interchannel Crosstalk

Power penalty from interchannel crosstalk can be reduced significantly by proper choice of optical filters before the photodetector [8],[20] and is primarily associated with direct detection. Like intrachannel crosstalk, interchannel crosstalk can arise from a number of

different sources. Fig. 2.6 shows two sources of this type of crosstalk. Fig. 2.6a shows how the inability of the filters in a demultiplexer to completely isolate neighboring channels can cause the λ_1 signal to get pass to the λ_2 channel and vice-versa. Fig. 2.6b shows how the wavelengths leak as a result of the imperfect isolation between

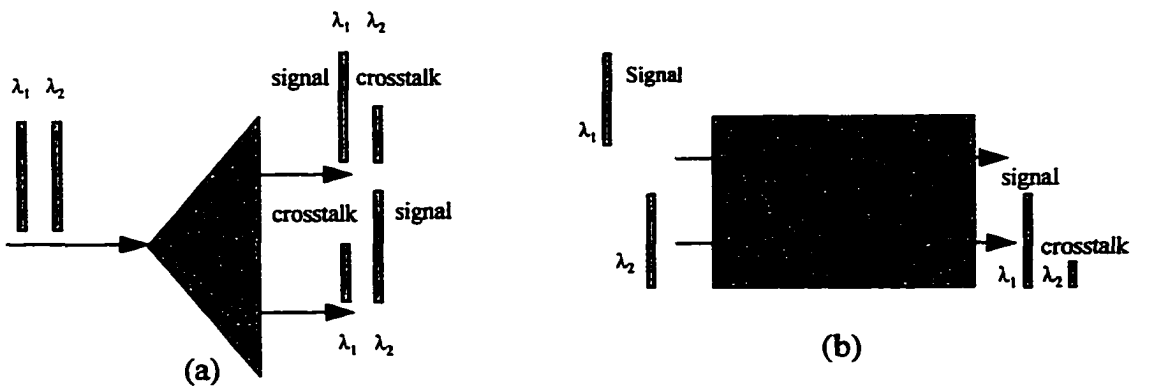

Figure 2.6 Sources of interchannel crosstalk. (a) Leakage of adjacent channels in optical demultiplexers, and (b) an optical switch with input signals at different wavelengths and incomplete port isolation.

the switch ports. For state of the technology filters, the damaging interchannel crosstalk terms normally originate from the two adjacent channels (channels at the end of the spectrum will see only one such crosstalk contributor) with negligible crosstalk contributed by the other channels.

2.3.2.5.3 Crosstalk Reduction

Crosstalk reduction is normally attacked at the device level rather than at the network level. The idea is that the lower the crosstalk of individual components in the network the better the cascadability of the components for an allowable crosstalk penalty. However, the architecture of the switch ultimately determines the crosstalk performance of the

device. Switch dilation [21] can dramatically reduce the crosstalk performance of optical switches. Spatial dilation and wavelength dilation are the two common approaches used to reduce crosstalk in optical switches. In a spatially dilated switch the signal passes through at least two stages in which crosstalk is further reduced with each additional stage. Fig. 2.7 shows how a 2 × 2 optical switch with crosstalk ϵ can have crosstalk reduced to ϵ^2 by adding some additional unused ports. Crosstalk reduction through spatial switch dilation increases the number of switching elements needed and thus increases the complexity and cost of the switch. Losses are also increased in the switch but this is often an acceptable tradeoff since optical amplifiers reduce the effects of losses. Fig. 2.7b is a symmetric architecture. Better performance can be obtained from the asymmetric architectures shown in Fig. 2.8a when there is a significant difference between the bar state and cross state crosstalk [22]. Fig. 2.8b shows a larger 4 × 4 nonblocking dilated switch. It is clear that the number of switching elements required for the dilated switch is more than that needed for the nondilated switch, but signals pass through only a single additional stage [21].

Wavelength dilation in switches is also used as another means of reducing interchannel crosstalk in WDM networks. Instead of using a single switch to handle several equally, closely spaced wavelengths, two switches can be used as shown in Fig. 2.9. One switch handles the even number wavelengths and the other handles the odd number wavelengths, effectively doubling the channel spacing as far as crosstalk generation effects are concerned. In the extreme case a separate switch can handle each wavelength. The cost scales with the number of switches. Placing a filter before the MUX in a DEMUX/MUX

pair can significantly improve the crosstalk performance of the device shown in Fig. 2.5 [20].

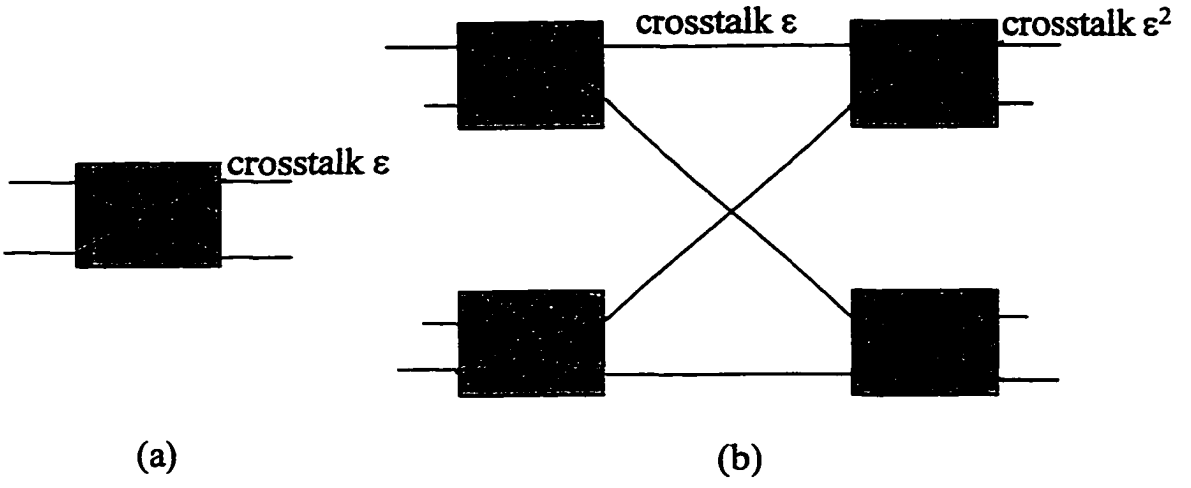

Figure 2.7 Crosstalk reduction via spatial dilation (a) A simple 2 × 2 switch. (b) A symmetrically dilated 2 × 2 switch with four 2 × 2 switches, each having an unused port for crosstalk reduction.

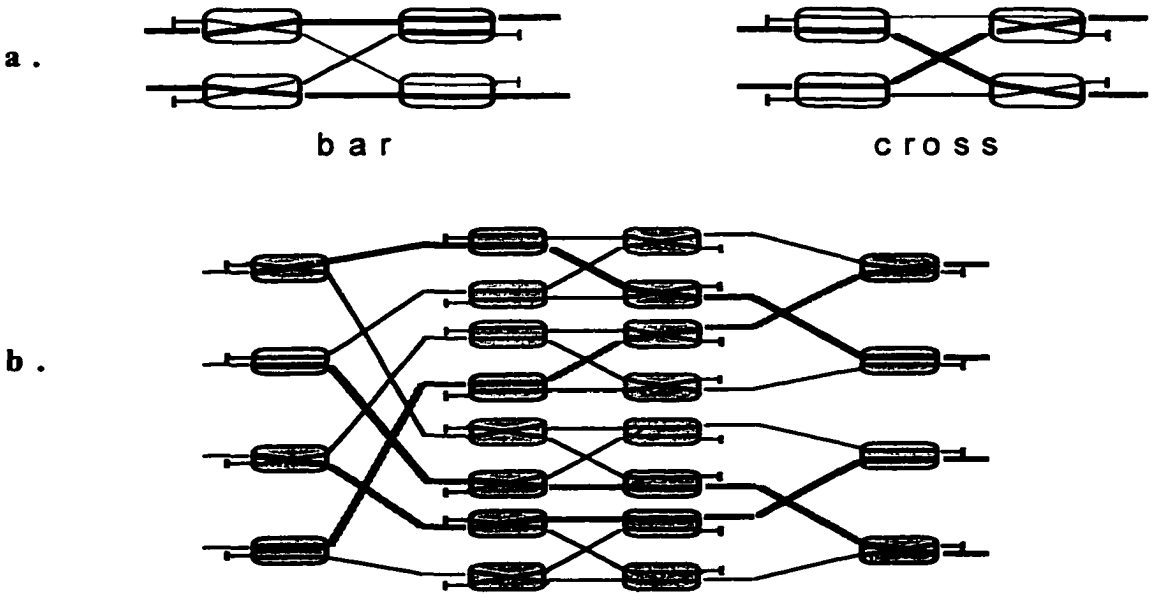

Figure 2.10 Dilated switches: (a) 2x2 dilated switch in bar and cross state. (b) 4x4 dilated and strictly nonblocking switch, in state (1-2, 2-4, 3-3,4-1) This configuration is sometimes called a router-selector.

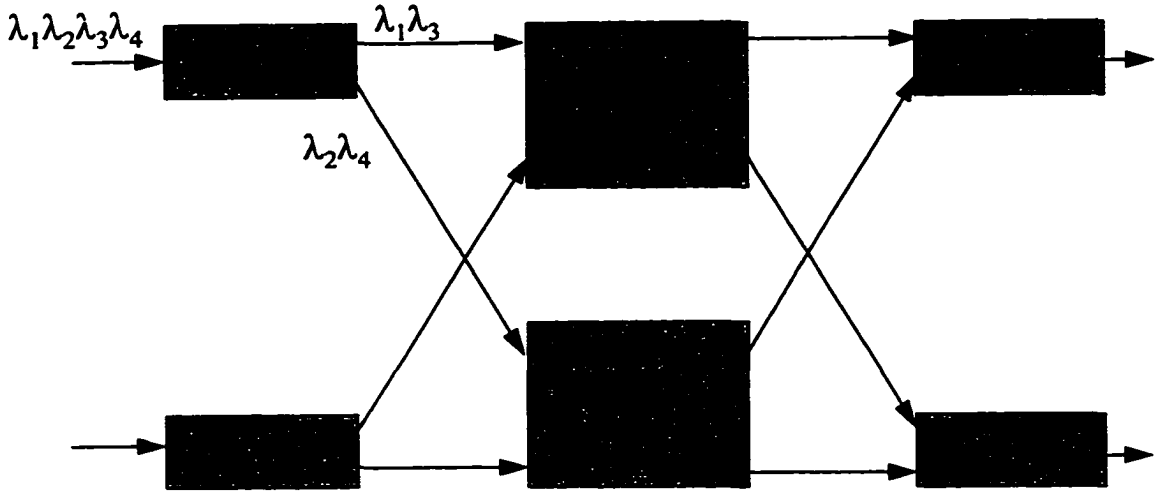

Figure 2.9 Crosstalk reduction via wavelength dilation. Mach-Zehnder interferometer (MZI) separates and combines the channels into two groups of even and odd number channels.

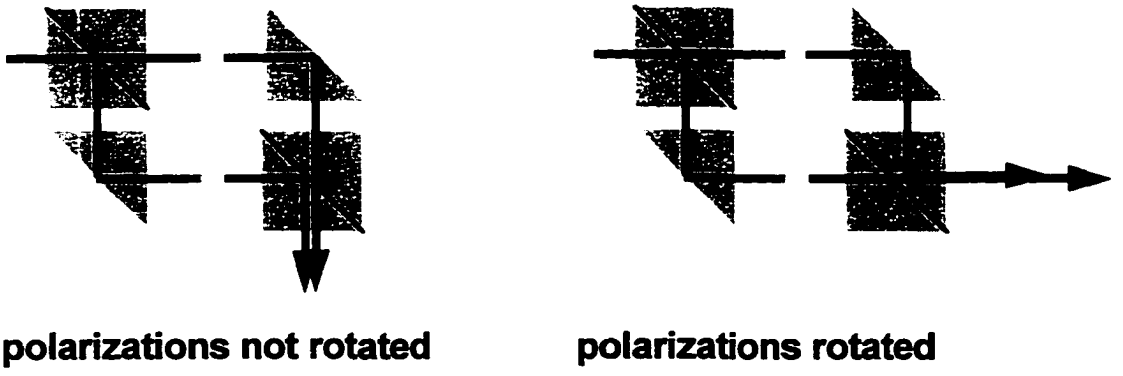

Figure 2.10 Polarization diversity allows a polarization dependent switching mechanism to provide polarization independent switching. In this example, the switching is effected using polarization rotation. The input is split into orthogonal polarizations using a polarization beamsplitter(PBS), and each is rotated separately; then the two output are combined in another. If polarizations are rotated the outputs take one path; if not they take the other.

2.3.2.6 Polarization Dependence

Like most optical components optical switches are in general required to show negligible polarization dependence. In particular, they are required to have low polarization dependent switching efficiency, low polarization dependent loss (PDL) and low polarization mode dispersion (PMD). Whereas some switching technologies are inherently polarization independent (e.g. optomechanical switches), some are intrinsically polarization dependent (e.g. waveguide switches). In addition, switches that are constructed from highly birefringent materials have high PMD. Polarization diversity [23] can be used as a means of making a polarization sensitive switch operate in a polarization insensitive mode. The technique involves a splitting of the polarizations at the input section of the switch, switching them separately through polarization optimized sections or by rotation of one polarization into the plane of the other where the switching efficiency is higher and, undoing the rotation if necessary and recombining at the output section of the switch. Fig. 2.10 shows an example of polarization independent switching based on polarization rotation. Switches based on liquid crystals, magneto-optics and some acousto-optic switches make use of this technique.

2.3.2.6.1 Polarization Dependent Loss (PDL)

PDL is the difference in loss between the two polarizations with best and worst losses in the switch. This difference can be significant in waveguide devices and can also present a problem in demultiplexers based on gratings. The amount of PDL that is tolerable depends on the application of the switch and the network architecture. If the signal passes

through many switches the accumulation of PDL can lead to significant variations in power levels. This can impose PDL constraints on individual switches. For a switch with N input ports it is required that $\Delta L \leq 0.1(1 + \log 2N)$dB [7]. Power equalizers that are used in some network elements (NE) to reduce power variations among different channels entering an EDFA can also correct for the slow changes in loss that occur when polarization drifts.

2.3.2.6.2 Polarization Mode Dispersion (PMD)

Birefringent devices or those in which the two polarizations follow different paths through the switch fabric can suffer polarization mode dispersion (PMD). PMD refers to the difference in time to traverse the switch fabric of the two polarizations. This can be a significant problem for high bit rate signals. For switches that employ polarization diversity the optical paths of the different polarizations should be the same lengths to avoid PMD.

2.3.2.6.3 Polarization Dependent Switching Efficiency

Some electrooptic switches require different voltages to switch the two orthogonal polarizations. Crosstalk can be unacceptable for one of the polarization in such cases, even though PDL may not be a problem. To make the switching efficiency polarization independent, a switching voltage as large as three times that for a single polarization device may be required [1]. This is commonly referred to as the overdriving technique and requires that the switching efficiency for both polarizations be a monotonic function

of the voltage. Polarization dependent switching efficiency can be eliminated in switches that employ polarization diversity technique.

2.4 Switch Architectures

Switches are either blocking or nonblocking depending on the connection pattern that is realizable. A switch is nonblocking if any unused input port can be connected to any unused output port. Depending on how the nonblocking function is realized and the constraints on connection set up, nonblocking switches are further subdivided into three categories, namely rearrangeable nonblocking, wide-sense nonblocking and strictly nonblocking [24-28]. If some connection patterns cannot be realized the switch is described as blocking. Most applications require nonblocking switches but in general nonblocking capability is achieved at the expense of more switching elements and thus larger switches. Less expensive, blocking switches with a small blocking probability might be justifiable deployed for some applications with the advantage of considerable cost savings. A switch is rearrangeable nonblocking if it is capable of any permutation of input to output connection. That is, any idle input may be connected to any idle output provided the existing connections may be rearranged. This can lead to brief interruptions of existing connections and will therefore be unacceptable for some applications. The advantage is fewer switching elements than the wide-sense and strictly nonblocking architectures to be defined shortly. A wide-sense nonblocking switch allows any input to be connected to any output without rearranging the existing connections but the connection pattern depends on the history of the existing connections, thus creating a

fundamental difficulty in constructing switch algorithms. A strictly nonblocking switch has a unique path from any input to any output. The required switch state is independent of the history of the existing connections and the number of connections. The price for such flexibility is increased switch size and thus increased cost of the switch. Fig. 2.11 shows examples of blocking, rearrangeable nonblocking, wide-sense nonblocking and strictly nonblocking architectures. Specific examples of each of these architectures are discussed in detail in [1].

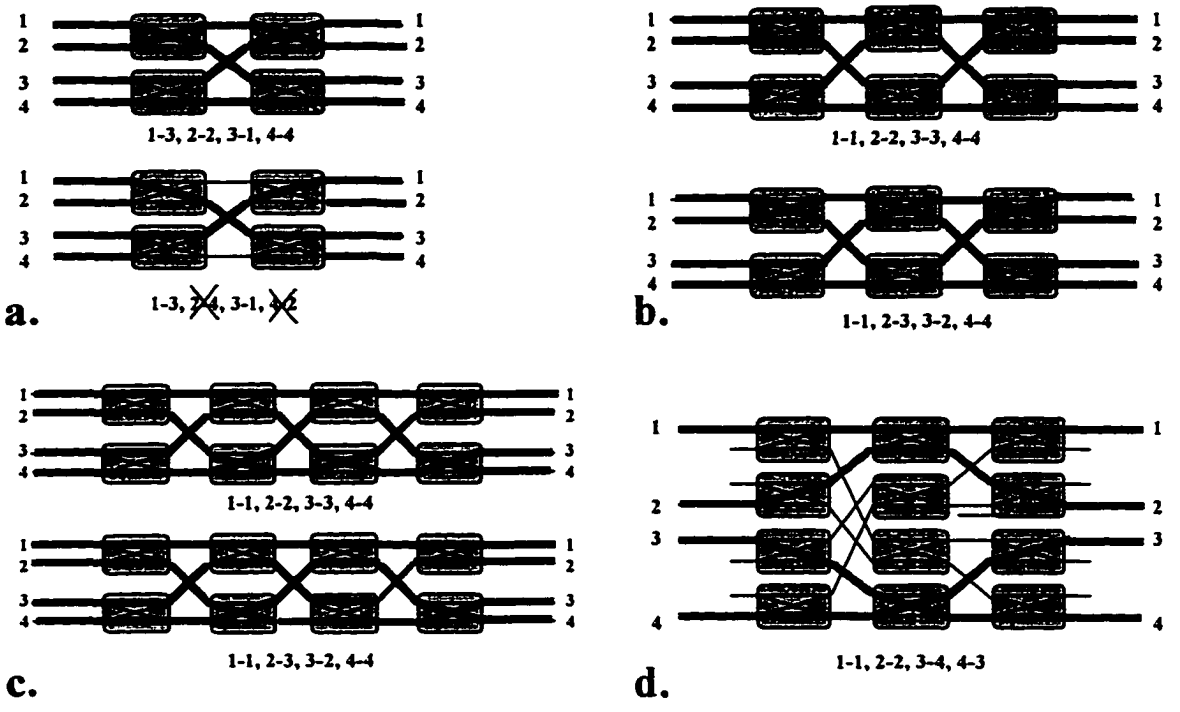

Figure 2.11 Examples of a. blocking, b. rearrangeably nonblocking, c. wide sense nonblocking, and d. strictly nonblocking 4x4 switch matrices constructed from 2x2 switch elements. In the blocking switch, some (upper) but not other (lower) connections can be made. In the rearrangeably nonblocking switch, all connections can be made, but the figure shows that some unchanged connections must take different paths if other connections are changed. In the wide sense and strictly nonblocking switches, no rearrangement is needed, and in the strictly nonblocking matrix, there is a unique path from each input to each output.

2.5 Switching Speed

The acceptable speed of an optical switch depends on the application of the switch. The time needed for switching has three major components:

1. Time to make the decision to switch
2. Time to initiate the switching (for example to change a voltage or current)
3. Time for the switch to respond.

Switching speed is normally given as the sum of the last two components above, ignoring the first contributor. Current speeds of optical switches ranges from the sub-nanoseconds obtainable with lithium niobate based devices to several hundred milliseconds required by large opto-mechanical switches. As we will see in chapter 4, slower switches account for more stable steady state operation of a network because of the slow response of EDFAs.

2.6 Scalability

In WDM networks two types of scaling is of interest for optical switches. First there is scaling to larger switch sizes and second, there is scaling to a larger number of wavelengths. Photonics device technology is relatively immature when compared to electronics device technology. However, rapid progress is been made in the areas of integrated photonics and integrated optoelectronics (combining the advantages of electronics and photonics). There are a number of fundamental obstacles that present themselves when large switch matrices are brought to the manufacturing stage. Two of these are the losses and the crosstalk. The dimension of the switch may be a function of

the acceptable loss and a minimum acceptable signal-to-noise ratio (SNR) [24]. Since optical circuits can be crossed in a plane without "short circuit," but not without crosstalk there are topological constraints [29]. Also, the sizes of the waveguide switches that can be made on a single substrate are limited to small switch dimensions. Large matrices require multiply substrates which substantially increases the cost of the switch and create other problems associated with the optical interconnects.

As pointed out before, the 1 × 2 and 2 × 2 optical switches are the elementary units of many larger switches. However, for certain opto-mechanical switches a single stage 1 × N switch can be made which can then be used in a two-stage configuration to construct an M × N switch, using M 1 × N and N M × 1 switches. Larger opto-mechanical switches can also be made from smaller intrinsically N × N opto-mechanical switches (N limited to 8). These large-scale opto-mechanical switches are only useful for applications that can tolerate hundreds of milliseconds switching speeds. Therefore, constraints such as cost, loss, speed, size and crosstalk are core considerations when determining switch scalability. Wavelength scalability depends on the wavelength selective components in the switch.

2.7 Latching vs Non-latching Switches

A latching switch remains in a given switch state until it is powered to another state. Once it is in a particular state, it remains there without the need for an active input. On the other hand, a nonlatching switch has to be constantly powered for it to remain in a given state. For some applications the "no power" state is of some importance. For the

latching switch the "no power" state is the present state. Some non-latching switches reverts to a default state, while others revert to an indeterminate state or can even absorb all the optical power, as in the case of switches based on optical amplifiers. A well-defined default "no power" state can be very useful for automatic routing to ensure some degree of survivability when power failures occur.

2.8 Reliability

The reliability of optical components is just as important as the cost and performance [30]. The packaged switches must be able to withstand harsh environmental conditions and have lifetimes on the order of that of the optical fibers and other components making up the network. Bellcore TR-NWT-001073 (January 1994), Generic Requirements for Fiber Optic Switches, outlines the reliability requirements. The temperature cycling test which takes the device through several temperature cycles from as low as -40° C to 75° C is a particular stringent test specified in the Bellcore document. A thermal aging test is also required as specified in the same Bellcore document. This test entails a testing of the switch's ability to withstand sustained high temperatures. The reliability of many optical components is not well known as these are relatively new devices which are yet to endure rigorous lab test and the always convincing field trials.

2.9 Other Switch Performance Issues

Some switches can support internal termination of connections and multicasting without additional hardware while others will need additional hardware. A means of verifying the

state of a switch can also be useful in some applications. Hardware verification of switch state can serve as a means of monitoring failures in optical switches that employ protection switching mechanisms.

2.10 Demultiplexer/Multiplexer Options

Demultiplexers and multiplexers are interchangeable devices. These devices will not be described in any detail here but rather a number of generic requirements will be stated and the different technologies in use will be given. In general low insertion loss, good optical isolation, polarization independent operation, stable spectral resolution with efficient use of the optical spectrum, flat spectral response, unity transmission in the passband, infinite rejection of all other channels and a sharp roll-off between the transmission and rejection bands are all desirable properties of the demultiplexers and multiplexers used in WDM networks. These ideal requirements are difficult to achieve and only approximations are possible. However, significant progress is been realized through continuous research. Currently, the wavelength separation and combination is done using gratings [31], interference filters [32], arrayed waveguide gratings [33] and acousto-optic tunable filters [34]. The construction of a multiwavelength switch for M input fibers each carrying N wavelengths is to separate the wavelengths coming from each of the M fibers using a demultiplexer, space switch each of the N wavelengths in its own M × M switch, and finally recombine the wavelengths with M multiplexers as shown in Fig. 2.12. The space switching technological options are the focus of this work.

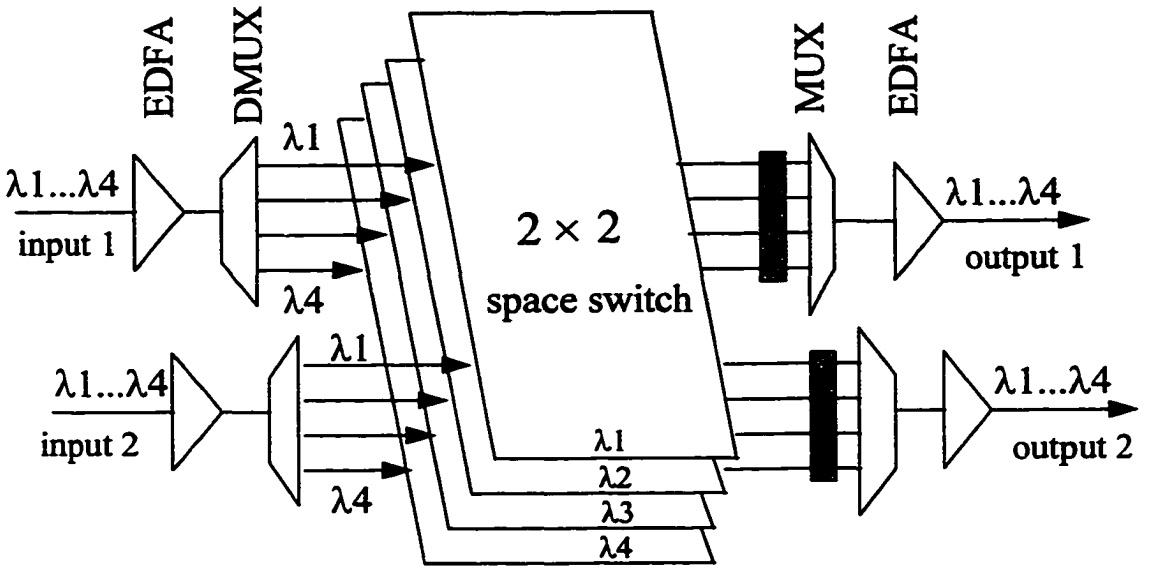

Figure 2.12 A wavelength selective cross-connect.

2.11 Optical Switching Technologies

This section covers the various optical space switching technologies that are currently deployed and those that are emerging in the marketplace. The construction and switching mechanism is used as the differentiating characteristics and intrinsic performance limitations are discussed. The current performance available for each technology is specified with the understanding that some of the numbers given are dated, since this is a rapidly developing field.

2.11.1 Opto-mechanical Switches

Opto-mechanical switches are the most mature switching technology available today. They have low insertion loss, low crosstalk, low PDL and are relatively inexpensive. The switching function is accomplished by some relative mechanical motion between input

and output fibers or by moving an optical element such as a lens between fibers. Most opto-mechanical switches make use of GRIN rod lenses for collimating the input and output lights. A collimated beam is easier to manipulate optically and coupling efficiency is enhanced when a collimated beam is focused onto the output fiber. There are three common methods of effecting switching in these lens based switches.

In the first approach a stepper motor controls the position of the GRIN rod lenses mounted on an armature at the input, aligning the desired output fiber and isolating the others. The switching time depends on the size of the switch matrix with typical values of 20 ms for a 2 × 2 switch and up to 125 ms for a 1 × 8 matrix.

In another arrangement the switching state is controlled by moving a mirror in and out of the optical path. The mirrors can be moved by either a stepper motor or a solenoid which can be latching. Both this approach and the previous operate by moving the optical element and thus their performance is similar.

In the third approach the optical elements are fixed and the fibers are aligned to achieved a desired connectivity. Piezoelectric controllers are usually used to allow for precise alignment. This approach also employs an active feedback mechanism to correct for small misalignments due to changing environmental conditions. As the switch matrix increases to larger dimensions, this approach has a speed advantage over the previous two.

Some opto-mechanical switches use a fiber directional coupler to vary the switch state. The coupling region is bent and stretched to change the coupling between the different input and output ports, effectively changing the state of the switch.

2.11.1.1 Micro-Optomechanical Switches

Laboratory demonstration of micromechanical switches have been reported [35-38]. These micro electromechanical system (MEMS) devices are tiny gadgets built to replace larger devices. Optical MEMS devices have also found applications as attenuators [37],[39-41]. The conventional optomechanical switches suffer from large size, large element mass, and slow switching time. Guided-wave solid-state switches are limited to small dimensions because of their high loss, high crosstalk, and long device lengths. Free-space micromachined optical switches (FS-MOS) promises to alleviate all these problems to some extent. Free-space interconnections allow for low loss and low crosstalk. Large compact crossconnects can be constructed by utilizing the batch-fabrication economy of monolithic integration. Currently these switches have switching times in the tens of microseconds, with small polarization dependence, and the losses are approaching acceptable levels. Devices with crosstalk less than -60 dB, PDL less than 0.3 dB, and loss less than 0.8 dB have been demonstrated [37-38]. These switches can be expected to seriously compete with opto-mechanical switches as their performance improves with each subsequent generation.

The typical performance of opto-mechanical switches is summarized below:

Loss: $\leq$ 1.0 dB for 2 $\times$ 2

Output port isolation: ≥ 50 dB

Backward Isolation: > 45 dB

Polarization dependence:

PDL: small, ≤ 0.2 dB

PMD ~ 0

Switching time (faster for smaller switch dimensions)

5 to several hundred milliseconds

2.11.2 Waveguide Switches

Optical waveguide switches account for a large number of the currently available optical switches. These switches are constructed from a wide variety of materials which largely determine their optical performance. They are constructed in glass, polymer, lithium niobate, silica, silicon, and semiconductor. In general there are two groups into which currently available waveguide switches are classified. These are the "digital switch" based on a waveguide y-branch, and the Mach-Zehnder interferometer shown in Fig 2.13a and Fig 2.13b respectively.

The digital switch is so called because of the "digital like", polarization independent characteristic response. There is no need for precise control of the voltage in an electro-optic based design of the digital switch. This allows several such switches to be controlled from the same voltage source. The amount of light that is coupled to each branch depends on the index symmetry. More light will be coupled into the branch with the larger effective index because of the mode sorting principle of asymmetric branching

[1]. The index change can be accomplished electro-optically, as in lithium niobate devices, thermally, as in polymer based devices, or by current injection, as in silicon waveguide devices.

The Mach-Zehnder interferometer (MZI) makes use of two interfering paths of different optical lengths. It consist of two 3-dB couplers with two uncoupled paths of different optical lengths in between. If the relative phase between the equal components of the light traversing each branch is exactly out of phase then all the light is recoupled to the input guide. If they are in phase the light gets coupled to the opposite guide. The response is periodic and the passbands are not flat, thus crosstalk performance for closely spaced channels in a WDM system are less than desired. Crosstalk performance can be improved by switch dilation and moderate on-chip integration (up to 8 × 8 matrices) is possible. These Mach-Zehnder waveguide devices are inherently polarization dependent and some means of compensating for the different response of the two polarizations is normally required. The losses are higher than the opto-mechanical switches but much higher speeds are possible as will be outlined in the following sections. The material from which the switch is made and/or the technology of the switch will be used to differentiate the switches in the following sections.

2.11.2.1 Lithium-niobate Waveguide Switches

Lithium-niobate is a ferroelectric compound with a high, anisotropic electro-optic coefficient. This means that switches made from this material can be switched rapidly with low voltage and that the different polarizations of the optical mode cannot be

switched equally. These devices account for the fastest available switches. Single switches used as modulators have been reported to switch as fast as 40 Gb/s. The interaction between the microstrips (The RC time constant) lines bringing voltage to the individual switching elements, limits the switching speeds to much lower values when large switching matrices are constructed. Losses are higher than the optomechanical switches and crosstalk values in single-stage switches of -20 to -30 dB are typical. In matrices these numbers are often worse. Switch dilation can improve the crosstalk performance for a given switch dimension at the price of more switching elements and consequently greater losses.

The dielectric properties of lithium-niobate devices vary as a function of direction within the crystal. The direction dependent relative dielectric constant ϵ_{ij} determines the relationship between the electric flux density D_i and the electric field strength E_i :

$$D_i = \varepsilon_{ij}\varepsilon_o E_j \tag{2.1}$$

The dielectric constant is proportional to the square of the index n.

Lithium niobate is highly birefringent ($\Delta n \sim 0.07$ at 1.55 nm) and has strongly polarization-dependent electro-optic coefficients as pointed out before. PMD can be large in these switches. The more compact the switch the less the effect but as much as 20-40 ps for 4 × 4 and 8 × 8 switch matrices are common. This PMD creates problems at OC192 rates but may be acceptable at OC48 and less rates, if the number of cascaded switches in a transparent path is small. Considerable complexity is involved in making

the Mach-Zehnder design polarization independent. However, high voltages can be used to overdrive the "digital optical switch" design to achieve polarization independent operation. These switches cost considerable more than their opto-mechanical equivalent. The typical performance of the lithium-niobate waveguide switch is summarized below:

loss: 2-3 dB

Output port isolation: 15 to 20 dB for a single stage. Crosstalk may depend on switch state.

Backward isolation: > 45 dB

Polarization dependence:

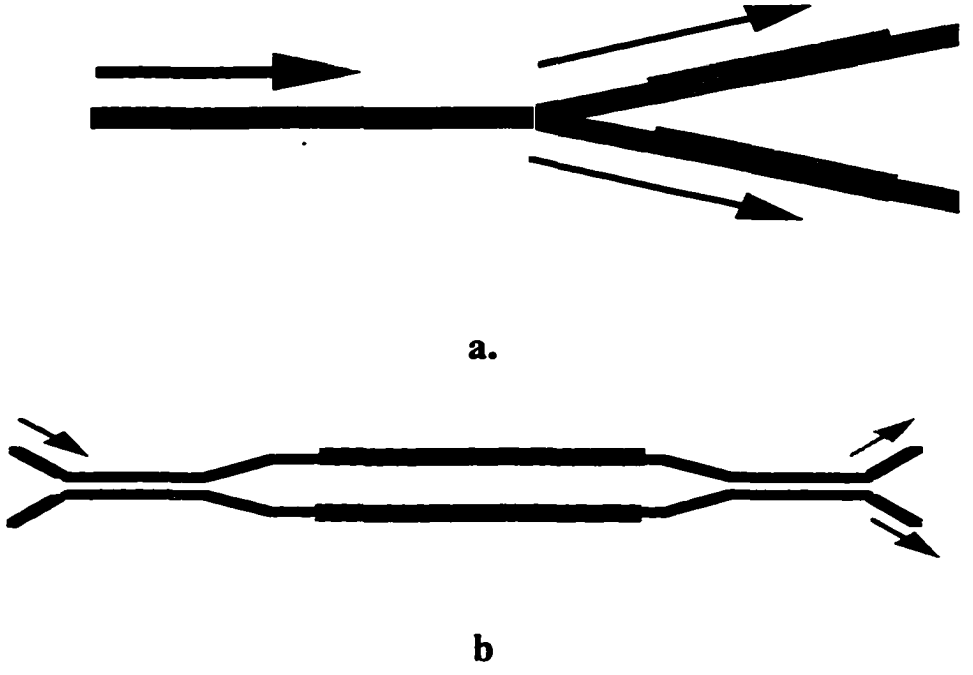

Fig. 2.13 Two configurations for waveguide switches: (a) The digital switch divides optical power if symmetric; breaking symmetry directs light to one branch. (b) The Mach-Zehnder interferometer has a periodic response to changing relative optical lengths of the two arms. Hatched regions indicate location of electrodes or heaters used to change refractive index.

PDL: 1-2 dB; greater in multistage designs.

PMD: A function of device length; ~25 ps for 10 cm.

Switching time: subnanoseconds (design and packaging dependent)

2.11.2.2 Silica Waveguide Switches

These switches are based on the thermo-optic effect since there is no electro-optic effect in glass. They are made by depositing the glass on a planar substrate. The 2 × 2 design is a Mach Zehnder interferometer with a heater on one branch to change the refractive index and thus effect a relative phase change with respect to the other branch. Due to the glass property these switches are not made in the "digital switch" form because of the difficulty of thermally isolating the two arms. These switches have low loss and small birefringence. Switches based on the thermo-optic effect are inherently slower than those based on the electro-optic effect with typical switching times of 1-3 msec. Another drawback is the relative high power consumption of these switches despite the fact that they can normally be switched with a small accurately controlled voltage. As much as 18 W is consumed by an 8 × 8 matrix and 600 mW by the 2 × 2 configuration. The typical performance of the silica waveguide switch is summarized below:

Loss: <1.5 dB for 2 × 2; <10 dB for 8 × 8

Output port isolation: 20 dB for 2 × 2; 10 dB for 8 × 8

Backward Isolation: >55 dB

Polarization dependence

PDL: small

PMD: small

Switching time < 3 msec

2.11.2.3 Polymer Waveguide Switches

Spin coating techniques have been used to form layers of polymers on different substrates which has resulted in a wide range of planar guided wave devices. Although some polymer devices have been constructed based on the electro-optic effect most are based on the thermo-optic effect, as losses are generally lower in the latter. Solid state optical switches have been constructed from thermo-optic polymers based on the Y-branch "digital switch" construction. The scalability is thought to be better than lithium niobate material as larger wafer sizes are possible. The optical mode sizes of the polymer based switches can be matched more easily to the standard single mode fiber than can be done in switches based on lithium niobate and semiconductor materials [42]. This reduces the losses due to different mode sizes. The switches can be made polarization and wavelength independent since the spin coating is nearly isotropic. The reliability of the switches has been questioned but improvements in polymer materials and the adhesives used to construct the polymer based devices have lead to the emergence of commercial products with acceptable reliability [42]. The typical performance of polymer waveguide switches is given below:

Loss: ~2.5 dB per switch stage; 2.5 dB for 1 × 2 to <5 dB for 1 × 8

Output port isolation: >30 dB for single stage

Backward isolation: > 50 dB

Polarization dependence:

PDL: ≤0.2 for 1 × 2 to <0.5 dB for 1 × 8

PMD: small; probably < 10% that of lithium niobate

Switching time: ~2 ms

2.11.2.4 Silicon Waveguide Switches

Mach-Zehnder constructed switches made using waveguides fabricated in silicon on silicon have been demonstrated. An oxide layer is used to optically separate the waveguide from the substrate. These devices are based on the relationship between refractive index and carrier density. The switching time is thus related to the mobility of the carriers and thus sub-microsecond speeds have been demonstrated in laboratory prototypes. The losses and crosstalk are currently higher than desired but improvements can be expected as the technology is not as mature as that for switches based on other waveguide materials. Typical switching performance will not be given here since any such data can be considered relatively premature at this time.

2.11.2.5 Semiconductor Waveguide Switches (InP)

Semiconductor waveguide switches are very attractive for WDM applications because of the potential increase of on-chip functionality. Indium Phosphorous (InP) switching technology has the advantages of been able to compensate for the switch fabric loss with monolithic integration of semiconductor optical amplifiers (SOA'S), compact size, high reliability and high speed. The losses are normally higher than glass, lithium niobate and

polymer waveguide switches but significant progress has been made to improve the losses of currently emerging switches. The switching mechanism can be provided by either electro-optically induced index changes or by current injection index changes. If SOAs are used in the device all-optical switching is possible. The PDL and crosstalk can be made very small and they intrinsically have negligible PMD. These switches can be lossless if integrated with optical amplifiers. However, the amplifiers can impose PDL and SNR limitations. A 4 × 4 laboratory prototype switch has been reported [43]. The typical performance of InP waveguide switches is given below.

Loss <2 dB

Output port isolation: ~40 dB

Polarization dependence:

PDL: <1 dB

Switching time: nanoseconds or less

2.11.3 Acousto-optic Switches

Acousto-optic switches come in two flavors. There are the lithium niobate designs and the all-fiber design which has been offered commercially. They have been thought to be very attractive for WDM applications because of their unique ability to process many wavelength channels simultaneously and independently [34],[44]. The principle of operation of the lithium niobate acousto-optic switches is based on the interaction of an acoustic wave used to generate a birefringence grating and an incoming polarized beam of light [34],[44-46]. The birefringence acts to cause a polarization transformation

between TE and TM polarizations. When used to switch several closely spaced channels at once these acousto-optic switches suffer from intolerable coherent crosstalk that has limited their usefulness in as far as multichannel space switching is concerned [34],[46],[47]. The crosstalk performance of the switch has been improved through dilation, apodization and pass-band flattening [45-46],[48-49]. Unlike the lithium niobate acousto-optic switches where the guided light is converted to a different polarization mode, in the all-fiber acousto-optic switch the light is converted to a different spatial mode. It is a wavelength dependent switch (different devices are required for the 1310 and 1550 nm windows) requiring about 200 mW of power to switch. It is wavelength tunable over approximately 100 nm. The typical performance of acousto-optic fiber switches is given below.

Loss < 1 dB for a 1 × 2

Output port isolation: 15 dB (within a narrow wavelength region)

Backward isolation: > 50 dB

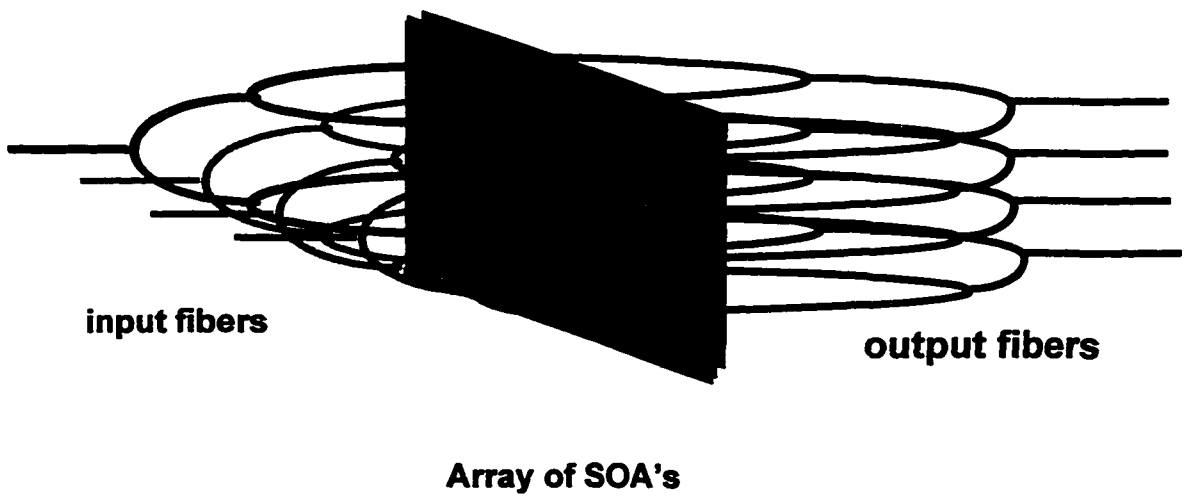

Figure 2.14 Schematic picture of a semiconductor gate array switch. Each of the SOA's can be ON or OFF.

Switching time: ~ 20 μsec

2.11.4 Semiconductor Gate Array Switches

The semiconductor gate array switch is constructed by integrating passive fabrics such as splitter/combiner with SOA gate switches as shown in Fig 2.14. Loss compensation and high contrast are inherent to this device. The currently available designs operate in the 1300 nm window over a 40 nm bandwidth. A different material will be required to accommodate 1550 nm window operation. There are transparency and scalability challenges to be addressed because of the PDL, signal distortion due to saturation and carrier dynamic effects, and SNR limitation imposed by the added ASE from the SOA. Manufacturing uniformity constraints have limited the current array sizes to 8 × 8. The switching speeds are in the nanoseconds to microseconds range, second only to the lithium niobate switches. The switch architecture allows multicasting, broadcasting, and internal termination of connections without additional hardware. The typical performance of the semiconductor gate array switch is given below.

Loss: 0 dB +/- 3 dB (Gain possible)

Output port isolation: 40 dB

Polarization dependence: 1-2 dB variation in throughput

PDL <1 dB

PMD: not relevant measure

Switching time: subnanoseconds to submicroseconds

2.11.5 Magneto-optic Switches

Currently available magneto-optic switches operates on the principle of polarization diversity. The polarization rotation is provided by a bistable magneto-optic Faraday rotator. The magneto-optic material (Bi-substituted iron garnet) is used to rotate the polarization of the incoming signal to the orthogonal plane when a magnetic field is applied. Depending on the direction of polarization rotation the switch is in either the bar or cross state. This is a latching, somewhat wavelength dependent switch. The typical performance is given below.

Loss: 1-2 dB

Output port isolation: >=25 dB

Backward isolation: > 50 dB

Polarization dependence: Relatively independent since polarization diversity is used.

Switching time: <1 msec; dominated by delay to respond.

2.11.6 Liquid Crystal Switches

Liquid crystal can be used to switch light because of their ability to rotate polarizations [50-53]. The switching mechanism is based on polarization diversity as illustrated in Fig. 2.10. The incoming light is separated into two orthogonal polarizations. The liquid crystal either rotates the polarization by 90° for one switch state, or does not change the polarization for the other switch state.

These switches are normally quite wavelength dependent, as the amount of polarization rotation is a function wavelength. The polarization rotation is also intrinsically

temperature dependent. Both the wavelength and the temperature dependence can be reduced by using several stages of polarization rotation. The operation and thermal stability of a prototype switch will be discussed in Chapter 3. Typical performance parameters for a single liquid crystal cell is given below.

Loss: 2-3 dB, depending on configuration

Output port isolation: 25 to 40 dB

Backward isolation: >50 dB

Polarization dependence: small (polarization diversity)

Switching time: ~ 30 msec

2.12 Conclusion

Our survey of existing and emerging WDM switching options shows that it is difficult to obtain all the desired properties in a single technology. Optomechanical switches give better optical performance than all other switch technology, with low loss, low crosstalk, and negligible polarization dependence. The main disadvantage is the switching speed which range from tens to hundreds of milliseconds depending on the size. Free-Space micromachined optical switches (FS-MOS) have been demonstrated in laboratories to overcome this drawback of mechanical-type switches, with submilliseconds switching times while retaining the excellent optical properties. Faster switches include:

1) Waveguide devices, with switching times ranging from less than a nanosecond to one or two milliseconds, depending on the material.

2) Acousto-optic switch devices, with switching times of 10-20 microseconds.

3) Magneto-optic switch devices, with switching times of a few hundred microseconds.

4) Semiconductor gate array switch fabrics, with switching time in less than a microsecond.

5) Liquid crystal based switches with switching times of a few to several milliseconds.

Optical switching is not a mature technology and the development of new components with improved and added features are been reported continually.

2.13 References:

[1] H. Scott Hinton, An Introduction to Photonic Switching Fabrics, Plenum Press: New York, 1993.

[2] P. F. Wysocki, J. Judkins, R. Espindola, M. Andrejco, A. Vensarkar, and K. Walker, "Broad-band erbium-doped fiber amplifier flattened beyond 40 nm using long-period grating," IEEE Photon. Technol. Lett., vol. 9, no. 10, pp. 1343-1345, Oct. 1997.

[3] Y. Sun, J. W. Sulhoff, A. K. Srivastava, J. L. Zyskind, C. Wolf, T. A. Strasser, J. R. Pedrazzani, J. B. Judkins, R. P. Espindola, A. M. Vengsarkar, and J. Zhou, "An 80 nm ultra wide band EDFA with low noise figure and high output power," IEE ECOC'97, Edingburg, Scotland, 1997.

[4] H. Masuda, S. Kawai, K.I. Suzuki, and K. Aida, "Ultrawide 75-nm 3-dB gain-band optical amplification with erbium-doped fluoride fiber amplifiers and distributed raman amplifiers," IEEE Photon. Technol. Lett., vol. 10, no. 4, pp. 516-518, 1998.

[5] A. Mori, Y. Ohishi, M. Yamada, H. Ono, Y. Nishida, K. Oikawa, and S. Sudo, " 1.5 mm broadband amplification by tellurite-based EDFAs," in Proc. Optical Fiber Communication (OFC'97), 1997, postdeadline paper PD1.

[6] A. K. Srivastava, J. L. Zyskind, J. D. Evankow, J. W. Sulhoff, Y. Sun, and M. A. Mills, "Very flat gain erbium-doped fiber amplifier using samarium-doped fiber," IEEE Photon. Technol. Lett., vol. 9, no. 12, pp. 1576-1577, 1997.

[7] Bellcore Technical Reference TR-NWT-001073, *Generic Requirements for Fiber Optic Switches*, Issue 1, January 1994.

[8] J. Zhou, M. J. O'Mohoney, and S. D. Walker, "Analysis of optical crosstalk effects in multi-wavelength switched networks," IEEE Phot. Technol. Lett., vol. 6, pp. 302-305, Feb. 1994.

[9] MONET 2nd quarterly report : Review, Tech Report, Multiwavelength Optical Networking Consortium, Jun. 1995.

[10] Y. D. Jin, Q. Jiang, and M. Kavehrad, "Performance degradation due to crosstalk in multiwavelength optical networks using dynamic wavelength routing," IEEE Phot. Technol. Lett., vol. 7, pp. 1210-1212, Oct. 1995.

[11] D. J. Blumenthal, P. Granestrand, and L. Thylen, "BER floors due to heterodyne coherent crosstalk in space photonic switches for WDM networks," IEEE Phot. Technol. Lett., vol. 8, pp. 284-286, Feb. 1996.

[12] E. L. Goldstein, L. Eskildsen, and A. F. Elrefaie, "Performance implications of component crosstalk in transparent lightwave networks," IEEE Phot. Technol. Lett., vil. 6, pp. 657-660, May 1994.

[13] E. L. Goldstein, L. Eskildsen, and Y. Silberberg, "Polarization statistics of crosstalk-induced noise in transparent lightwave networks," IEEE Phot. Technol. Lett., vol. 7, pp. 1345-1347, Nov. 1995.

[14] N. Antoniades, I. Roudas, R. E. Wagner, J. L. Jackel, and T. E. Stern, "Crosstalk Performance of a wavelength selective cross-connect mesh topology," in Proc. OFC'98, San Jose, CA, 1998.

[15] N. Antoniades, I. Roudas, R. E. Wagner, T. E. Stern, J. L. Jackel, and D. H. Richards, "Study of Performance Degradations due to Crosstalk in a Wavelength Selective Cross-connect Mesh Topology," submitted to IEEE Photonics. Technol. Lett.

[16] T. H. Gilfedder, D. K. Hunter, L. Andonovic, "Crosstalk induced interferometric noise performance degradation of dilated optical TDM switching architectures,", IEE ECOC'97, Edinburg, Scotland, Sept. 1007.

[17] P. J. Legg, D. K. Hunter, I. Andonovic, and P. E. Barnsley, "Inter-Channel crosstalk phenomena in optical time division multiplexed switching networks," IEEE Photon. Technol. Lett., vol. 6, no. 5, pp. 661-663, 1994.

[18] P. J. Legg, M. Tur, and I. Andonovic, "Solution paths to limit interferometric noise induced performance degradation in ASK/Direct detection lightwave networks," J. Lightwave Technol., vol. 14, no. 9, pp. 1943-1954, 1996.

[19] Y. D. Jin, M. Kavehrad, "An optical cross-connect system as a high-speed switching core and its performance analysis," J. Lightwave Technol., vol. 14, no. 6, pp. 1183-1197, 1996.

[20] C. P. Larsen, L. Gillner, M. Gustavsson, "Linear crosstalk properties of large WDM cross-connects," IEE ECOC'97, Edingburg, Scotland, Sept. 1997.

[21] Krishnan Padmanabhan and Arun N. Netravali, "Dilated Networks for Photonic Switching," IEEE Trans. on Comms. vol. com-35, no. 12, pp. 1357-1365, 1987.

[22] G. Hugh Song, "Asymmetric dilation of multiwavelength cross-connect switches for low-crosstalk WDM optical networks," J. Lightwave Technol. vol. 15, no. 3, p. 430-436, 1997.

[23] B. E. A. Saleh, M. C. Teich, Fundamentals of Photonics, New York: John Wiley and Sons, Inc., 1991.

[24] R. A. Spanke, "Architectures for guided-wave optical space switching systems," IEEE Comm. Mag. vol. 25, no. 5, May 1987, pp. 42-48.

[25] Ron. A. Spanke, "Architectures for large nonblocking optical space switches,", IEEE J. Quantum Electronics, vol. QE-22, no. 6, pp. 964-967, 1986.

[26] R. Ramaswami and K. N. Sivaranan, " Optical Networks: A practical perspective," Morgan Kaufmann Publishers, Inc. San Francisco, California, 1998.

[27] R. A. Spanke, and V. E. Benes, "An n-stage planar optical permutation network," Applied Optics, 26, April 1987.

[28] C. Clos, "A study of non-blocking switching networks," Bell Syst. Tech. J. 32, pp. 406-424, 1953.

[29] L. Thylen, G. Karlsson, O. Nilsson, "Switching technologies for future guided wave optical networks: potential and limitations of photonics and electronics," IEEE Comm. Mag. Feb. 1996, pp. 106-113.

[30] J. L. Spencer, "Reliability of Optoelectronic Components and Its Network Implications," Proc. Opt. Fiber Commun. Conf., OSA Tech. Dig. Series, vol. 8, 1995, pp. 100 - 101.

[31] H. N. Rourke, S. R. Baker, V. Baker, R. S. Baulcomb, K. C. Byron, S. J. Clements, T. J. Cullen, S. Davis, A. Fielding, D. Goodchild, "A low loss 4-channel wavelength demultiplexer based on fiber Bragg gratings," IEE ECOC'96, Oslo, paper Wed. 1.7.

[32] Neil A. Jackman, "Multilayer optical filters with random errors," Bell Labs Technical Journal, Jan- March 1998, pp. 112-121.

[33] Katsunari Okamoto, "Fundamentals, Technology and Application of AWGs," ECOC'98, Madrid, Spain, Sept. 1998.

[34] A. d'Alessandro, D. A. Smith, and J. E. Baran, "Multichannel operation of an integrated acousto-optic wavelength routing switch for WDM systems," IEEE Photon. Technol. Lett., vol. 6, no. 3, pp. 390-393, 1994.

[35] L. Y. Lin, E.L. Goldstein, J. M. Simmons, and R. W. Tkach, "High-density Connection-symmetric Free-space Micromachined Polygon Optical Crossconnects with Low Loss for WDM Networks," Optical Fiber Communication Conference 98, San Jose, California, Paper PD 24.

[36] Joseph Ford, James A. Walker, Vladmir Aksyuk, and David J. Bishop, "Wavelength-Selectable Add/Drop with Tilting Micromirror," LEOS'97, paper PD 2.3.

[37] C. Randy Giles, "Lightwave Micromachines," ECOC'98, Madrid, Spain, Sept. 1998.

[38] L. Y. Lin, E. L. Goldstein, and R. W. Tkach, "Free-Space Micromachined Optical Switches with Submillisecond Switching Time for Large-Scale Optical Crossconnects," IEEE Photonics Technol. Lett., Vol. 10, no. 4, pp. 525-527.

[39] J. E. Ford, J. A. Walker, K. W. Goossen, and C. C. Chang, "Passband-Free Dynamic WDM Equalization," ECOC'98, Madrid, Spain, Sept. 1998.

[40] B. Barber, C. R. Giles, V. Askyuk, R. Ruel, L. Stulz, and D. Bishop, "A Fiber connectorized MEMS Variable Optical Attenuator," IEEE Photonics Technol. Lett. Vol. 10, no. 9, pp. 1262-1264.

[41] Joseph E. Ford, James A. Walker, Dennis S. Greywall, and Keith W. Goossen, "Micromechanical Fiber-Optic Attenuator with 3 μs Response," Journal of Lightwave Technol. Vol. 16, no. 9, pp. 1663-1670.

[42] T. A. Tumolillo, Jr. , M. Donckers, and W. H. G. Horsthuis, "Solid state optical space switches for network cross-connect and protection applications," IEEE comm. mag. Feb. 1997, pp. 124-130.

[43] MONET 14th quarterly report: Review, Tech. Report, Multiwavelength Optical Networking Consortium, June 1998.

[44] D. A. Smith, R. S. Chakravarthy, Z. Bao, J. E. Baran, J. L. Jackel, A. d'Alesandro, D. J. Fritz, S. H. Huang, X. Y. Zou, S. M. Hwang, A. E. Willner, and K. D. Li, "Evolution of the acousto-optic wavelength routing switch," J. Lightwave Technol., vol. 14, no. 6, pp. 1005-1019, 1996.

[45] D. A. Smith, A. d'Alessandro, J. E. Baran, D. J. Fritz, J. L. Jackel, and R. S. Chakravarthy, "Multiwavelength performance of an apodized acousto-optic switch," J. Lightwave Technol., vol. 14, no. 9, pp. 2044-2051, 1996

[46] J. L. Jackel, M. S. Goodman, J. E. Baran, W. J. Tomlinson, G. K. Chang, M. Z. Iqbal, G. H. Song, K. Bala, C. A. Brackett, D. A. Smith, R. S. Chakravarthy, R. H. Hobbs, D. J. Fritz, R. W. Ase, and K. M. Kissa, "Acousto-optic tunable filters (AOTF's) for multiwavelength optical cross-connects: crosstalk considerations," J. Lightwave Technol., vol. 14, no. 6, pp. 1056-1066, 1996.

[47] G. Hugh Song, "Time-Dependent analysis of acousto-optic tunable filters for multichannel optical switching," J. Lightwave Technol., vol. 15, no. 3, pp. 519-528, 1997.

[48] D. A. Smith and J. J. Johnson, "Sidelobe suppression in an acousto-optic filter with a raised cosine interaction strength," Appl. Phys. Lett., vol. 61, pp. 1025-1027, 1992.

[49] D. A. Smith, J. J. Johnson, B. L. Heffner, K. W. Cheung, and J. E. Baran, "Two-stage integrated-optic acoustically tunable optical filter with enhanced sidelobe suppression,", IEEE Electronics Lett., vol. 25, no. 6, pp. 398-399, 1989.

[50] J. S. Patel, and Y. Silberberg, "Liquid crystal and grating-based multiple-wavelength cross-connect switch," IEEE Photonics Technol. Lett., vol. 7, no. 5, pp. 514-516, 1995.

[51] Kuang-Yi Wu, and Jian-Yu Liu, "Liquid-crystal space and wavelength routing switches," IEE ECOC'97, Edingburgh, Scotland, Sept. 1997, paper MC4.

[52] F. Pain, R. Coquille, B. Vinouze, N. Wolffer, and P. Garvey, "High contrast nematic liquid crystal polarization controllers: application to a 4 × 4 free space optical switch at 1.5 μm,", ECOC'97, Edinburg, UK, Sept. 1997.

[53] P. G. de Gennes, "The Physics of Liquid Crystals," Oxford University Press, 1974.

CHAPTER 3

EXPERIMENTAL CHARACTERIZATION OF A NOVEL LIQUID CRYSTAL CROSSCONNECT SWITCH

3.1 Background

Liquid crystals (LC) are a phase of matter whose order is intermediate between that of a liquid and that of a crystal. They have become very attractive for WDM switching applications because of their ability to rotate polarization [1-3]. In Section 3.1 the operating principles of a prototype 2 × 2 liquid crystal cross-connect (LXC) switch used to interconnect independent rings in the MONET project [4] will be presented. Our measurements of the thermal stability of the switch will also be presented and the reliability commented on in Section 3.2.

Liquid crystals come in various forms with different materials constituting the liquid crystal itself. The liquid crystal that has been under serious investigation for WDM switching applications is the Twisted Nematic type. A Twisted Nematic liquid crystal cell [5] is made up of:

1. Two bounding plates (usually glass slides), each with a transparent conductive coating (usually indium tin oxide (ITO)) that acts as an electrode.
2. Spacers to control the cell gap precisely.
3. Two crossed polarizers (the polarizer and analyzer) in some cases.
4. The nematic liquid crystal material.

This chapter describes the operation and the experimentally determined thermal stability of a prototype liquid crystal crossconnect (LXC) switch. The general conclusions are applicable to any switch based on liquid crystal technology.

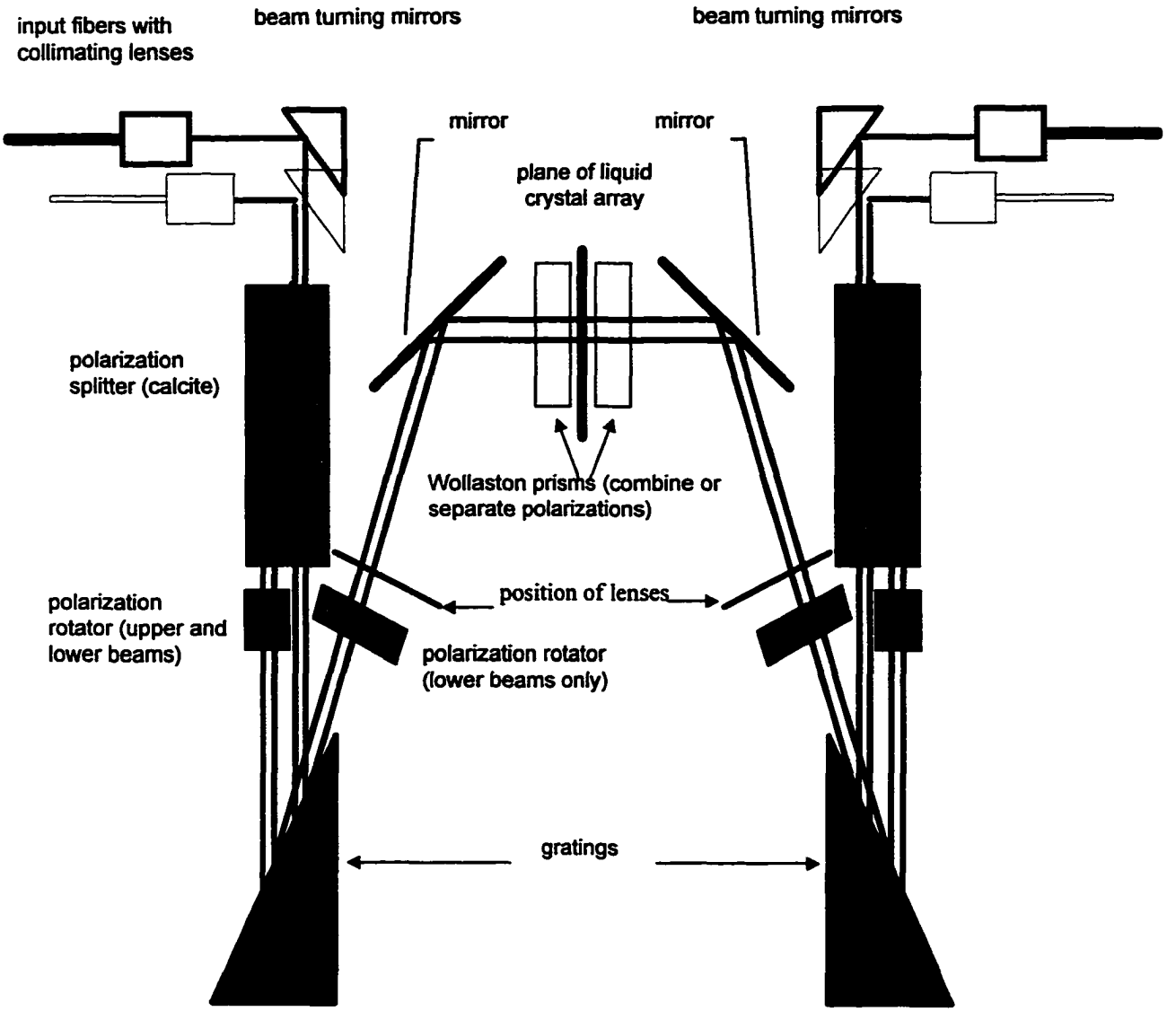

Fig. 3.1 Multiwavelength liquid crystal switch, top view

3.1.1 Design and Operation Principles

A 2 × 2 prototype multiwavelength liquid crystal cross-connect (LXC) switch is shown schematically in Fig. 3.1. The switching mechanism is based on polarization diversity as shown in Fig. 2.10. A brief description of the operation of the prototype device shown in Fig. 3.1 is as follows: The LXC switch consists of two input and two output fibers connected via an optical path in which the wavelength selection takes place. The input beams are vertically offset from each other. Both beams are separated into their vertical and horizontal polarizations by the polarization splitters (calcite blocks). The half-wave plate at the output face of the calcite block rotates the polarization of the ordinary beams into the horizontal plane. This ensures that the beams encountering the grating are in a single polarization state (perpendicular to the grooves of the diffraction grating); that which gives the maximum diffraction efficiency for the grating. The polarization rotation also accommodates the switching at the liquid crystal array via polarization rotation. After the wavelength spectrum is spread by the grating, the lower two beams pass through another half-wave plate that rotates the polarization into the vertical plane. Therefore, the beams from the separate inputs have orthogonal polarizations after this optical adjustment. A lens is used to focus the light which then passes through a Wollaston prism after reflection from a mirror. The Wollaston prism causes the upper and lower beams to overlap. After passing through the Wollaston prism the beams encounter the liquid crystal array. Each of the wavelength channels is either polarization rotated or remains in the same polarization state, depending on the "voltage controlled" desired

switch state. The beams are then processed by the mirror-image optics on the output side of the switch before they are collimated and sent to the appropriate output fibers.

3.1.2 Liquid Crystal Cells

The liquid crystal cell array lies in the region of the switch where the wavelengths are separated. Each cell operates on a single spectral slice and is independently controlled by a voltage source. The cell is designed such that with no applied voltage the polarization of the incoming light is rotated by 90°, and such that when a large enough voltage is applied, the polarization of the incoming light is preserved. The amount of polarization rotation is wavelength dependent, and therefore the switching efficiency is wavelength dependent. Wavelength dependence can be reduced by using multiple stages of polarization rotation which can be accomplished using passive materials. Input light which undergoes polarization rotation is transferred to the complementary output of the switch, i.e.,. input 1 to output 2 and input 2 to output 1. For the unrotated polarization light, the input light goes to the corresponding outputs. In the former case the switch is in the cross state and for the latter case it is in the bar state for the wavelengths involved.

The polarization rotation which accommodates the switching is accomplished by carefully designed twisted nematic liquid crystal cells. A thin layer of polymer is used to coat the transparent electrodes in contact with the LC. The layer of polymer at one surface of the cell is brushed in a perpendicular direction to that at the other surface. The nematic LC molecules tend to orient with their long axis parallel to these directions. When there is no applied voltage the nematic director undergoes a smooth 90° twist from

the orientation of the rub at one surface to the orientation of the rub at the other surface. The twisted arrangement of the LC molecules acts as a birefringent optical waveguide which rotates the plane of polarization by a quarter cycle such that light emerging from the cell has an orthogonal polarization to the light entering it. With a large enough voltage (AC) the molecules align themselves with the electric field and there is no polarization rotation (no birefringence) of the light.

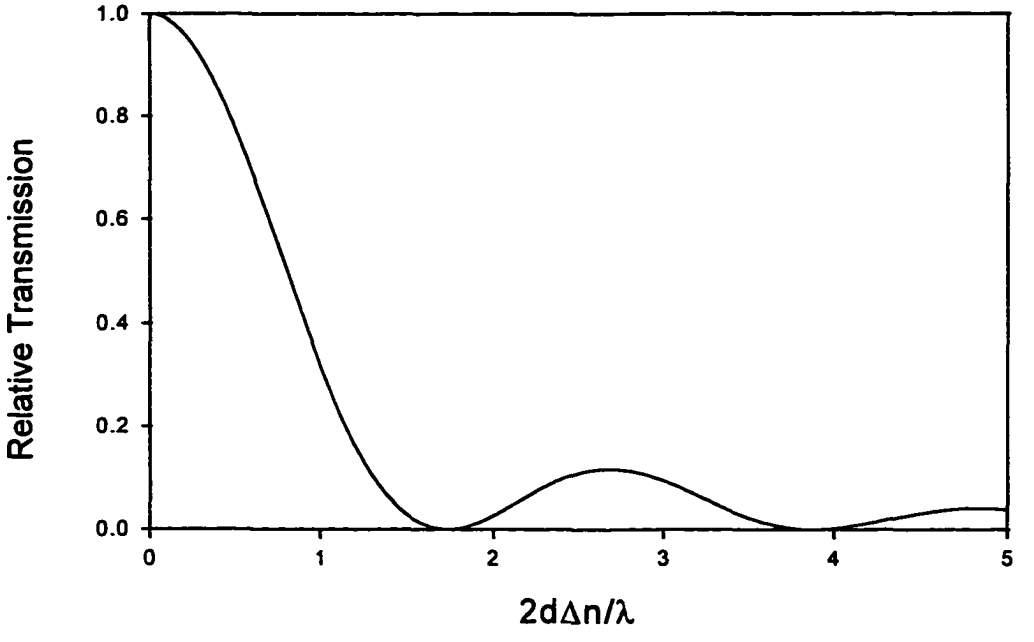

Figure 3.2 Relative transmission through parallel linear polarizers of a twisted nematic liquid crystal cell.

For a uniform twist, the polarization of the output light at a particular wavelength λ is dependent on the local birefringence (Δn) and on the thickness of the cell (d). The relative transmission (T) of such a cell placed between parallel linear polarizers is given by:

$$T = \frac{\sin^2(\frac{\pi}{2}\sqrt{1+a^2})}{1+a^2} \tag{3.1}$$

where $a = 2d\Delta n/\lambda$. For a narrow wavelength band λ can be considered constant but for a wider spectrum this assumption is not valid. The transmission (T) given in equation (3.1) is plotted in Fig 3.2. From the figure we see that for a given birefringence there is a set of discrete values of cell thickness (the minima) for which the polarization rotation is precisely 90°. The prototype LXC switch operates at the first minimum ($a = \sqrt{3}$). Accurate control of the thickness is essential for good crosstalk performance of the LXC switch. The crosstalk of the cross state is in general worse than the bar state since a high enough voltage will align the molecules with the electric field, reducing the birefringence to effectively zero. Therefore, the state of polarization (SOP) of the light and thus the switching can be controlled more accurately.

3.2 Thermal Stability of the LXC

The performance of the LXC is very temperature dependent. Temperature changes can affect the viscosity of the liquid crystal material. This affects the local birefringence of the LC molecules and therefore the value of $a = 2d\Delta n/\lambda$ changes, leading to incomplete or

excess polarization rotation. This can lead to degraded crosstalk performance of the LXC switch. At a high enough temperature (clearing temperature) the liquid crystal becomes optically isotropic and thus no polarization rotation can take place. Different liquid crystals have different clearing temperatures with typical values ranging from about 60°C to more than 100°C. The alignment of the optical elements making up the switch can also be affected by temperature.

In our laboratory the thermal stability of the prototype LXC was measured under the following conditions. First, we measured the LXC switch box with a dummy cell (one with no liquid crystal material) in place. Second, the liquid crystal array itself was measured in a separate fixture. This was done to separate the thermal effects due to the misalignment of the optical elements in the switch box which affects loss and wavelength registration, from the thermal effects due to the birefringence changes of the liquid crystal itself, which primarily affect the crosstalk performance of the switch.

3.2.1 Thermal Stability of the Optical Box

The switch box was placed in a large temperature controlled oven and the throughput over a narrow wavelength range determined for a broadband light source provided by an EDFA placed outside the chamber. The throughput for single polarization light was recorded using an optical spectrum analyzer. The internal temperature of the oven was then cycled from 20°C to 50°C and then back to 20°C. Since a dummy liquid crystal cell was used for this measurement only the loss and wavelength registration for the bar state of the switch could be recorded. This was sufficient for the purposes of the measurement

which was to observe if temperature induced movements of the of the optical components affected the loss and wavelength registration of the optical elements in LXC (i.e. minus the liquid crystal itself).

Both the average loss and the loss spectrum showed considerable temperature dependence over the temperature range. The output for one polarization at 21.7°C and 50.4°C were compared. As the temperature increased the throughput reduced by as much as 6 dB. The loss variation was also observed to be irreversible. After several thermal cycles the loss spectrum at the same temperatures varied by as much as 2 to 8 dB depending on the wavelength. The wavelength registration shifted slightly with temperature. However, the observed shifts were thought to be tolerable since the channels are wide and flat. The variation in loss observed for the optical elements in the switch box of the prototype LXC switch shows that improvement in the design, construction, and materials is necessary if the switch is to be operated in an environment with substantial temperature changes, and not that there are intrinsic problems in the switch technology itself. Much more stable operation has been observed over several months in a laboratory environment with only a few degrees daily temperature swing.

3.2.2 Thermal Stability of Liquid Crystal Cell

The fixture used to measure the thermal properties of the liquid crystal array is shown schematically in Fig 3.3. The fixture provides the same polarization splitting, rotation and combining as the optical box, but does not perform wavelength separation. The liquid crystal is controlled by a voltage source which determines whether light will be focused

into the output fiber (Fig. 3.3a) or will be directed away from the output fiber (Fig. 3.3b). The liquid crystal was mounted in the fixture and the entire fixture placed in a small oven. The throughput as a function of the applied voltage was measured by a power meter for a set of temperatures between room temperature (23°C) and 50°C.

For a liquid crystal fabricated with an ideal thickness the set of curves shown in Fig. 3.4 were observed. For low voltage the polarization is rotated and consequently the throughput is low. As the voltage increases and the intermolecular forces are overcomed, the birefringence of the cell is lost and the throughput is increased. As the temperature increases the birefringence is reduced due to greater randomness in the LC orientation,

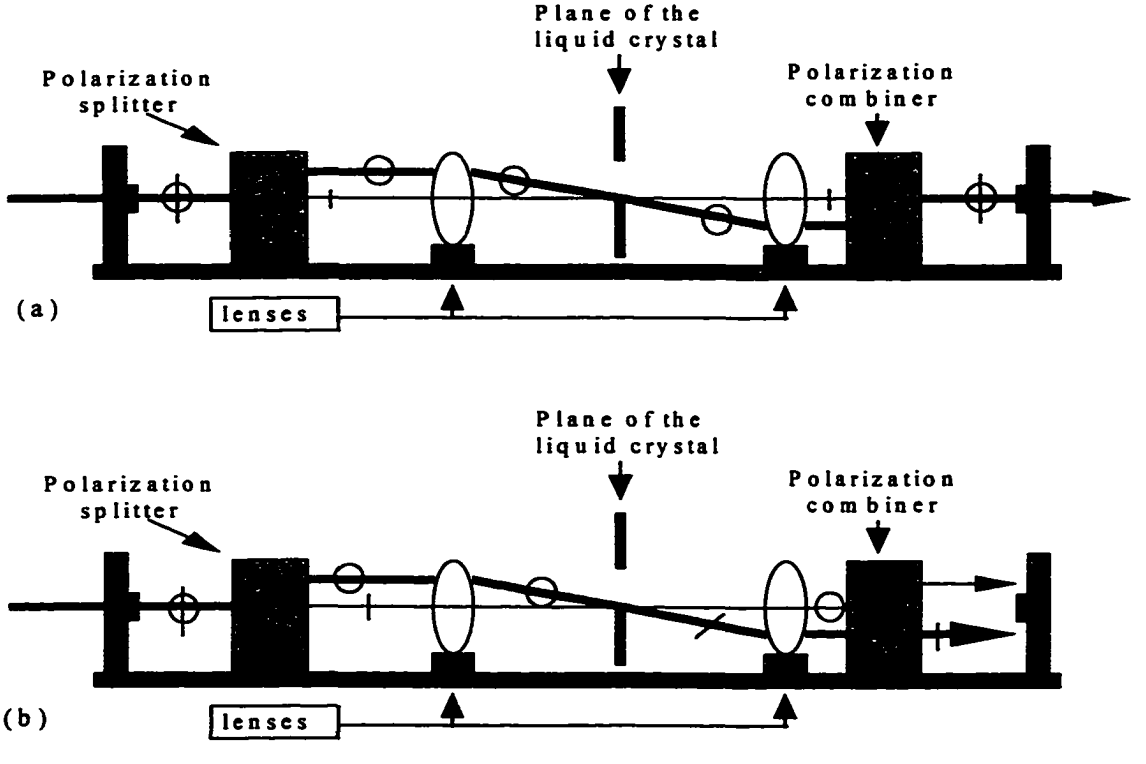

Figure 3.3 Fixture for measuring liquid crystal switching efficiency. (a) Optical path when polarization is not rotated. (b) Optical path when polarization is rotated.

and consequently incomplete polarization rotation results. As a result the minimum output and thus the crosstalk is higher for higher temperatures. Fig. 3.5 shows the throughput obtained for a cell with thickness greater than the ideal. Unlike the previous case, the throughput at zero voltage is not a minimum.

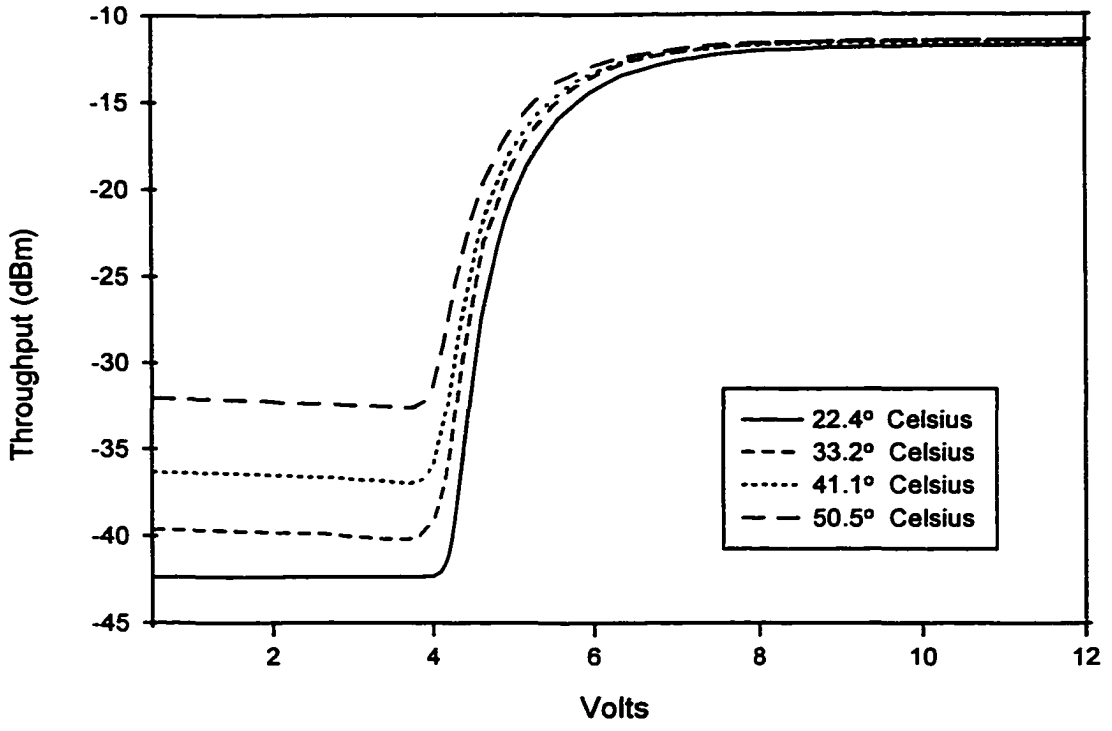

Figure 3.4 Output of liquid crystal cell with near ideal thickness, as function of voltage, for four temperatures.

As the voltage increases the birefringence decreases until $a = 2d\Delta n/\lambda$ reaches a value that produces minimum output. With further increase of the voltage the birefringence is further reduced and the output increases to some saturation value. As the temperature is increased the birefringence of the LC is reduced and consequently a smaller voltage is required to achieve the birefringence that gives a minimum as seen in Fig. 3.5. Fig 3.5

also shows that a cell that is thicker than the ideal can be tuned to a minimum output however, such a cell has a very sharp minimum, and would therefore require a sustained precise control of the voltage to realize good crosstalk performance.

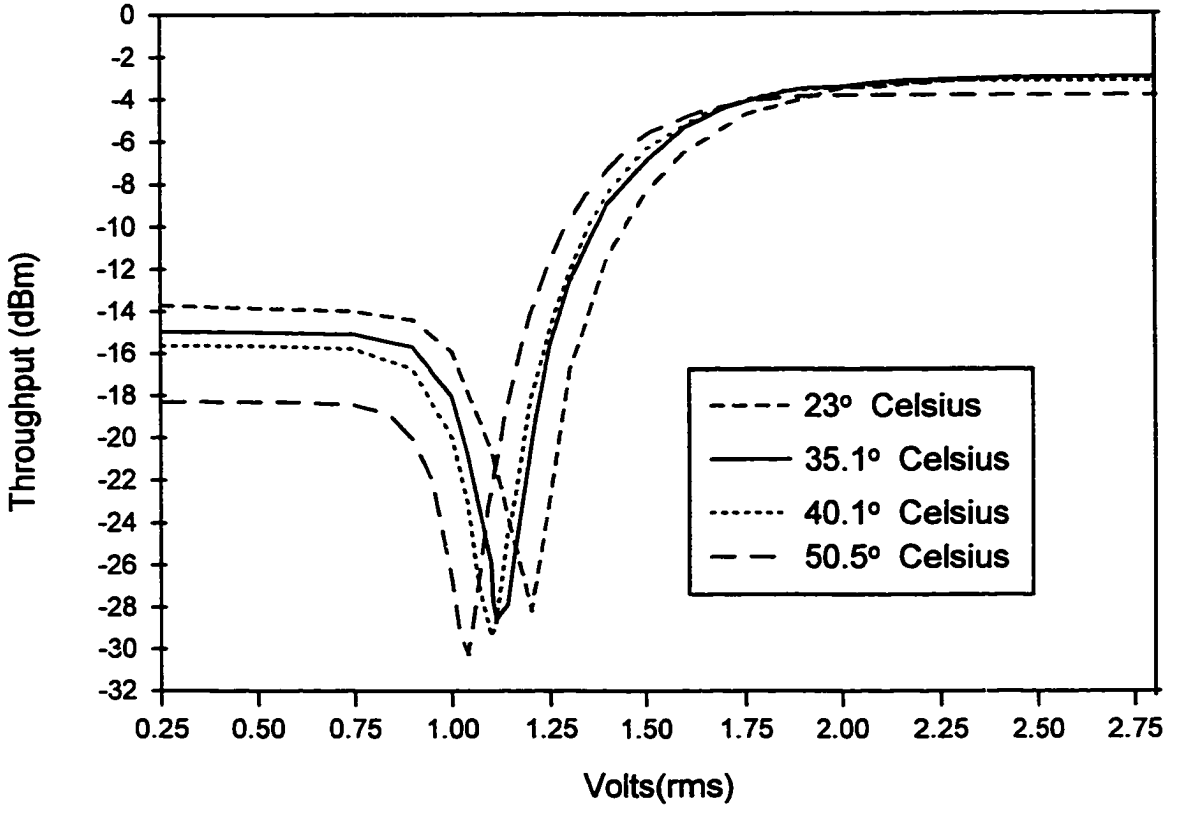

Figure 3.5 Output of liquid crystal cell with thickness greater than the ideal, as a function of voltage, for four temperatures. (Liquid crystal material is not the same as for the cell characterized in Fig. 3.4)

The measured prototype LXC had not been optimized for good thermal behavior and substantial improvement in performance is expected from the emerging switches in the marketplace based on this technology. The typical performance parameters for a single liquid crystal cell is given below:

Loss: 2-3 dB, depending on configuration

Output port isolation: 25 to 40 dB

Backward isolation: >50 dB

Polarization dependence: small (polarization diversity)

Switching time: ~ 30 msec

3.3 References

[1] J. S. Patel, and Y. Silberberg, "Liquid crystal and grating-based multiple-wavelength cross-connect switch," IEEE Photonics Technol. Lett., vol. 7, no. 5, pp. 514-516, 1995.

[2] Kuang-Yi Wu, and Jian-Yu Liu, "Liquid-crystal space and wavelength routing switches," IEE ECOC'97, Edingburg, Scotland, Sept. 1997, paper MC4.

[3] F. Pain, R. Coquille, B. Vinouze, N. Wolffer, and P. Garvey, "High contrast nematic liquid crystal polarization controllers: application to a 4 × 4 free space optical switch at 1.5 μm,", ECOC'97, Edinburgh, UK, Sept. 1997.

[4] R. E. Wagner, R. C. Alferness, A. A. M. Saleh, and M. S. Goodman, "MONET: Multiwavelength optical networking," IEEE Journal of Lightwave Technol. June 1996. pp. 1349-1355.

[5] P. G. de Gennes, "The Physics of Liquid Crystals," Oxford University Press, 1974.

CHAPTER 4

SWITCHING DYNAMICS AND ITS IMPLICATION ON MULTI-CHANNEL EDFA STABILIZATION: EXPERIMENTAL RESULTS

4.1 Background

The advent of EDFAs has revolutionized the field of optical communications in two ways. First their large optical gain allows long-haul unregenerated systems with optical repeaters spaced more than 100 km. Second, their large optical bandwidth and slow gain dynamics, which allows them to simultaneously accommodate multiple optical channels without significant crosstalk, makes it possible to increase capacity by an order of magnitude using several WDM high bit-rate channels [1-2]. Optical amplifiers and wavelength-multiplexing technology are transforming lightwave communications by providing cost-effective upgrades that will increase the transmission capacity of telecommunication networks significantly [3-5]. Successful deployment of these advanced systems requires a thorough understanding of optical amplifiers and the optical fiber medium, as their requirements interrelate through optical bandwidth, noise, dispersion, optical nonlinearities, and their impact on signal transmission. Optical fiber has emerged as the undisputed transmission medium of choice because it offers unrivaled transmission capacity at a cost lower than any other medium. Many companies and consortia are continuously pursuing research to explore the efficient uses of the wide bandwidth of low-loss single-mode fibers for long-distance transport as well as high-throughput computer networking and distribution of broadband services. EDFAs consist of a short length of optical fiber containing a low concentration of erbium ions and a

semiconductor laser that excites these ions to provide gain in the 1550 nm wavelength region. Unlike conventional lightwave repeaters, these amplifiers can boost the power of lightwave signals without the need for opto-electronic conversion. The process is independent of data rate and can accommodate many wavelength-division-multiplexed (WDM) channels with negligible interchannel crosstalk as pointed out before. Conventional EDFAs have a usable optical bandwidth (BW) of approximately 35 nm and therefore offer a simple and cost-effective means to exploit a portion of the approximate 200 nm transmission capacity inherent in single-mode optical fibers. EDFAs have therefore set the stage for improved operation flexibility, reliability, and have made optical networking functionality realizable, potentially at lower cost than with optoelectronic generators.

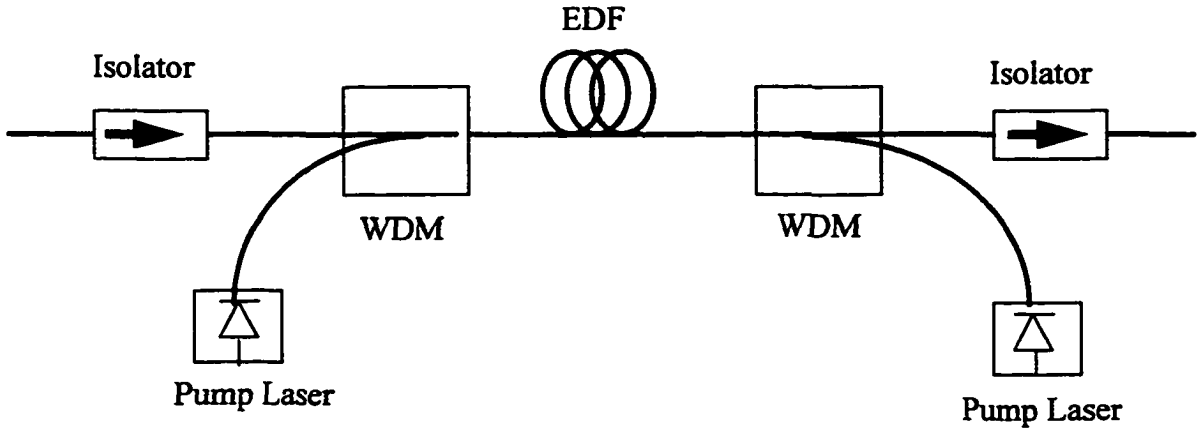

Figure 4.1 Typical EDFA configuration. This is a bi-directionally pumped configuration but co-pumped and counter-pumped configurations have similar configurations except for the absence of the corresponding pump laser and WDM.

4.1.1 General EDFA Properties

Fig. 4.1 shows a simplified diagram of an EDFA configuration. Optical filters (not shown in the figure) can be used to alter the amplifier spectral characteristics, and optical isolators to prevent the amplifier from oscillating due to unwanted reflections. Additionally, couplers may be used to enable performance monitoring and as shown, to couple power from the pump laser to the erbium-doped fiber (EDF). EDFAs can be forward pumped, backward pumped, or bi-directionally pumped, with each configuration having its own advantages and disadvantages. The EDFA can be consructed from a single or several stages of EDF. The erbium-doped fiber is fabricated by selective doping during manufacturing to confine the erbium ions to the single-mode fiber core [6]. The doped region of the fiber is the critical portion of the EDFA. When this region is optically pumped efficiently it becomes an amplifying medium in the 1520-1600 nm wavelength window. Within the glass the erbium associates with oxygen and exist in the Er^{3+} ionization state, having energy state transitions appropriate for optical amplification in the 1550-nm wavelength region. Fibers are generally characterized by their associated absorption and emission spectra. The former represents the characteristic absorption of a short length of fiber when illuminated by a white-light source. Observations of this spectrum show the absorption bands 530, 660, 800, 980, or 1480 nm as the most promising pump wavelengths. The emission spectrum is measured with a large pump power at 980 or 528 nm to completely invert the Er^{3+} population to a metastable level. The pump wavelengths 980 and 1480 nm are most commonly deployed, as they offer the best compromise between efficiency, and hence gain, and noise performance [7-8]. Also,

excited state absorption (ESA), the phenomenon where atoms can be excited to a fourth energy level by absorption of a pump or a signal photon from the metastable level 2 to be discussed below, does not occur when these two pump wavelengths are deployed. Fig. 4.2 shows a typical absorption and emission (fluorescence) spectra for a commercially available EDF. The shapes of the absorption and emission spectra can be explained by the associated energy-level transitions represented schematically by Fig. 4.3. The energy levels $^4I_{15/2}$, $^4I_{13/2}$ and $^4I_{11/2}$ are not discrete energy levels but a number of closely spaced states commonly known as a manifold. The degeneracy of these levels are enhanced by the Stark effect, due to the influence of codopants such as aluminum and the anistropic nature of the glass host. The shape of the emission spectral envelope depends totally on the nature of the transition between the manifolds. Aluminum introduces additional splitting which in turn increases the number and the range of allowed transitions, with a consequent flatter spectrum and thus increased usable bandwidth of the fiber [9]. Each of the energy levels is characterized by a total orbital momentum j; each split into a manifold of $g = j + 1/2$ energy sublevels [10], where g is the total level degeneracy. As a result of intramanifold thermalization the simplified representation in which each manifold is considered a single level is quite accurate at normal operating temperatures. The effect of the thermalization is to maintain a constant population distribution within the manifolds (Boltzman's distribution). The fact that the main energy levels are split with uneven internal subpopulation distributions also makes it possible to pump Er^{3+} glass directly in level 2 (as opposed to level 3) and to achieve overall population inversion between levels 1 and 2. Amplification is a three-level process in EDFAs, and

consequently unlike the four-level system, reabsorption of signal energy can take place if population inversion is not complete. In fact, an unpumped amplifier attenuates the input signal because of absorption by ground-state ions. In 980 nm pumped amplifiers absorption of pump light excites the erbium ions from the lower level ($^4I_{15/2}$) ground state to the $^4I_{11/2}$ state, the lifetime of which is extremely short, being on the order of 1 μs. A nonradioactive decay to the $^4I_{13/2}$ state follows. This is the long-lived metastable state, as the spontaneous lifetime is extremely long, on the order of 10 ms. From this level two events are possible.

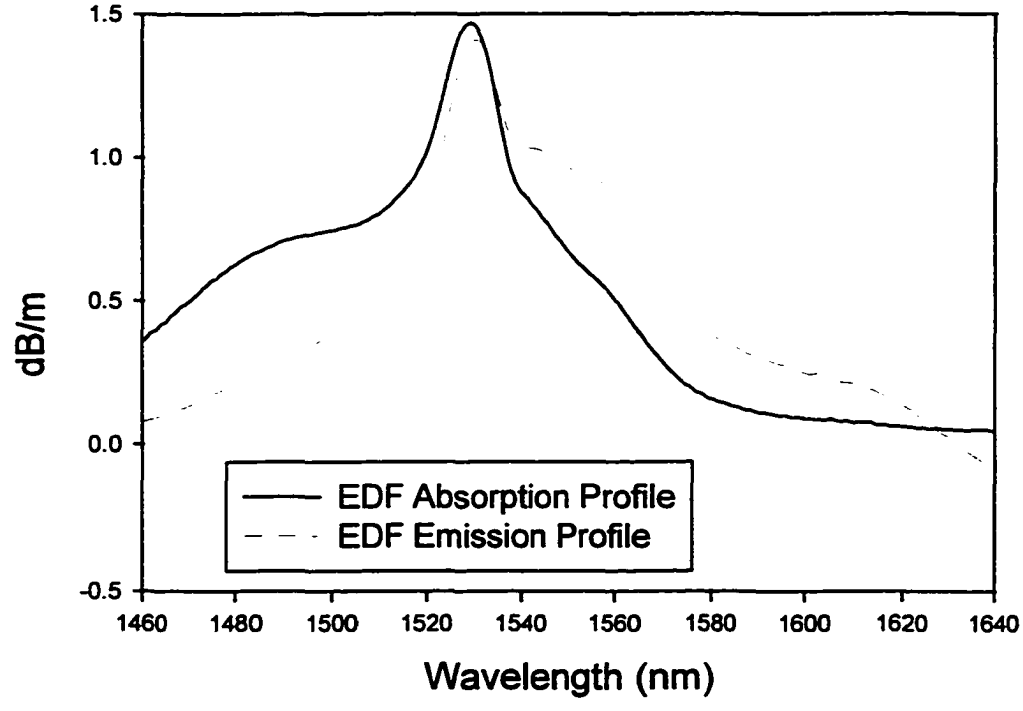

Figure 4.2 Example of the absorption and emission profile for a commercially available EDF. This is the EDF that is used for all the simulations presented in this thesis.

1. An excited ion decays naturally to the ground state, generating a photon of random phase.
2. Through stimulated emission by a signal photon, excited ions emit photons in phase with the signal frequency. This process continues as the signal passes through the gain medium, producing an amplified replica of the input signal at the EDFA output. Amplification takes place for signal photons in the approximate wavelength region from 1520-1600 nm, corresponding to the energy difference of the metastable and ground-state of the erbium ion. Therefore, the net result is a transition to the ground-state, resulting in an additional photon of the same wavelength and phase.

Both the signal and spontaneous photons are amplified as they propagate along the length

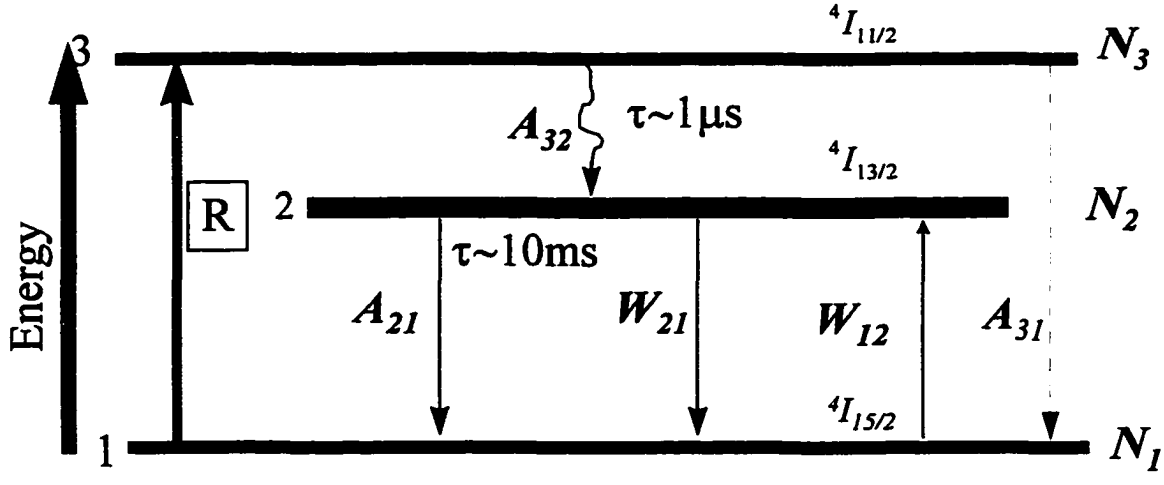

Figure 4.3 A simplified energy level diagram of erbium ions and the associated transitions corresponding to a basic three-level laser system. The Wij terms represents processes due to stimulated emission and absorption while the Aij terms represent the natural radiative and non-radiative decay processes.

of the doped fiber. The amplified spontaneous emission (ASE) is not related to the signal and constitutes noise in the device. It is produced over the whole gain spectrum of the amplifier and is nearly proportional to the gain. The EDFA can be designed to operate close to the quantum limit for minimum ASE noise [11].

4.1.1.1 Pumping at 1480 nm vs 980 nm

Choosing the pump wavelength to be 1480 nm is a good compromise between having a strong ground state absorption in order to excite the erbium ions, and a weak gain coefficient to minimize pump stimulated emission [12]. Key advantages of pumping at 980-nm are that the effective gain coefficient at the pump wavelength is practically zero because of the three-level property, pump stimulated emission does not occur, higher slope efficiency (power vs laser current), higher small signal gain per mW pump, lower noise figure (near theoretical limit of 3 dB), and larger signal to pump wavelength separation than 1480 nm pumps. Practically, the last advantage means greater ease of filtering remnant pump from signal, using a wavelength division multiplexer. There is a pump threshold power, dependent on pump wavelength, signal power and wavelength, and fiber length, above which the amplifier exhibits gain where the amplification from stimulated emission of the metastable ions more than compensates loss from ground-state absorption. When the pump power is varied there is a changing range of wavelengths over which the fiber is amplifying and outside which the fiber is lossy. As the pump power is increased, fiber transparency is followed by a regime of fiber amplification, starting from long wavelengths. This is because the ground-state absorption which

reduces gain is lower at longer wavelengths. Amplified signal output power increases with increasing pump power in a three-level system.

4.2 Gain Dynamics

Although EDFAs are a key technology enabling the realization of transparent WDM communication, and despite their unsurpassed performance, a number of significant technological challenges remain. These challenges become increasingly severe as the network grows in complexity and reach. In a large reconfigurable network, dynamic reconfiguration exacerbates the difficulties and imposes stringent demands on all components. One of the most significant of these challenges is commonly refered to as "transient cross-saturation" or "gain dynamics". This is seen in Fig. 4.4a where the loss of the strong signal channel causes the power in the surviving channel to increase and take its place. Fig. 4.4b shows the time resolved response of the surviving channel (top trace) for the adding and dropping of a channel (bottom curve). As is clear from the figure, the surviving channel experiences power excursions that rougly complements those of the channel that is being modulated.

A number of experimentally demonstrated methods to prevent these unwanted power excursions of surviving channels in EDFAs have been reported. These include gain clamping via the construction of ring lasers [13-14], or of lasers with cavities defined by fiber Bragg gratings [15-16], or using stimulated brillouin scattering [17-18], fast pump control [19-21] and insertion of a compensating signal [22-23]. Inserting a compensating signal into the first EDFA has been reported to be effective in stabilizing chains of six

[24] and eight [25-26] EDFAs. A simpler approach which employs an all-optical feedback mechanism at the first EDFA for clamping the gain of individual channels and the generation of a compensating signal, which is propagated throughout the entire chain has also been reported [27].

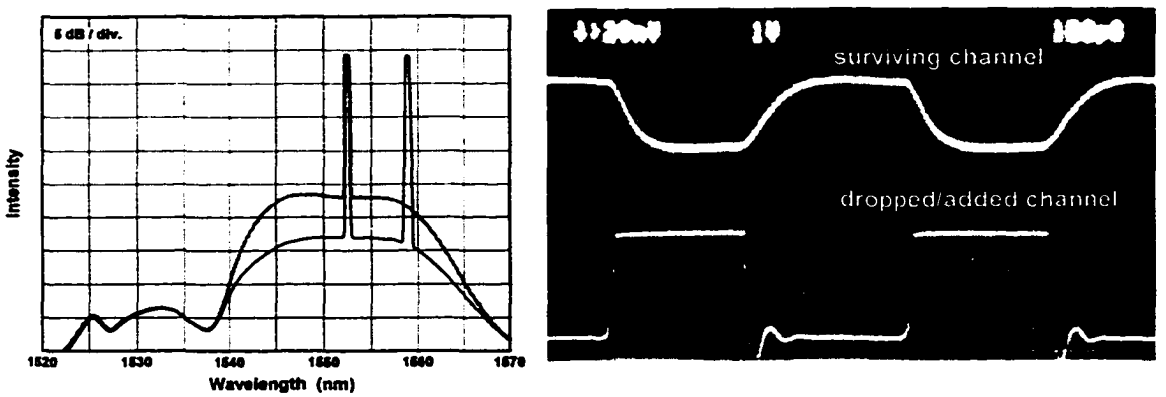

Figure 4.4 EDFA cross gain saturation. (a) When the "strong" signal is dropped the power in the surviving channel increases and take its place. (b) Time resolved response for dropping and adding half the number channels.

This chapter presents experimental results of gain dynamics for individual and cascaded stabilized EDFAs. First, we briefly describe a number of different methods for stabilizing the gain of EDFAs. We then show our all-optical method for gain-clamping chains of saturated EDFAs [27].

4.2.1 The Problem

The number of wavelength channels passing through an EDFA in a multiwavelength network will vary as a result of network reconfiguration, network growth to larger number of channels, or component failures that can cause one or more channel to drop out. Because these amplifiers are operating near saturation, and since the total output power of a saturated EDFA is very nearly constant, independent of the number of channels, the gain experienced by each channel will, therefore, depend on the number of channels present. This will induce time-varying perturbations, via transient cross-saturation in the amplifier, on other wavelengths as seen in Fig. 4.4b. These perturbations, which in general accumulate along the amplifier chain, may grow large in systems that undergo reconfiguration. Cross-saturation in the network's EDFAs will induce power transients in the surviving channels, the speed of which is proportional to the number of amplifiers in the network. The increased gain when channels are dropped can give rise to surviving channel errors since the power of the surviving channels may surpass the thresholds for nonlinear effects such as Brillouin scattering. Rapidly changing gain, due to channel drop or addition, can lead to errors as the receiver's ability to adapt to changing power levels is exceeded. Since we can assume that EDFAs will not be used in multiwavelength optical networks unless information in one channel is not degraded by any changes in other channels, both steady state gain and fast transients must be controlled. The transient gain changes that occur at the time of channel dropping present a particular challenge in amplifier cascades. While typical time scales for gain changes in

a single amplifier are tens of microseconds, the time constant for a chain of N amplifiers

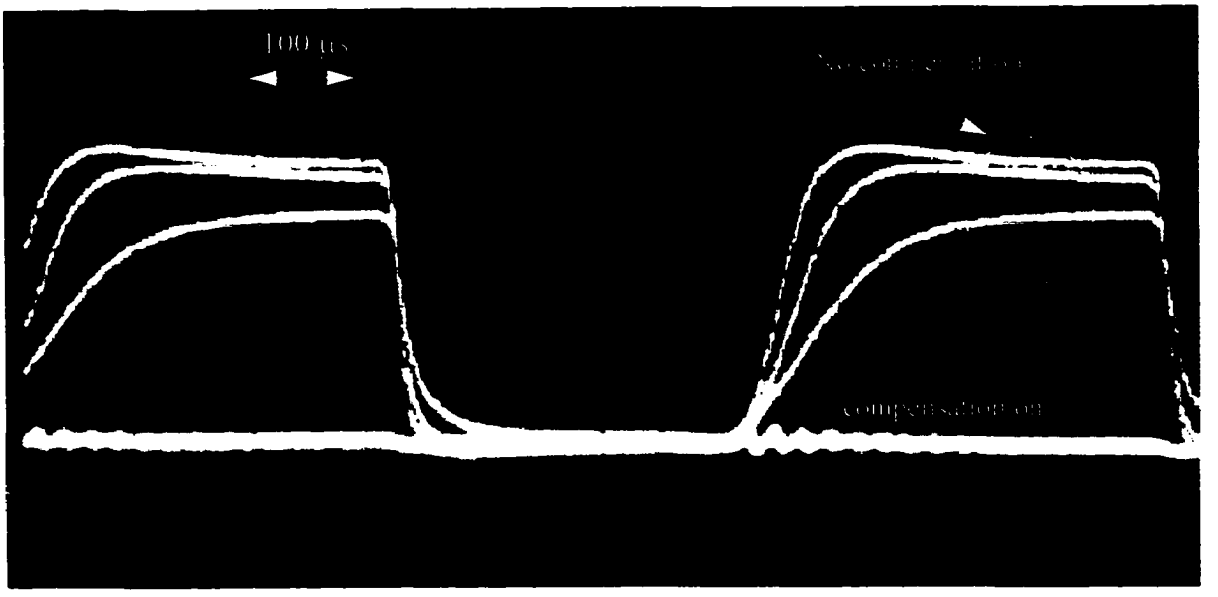

Figure 4.5 Fast power transients in a chain of three EDFAs for the surviving channel when channels are added and dropped. The figure also shows the clamping of the power excursions (lower trace) when compensation is introduced.

is 1/N times shorter than that of a single amplifier [28]. Fig. 4.5 shows this reduction of the time constant for a chain of three EDFAs. Thus long chains of amplifiers will require faster control to limit the undesirable power excursions, presenting a greater gain stabilization challenge.

4.3 Gain Stabilization Options

The main objective of stabilization is to maintain constant per-channel output power without degrading the signal-to-noise ratio (SNR), regardless of the number of channels present. The basic requirement is that any given channel passing through an optical amplifier shall not be adversely affected by anything that happens to any of the other

channels passing through the same amplifier. Some stabilization schemes accomplishes this task better than others. Even in the absence of channel dropping or addition the variations in power of one channel can cause power variations at other channels in saturated EDFAs. This occurs because the gain or the level of inversion of the EDFA depends on the total input power. If the input power of one channel increases, the level of inversion will be reduced. Consequently, the gain of the amplifier reduces resulting in lowered output power for the other channels. If all channels experience the same change in power, the self-healing effect of saturated EDFAs ensures that the output power per channel will remain nearly constant as the gain is automatically adjusted. The proposed solutions for alleviating the cross saturation effect in saturated EDFAs fall into three main groups: gain clamping, control of pump power to shift saturation power, and use of non-saturated EDFAs.

4.3.1 Gain Clamping

The EDFA is saturated when changes in the input power do not produce a commensorate change in the output power. That is, the output power remains fixed at the rated saturated output power of the EDFA. This saturated output power depends on the EDF design and is directly proportional to the pump power over a certain range of pump powers. As we will see later, this dependence on pump power can be used to stabilize the gain or the power per channel of the EDFA. Because the EDFA gain spectrum is not flat the minimum input power that drives the EDFA into saturation varies slightly depending on

the wavelengths of the input signals. The gain of the saturated EDFA depends strongly on the total input power and only slightly on the nonflat gain. Therefore, the gain can be made almost fixed if the total input power is kept constant. This can be accomplished by adjusting a compensating channel to keep the total input power constant when channels are added or dropped. The gain-clamped EDFA is designed such that the compensating channel has a particular power level relative to the signals when all channels are present. Any disproportionate disrribution of the power levels of the signals at the input is amplified and replicated at the output. Higher input power than designed for can reduce the compensating signal level to zero. The minimum total input signal power that reduces the power in the compensating channel to zero is refered to as the critical input power P_c [29]. For the range of input signal powers below P_c, the gain of the EDFA is fixed. A stronger compensating channel increases the maximum input signal power that can be tolerated before the gain-clamping property is lost, but this also means that the average gain of the EDFA will be lower.

4.3.1.1 Gain Clamping using a Compensating Channel

There are a number of different schemes that are used to gain clamp an EDFA using a compensating channel. All-optical gain clamping which automatically generates a compensating channel is achieved by embedding the erbium-doped fiber in a laser cavity defined by wavelength selective elements, wavelength selective couplers in Fig. 4.6a and fiber Bragg gratings in Fig. 4.6b. If a filter is used to select the lasing wavelength, the

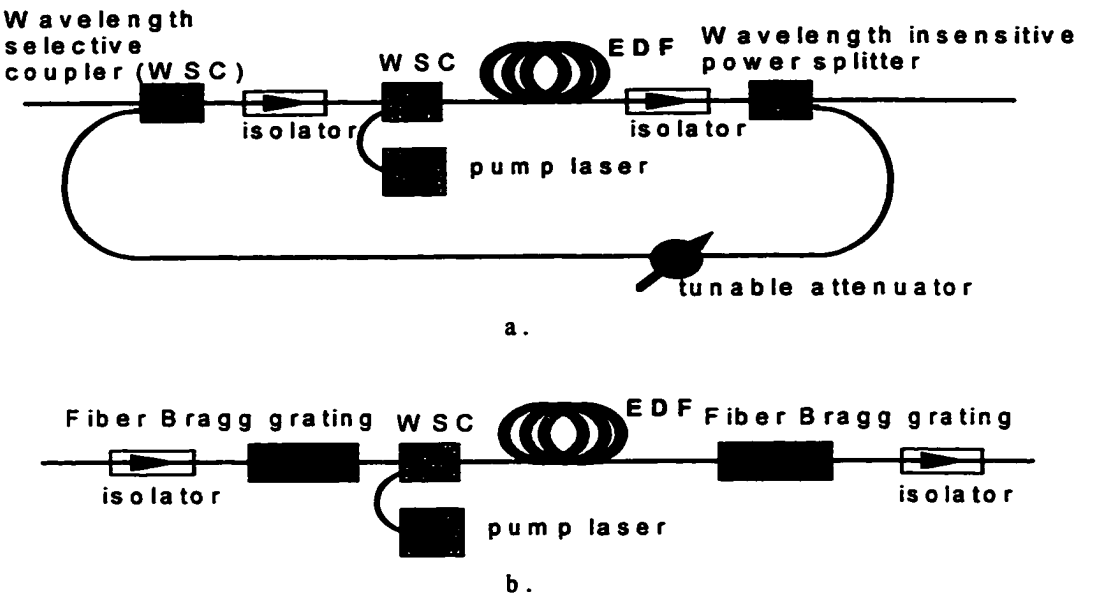

Figure 4.6 EDFA gain stabilization using (a) wavelength selective optical feedback and a wavelength insensitive output coupler, (b) fiber Bragg grating to select the stabilization wavelength.

interplay of polarization instabilities and PDLs can cause gain drift of > 0.5 dB. The gain drift is due to polarization fading of the feedback channel that is selected by the filter. Faraday rotator mirrors can be used to suppress this gain drift [30]. Much of the work in this thesis is based on this type of EDFA and a detailed description of its behavior for a single EDFA and chains of EDFAs will be given later in this chapter.

The compensating channel can also be generated as shown in Fig 4.7. In Fig. 4.7a an optical tap at the input monitors the total input power and provides information which is used to adjust the power of the compensating channel. This approach can also be used to stabilize chains of EDFAs [25-26]. Experimental results have shown that this method can be somewhat faster than the all-optical feedback approach. Gain clamping was achieved

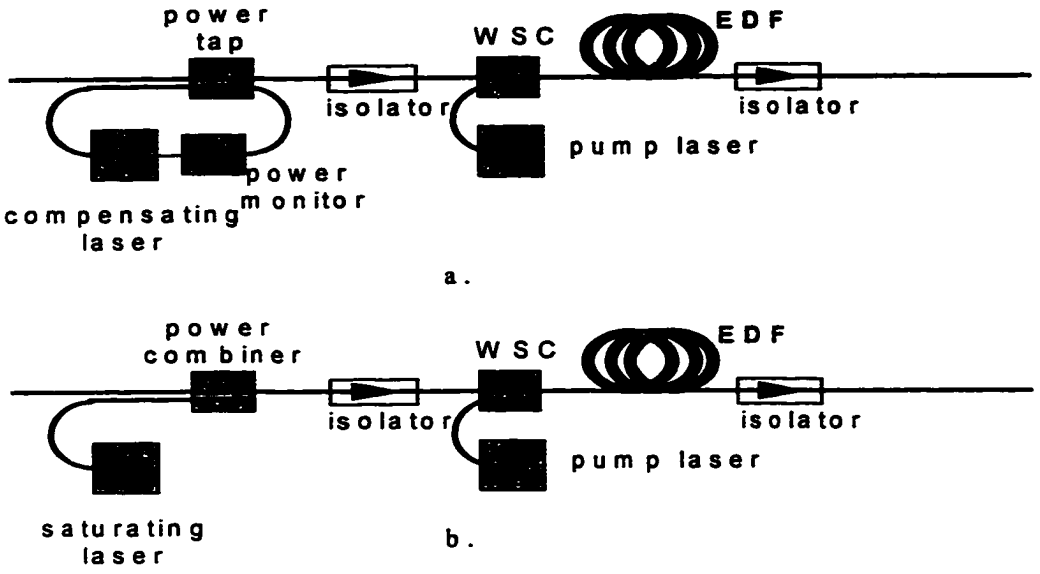

Figure 4.7 EDFA gain stabilization by (a) Tapping the input power and using a compensating laser to keep the total input power constant, (b) using a fixed strong saturating laser to limit the gain excursion of the EDFA.

in a few tens of microseconds [26]. Fig. 4.7b shows a passive approach used to limit the gain excursion when the number of channels changes in an EDFA. A relatively strong laser provides a fixed output power that dominates and deeply saturates the EDFA. Because of the strong saturating signal, changes in the much lower powered signal channels produce a relatively small perturbation of the average inversion level of the EDFA and thus changes in gain are substantially limited.

4.3.1.2 Gain Clamping using Stimulated Brillouin Scattering

In this approach a counter propagating probe signal is inserted at the output of a two-stage EDFA [17-18]. The isolator that is normally placed at the output of the EDFA is

replaced by a circulator. In between the stages a span of dispersion compensating fiber (DCF) is used to compensate the chromatic dispersion of the previous span.When the number of input channels decreases, the gain of the probe beam increases. The amplified probe beam stimulates the Brillouin scattering from the DCF and therefore increases the Stoke's field that re-enters stage two of the EDFA. In so doing, the gain of the EDFA is clamped.

4.3.2 Changing Saturation level by Pump Power Control

The total input signal power combined with the optical pump power determines the saturation point of the EDFA and therefore the level of population inversion. If for example, the total input power decreases and the pump power remains constant, the average inversion and thus the gain of the EDFA increases. If the reduction of input power is accompanied by a corresponding reduction of pump power, the level of inversion and thus the gain can be kept fixed. The speed of stabilization in pump controlled EDFA depends on the time required to change the pump and on the dynamic response of the EDFA once the pump power is adjusted. How the pump power is controlled determines whether the EDFA will behave as a fixed gain or as a fixed average output power EDFA. Fig. 4.8 illustrates two different means of adjusting the pump power with different results. In Fig. 4.8a the total input power is monitored and the pump adjusted to keep the population inversion and thus the gain fixed. Pump control can also be achieved by monitoring the excess pump-loss at the EDFA output [31-32] or keeping

the maximum channel power constant by dynamically tracking the signal with the highest power [33]. Fig. 4.8b shows a means of monitoring the number of channels entering the EDFA, and then adjusting the pump power to the level appropriate for the number of channels. The optical tap is place at the output of the EDFA instead of at the input because a substantial amount of power is required to spectrally resolve the output such that the channels can be counted, and also because a better noise figure can be realized in this way. Counting the number of channels keeps the average output power per channel constant, but unless the power per channel is monitored carefully fixed gain operating is not achieved. If the power in one channel changes the other channels will experience a complementary change in power. Therefore, the gain of the EDFA is modulated by any change in the input power of the channels.

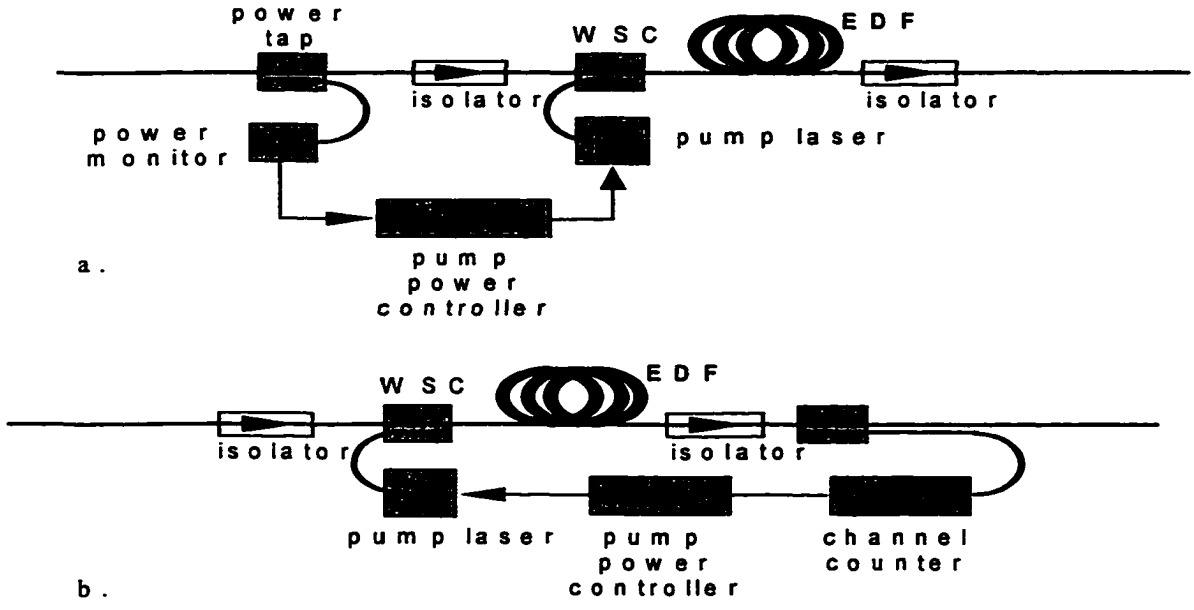

Figure 4.8 Gain stabilization or average output power stabilization by pump power control. (a) Pump power is adjusted based on variations of the total input power. (b) Pump power is adjusted for the number input channels.

4.3.3 Non-saturated EDFAs

For extremely high pump powers, short EDF lengths, and low input powers the EDFA will operate in the non-saturated regime. The advantage of operating in this region is that the gain variations as channels are added or dropped are much smaller than in saturated EDFAs. Simulation has been used to show that when 6 of 8 channels are dropped, the per channel power change in an overpumped EDFA is about 0.6 dB, nearly an order of magnitude less than would occur in a saturated EDFA with the same number of channels dropped [34]. The simplicity of this approach is very attractive but there are a number of disadvantages:

1) The losses must be controlled very accurately as excess loss cannot be compensated for as in a saturated EDFA. At the same time, lower than expected losses can drive the EDFA closer to or into the saturated regime, thus reducing its gain controllability.

2) Higher pump power than for saturated EDFAs with the same gain is required and the pumping efficiency is lower. There are also reliability issues associated with these higher power pumps.

3) The required lower input power of these EDFAs means that signal-to-noise ratio (SNR) at the output will be lower than that obtained with saturated EDFAs even though the noise figure may be similar.

4.4 Dynamic All-optical Automatic Gain Control

This section discusses experimental results of gain clamping a single EDFA and our approach for stabilizing a chain of EDFAs. The all-optical stabilization scheme used here assumes the basic configuration of laser-gain controlled EDFAs, in which automatic gain control is achieved by introducing lasing at a particular wavelength in a ring laser configuration as shown in Fig. 4.6a. The wavelength selective coupler at the input selects the lasing wavelength while conserving the input signal. The method of selecting the lasing wavelength avoids the gain drift problems associated with the use of filters [30] as less polarization sensitivity is associated with the wavelength selective coupler. A variable attenuator allows feedback adjustment. With proper choice of attenuation, the gain is clamped for any number of input channels. First, we examine and analyze a number of factors which affect the transient power excursion of the surviving channel in an all-optically stabilized EDFA such as attenuator level in the optical feedback loop, switching speeds, and length of the feedback loop. We then present our Type 1 approach for stabilizing a chain of EDFAs [27]. In Type 1 chain stabilization, a ring laser at the first EDFA acts both to clamp the gain and generate a compensating signal at wavelength λ_c which takes the place of the dropped channel λ_D in the subsequent EDFAs. In Chapter 5, we will use simulations to expand on this analysis by presenting a more detailed description of the all-optical gain clamped EDFA and compare our Type 1 chain stabilization approach with the conceptually simpler Type 2 approach. In a Type 2 chain each of the EDFAs is gain clamped individually. Section 4.4.1 describes the experimental setup, section 4.4.2 describes the behavior of an individual gain clamped EDFA as a

function of feedback level, switching speed, and cavity length. Section 4.4.3 presents our Type 1 chain stabilization approach.

4.4.1 Experimental Setup

Fig. 4.9 shows the experimental arrangement for testing the chain of amplifiers. Two wavelengths are input, each with approximately -3 dBm power. One channel is chopped at rates of up to a few kilohertz, simulating the loss and addition of half of the channels in a multiwavelength system, and the power at the other channel monitored. A variable attenuator between the first and second EDFA simulates varying fiber link losses. An

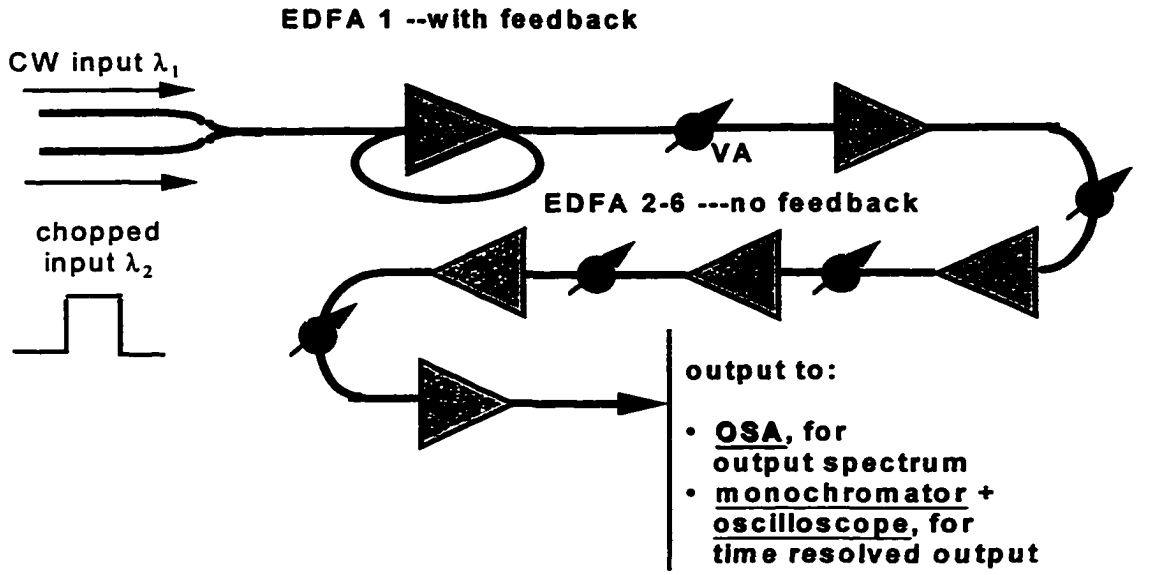

Figure 4.9 A six-EDFA chain (Type 1) with the first a fixed-gain amplifier and all others unmodified.

Optical Spectrum Analyzer (OSA) was used to observe the spectrum and provide an output to an oscilloscope via its monochromator output. Therefore, both the spectrum and

the time resolved power of each wavelength were observed. We monitored the output at different points of the chain to record the evolution of the signals as the length of the chain increased.

4.4.2 Performance of a Single Gain-Clamped EDFA

This section examines the effects of cavity loss, switching speeds, and cavity length on the transient power excursions in the surviving channel. There are other factors that affect the transient power excursions in the surviving channel, some of which will be presented in our simulation analysis in Chapter 5. However, here we focus on our experimentally tested results.

4.4.2.1 Typical Behavior

Fig. 4.10 shows the static and time resolved results of all-optically stabilizing a single EDFA. The unstabilized results were shown in Fig. 4.4. The increase in power of the surviving channel seen in Fig. 4.4a does not occur in this case as the compensating (lasing) signal takes the place of the dropped channel as seen in Fig. 4.10a. Likewise, the power excursions experienced by the surviving channel in Fig. 4.4b is not observed in Fig. 4.10b as the power variations of the dropped/ added channel are now counteracted by the lasing signal. A more detailed examinination of the relationship between the surviving, dropped/added, and lasing signal will presented in the simulation results in Chapter 5.

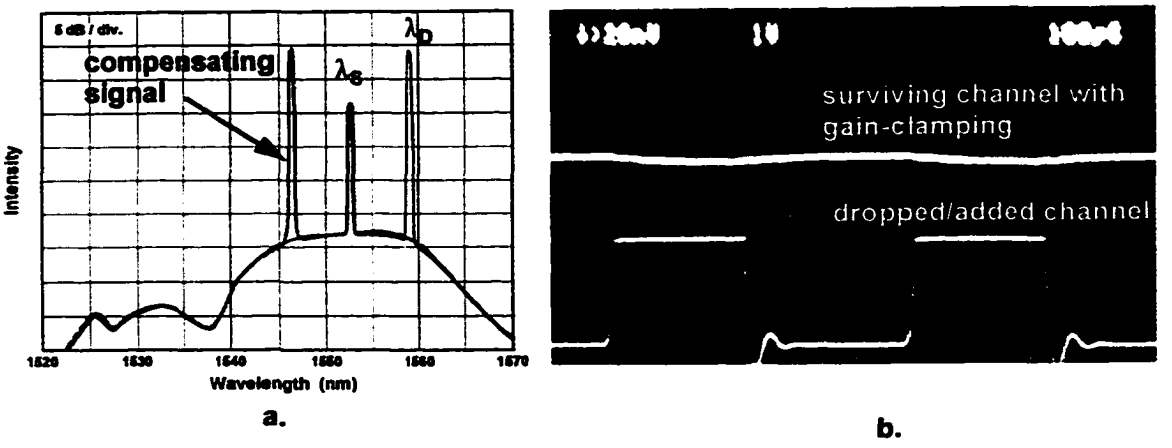

Figure 4.10 Gain clamped EDFA. (a) Spectrum showing the compensating signal taking the place of the dropped channel, thus keeping the gain of the the surviviving chanel fixed. (b) Time resolved results for the dropping and adding of half the number of channels.

4.4.2.2 Feedback level (attenuator/cavity loss)

An important parameter that affects the transient power excursions in the surviving channel is the amount of loss (α) in the feedback loop and consequently the amount of gain that can be sacrificed without seriously affecting the network performance. If there is no lasing when all signal channels are present, the lasing signal must grow from the ASE noise. The early stages of the growth are slow, making it difficult for the lasing signal to catch up with the increased gain, and ultimately leading to over and undershoots. As the loss is decreased, there is lasing even when all signal channels are present. When a channel is dropped the lasing signal increases, but because it is building up from a higher level, it reaches the level at which it clamps the gain more rapidly and the overshoots are less. Thus, the power excursion of the surviving channels can be made significantly less, but at the expense of reduced gain, as shown in Fig. 4.11a. A lower

power excursion of surviving channels is certainly preferable, but the lowered gain is not

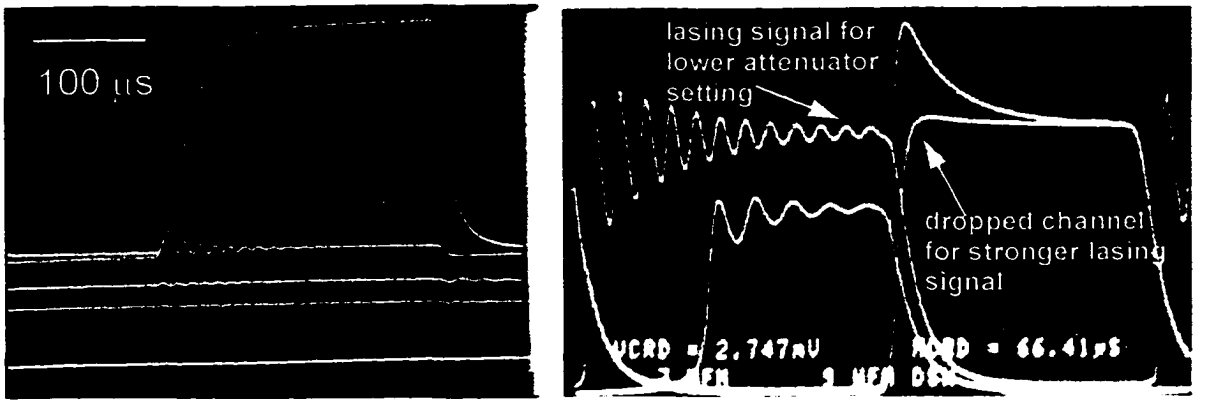

a. b.

Figure 4.11 (a) Transient response to dropping four of eight channels, for different attenuator settings. (b) Transient response of the compensating and dropped/added channel for two different attenuator settings

and can compromise network performance. Fig. 4.11b shows the lasing and the dropped channel for two different attenuator settings. For the lower attenuator setting the feedback (lasing) signal is stronger (upper oscillating trace) and responds to the dropped channel faster than for the higher attenuator setting. The overshoots are significantly limited by the stronger lasing signal as seen in the figure.

4.4.2.3 Switching Speed

For a given attenuator loss, the power excursion of the initial transients is also dependent on the speed with which channels are added and dropped. Figs. 4.12a and 4.12b show the surviving channel for a fast and a slow switching speed respectively. Clearly, the power excursions are greater and the oscillations last longer for faster switching speeds. This occurs because at slower switching speeds the feedback signal is better able to adjust and

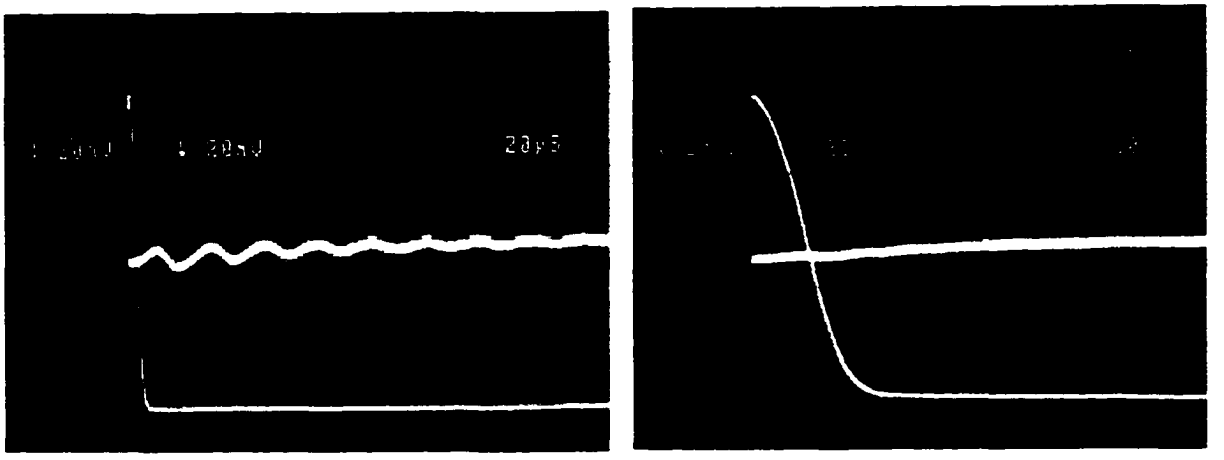

a. b.

Figure 4.12 Transient response of the surviving channel for (a) a fast dropping of channels and (b) a slower dropping of channels.

follow the changes in gain (average inversion) and compensate to maintain the total ouput power of the amplifier. At faster switching speeds, however, the feedback signal cannot adjust to follow the more rapid changes in gain, causing both the feedback and surviving channels to over and undershoot, and experience a decaying power oscillation.

4.3.2.4 Length of Lasing Cavity

To test the effect of cavity length on the gain stabilization technique the transient responses of the signals were compared for two different cavity lengths. The cavity length was increased by inserting an extended length of fiber in the feedback path. The extra fiber adds loss to the feedback path and therefore the variable attenuator was adjusted for the same steady state gain as obtained with the shorter loop. The power excursions of the surviving channel are clamped more rapidly, and are therefore less for shorter cavity lengths. Fig. 4.13 shows that after the channel is dropped the compensating channel

responds faster and has a lower power excursion for a shorter cavity length than it does for the longer cavity. This is because of the longer propagation time (longer delay) of the lasing signal for the longer feedback path.

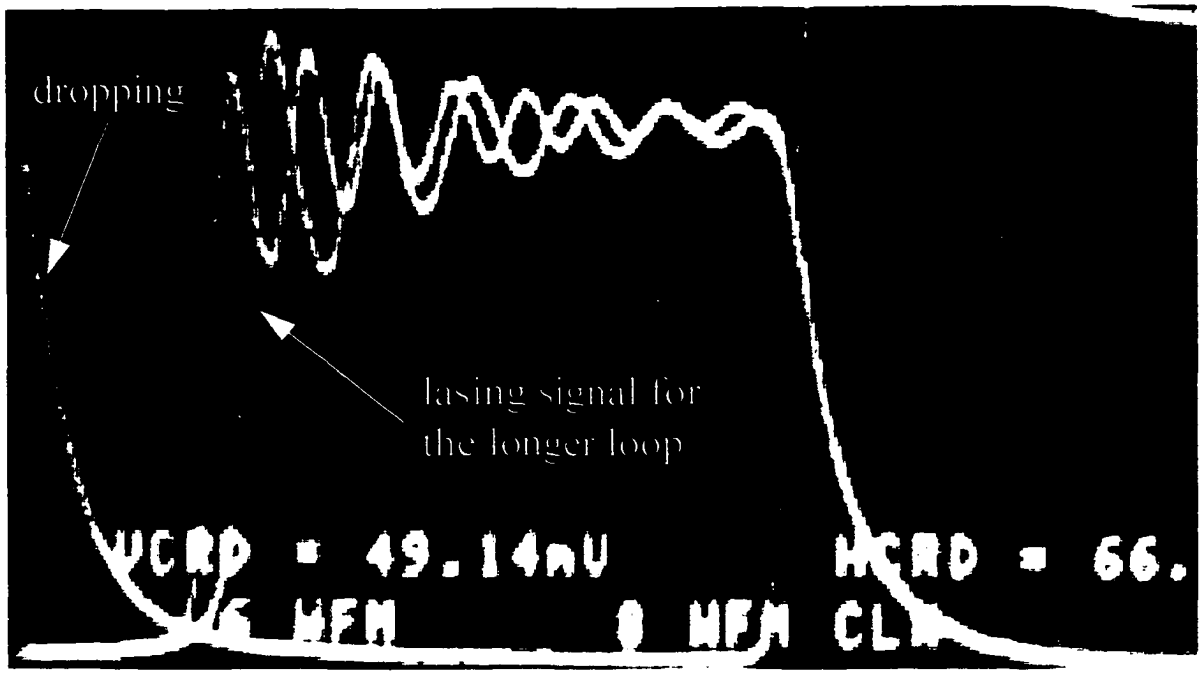

Figure 4.13 Comparing the transient response of the lasing signal for a short and a long lasing cavity.

4.4.3 EDFA Chain Stabilization

We now consider how the degradations observed in a single gain-clamped EDFA compound in a Type 1 chain of amplifiers. We will present our experimental results for the power excursions of the surviving channel in a six-EDFA chain and also show bit-error-rate (BER) measurements for the surviving channel in a three-EDFA chain.

4.4.3.1 Type 1 Stabilization (Lasing Only at the first EDFA)

In this type of chain stabilization, shown in Fig. 4.9, the ring laser acts both to clamp the gain and to generate a compensating signal at wavelength λ_C which takes the place of the dropped channels in the subsequent EDFAs. For this approach we obtained stabilization of the EDFA chain in three steps.

1. The gain in the first EDFA is clamped via an all-optical feedback in a ring laser configuration.
2. A compensating signal is generated in the same ring laser (first EDFA), via the same feedback mechanism that clamps the gain, and is inserted into the output fiber, via a wavelength insensitive coupler, with the same power relative to the output surviving signals.
3. The compensating signal is transmitted to subsequent amplifiers in the chain, which do not need to be modified.

As long as the compensating signal lies within the flat gain region of the EDFA, so that its intensity relative to that of the real signals remains constant as it passes through several amplifiers, the remaining amplifiers see a constant average input power [27]. Thus, reusing the compensating signal allows modifying only the first EDFA to stabilize the entire chain. To the extent that the gain of the compensating signal differs from that of the real signal it replaces, it will over or under compensate in the following EDFAs, with the result that the stabilization of the chain will be less than desired. This issue will be discussed in the simulation results presented in Chapter 5.

4.4.3.1.1 Experimental Results for Type 1 Chain

A six-EDFA chain with attenuators between amplifiers representing the span losses as shown in Fig. 4.9 was stabilized as above. The EDFAs were not of the same kind. Three were single-stage EDFAs from one vendor, and the other three were from a second vendor. One of the second vendor's EDFAs was of a two-stage configuration, while the other two were single-stage configurations. Two signals, each with one to 7 times the power of a signal we expect to use in our 8-wavelength system, were the inputs to the chain of EDFAs. A chopper was used to modulate one channel to simulate the rapid adding and dropping of channels. The power excursions of the surviving channel after the sixth EDFA for the adding and dropping of 4 of 8 channels is shown in Fig. 4.14. Without compensation, the power change was ~3 dB. With compensation the worst case power excursion was 0.25 dB, with a damped ~20 μs period relaxation oscillation. All the EDFAs beyond the first in the Type 1 chain operate in the saturated regime and therefore the output power of the signals can be recovered when there is excess span loss. When the attenuator between the first and second EDFAs was varied by more than 6 dB, output power changed by less than 0.5 dB at the output of our six-EDFA Type 1 chain [35].

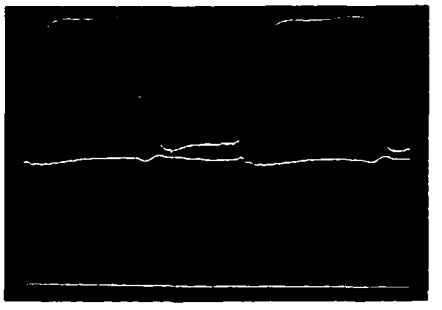

Figure 4.14 Output of surviving channel after 6 EDFAs, with (middle trace) and without (upper trace) stabilization. The bottom line represents the absence of output.

Fig. 4.15a shows the output power of the surviving channel after the last of a three-EDFA chain. The figure shows the response with and without Type 1 stabilization for the rapid adding and dropping of seven of eight channels. Fig. 4.15b shows BER measurements for the surviving channel at the output of the chain for a 2.5 Gbps psuedo-random sequence. The power penalty for the compensated EDFA was < 0.5 dB when the

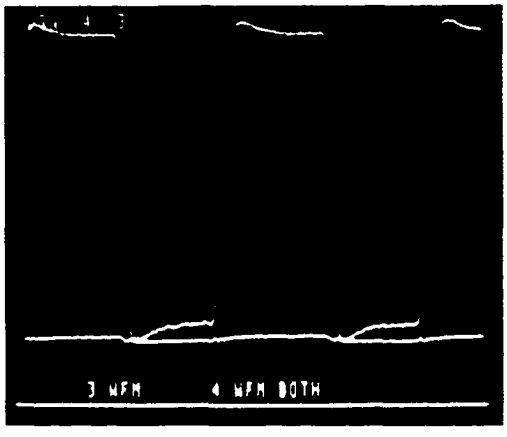

a.

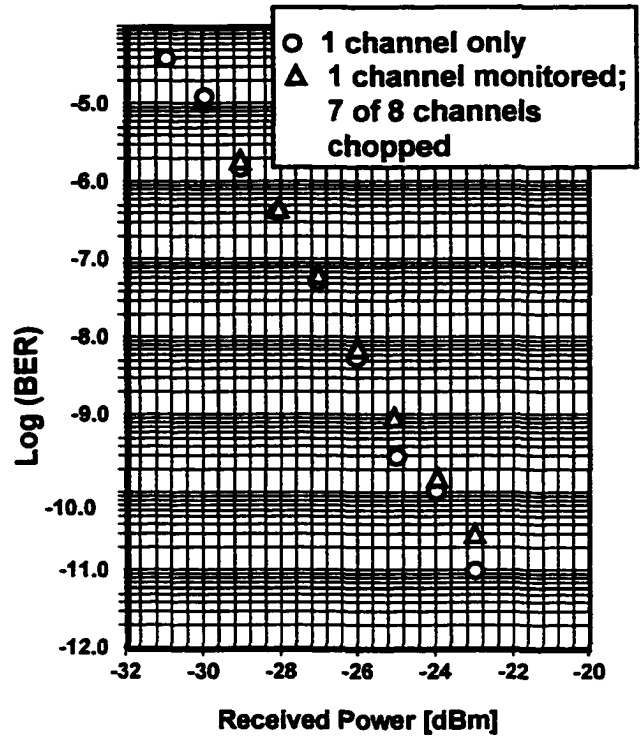

b.

Figure 4.15 (a) Power in surviving channel after power equivalent to 7 of 8 channels has been chopped with and without stabilization. (b) BER measurement for the surviving channel, o with eight channels present at all times, and Δ with 7 of 8 channels chopped.

chopper was operational compared to when all signals are present at all times. Without stabilization the BER was exceedly high as the test set was unable to synchronize with the rapidly changing power levels. Therefore, the Type 1 stabilized chain was able to

effectively protect the surviving channel from errors for this worst case scenario of the dropping of seven of the eight channels.

4.5 Conclusion

An experimental evaluation of gain dynamics for a single and chains of EDFAs and the impact on multiwavelength communication systems has been presented. A brief description of a number of different methods of stabilizing a saturated EDFA when the number of channels at the input changes was presented. Results of our experimentally demonstrated method of stabilizing chains of saturated EDFAs were also presented. The main objective was to understand how nearly one can maintain constant per-channel output power with a minimally degraded SNR, regardless of the number of channels present.

Specifically, we have shown experimentally that the lower the losses in the feedback loop, the slower the switching speeds and the shorter the length of the cavity, the smaller the power excursions experienced by the surviving channel in an all-optical gain clamped EDFA. Therefore, the switching speed at the network element, the loss in the feedback loop, and the length of the lasing cavity at the first amplifier all determine the cumulative effect at the end of the EDFA chain. The chains were constructed using EDFAs made by different vendors with very different operating points, thus showing the robustness of our Type 1 stabilization technique.

4.6 References

[1] E. Desurvire, C. R. Giles, and J. R. Simpson, "Gain dynamics of erbium-doped fiber amplifiers," SPIE Vol. 1171 Fiber Laser Sources and Amplifiers (1989).

[2] C. R. Giles, and E. Desurvire, "Transient gain and cross talk in erbium-doped fiber amplifiers," Optics Letters, vol. 14, no. 16 Aug. 1989, pp. 880-882.

[3] R. J. Mears, L. Reekie, I. M. Jauncey, and D. N. Payne, "Low-noise Erbium-doped fiber amplifiers operating at 1.54 μm," Electron. Lett. vol. 23 pp. 1026-1028. Sept. 1987.

[4] E. Desurvire, J. R. Simpson, and P. C. Becker, "High-gain Erbium-doped traveling-wave fiber amplifier," Opt. Lett., vol. 12, pp. 888-890, Nov. 1987.

[5] E. Snitzer et al., "Erbium fiber laser amplifier at 1.55 μm with pump at 1.49 μm and Yb sensitized Er oscillator," postdeadline papers, in OFC '88, OSA, Washington, DC 1988, paper PD2.

[6] B. J. Ainsle, "A review of the fabrication and properties of Erbium-doped fiber for optical amplifiers," J. Lightwave Tech., vol. 9, no. 2, pp. 220-227, 1991.

[7] R. I. Laming et al., "Efficient pump wavelengths of Erbium doped fiber optical amplifiers," Electron. Lett., vol. 25, pp. 12-14, 1989.

[8] H. V. Pommer et al., "Noise and gain performance for Erbium-doped fiber amplifier pumped at 980 or 1480 nm," Fiber Laser Amplifiers II, M. J. F. Digornet, ED., Proc. SPIE, vol. 1373, pp. 254-265, 1990.

[9] W. J. Miniscalco, "Erbium-doped glasses for fiber amplifiers at 1500 nm," J. Lightwave Tech., vol. 9, no. 2, pp. 234-250, 1991.

[10] E. Desurvire, Erbium-Doped Fiber Amplifiers: Principles and Applications, (John Wiley & Sons, NY, 1994)

[11] C. R. Giles et al., "Noise performance of Erbium-doped fiber amplifiers pumped at 1.49 mm, and application of signal preamplification at 1.8 Gbits/s," IEEE Photonics Tech. Lett., vol. 1, pp. 367-369, 1989.

[12] Randy Giles, Tingye Li, "Optical amplifiers transform long-distance lightwave telecommunications," Proceedings of the IEEE, vol. 84, no. 6. June 1996, pp. 870-883.

[13] M. Zirngibl, "Gain Control in Erbium-Doped Fiber Amplifier by an all-optical feedback loop," Electron. Lett., 27, 560-561 (1991).

[14] Haruo Okamura, "Automatic Optical Loss Compensation with Erbium-Doped Fiber Amplifiers," J. Lightwave Technology, 10, 1110-1116 (1992).

[15] J. F. Massicott, S. D. Willson, R. Wyatt, J. R. Armitage, R. Kashyap, D. Williams, and R. A. Lobbett, "1480 nm pumped erbium doped fiber amplifier with all optical automatic gain control." Electron. Lett.,. 30 962-964 (1994).

[16] M. Fake, J. Simmons, J. Massicott, R. Wyatt, "Optically stabilized EDFA for in-band WDM system," in proc. of OFC'95, paper TuP3.

[17] Seung Hee Lee and Seong Ha Kim, "Performance of all optical gain-clamped EDFA in 8 channel × 10 Gbps WDM using stimulated brillouin scattering," ECOC'98, Madrid, Spain, Sept. 1998.

[18] Seung Hee Lee, and Seong Ha Kim, "All-optical gain-clamped erbium-doped fiber amplifier for wavelength-division multiplexed networking using stimulated Brillouin scattering," in proc. of OFC'98 San Jose, CA. paper WM52.

[19] A. K. Srivastava, Y. Sun, J. L. Zyskind, J. W. Sulhoff, C. Wolf, R. W. Tkach, "Fast Gain Control in Erbium-Doped Fiber Amplifier," in Optical Amplifier and Their Applications, Vol. V of 1996 Trends in Optics and Photonic Series (Optical Society of America, Washington, D. C., 1996) p. 24.

[20] A. K. Srivastava, Y. Sun, J. L. Zyskind, and J. W. Sulhoff, "EDFA Transient Response to Channel Loss in WDM Transmission System," IEEE Photonics Technol. Lett., vol. 9, no. 3, pp. 386-388, 1997.

[21] Seo Yeon Park, Hyang Kyun Kim, Gap Yeol Lyu, Sun Mo Kang, and Sang-Yung Shim, "Dynamic Gain and Output Power Control in a Gain-Flattened Erbium-Doped Fiber Amplifier," IEEE Photonics Technology Lett. vol. 10, no. 6, pp. 787-789, 1998.

[22] F. Shehadeh, R. S. Vodhanel, C. Gibbons, and M. Ali, "Comparison of gain control techniques to stabilize EDFAs for WDM networks," in Technical Digest of Optical Fiber Communications (Optical Society of America, San Jose, CA, 1996) paper WM8.

[23] E. Desurvire, M. Zirngibl, H. M. Presby, and D. DiGiovanni, "Dynamic Gain Compensation in Saturated Erbium-Doped Fiber Amplifiers," IEEE Photonics Technol. Lett. Vol. 3, no. 5, pp. 453-455, 1991.

[24] B. Clesca, V. Harvard, S. Gauchard, V. Rodriques, E. Lantoine, D. Cravec, and F. X. Ollivier, "Upper limit and control scheme for power channel in optically-amplified WDM systems", in Proceedings of European Conference on Optical Communications (Oslo, 1996) paper WeP.31.

[25] J. L. Zyskind, A. K. Srivastava, Y. Sun, J. C. Ellison, G. W. Newsome, R. W. Tkach, A. R. Chraplyvy, J. W. Sulhoff, T. A. Strasser, J. R. Pedrazzani and C. Wolf, " Fast link

control protection for surviving channels in multiwavelength optical networks," in Proceedings of European Conference on Optical Communications (Oslo, 1996) postdeadline paper.

[26] A. K. Srivastava, J. L. Zyskind, Y. Sun, J. Ellson, G. Newsome, R. W. Tkach, A. R. Chraplyvy, J. W. Sulhoff, T. A. Strasser, C. Wolf, and J. R. Pedrazzani, "Fast-Link Control Protection of Surviving Channels in Multiwavelength Optical Networks," IEEE Photonics Technol. Lett. vol. 9, no. 12, pp. 1667-1669, 1997.

[27] J. L. Jackel and D. Richards, "All-optical stabilization of multi-wavelength EDFA chains: a network-level approach," in Proceedings of LEOS'96 (IEEE Laser and Electro-Optics Society) postdeadline paper.

[28] J. L. Zyskind, Y. Sun, A. K. Srivastava, J. W. Sulhoff, A. J. Lucero, C. Wolf, and R. W. Tkach, "Fast Power Transients in Optically Amplified Optical Networks," Optical Fiber Communication Conference (Optical Society of America) postdeadline paper PD31.

[29] A Yu and M. J. O'Mahony, "Modeling of laser-controlled erbium-doped fiber amplifiers," in Technical Digest of Optical Fiber Communication (Optical Society of America, San Jose, CA, 1996) paper WK14.

[30] Y. Takushima and K. Kikuchi, "Gain stabilization of all-optical gain-clamped amplifier by using Faraday rotator mirrors," Electronics Lett. vol. 34, No. 5, March, 1998, pp. 458-459.

[31] J. C. van der Plaats, F. W. Willems, and A. M. J. Koonen, "Dynamic pump-loss controlled gain-locking system for erbium-doped fiber amplifiers in multi-wavelength networks," ECOC'97, Edinburgh, UK, Sept. 1997.

[32] M. Karasek, and J. C. van der Plaats, "Analysis of Dynamic Pump-Loss Controlled Gain Locking System for Erbium-Doped Fiber Amplifiers," IEEE Photonics Technol. Lett. vol. 10, no. 8, pp. 1171-1173, 1998.

[33] H. Suzuki, N. Takachio, O. Ishida, and M. Koga, Dynamic gain control by maximum signal power channel in optical linear repeaters for WDM photonic transport networks," IEEE Photonics Technol. Lett. vol. 10, no. 5, pp. 734-736.

[34] M. Karasek and F. W. Willems, "Suppression of Dynamic Cross Saturation in Cascades of Overpumped Erbium-Doped Fiber Amplifiers," IEEE Photonics Technol. Lett. vol. 10, no. 7, pp. 1036-1038, 1998.

[35] Janet Lehr Jackel, and Dwight Richards, "All-optical stabilization of cascaded multichannel EDFAs with changing number of channels," in proc. of OFC'97, Dallas, TX. Feb. 1997, paper TuP4.

CHAPTER 5

SWITCHING DYNAMICS AND ITS IMPLICATION ON MULTI-CHANNEL EDFA STABILIZATION: SIMULATION RESULTS

5.1 Introduction

Experimental results of an all-optical method of stabilizing the gain of a single and chains of EDFAs were presented in Chapter 4. The transient degradations experienced by surviving channels when channels are switched in a chain of saturated EDFAs, and how some of the effects of this switching can be reduced were explained in that chapter. This chapter expands on this work by presenting a detailed theoretical analysis of gain dynamics for individual and cascaded stabilized EDFAs. A dynamic simulation tool is used for modeling the behavior of a single amplifier and different amplifier chains with and without stabilization. The simulations are not intended to verify our experimental results but rather to help in the understanding of the gain dynamics of all-optically stabilized EDFAs and EDFA chains. The model assumes homogenous gain but uses specifications for slightly different EDFAs than those measured. The dynamic simulation tool is used to model the behavior of a single all-optically gain-clamped EDFA and to compare two different approaches to stabilizing amplifier chains based on this type of EDFA, including our experimentally tested method, presented in Chapter 4. Finally, the simulation tool is used to model the behavior of a pump controlled EDFA and its compatibility with the all-optical feedback method. Compatibility can be an issue in a network with multivendor equipment employing different gain stabilization schemes such as the MONET DC network [1].

5.2 Dynamic All-optical Automatic Gain Control: Simulations

This section presents simulation results that aids us in our understanding of some of the experimental results presented in the previous chapter. We expand our analysis to take into account effects that were not carefully examined in the experiment. The all-optical stabilization scheme used here is the same as was tested experimentally and presented in Chapter 4, in which automatic gain control is achieved by introducing lasing at a particular wavelength in a ring laser configuration as shown in Fig. 4.6a. As was the case in Chapter 4, first, we examine and analyze the relevant factors which affects the transient power excursion of the surviving channel in a single all-optically stabilized EDFA such as attenuator level in the optical feedback loop, switching speeds, the number of wavelengths dropped or added, the choice of lasing wavelength, and the choice of pump wavelength. Using this performance analysis of the single EDFA as a guideline, we present and compare two different approaches to chain stabilization, including our experimentally tested Type 1 approach [2]. Recall that in Type 1 chain stabilization, a ring laser at the first EDFA acts both to clamp the gain and to generate a compensating signal at wavelength λ_C which takes the place of the dropped channels λ_D in the subsequent EDFAs. Type 2 stabilization is the conceptually simpler method of gain clamping each of the EDFAs individually. As will be shown, each of these approaches creates demands on the EDFAs or on the chain as a whole.

We will show the effects on gain flatness, initial power transients and noise figure (NF) of the stabilized EDFA and show how to minimize some of the limitations that

degradations in any of these can impose on the stabilization techniques. We show how any degradation at the first EDFA has a cumulative effect at the output of all subsequent EDFAs in the chain. This has the important implication that the achievable length of the chain is a function of the design parameters of the first EDFA in the chain.

Section 5.2.1 presents the dynamic amplifier simulation model. Section 5.2.2 describes the system model and the individual EDFA design which was chosen to optimize gain flatness for eight wavelengths over the wavelength range of interest. Section 5.2.3 describes the behavior of an individual gain flattened EDFA as a function of feedback level, switching speed, number of channels added or dropped, choice of feedback wavelength, and choice of pumping wavelength. Section 5.2.4 presents and compares two different approaches to chain stabilization.

5.2.1 The Dynamic Amplifier Model

The EDFA model assumes a commercially available alumino-germano silicate fiber, and thus all of the numerical conclusions reported here apply to this specific fiber. The absorption and emission profiles are plotted in Fig. 4.2. However, our results can be applied more generally to any other EDFA configuration taking into account its specific characteristics. The fiber is completely characterized by only four parameters; the Er^{3+} absorption coefficient $a(\lambda)$, the gain coefficient $g(\lambda)$, the fiber excess loss l (0.0033 dB/m), and fiber saturation parameter $\zeta = An_t/\tau = 5.58 \times 10^{14}\ m^{-1}s^{-1}$. Here A is the erbium core area, n_t is the ion density, τ is the metastable lifetime (10 ms). Forward

pumping schemes with 80 mW of pump power are assumed throughout the calculations. An optical isolator is also assumed to be placed after each amplifier.

The dynamic model used here is based on the spectrally resolved numerical model of Giles [3] which assumes a homogeneous broadened gain medium. The forward and backward ASE spectra are well resolved in 651 wavelength bands ($\Delta\lambda$ = 0.2 nm intervals) over the 1470 nm to 1600 nm range. The model uses both the space and time dependent rate (Eqn. 18) and propagation (Eqn. 20) equations of [3], which are repeated below as equations (5.1) and (5.2) respectively:

$$\frac{d\bar{n}_2}{dt} = \sum_k \frac{P_k(z)\sigma_{ak}\Gamma_{k,1}\bar{n}_1}{h\nu_k \pi b_{eff}^2} - \sum_k \frac{P_k(z)\sigma_{ek}\Gamma_{k,2}\bar{n}_2}{h\nu_k \pi b_{eff}^2} - \frac{\bar{n}_2}{\tau}. \tag{5.1}$$

$$\frac{dP_k}{dz} = u_k(\alpha_k + g_k^*)\frac{\bar{n}_2}{\bar{n}_t}P_k(z) + u_k g_k^* \frac{\bar{n}_2}{\bar{n}_t} mh\nu_k - u_k(\alpha_k + l_k)P_k. \tag{5.2}$$

$$\alpha(\lambda) = \sigma_a(\lambda)\Gamma(\lambda)n_t \tag{5.3}$$

$$g^*(\lambda) = \sigma_e(\lambda)\Gamma(\lambda)n_t \tag{5.4}$$

$$n_t(r,\phi,z) = n_1(r,\phi,z) + n_2(r,\phi,z). \tag{5.5}$$

The first term of equation (5.1) represents the metastable population through absorption of light, the second term represents the stimulated emission which causes depletion of the metastable level and the last term represents spontaneous emission from the metastable level. Using equations (5.3) and (5.4), defining a new fiber parameter, $\zeta = \pi b_{eff}^2 \, \bar{n}_t / \tau$, the ratio of the linear density of ions to the metastable lifetime, assuming that $\Gamma_{k,1}$ and $\Gamma_{k,2}$ are

nearly equal (i.e. the erbium ions are well confined to the center of the optical modes), equation (5.1) becomes:

$$\frac{d\overline{n}_2}{dt} = \sum_k \frac{\alpha_k \frac{\overline{n}_1}{\overline{n}_t}}{h\nu_k \pi b_{eff}^2} P_k(z) - \sum_k \frac{g_k^{\cdot} \frac{\overline{n}_2}{\overline{n}_t}}{h\nu_k \pi b_{eff}^2} P_k(z) - \overline{n}_2 / \tau \tag{5.6}$$

simplifying further we have:

$$\frac{d\overline{n}_2}{dt} = \sum_k \frac{\alpha_k \overline{n}_1}{h\nu_k \zeta \tau} P_k(z) - \sum_k \frac{g_k^{\cdot} \overline{n}_2}{h\nu_k \zeta \tau} P_k(z) - \frac{\overline{n}_2}{\tau} \tag{5.7}$$

Letting $\overline{n} = \frac{\overline{n}_2}{\overline{n}_t}$ and using equation (5.5) equation (5.7) becomes

$$\frac{d\overline{n}}{dt} = \sum_k \frac{\alpha_k P_k(z)}{h\nu_k \zeta \tau}(1-\overline{n}) - \sum_k \frac{g_k^{\cdot} P_k(z)}{h\nu_k \zeta \tau} \overline{n} - \overline{n} / \tau \tag{5.8}$$

The parameter ζ can be determined from measurements of the fiber saturation power P_k^{sat} as, $\zeta = P_k^{sat}(\alpha_k + g_k^{\cdot}) / h\nu_k$ [4-5]. Solving equations (5.2) and (5.8) iteratively is the foundation of the numerical EDFA model used here. The procedure demands that the boundary conditions at z = 0, L for the k beams be specified. Both equations are integrated over space (z), optical frequency (k), and time (t). A numerical analysis method such as the Runge-Kutta algorithm can be used to solve the equations [6].

The space and time are decomposed into a grid of M x N discrete bins Δz and Δt, respectively. The space equations are integrated iteratively for each time $t = m\Delta t$ (m = 1, 2,...,N). The initial conditions of the system for the metastable state population [i.e., $n_2(z,t = 0)$], are given by solving the steady state inversion equation (Eqn. 19) of [3],

repeated below as equation (5.9). In the steady state regime where the populations are time invariant, i.e. $dn_i/dt = 0$, equation (5.1) provides the static solution:

$$\frac{\overline{n}_2}{\overline{n}_t} = \frac{\sum_k \frac{P_k(z)\alpha_k}{h\nu_k \zeta}}{1 + \sum_k \frac{P_k(z)(\alpha_k + g_k^*)}{h\nu_k \zeta}} \tag{5.9}$$

This condition is applicable for CW beams and those modulated at frequencies in excess of 10 kHz [7-8]. The initial power levels at each discrete point of the fiber is obtained by substituting equation (5.9) into equation (5.2). The algorithm uses the initial conditions to evaluate the inversion for the first time step Δt. The calculated value of the inversion is then used to calculate the signal, ASE noise spectrum, and power in the pump as a function of position. These powers are then used to evaluate the inversion at the next time step 2Δt. By this computationally intense iterative process, we were able to capture and accurately characterize the dynamic behavior of the EDFA.

5.2.2 The System Model

Except where explicitly stated, and for simplifying the analysis, the system model presented in these simulations assumes two input channels at 1549.4 and 1551 nm, with input powers of -8 dBm/channel, simulating 8 channels with -14 dBm input each. Dropping one of these channels is equivalent to the loss of 4 of the eight channels. The signal at 1551 nm is taken as the surviving channel. In some cases, when it was necessary to strictly simulated the eight channels, these channels were spaced 1.6-nm apart in the

1549.4 to 1560.6 nm amplifier band to conform to the proposed ITU standard wavelength grid. In some cases the span loss between amplifiers was adjusted to maintain the same output power for the surviving channel at each EDFA output, but in other cases the span loss between amplifiers was kept constant. The noise figure (NF) results presented here do not take into account any degradation due to coupling losses at the input and is derived from the actual input power coupled into the EDFA.

5.2.2.1 Amplifier Operating Point

Although the ultimate consideration is to design an EDFA configuration which is capable of maintaining constant per-channel output power with a minimally degraded SNR, regardless of the number of channels present, we are also concerned with achieving maximum gain and minimum spectral gain variations. To optimize the amplifier for both we used the optimization method reported in [9]. The method determines the optimum erbium fiber length required to maximize the individual amplifier gain subject to the constraint of minimizing the spectral gain variations, for a given input signal levels and pump power. With the amplifier characteristics used here, the optimum amplifier length, L_{opt}, is found to be 50 m. At L_{opt}, the maximum least-favored signal gain from among all of the eight signals used in the simulation is 20 dB, and the associated minimum spectral gain variations is about 2 dB. Therefore, we have assumed an amplifier length of 50 m throughout the simulations presented in this thesis. However, our conclusions can be applied qualitatively to a wide range of EDFAs.

5.2.3 Performance of a Single Gain-Clamped EDFA

The main objective of this section is to examine the effects of cavity losses, switching speeds, the number of wavelengths dropped/added, and choice of lasing and pump wavelengths on the transient power excursions in the surviving channel. In Chapter 4 the effects of cavity length, which is not covered here, and a subset of these effects were examined experimentally. The analysis here is simulation based and mirrors our work presented in [10-14]. The goal is to use the simulation to aid in our understanding of the experimentally observed effects and to study effects that were not covered in our experimental work.

5.2.3.1 Typical Behavior

Fig. 5.1a shows a typical case of the transient response of the output power of the surviving signal (λ_S), the lasing (compensating) signal (λ_C) and the dropped signal (λ_D), when four out of eight signals are dropped or added, and when the power in the lasing signal is equivalent to that of one signal channel when all signal channels are present. As can be seen from the figure, both the surviving and compensating signals experience initial power excursions and relaxation oscillations before steady state is reestablished. We will show that the frequency and damping constants of these oscillations are directly related to the cavity loss, which determines the power in the lasing wavelength when all channels are present, the speed at which the number of channels changes, the number of

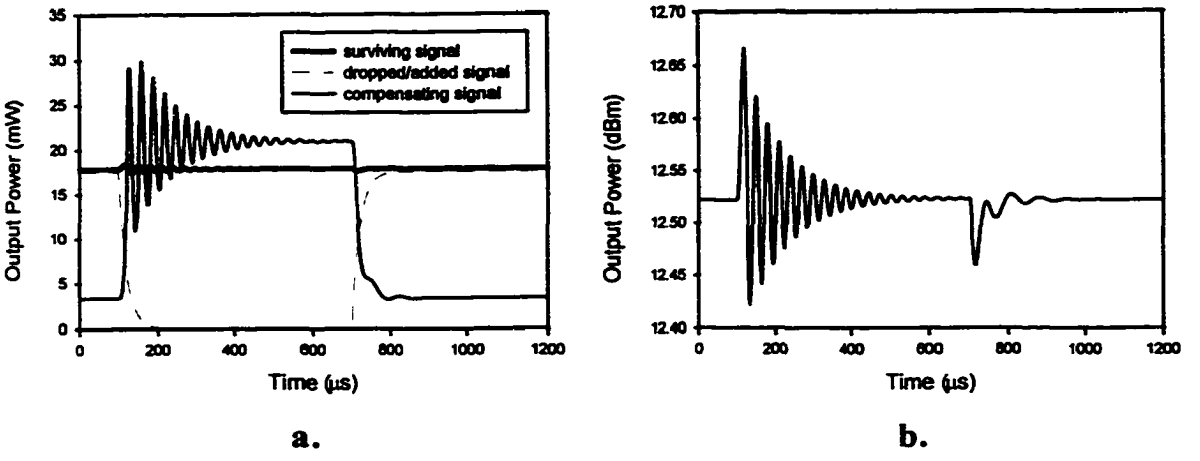

Figure 5.1. Typical transient response for the dropping/adding of 4 of 8 channels. The lasing signal is equivalent to that of one signal channel when all signal channels are present. (a) The transient response of the surviving, dropped/added and lasing signals output power. (b) The surviving channel from (a) with an expanded vertical scale. Note the difference in frequency and the transient power excursions of the drop case with respect to the add case.

channels dropped or added, the pumping wavelength and, to a lesser extent, the choice of lasing wavelength. It has been shown that these power excursions have two contributions: a static contibution due to the spectral hole burning, and a dynamic contribution due to relaxation oscillations in the laser [15-17]. Since the dynamic model used here assumes a completely homogenous gain, the power excursion shown in Fig. 5.1 are totally due to the dynamic contribution owing to the relaxation oscillations. The relaxation oscillations of the compensating signal lag that of the surviving signal slightly in time phase, but the frequency of oscillations are identical.

Fig. 5.1b shows the surviving signal of Fig. 5.1a on an expanded vertical scale. As can be seen from the figure, both the frequency and amplitude of the transient power excursions of the surviving channel are lower in the case of adding channels versus that

of dropping channels. These simulation results are in good qualitative agreement with the experimental results reported in [15-17]. Both simulation and experiment indicate that dropping of channels results in much more severe effects on the surviving channels. Therefore, we have focused our analysis on the dropping of channels case rather than the adding.

5.2.3.2 Feedback level (attenuator/cavity loss)

As discussed in Chapter 4, an important parameter that affects the transient power excursions in the surviving channel is the amount of loss (α) in the feedback loop and consequently the amount of gain that can be sacrificed without seriously affecting the network performance. Fig. 4.11a which is repeated below as Fig. 5.2b for comparison with the simulation result presented in Fig. 5.2a, showed the experimental result of the tradeoff between gain and stability. As both the simulation and experimental results show, the power excursion of the surviving channels can be made significantly less, but at the expense of reduced gain. A lower power excursion of surviving channels is certainly preferable, but the lowered gain is not and can compromise network performance. In addition, the increased gain compression increases gain tilt [18] and the noise figure, as seen in Figs. 5.3a and 5.3b respectively. However, all of these problems can be minimized if the EDFA is designed to operate with a total input power that includes the compensating signal. Simply increasing the pump power can restore the desired level of EDFA saturation.

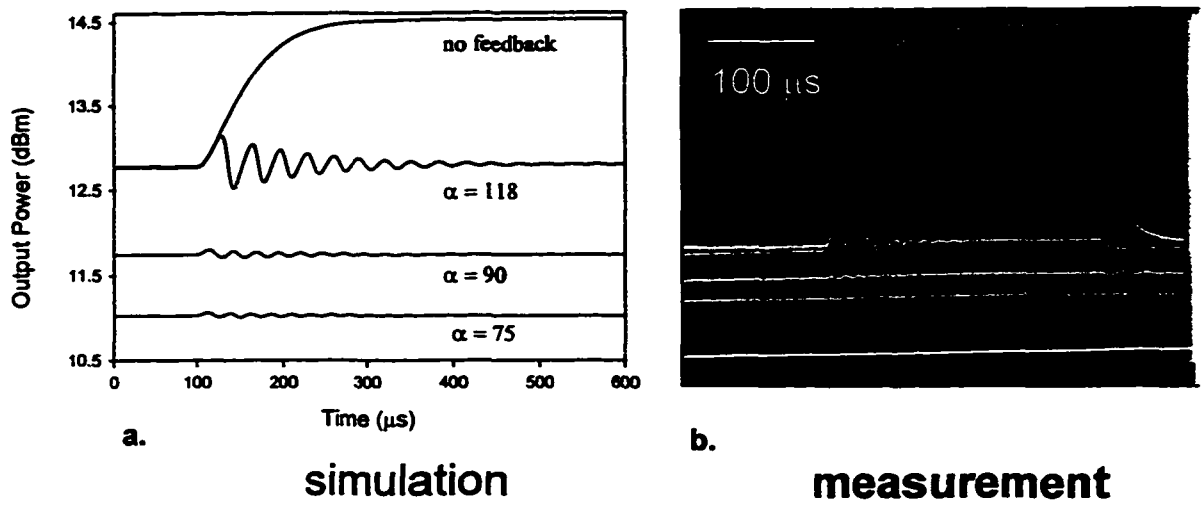

Figure 5.2 Transient response to dropping four of eight channels, for different attenuator settings. The simulation results show the same behavior as the experimental results.

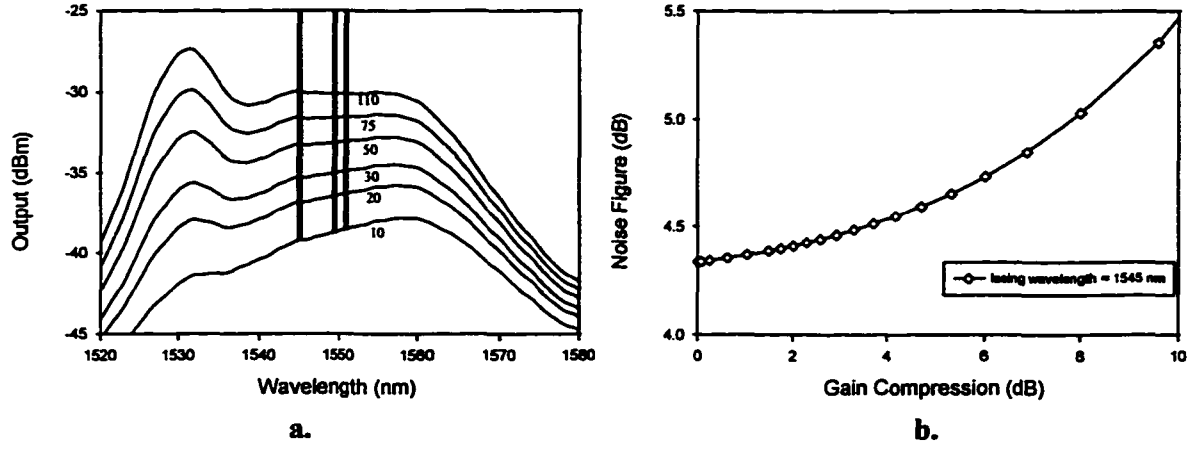

Figure 5.3 Lowering attenuator setting (increased gain compression) for a lasing wavelength of 1545 nm. (a) Gain tilt as a function of wavelength. (b) Noise figure as a function of added gain compression. Gain compression of 0 corresponds to no feedback.

5.2.3.3 Switching Speed

The simulation is in agreement with the experimental conclusion that for a given attenuator loss, the power excursion of the initial transients is also dependent on the speed with which channels are added and dropped. Fig. 5.4 shows that the power excursions are greater for faster switching speeds. The reasoning behind this observation was given in Section 4.4.2.3 of the previous chapter. Therefore, the slower switches discussed in Chapter 2, such as the optomechanical designs, will produce less transient power excursions when used to reconfigure the network when channels or added or dropped or as a result of protection switching.

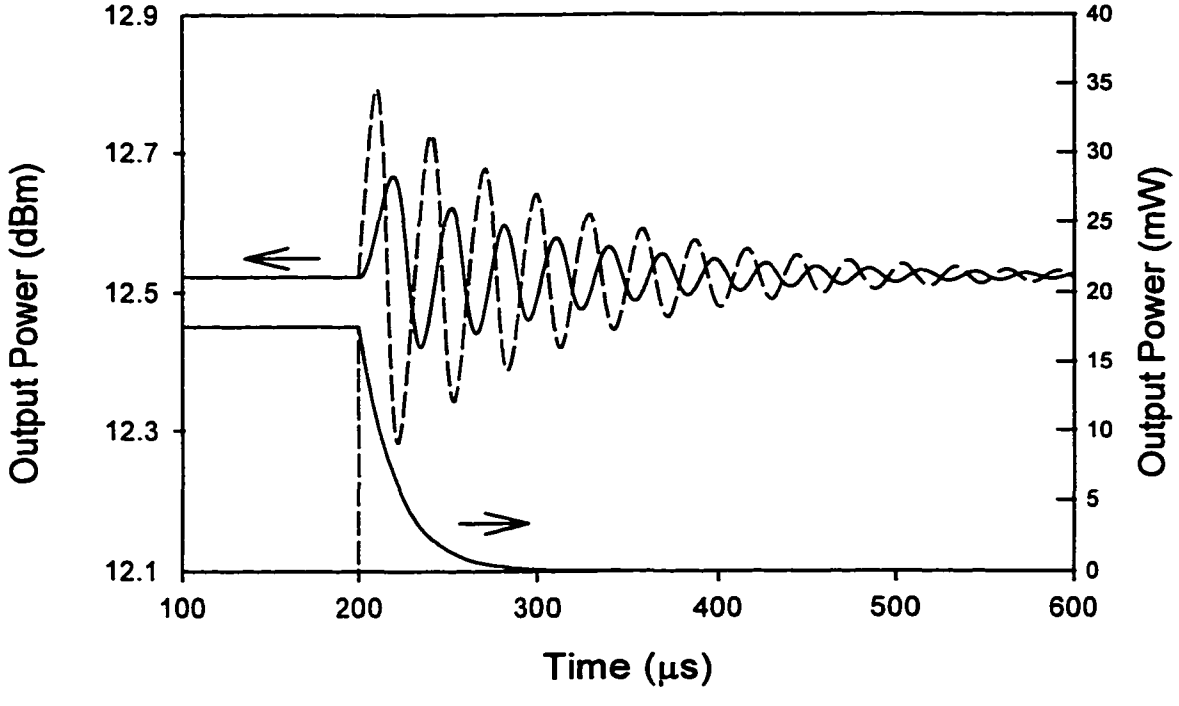

Figure 5.4 Transient response (upper curves) to dropping four of eight channels when drop is instantaneous and when drop takes approximately 100 μs. Lower curves show channel drop on the same time scale.

5.2.3.4 Number of Channels Dropped/Added

For a given attenuator loss and switching speed, both the frequency and amplitude of the power excursions experienced by the surviving channels are a function of the number of channels in the system. Fig. 5.5a shows an example of the dynamics of the eighth channel (1560.6 nm), when 1, 4, and 7 channels are switched, respectively. Figures 5.5b and 5.5c show the corresponding absorbed pump power and power excursions of the compensating

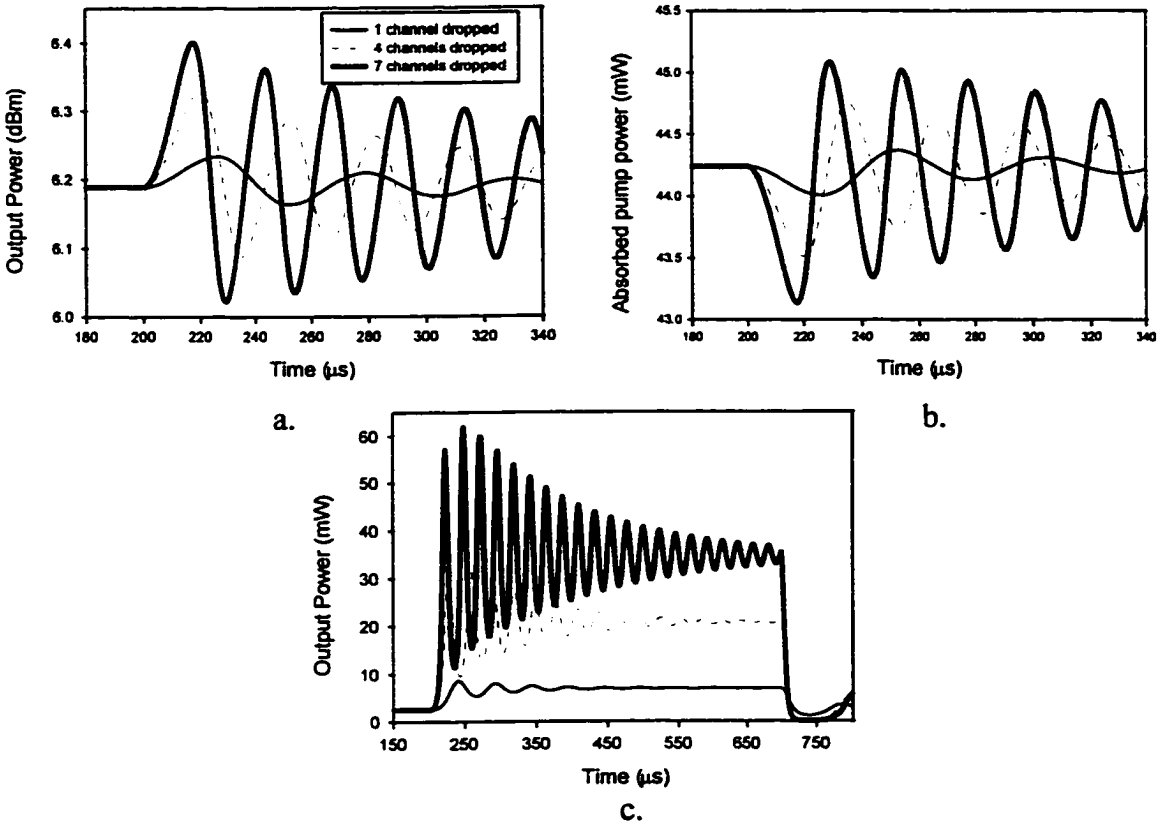

Figure 5.5 Transient response when one, four, and seven channels are switched respectively. (a) Transient response of channel 8 (1560.6 nm). (b) Absorbed pump power. (c) The compensating (lasing) channel. Note that both the frequency and the amplitude of the power excursions increases as the numbe of channles switch increases.

channel. Clearly, as the number of switched channels increases, the compensating channel has higher power and both the frequency and amplitude of the power excursions experienced by the surviving channels increase. The oscillations of the absorbed pump power are out of phase with the oscillations of the surviving channel as one would expect. The speed at which the gain rises is proportional to the number of channels dropped, so as the number of dropped channels increases both the initial gain transient and the resulting signal oscillations are larger.

5.2.3.5 Choice of Feedback (Lasing) Wavelength

It is possible to achieve the same steady state signal gain in an all-optical gain controlled EDFA configuration using different lasing wavelengths. Since the gain of the EDFA is wavelength dependent, lasing wavelengths with higher gains will require higher attenuator losses in the feedback path. The steady state behavior in terms of output powers may be the same; but the transitions and the noise figure of individual surviving channels are somewhat wavelength dependent. Note that residual power excursions related to spectral hole burning resulting from inhomogeneity, as has been shown experimentally [15], becomes less significant as the lasing wavelength approaches the spectral band occupied by signal wavelengths. As noted before, the effects of inhomogeneity are not taken into account in this analysis. We believe these effects will not seriously impair the effectiveness of laser gain control as has been shown experimentally [2].

The choice of a lasing wavelength for a system design is somewhat constrained. First, filtering considerations might rule that it should not be within our useful signal band. Second, if the compensating signal is to propagate along the entire chain as in Type 1 chain stabilization, it must lie within the flat gain region of the EDFA, so that its intensity relative to that of the real signals remains constant [2]. This means that the choice of lasing wavelength is somewhat more constrained in the case of Type 1 chain stabilization. This issue was discussed in Section 4.4.3.1.

We will define a gain recovery time, t_{rec}, as the time it takes the surviving signal to return to within a hundredth of a dB of its steady state value after channels are dropped.

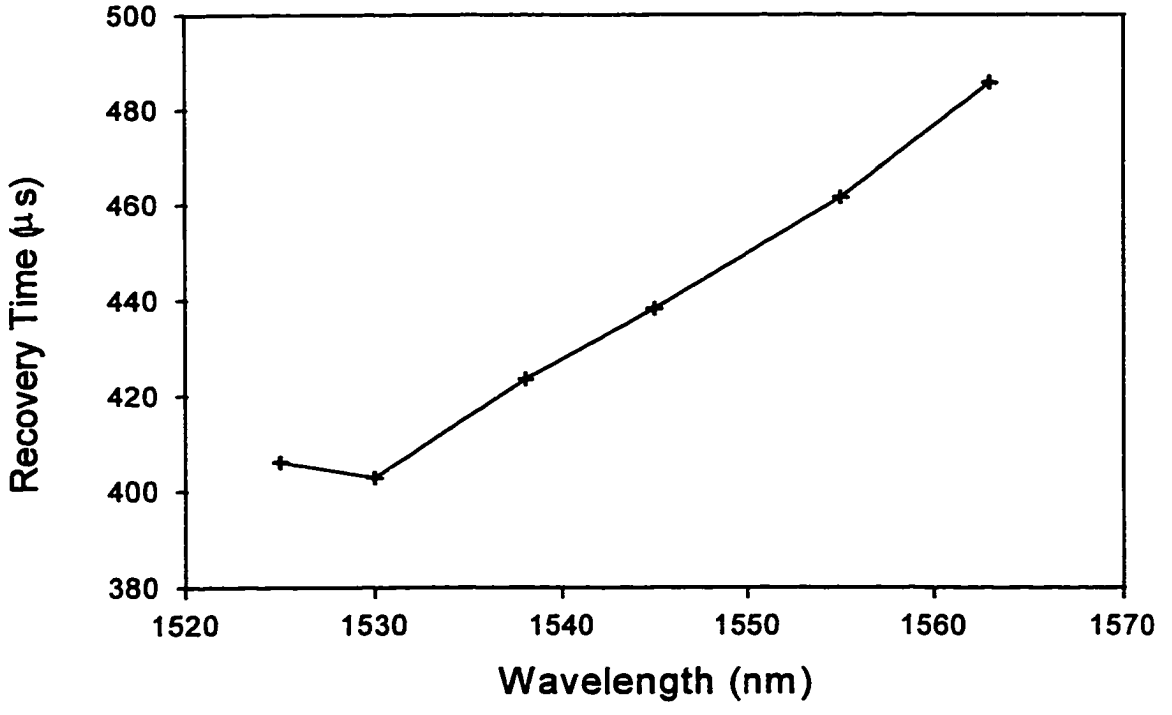

Figure 5.6 Recovery time (from time of drop to when the output power returns to within a hundredth of a decibel of its steady-state value) for a discrete set of lasing wavelengths.

Fig. 5.6 shows how t_{rec} varies for a discrete set of lasing wavelengths. Wavelengths that result in higher transient power excursions exhibit longer (lower oscillation frequency) gain recovery times. These effects can be explained by the differences of differential gains of the surviving and compensating signals, for changes in the average inversion [3]. This ratio is expressed as [3]:

$$\frac{dg_s}{dg_c} = \frac{\sigma_e^s + \sigma_a^s}{\sigma_e^c + \sigma_a^c} \tag{5.10}$$

Where σ_e and σ_a are the EDFA's wavelength dependent emission and absorption cross-sections, respectively. For compensating wavelengths with larger denominators on the

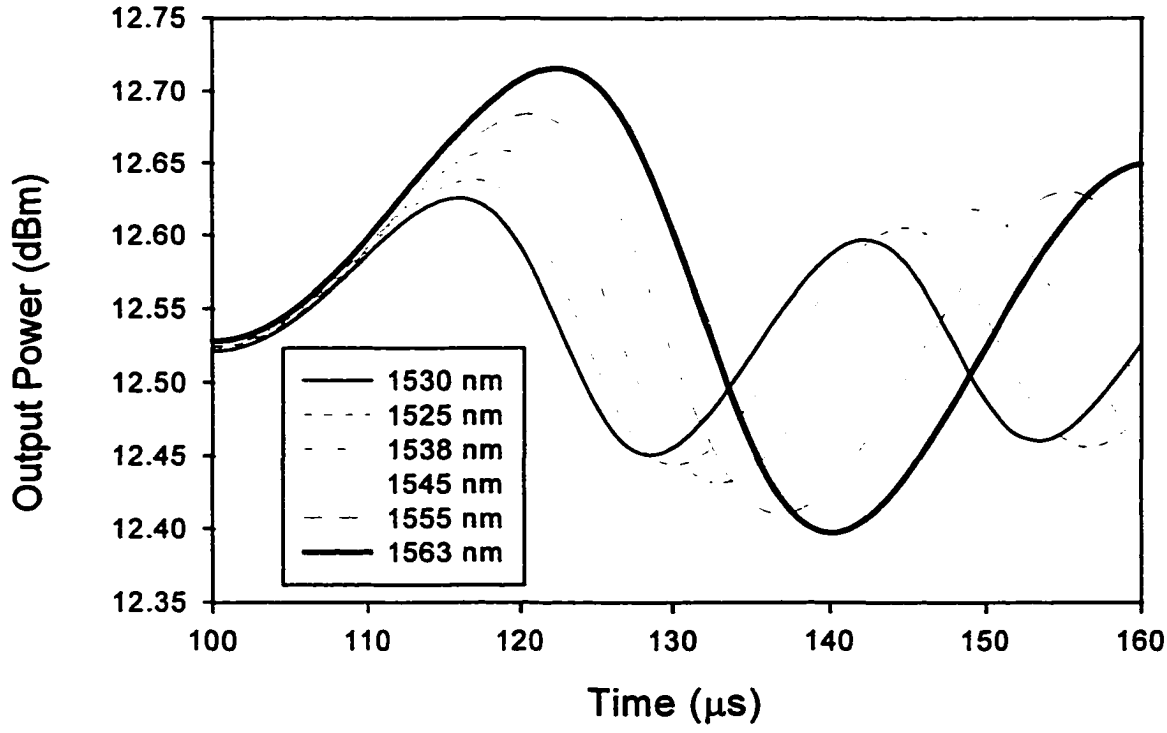

Figure 5.7 Transient response of the surviving channel for different lasing wavelengths. Note the tradeoff between oscillation frequency and power excursions.

RHS of (5.10), e.g. those compensating signals which are close to the 1530-nm gain peak, the differential gain for the signal as a result of changes in the average inversion is smaller, and thus smaller power excursions result. The set of curves in Fig. 5.7 represent a sequence of decreasing denominators in (5.10), starting from maximum value at the 1530 nm curve at the bottom (minimum power excursions) to the minimum value at the 1563 nm curve at the top (maximum power excursions).

5.2.3.5.1 Noise Figure

The noise figure of an all-optically gain controlled EDFA is subject to degradation due to

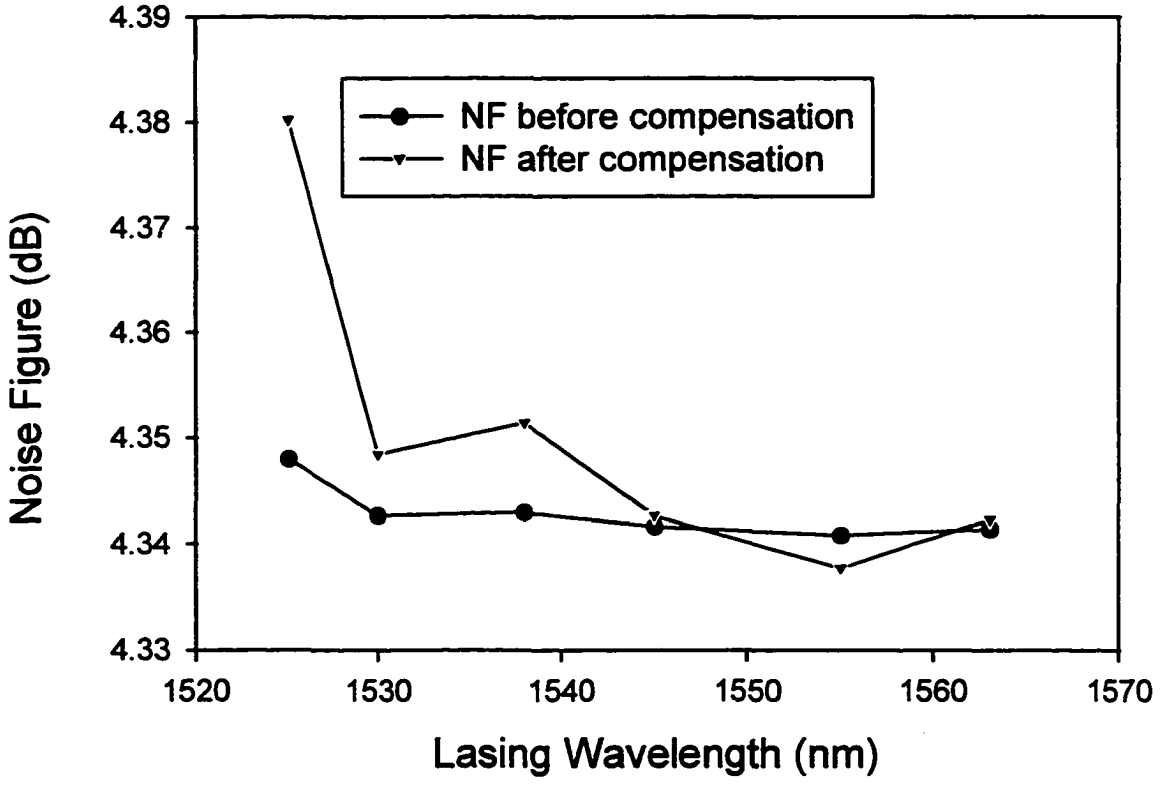

Figure 5.8 The effects of the compensation process on the noise figure of the surviving signal at 1551 nm, for a discrete set of lasing wavelengths. The steady state output power of the surviving signal is the same in all cases.

the amplifier's inherent operation in the deeper saturated regime. The noise figure can be estimated from the average inversion along the EDFA length [19]. Depending on the choice of lasing wavelength, the compensation process itself can slightly degrade or improve the noise figure at a particular signal wavelength because wavelengths with different gain produce different spatial variation in the inversion. Fig. 5.8 shows how the compensation affects the noise figure at a signal wavelength of 1551 nm for a discrete set of lasing wavelengths when half the channels are dropped and the compensating channel is approximately equivalent to 1 signal channel when all signals are present. Optimizing the noise figure at the end of a chain of EDFAs is equivalent to optimizing the noise figure at the first EDFA [18].

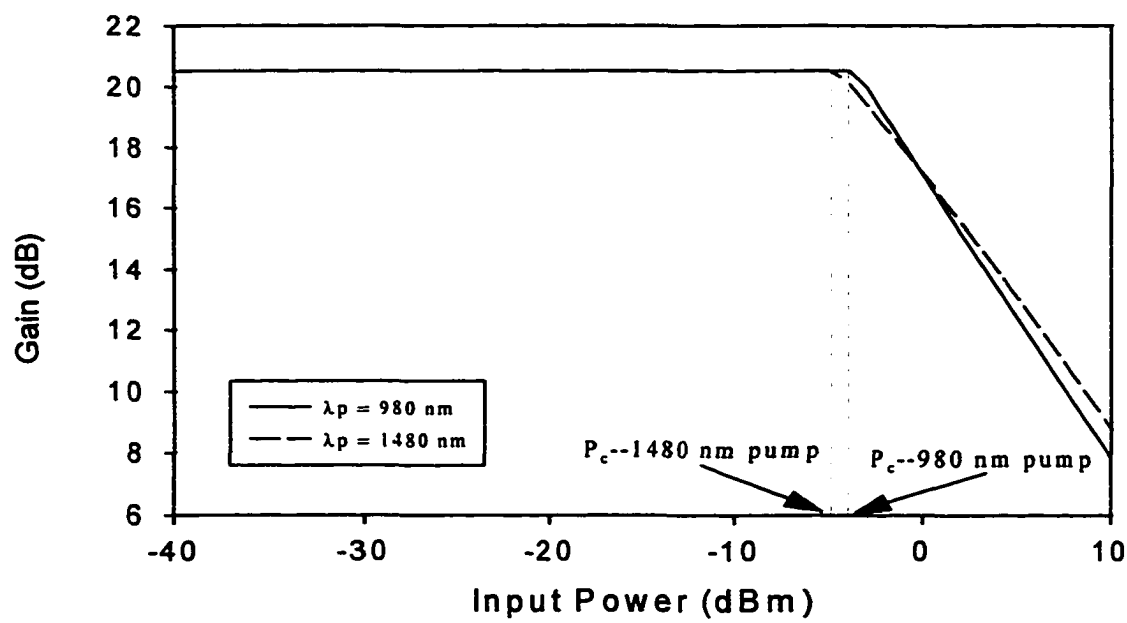

Figure 5.9 Typical gain vs input power curves for 1480 nm and 980 nm pumping with the same pump power.

5.2.3.6 Choice of EDFA Pump Wavelength

In Chapter 4 a brief comparison of the most popular pump wavelengths for the EDFA was given. Here, the transient response of the all-optical gain-clamped EDFA for 980 nm and 1480 nm pumping schemes is compared. For the gain-clamped EDFA the population inversion is set at the level that provides gain at the lasing wavelength that exactly cancels the losses in the feedback loop. This level of inversion is independent of the pump wavelength that is used. In fact, this level of inversion is also independent of the pump power to a certain extent. Higher pump power results in a higher critical input power and therefore also means that the power in the compensating channel is increased. As Fig. 5.9 shows, a 980 nm pumped EDFA results in a slightly higher critical input power than the 1480 nm pumped EDFA for the same input pump power [19]. The figure also shows that the gain of the surviving channel is the same for both pumping schemes as indicated before. Even though the gains are the same for both pumping schemes, more pump power is absorbed by the EDF for 980 nm pumping. Therefore, for all else being equal, the compensating channel normally has higher power in the 980 nm pumped EDFA than in the 1480 nm pumped EDFA. Since the frequency and the damping constant of the oscillations experienced by the surviving channel in the all-optical gain clamped EDFA depends on the power in the compensating channel, the transient behavior differs with the pump wavelength even though the steady state response is similar. In particular, as shown in Fig. 5.10, the higher power of the compensating channel for the 980 nm pumped EDFA results in a higher frequency of oscillation and a longer damping constants for the signals. Fig. 5.10a shows that even though the initial

power excursions of the oscillating power level of the surviving channel are higher in the 1480 nm pumped case, the gain is clamped more rapidly as the damping constant is shorter.

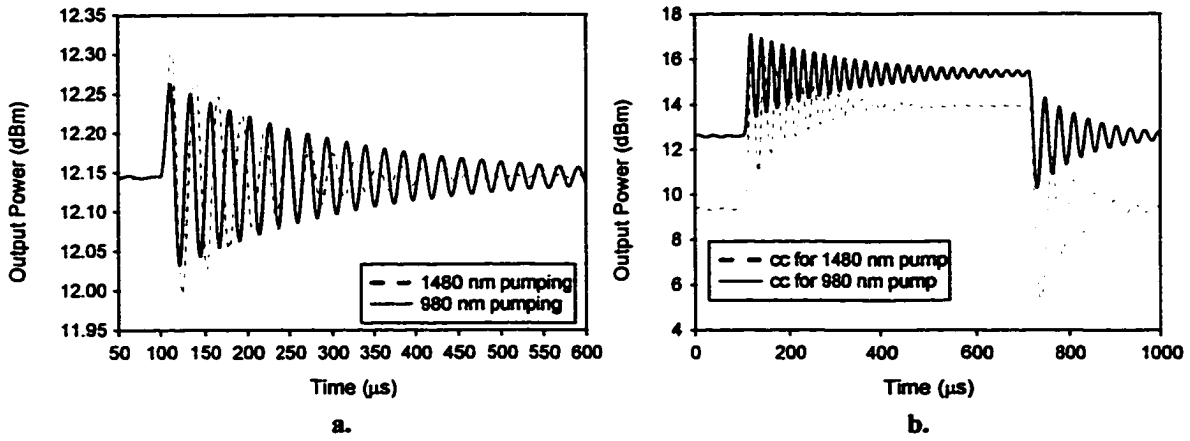

Figure 5.10 Comparison of 1480 nm and 980 nm pumping schemes in an all-optically gain-clamped EDFA with the same pump powers. (a) Oscillations of the surviving channel when channels are dropped. Note the different damping constants and oscillation frequencies. (b) The compensating (lasing) signal dropping and adding of channels.

5.2.4 EDFA Chain Stabilization

We now consider how the degradations observed in a single gain-clamped EDFA compound in a chain of amplifiers of either Type 1 or Type 2. We highlight the

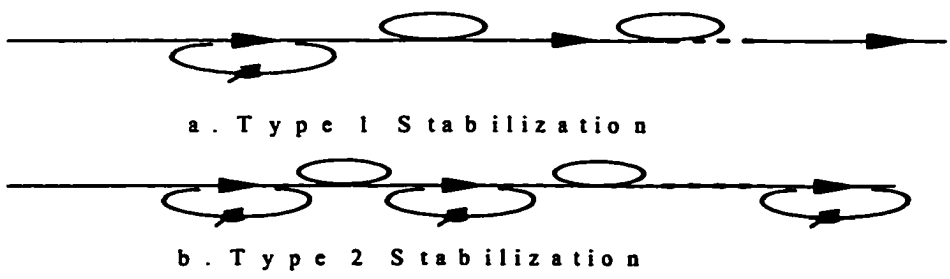

Figure 5.11 Two ways to do all-optical chain stabilization

robustness of these approaches and also show some of their limitations.

5.2.4.1 Type 1 Stabilization (Lasing Only at the first EDFA)

In the first type of chain stabilization, shown in Fig. 5.11a, the ring laser acts both to clamp the gain and to generate a compensating signal at wavelength λ_C which takes the place of the dropped channels in the subsequent EDFAs. The experimental results presented in Section 4.4.3 are based on this type of chain. For this approach stabilization is obtained as explained in Section 4.4.3.1.

5.2.4.1.1 Simulation Results for Type 1 Chain

Fig. 5.12 shows the surviving signal at 1551 nm at the output of a chain of six EDFAs, after dropping the channel at 1549.4 nm. The lasing wavelength at the first EDFA was placed at 1545 nm, which is outside of our intended set of signal wavelength and at the same time on the flat region of the spectrum, as discussed in Section 4.4.3.1. The loss between amplifiers has been adjusted to give constant steady state output power for the surviving channel. When all signal channels are present the lasing signal has power equivalent to one of eight channels. In a chain of EDFAs, the power excursion increases with the number of amplifiers, as shown in Fig. 5.12 for the first, third, and sixth amplifiers. The extent to which these effects are amplified at the end of the chain depends on how much we are able to limit the initial power excursions at the first EDFA. We have seen that smaller power excursions result from lower losses in the feedback loop,

slower switching speeds and smaller numbers of dropped channels. We have also seen that the power excursions will differ slightly for different lasing and pumping

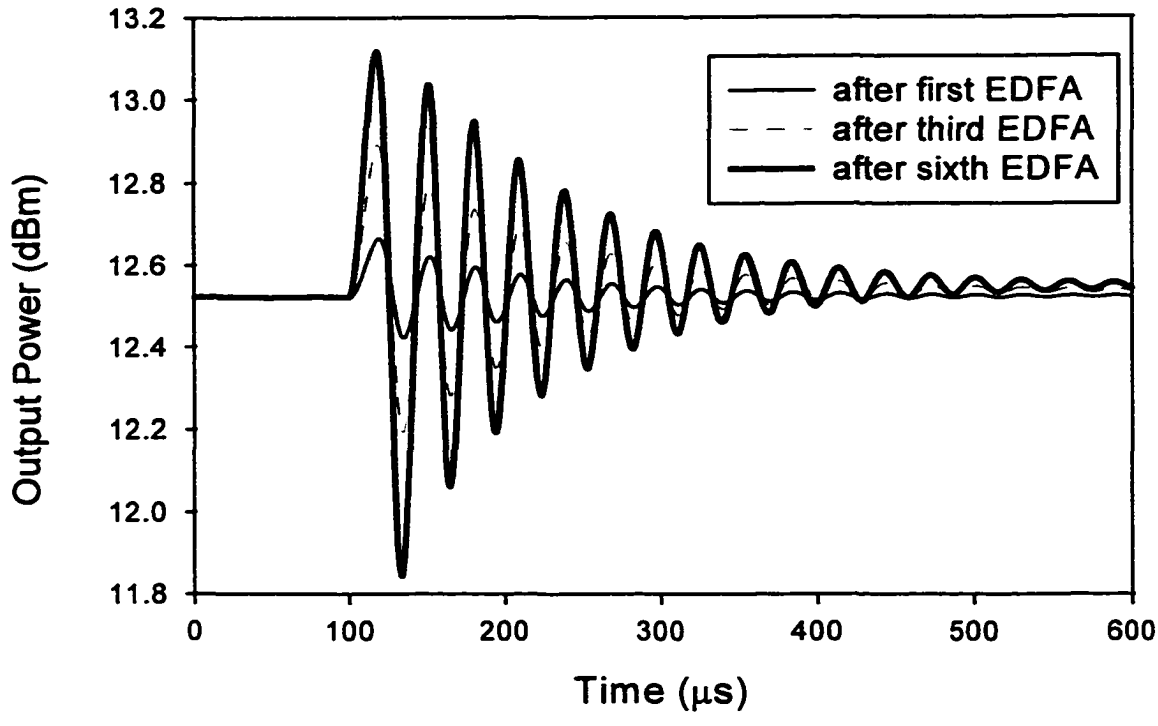

Figure 5.12 Type 1 stabilization, for one, three, and six EDFAs, with λ_c = 1545 nm, in the flat gain region. Output power has been equalized at each stage.

wavelengths. Therefore, the loss in the feedback loop, the switching speed at the network element, the number of channels dropped or added, the choice of lasing wavelength, and the choice of pumping wavelength at the first amplifier all determine the cumulative effect at the end of the EDFA chain. The smaller the power excursions exhibited at the first EDFA the smaller the chain impairment. Fig. 5.13 shows how the difference in switching speeds shown in Fig. 5.4 affects the power excursion and time constant at the output of the sixth amplifier in the chain. Lower power excursions resulting from slower

switching speeds at the first EDFA, results in lower power excursions in the subsequent EDFAs.

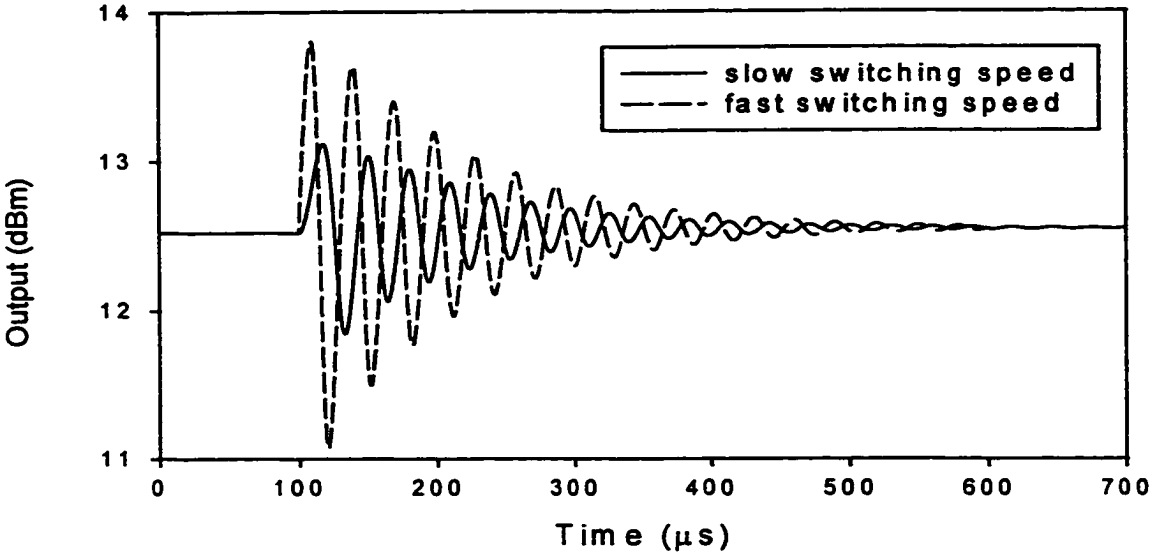

Figure 5.13 The power excursions of the surviving channel after six EDFAs for the two switching speeds shown in Fig. 5.4

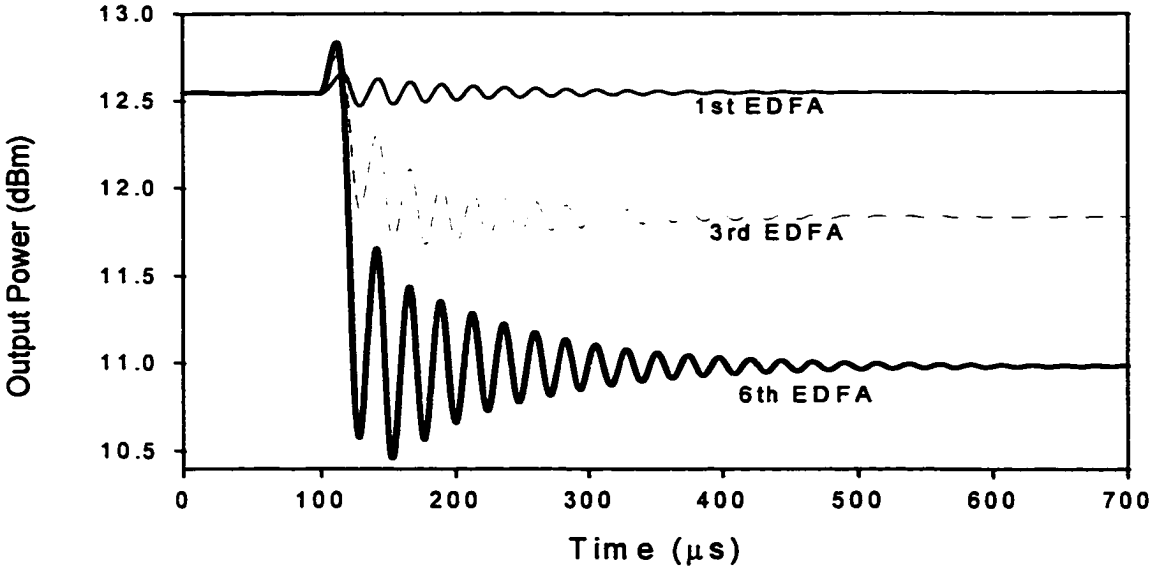

Figure 5.14 Type 1 stabilization, for 1, 3, and 6 EDFAs, with λ_c = 1530 nm, i.e., with greater gain than the drop and surviving signals. Steady-state output power has been equalized at each stage. Compare with Fig. 5.12.

Fig 5.14 shows the effects of non flat gain. The figure shows the surviving signal after the first, third and sixth EDFAs for a case of overcompensation, where the lasing wavelength is placed on the ASE peak at 1530 nm. The output power of the surviving channel is progressively lowered as the power in the compensating signal increases, accounting for more of the saturated output power of the EDFA. To effectively stabilize the chain using this approach it is imperative that the compensating signal be on the flat part of the spectrum so that the difference in gain between it and the signals is as small as possible. In Figs. 5.12-5.14, the loss between amplifiers has been adjusted to give constant output power for the surviving channel at each stage. Figs. 5.15a and 5.15b present two results in which the loss between amplifiers was kept constant and a lasing wavelength of 1545 nm was used. Fig. 5.15a shows that the power in the surviving channel increases because of the non flat gain of the EDFA (λ_S has higher gain than λ_D). However, the output power transients grow only slowly as seen in the figure after 1, 6 and 20 EDFAs. Fig. 5.15b

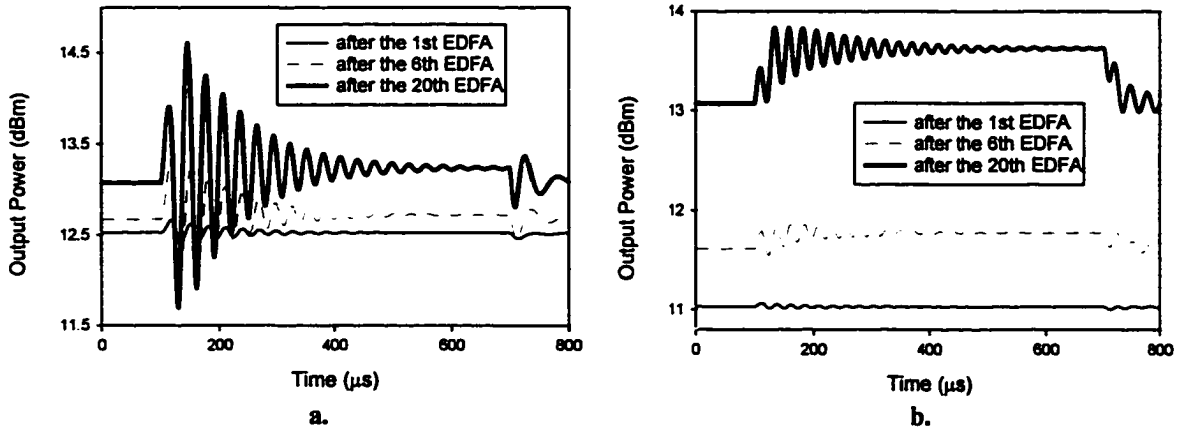

Figure 5.15 Type 1 stabilization, for one, six, and 20 EDFAs with λ_c = 1545 nm, in the flat gain region. The losses are the same between each stage. (a) Loss in the feedback loop at the first EDFA is 20.4 dB. (b) Loss in the feedback loop at the first EDFA is 18.75 dB.

shows that for an approximate 1.5-dB reduction in the gain of the surviving signal at the first EDFA (1.65 dB reduction in the feedback attenuator level), the output power excursions can be made much less, but because of the increased gain tilt due to the EDFA operating in deeper saturation, the differences in the steady state levels are considerable more. The figure also shows some degree of undercompensation brought about by the increased gain tilt. The increased gain tilt occurs because the presence of the lasing signal has moved the amplifier further away from its optimum operating point. A redesign of the EDFA such that mimimum gain variation occurs with the total input power including the compensating signal, will eliminate, or at least reduce the gain tilt. Thus, these figures show the importance of using EDFAs designed with the correct total input power in mind. The larger the chain to be traversed the flatter are the gain requirements.

5.2.4.2 Type 2 Stabilization (Lasing at Each EDFA)

Type 2 stabilization, shown in Fig. 5.11b, is the conceptually simpler method of gain clamping each of the EDFAs individually. Stabilization is achieved in the following two steps:

1. The gain experienced by individual channels at each EDFA is clamped via all-optical feedback in a ring laser configuration at each amplifier.
2. We filter the compensating signal generated in each stage by using a wavelength selective coupler at both the outputs and inputs.

One concern in using this approach is the possibility of distortion in the initial transients. Fig. 5.16 shows the output after the first, third, and sixth amplifiers for a lasing wavelength of 1545 nm at each amplifier. The response differs from that of Type 1 in three ways. 1) There is a significant difference between the initial over and undershoots. 2) The output power is clamped more rapidly. 3) The oscillations of the surviving channel are noticably distorted after the sixth amplifier. All three effects are somewhat related.

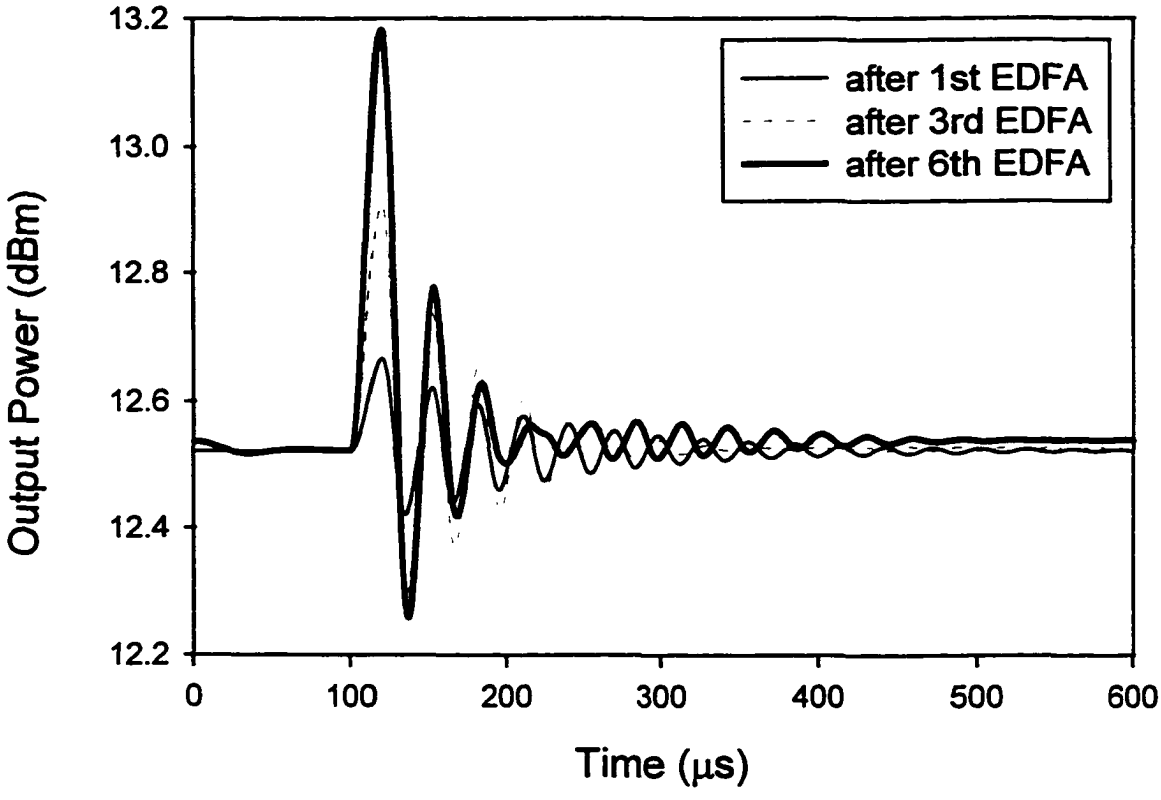

Figure 5.16 Type 2 stabilization, for one, three, and six EDFAs with λc = 1545 nm. Note that the transients die down faster than in Fig. 5.12. The steady state output power of the surviving channel has been equalized at each stage.

When channels are dropped, for all but the first EDFA in the chain, the input is an oscillatory signal from the previous stage. The initial overshoot of the surviving signal

occurs on a much faster time scale than the lagging lasing signal can build up to compensate for the dropped channel. The faster power overshoots of the surviving channels limit the power available to the compensating signals to lower values for longer chains. For long enough chains the fast power transients can actually cause the first peak of the compensating signal to be below its steady state power level. The undershoot of the surviving signal is proportional to the overshoot of the lasing signal. Therefore, since the fast power transient in the surviving channel has suppressed the overshoot of the compensating signal, very little of the undershoot of the surviving signal is associated with the compensating signal for longer chains.

As was clear from Fig. 5.12, in the absence of a lasing signal the undershoots of the oscillatory input signal entering the subsequent amplifiers in the chain grow as a result of fast power transients. If there is already a lasing signal present as in Fig. 5.16, when the oscillating input signal goes below its steady state value this is sensed by the now built up lasing signal which acts to counter this in much the same way it would compensate for a dropped channel. In this way, the undershoots of the surviving signal are clamped. The built up lasing signal at each amplifier is now able to clamp the second overshoot peaks to much smaller power excursions than the first occurrence. Rather than causing the oscillation, the lasing signal is now helping to damp it. The clamping of the output power of the surviving channels is thus accelerated.

The phase difference between the oscillating input signal going into the EDFAs beyond the first, and the lasing signal stabilizing the particular EDFA can lead to distortion in the

oscillations of the output surviving signals. Each subsequent amplifier can add its own distortion to an already distorted signal. The effect of this distortion on data format needs to be further investigated.

5.2.5 Comparing the Two Approaches

As Fig. 5.17 shows, it is possible to stabilize a chain of EDFAs using either Type 1 or Type 2 stabilization. As stated before, the initial overshoot of the surviving channel occurs on a must faster time scale than the lagging lasing signal can compensate for it and thus, the first peak in the transient is similar for both the Type 1 and Type 2 chains.

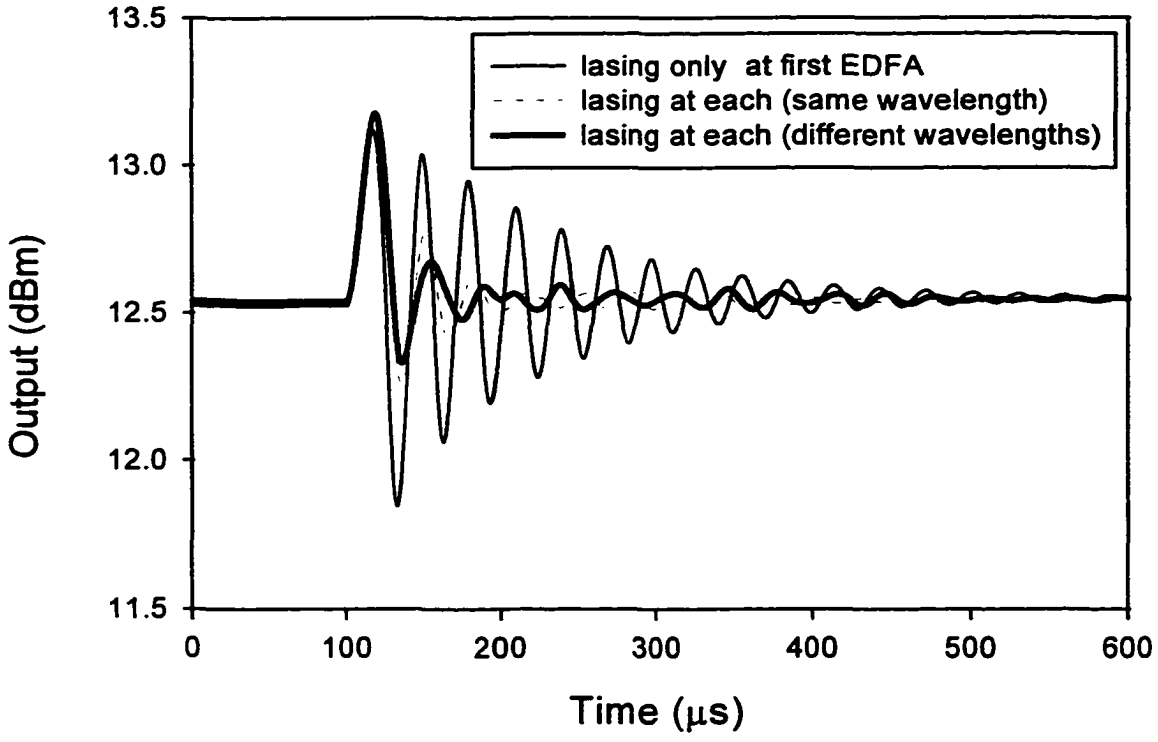

Figure 5.17 Comparing the transient response of Type 1 and 2 after a chain of six EDFAs, for the same and different lasing wavelengths at each EDFA. Note the faster clamping of the power excursions using Type 2 stabilization.

However, as as is obvious from Fig. 5.17 the power excursions are clamped more rapidly in the Type 2 approach, as stated before. There are some obvious distortion in the transients seen in the Type 2 case which are not seen in the Type 1 case. Another striking difference between the two approaches is seen in Fig. 5.18. For a 3 dB excess loss between the first and second EDFAs it is possible to recover the output power of the surviving signal to within a fraction of a dB after 6 EDFAs using Type 1 stabilization. On the other hand, using Type 2, we suffer about 3-dB reduction in the surviving channel output power. We showed experimentally that when the attenuation between the first and second EDFA in a six-EDFA Type 1 chain was varied by more than 6 dB output power changed by less than 0.5 dB [20].

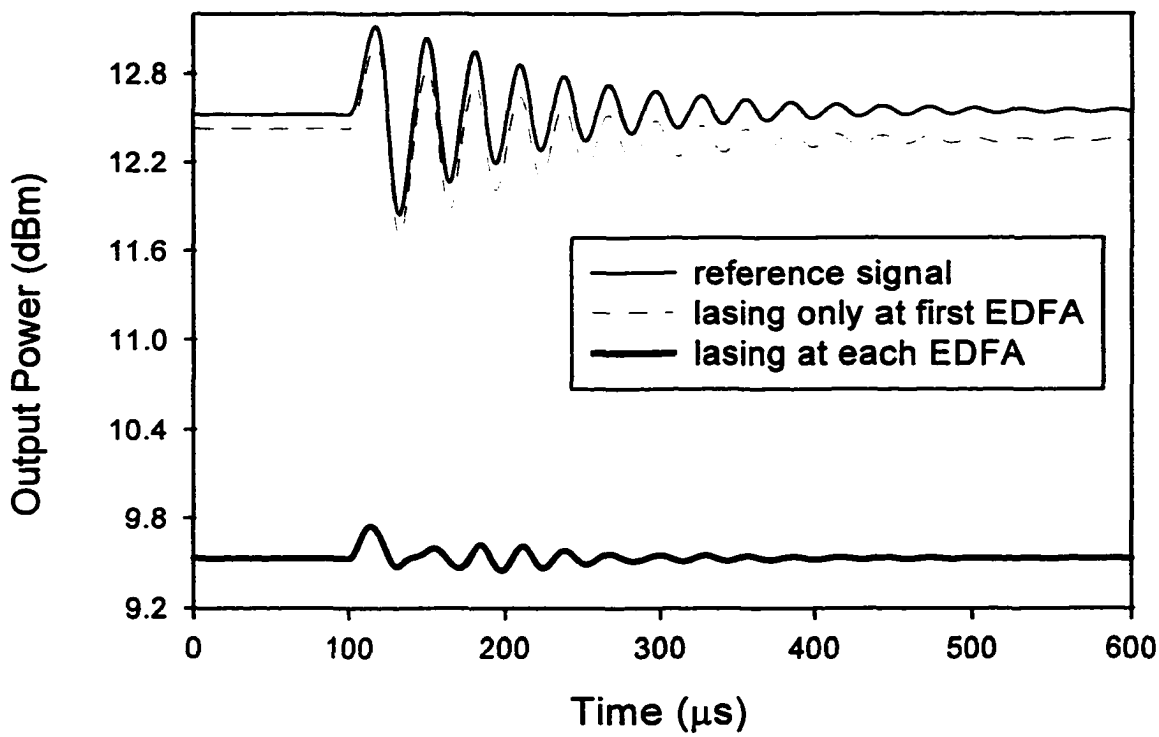

Figure 5.18 Comparison of Type 1 and 2 stabilization, after six EDFAs, when an excess 3-dB loss is inserted between the first and second EDFAs. Output poweris recoved in Type 1, but not in Type 2.

These results help us compare the two types of chain stabilization which we summarize in Table 5.1. Type 1 is less expensive to implement, since it requires modification of only the first EDFA, but it is sensitive to deviations from gain flatness. For short EDFA chains, where changes due to the different gains of the signal and compensating channels have little chance to accumulate, Type 1 stabilization appears to have an advantage. For long chains, we will need either to control the gain flatness very accurately, to accept some signal level variation due to non-flat gain, or to control the gain at every EDFA, as is done in Type 2. In this case, we see that it is necessary to control the loss budget of the chain more accurately than is necessary when using Type 1 stabilization. The obvious advantages of Type 2 stabilization are that lasing at each EDFA relaxes the requirement on gain flatness and that, as seen in Fig. 5.17, where Type 2 stabilization is possible even when all EDFAs use different lasing wavelengths, the choice of lasing wavelength is

	Cost	**Gain Flatness**	**Loss Budget**	**Speed of clamping**	**Distortion in Transients**
Type 1	Lower	sensitive (long chains)	More tolerant to excess loss	slower for chains	No
Type 2	higher	not very sensitive	accurate control needed	faster for chains	Yes impact?

Table 5.1 A brief comparison of Type 1 and Type 2 Chain Stabilization.

more relaxed than that of the first approach. Furthermore, the output power variations are smaller for longer chains than when Type 1 stabilization is used, and the initial power excursions of surviving signals can be made to clamp faster. However, lasing at each amplifier also makes the oscillations of the surviving signals susceptible to distortion. Thus, both of these techniques can be used to compensate for changing numbers of WDM channels, but the demands they place on the EDFA chain are different.

5.3 Amplifier Gain Stabilization Compatibility

The advantages of WDM technology over traditional single wavelength electronics based technology have led to more and more vendors becoming involved in the development and deployment of the equipment that make up the network. Competition is good for the customer from an economic point of view but it makes the overall engineering of the network more difficult. In order for the network to work as a whole, the interoperability of different vendors equipment must be assured. Here, we examine through simulation the compatibility of two different gain stabilization schemes such as is to be deployed in the MONET DC network [1]. In particular, we examine the compatibility of the Type 1 chain approach as disscussed above with a scheme that counts the number channels entering the EDFA and adjustes the pump power accordingly [21-22]. These two methods of gain control are intrinsically incompatible. Recall that for the Type 1 chain the compensating channel generated in the first EDFA is propagated to all the inline EDFAs downstream. Therefore, all the amplifiers expect a stabilizing channel along with the

signal channels. For an approach that counts the number of signal channels and adjusts the pump to the level appropriate for that number of channels, an extra stabilizing channel will reduce the gain of the EDFA as more input power than expected will enter the EDFA. Consequently, passing signals from a system based on the Type 1 approach to one that uses a pump controlled scheme and vice versa requires slight modifications in the system design. In particular, going from an EDFA based on the Type 1 approach to one based on the pump controlled approach, a filter is inserted in between to strip off the compensating channel (stabilizing wavelength). Going in the opposite direction, from a pump controlled EDFA to one that expects a stabilizing wavelength but does not self generates it (such as the input EDFA in a NE developed based on the Type 1 approach), the EDFA is gain clamped similarly to the first EDFA in the Type 1 chain.

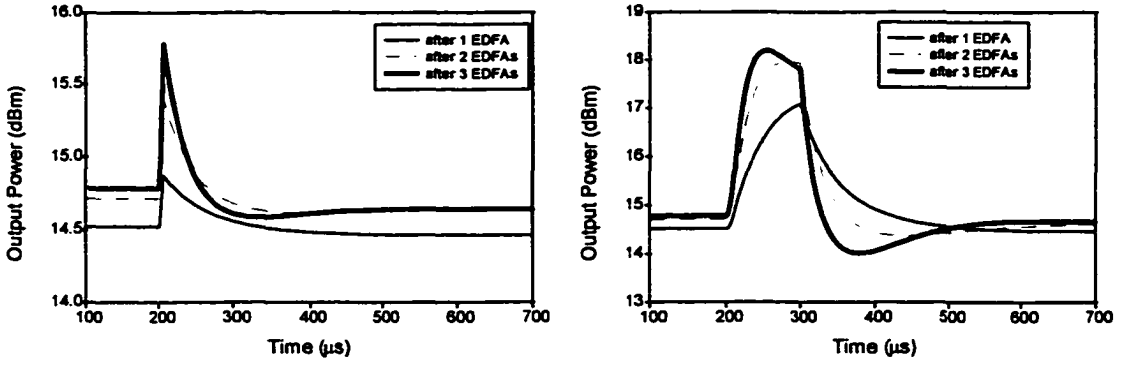

Figure 5.19 Simulated response to channel dropping of amplifiers with pump power control. The figure shows power in the surviving channel after 4 of 8 channels are dropped in the first, second and third EDFA. (a) Assumes that channel dropping occurs in 1 μs and pump power is controlled within 6 μs. (b) Assumes that channel dropping occurs in 10 μs and pump power control within 90 μs.

5.3.1 Simulation Results

Fig. 5.19 shows the simulated response of the per channel transients for a pump controlled three-EDFA chain with two different speeds of response of the pump control circuitry. Clearly, the shorter the time required to change the pump power, the lower the power excursions and the faster the surviving signals are stabilized. In simulating the compatibility of the two approaches we assumed add or drop occurs over 1 μs and pump control occurs 6 μs later, as in Fig. 5.19a. Fig. 5.20 shows the single amplifier response

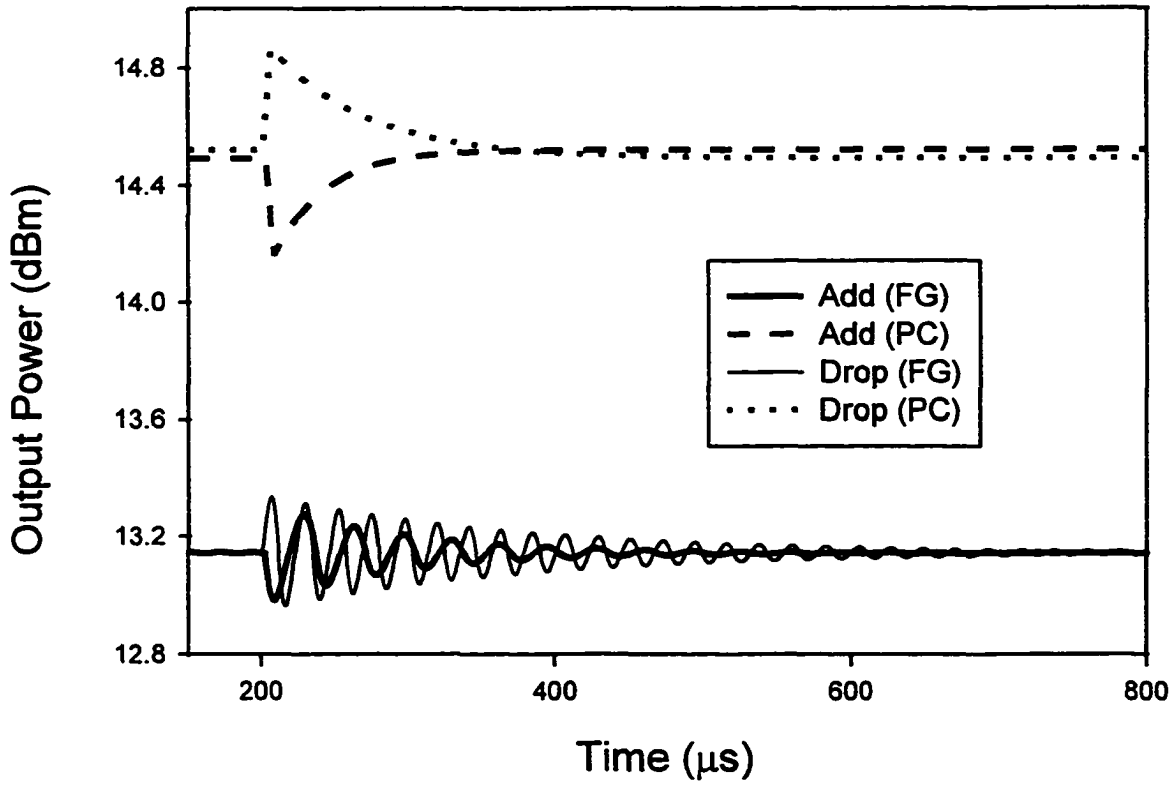

Figure 5.20 Single-EDFA response of the surviving channel for the dropping of four of eight channels for the all-optical fixed gain (FG) approach and the pump controlled (PC) approach. Speed of the pump response circuitry is the same as in Fig. 5.19a.

of both approaches for the adding and dropping of channels. As seen in the figure, the

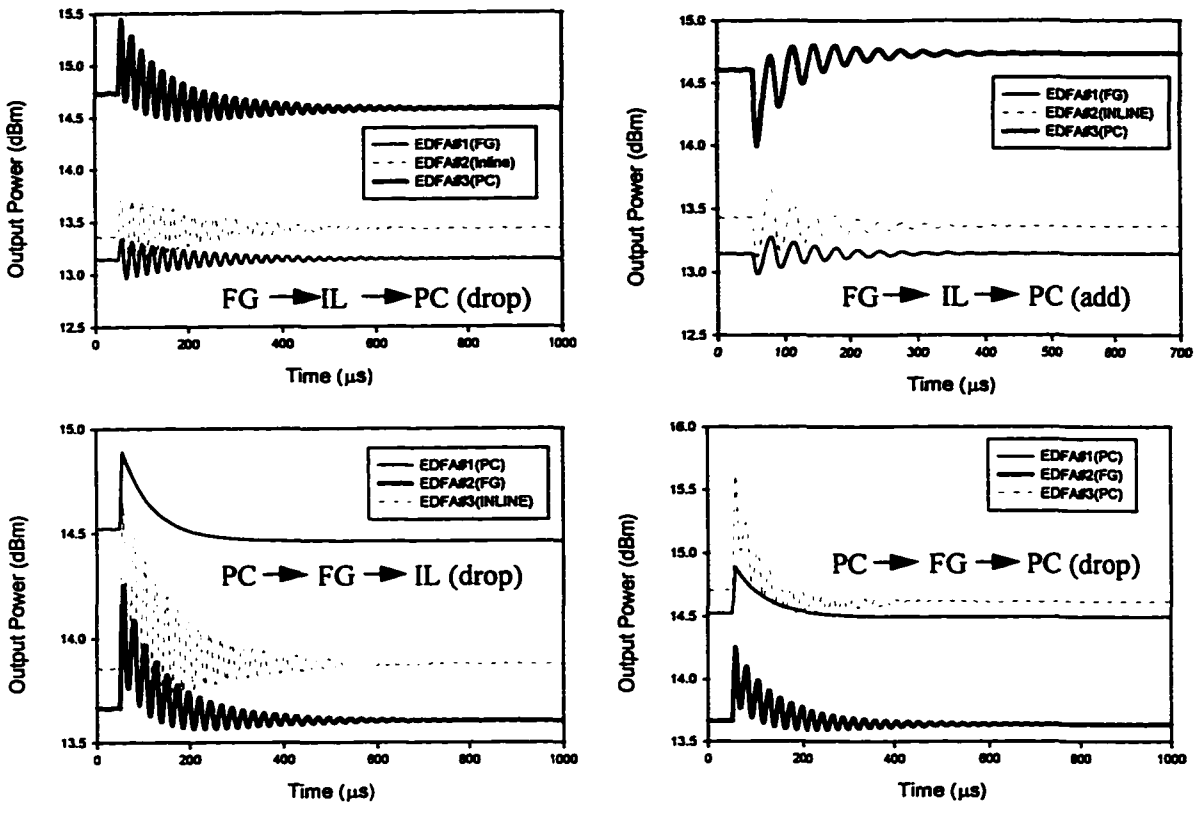

Figure 5.21 Transient power in surviving channel after 4 of 8 channels are dropped or added for various sequences of EDFAs. Fixed gain (FG), Inline (IL), pump controlled (PC) refers to the differently stabilized EDFAs as discussed.

pump control scheme has an exponential response with stabilization occuring in a few hundred microseconds, while the all-optical feedback approach has a damped oscillatory response with stabilization occuring in a similar time frame. Fig. 5.21 shows samples of simulations of per channel transients when 4 of 8 channels are added or dropped for various sequences of Type 1 and pump controlled EDFAs. For illustration purposes, the first EDFA of the Type 1 chain (with feedback loop) is referred to as FG (fixed gain), the other Type 1 EDFAs (without feedback loop) are referred to as IL (inline), and the pump

controlled EDFAs are referred to as PC (pump control) in the figures. The transient degradations after 3 EDFAs involving different designs are not significantly different from the transients observed for a homogeneous chain. Therefore, the general conclusion is that the impairments appear to be roughly additive as no unexpected interaction between the different stabilization schemes were observed when the EDFAs were modified as above. A stonger compensating channel for the Type 1 approach and a faster pump response time for the pump controlled scheme would reduce the size and duration of the transients.

5.4 Conclusion

A theoretical analysis of gain dynamics for a single and chains of EDFAs and the impact on multiwavelength communication systems has been presented. A dynamic simulation tool was used for modeling the behavior of a single EDFA and amplifier chains, with different methods of stabilization. The main objective was to understand how nearly one can maintain constant per-channel output power with a minimally degraded SNR, regardless of the number of channels present. Using an amplifier designed to optimize gain and minimize gain variation when 8 channels are present, we have examined the factors that affect the transient power excursions in the surviving channel. We modeled and compared the behavior of three different approaches to chain stabilization. We highlighted the robustness of these approaches and also showed some of their limitations and advantages.

In modeling the individual EDFA, we have observed the effects on gain flatness, initial power transients and noise figure (NF) and explored the limitations that any of these degradations can impose on the stabilization techniques. We showed how any degradation at the first EDFA has a cumulative effect at the output of all subsequent EDFAs in the chain. Specifically, we have shown that the lower the losses in the feedback loop, the slower the switching speeds and the smaller the numbers of dropped channels, the smaller the power excursions experienced by the surviving channel in an all-optical gain clamped EDFA. We have also shown that the power excursions will differ slightly for different lasing and pump wavelengths. Therefore, the switching speed at the network element, the loss in the feedback loop, the number of channels dropped/added, and the choice of lasing and pump wavelengths at the first amplifier all determine the cumulative effect at the end of the EDFA chain.

For the pump controlled EDFA we showed that the faster the response time of the pump control circuitry the smaller the size and duration of the transients. The compatibility of Type 1 stabilized EDFAs and pump controlled EDFAs was verified as the impairments were found to be roughly additive.

Although these calculations were made assuming a specific EDFA, they are in good qualitative agreement with experiment results obtained with several EDFAs and short EDFA chains of different construction. This modeling technique can be useful in understanding and optimizing the behavior of EDFAs in multiwavelength communications.

5.5 References

[1] Multiwavelength Optical Networking (MONET) Consortium, 15th Quarterly Report, September, 1998.

[2] J. L. Jackel and D. Richards, "All-optical stabilization of multi-wavelength EDFA chains: a network-level approach," in Proceedings of LEOS'96 (IEEE Laser and Electro-Optics Society) postdeadline paper.

[3] C. R. Giles and E. Desurvire, "Modeling Erbium-Doped Fiber Amplifiers", J. Lightwave Technology, vol. 9, no. 2, pp. 271-283, 1991.

[4] A.A Saleh, R. M. Jopson, J. D. Evankow, and J. Aspell, "Modeling of gain in erbium-doped fiber amplifiers," IEEE Photon. Tech. Lett., Oct. 1990

[5] C. R. Giles and D. DiGiovanni, "Spectral dependence of gain and noise in erbium-doped fiber amplifiers," Photon. Tech. Lett., vol.2, no. 11, pp. 797-800, 1990.

[6] R. W. Hamming, Numerical Methods for Scientist and Engineers. New York: Dover Publications, 1973.

[7] C. R. Giles, E. Desurvire, and J. R. Simpson, "Transient gain and cross talk in erbium-doped fiber amplifiers," Opt. Lett., Vol. 14, pp. 880-882,1989.

[8] R. I. Laming, L. Reekie, P. R. Morkel, and D. N. Payne, "Multichannel crosstalk and pump noise characterization of Er^{3+} -doped fiber amplifier pumped at 980 nm," Electron. Lett., vol. 25, pp. 455-456, 1989.

[9] M. A. Ali, A. F. Elrefaie, R. E. Wagner and S. A. Ahmed, " A Detailed Comparison of the Overall Performance of 980 and 1480 nm Pumped EDFA Cascades in WDM

Multiple-Access Lightwave Networks", J. Lightwave Technology, vol. 14, pp. 1436-1448, 1996.

[10] Janet L. Jackel and Dwight H. Richards, "All-Optical Stabilization of Multi-wavelength Erbium-doped Fiber Amplifiers with Changing Number of Channels," OSA Trends in Optics and Photonics, Vol. 12, System Technologies (Optical Society of America, Washington, DC, 1997).

[11] Dwight H. Richards, Janet L. Jackel, and Mohamed Ali, "A Theoretical Investigation of Dynamic All-Optical Automatic Gain Control in Multichannel EDFAs and EDFA Cascades," IEEE Journal of Selected Topics in Quantum Electronics, vol. 3, no. 4, pp. 1027-1036, August, 1997.

[12] D. H. Richards, J. L. Jackel, and M. A. Ali, "Multichannel EDFA Chain Control: A Comparison of Two All-optical Approaches," IEEE Photonics Technol. Lett., vol. 10, no. 1, pp. 156-158, 1998.

[13] D. H. Richards, M. A. Ali, J. L. Jackel, "EDFA Chain Control: A Comparison of Two Approaches," In Proc. LEOS'97, Montreal, Quebec, Aug. 1997, Paper FB2.

[14] D. H. Richards, M. A. Ali, and J. L. Jackel, "A Theoretical Investigation of Dynamic Automatic Gain Control in Multi-channel EDFA Cascades," ECOC'97, Edinburgh, UK, September, 1997.

[15] G. Luo, J. L. Zyskind, Y. Sun, A. K. Srivastava, J.W. Sulhoff and M.A. Ali, "Relaxation Oscillations and spectral hole burning in laser automatic gain control of EDFAs", in Technical Digest of Optical Fiber Communication Conference (Optical Society of America, Dallas, TX, 1997) paper WF4.

[16] G. Luo, J. L Zyskind, J. A. Nagel, and Mohamed Ali, "Experimental and Theoretical Analysis of Relaxation-Oscillations and Spectral Hole Burning Effects in All-Optical Gain-Clamped EDFAs for WDM Networks," Journal of Lightwave Technol. vo. 16, no.4, pp. 527-533, 1998.

[17] B. Landousies, T. Georges, E. Delevaque, R. Lebref and M. Monerie, "Low power transients in multichannel equalized and stabilized gain amplifier using passive gain control.", Electron. Lett., 32, 1912-1913, 1996.

[18] E. Desurvire, "Erbium-doped Fiber Amplifiers", New York: Wiley, 1994.

[19] A Yu and M. J. O'Mahony, "Modeling of laser-controlled erbium-doped fiber amplifiers," in Technical Digest of Optical Fiber Communication (Optical Society of America, San Jose, CA, 1996) paper WK14.

[20] Janet Lehr Jackel, and Dwight Richards, "All-optical stabilization of cascaded multi-channel EDFAs with changing number of channels," in proc. of OFC'97, San Jose, CA, Feb. 1997.

[21] A. K. Srivastava, Y. Sun, J. L. Zyskind, J. W. Sulhoff, C. Wolf, R. W. Tkach, "Fast Gain Control in Erbium-Doped Fiber Amplifier," in Optical Amplifier and Their Applications, Vol. V of 1996 Trends in Optics and Photonic Series (Optical Society of America, Washington, D. C., 1996) p. 24.

[22] A. K. Srivastava, Y. Sun, J. L. Zyskind, and J. W. Sulhoff, "EDFA Transient Response to Channel Loss in WDM Transmission System," IEEE Photonics Technol. Lett., vol. 9, no. 3, pp. 386-388, 1997.

CHAPTER 6

A NOVEL SHARED OPTICAL PROTECTION SWITCHING APPROACH FOR 4-FIBER WDM RING NETWORKS

6.1 Introduction

Network survivability is necessary for high speed optical networks carrying increasingly larger amounts of traffic. Technological advances have led to an increase in both the number of wavelengths and the bit rates that are being deployed in dense-wavelength division multiplexed (DWDM) networks. The consequences of a fiber cut or an optical fiber amplifier (OFA) failure are correspondingly magnified. The ring topology has become the de facto standard for intra-LATA, inter-office and loop deployment due to the improved survivability and bandwidth sharing that it offers [1].

SONET (Synchronous Optical Network) is currently the transmission and multiplexing standard for high-speed signals deployed by the Local Exchange Carriers (LEC) and Inter-exchange Carriers (IXC) in North America. A similar standard SDH (Synchronous Digital Hierarchy) has been adopted by telephone companies in Europe and Japan. All traffics traversing these networks are groomed at the transmitting end to satisfy the SONET/SDH format and the complementary processing done at the receiving end for traffic that is inherently non-SONET/SDH. Network survivability is almost always a SONET function, which imposes no limitation since only SONET formatted signals are transmitted. However, with the deployment of the underlying WDM layer a wider vision of survivability is under consideration [2]. Some network designers are pointing out

considerable economical advantages to be realized with a complete elimination of the SONET layer [3-5]. This will enable signals to be directly interfaced at the WDM layer, providing considerable cost savings and at the same time creating a more transparent network, as both SONET and non-SONET signals will be transmitted over the same fiber. In particular, researchers are proposing the direct mapping of ATM (Asynchronous Transport Mode) and IP (Internet Protocol) traffic to the WDM layer, bypassing the SONET equipment[3-6]. Although there are survival mechanisms built into these data-centric ATM switches and IP routers, restoration is in general slower than desired. Therefore, if nothing else, a significant speed advantage can be realized by protecting these types of traffic at the optical WDM layer. By so doing, and in accordance with layered architecture schemes, the survivability of the traffic is enhanced as there are multiple levels of protection. This in itself presents a non trivial problem; that of the proper interworking of the various levels of protection, that are more often than not developed independently of each other. Some means of coordination must be provided as redundancies at best, and contention at worst, can arise.

At the WDM layer there are two basic approaches to providing service reliability: 1) Automatic Protection Switching (APS) for both WDM point-to-point and WDM ring architectures, and 2) Using reconfigurable Optical Cross-Connect (OXC) Systems to provide WDM mesh restoration. WDM protection requires 100% redundancy and could result in a somewhat higher cost than WDM restoration. However, WDM protection allows simpler Network Elements (NEs), simpler technologies and operation procedures, simpler interworking, faster protection, and is based on more widely available

components. These advantages have made WDM protection the overwhelming choice for providing the 'first line of defense' in ensuring network survivability. On the other hand, WDM restoration can take seconds or even minutes depending on whether a distributed or a centralized management scheme is implemented. It has the advantage of being able to restore the network under multiple failure scenarios, at the same time making more efficient use of the available bandwidth [7]. If the cost can be justified, the overall survivability of the network can be improved by implementing some degree of WDM restoration to serve as the 'second line of defense,' to recover from some failure situations. In WDM networks the key network elements for realizing restoration are the wavelength selective crossconnects (WSXC) and the wavelength interchange crossconnects (WIXC) [4],[8]. WDM restoration schemes are covered at length in references [4],[9-15]. This work will focus on the 'first line of defense': WDM protection schemes.

This chapter will present a brief overview of the different optical protection switching schemes for currently deployed SONET ring networks. Alternative WDM architectures that closely mirrors each SONET implementation will then be presented. The types of failures that are likely in a WDM network are discussed with a view of how recovery can be realized. A discussion of the time scale to respond to failures and how this affects multilayer protection in a layered architecture is also presented. A detailed theoretical analysis of the difficulty of detecting fiber cuts in a transparent WDM network is presented. Different methods of detecting fiber cuts are evaluated and studied through simulation of a 3-WADM ring network with shared optical protection switching. The

focus of the simulations is on the dynamic effects of protection switching at the optical layer in a ring network with several in-line EDFAs between network elements (NE).

6.2 Background: Protection Concepts

Protection switching mechanisms fall in two fundamental categories: 1+1 protection and 1:N protection, where in the simplest case N = 1. The nature of the protection is often categorized as 1+1 Electrical or Optical Facility Protection or 1:N Electrical or Optical Facility or Equipment Protection [16]. At the network level, the protection provided is often a combination of different categories of protection. For instance, 1:N SONET APS could be offered at the client layer with 1:1 or 1+1 optical layer protection in a SONET/WDM combined protection scheme. These concepts can be applied to both point-to-point and ring architectures.

In 1+1 protection, traffic is sent over disjoint routes from the source to the destination via separate fibers. At the transmitting end a splitter can be used to direct data from a single laser source to both fibers. The transmission on both fibers is monitored at the destination and one selected for reception. The fiber carrying the selected transmission is called the working fiber and the other is called the protection fiber. If the transmission via the working fiber is degraded because of an amplifier failure or a fiber cut, the receiver switches to the protection fiber. This type of protection can be very fast as no signaling protocol is required between the transmitter and the receiver.

In 1:N protection, N working fibers share a single protection fiber. However, only failure of a single working fiber can be handled. Unlike the 1+1 protection scheme, traffic is not bridged to both fibers and under normal operation in which all the working fibers are intact, the protection fiber carries no traffic. If extra transmitters and receivers are provided, the protection fiber can be used to transmit preemptible lower-priority traffic, increasing the overall throughput of the network. In a SONET implementation of 1:1 protection an automatic protection signaling (APS) protocol is required to coordinate the switching at the transmitting and receiving ends.

After the restoration of a fiber in a 1+1 protection scheme, the repaired fiber becomes the protection fiber and the previous protection fiber assumes the role of the current working fiber. After a fault is repaired in a 1:N protection scheme, it is desirable to free the protection fiber so it can revert to its shared protection of N working fibers, or return to the transmission of lower-priority traffic. This type of protection is called reverting and can be executed automatically or manually.

Each link in a network carries traffic originating from and destining for different pairs of nodes. The traffic on a particular link can be protected by either path switching or line switching. In path switching (protection) the survival of each individual traffic stream is handled by the particular source and destination involved, regardless of where along the route the failure is located. In line switching, the failure is handled by the nodes adjacent to the fault, independently of the source and destination of each traffic stream. Line switching can be categorized as either span protection or line protection. In span

protection, the traffic between the two nodes adjacent to the failure is restored by switching to another fiber between the same two nodes. In line protection, the traffic is switched to a different route through the network between the same two nodes. In a ring network, line switching involves routing the traffic on the longer protection path all the way around the ring to the adjacent node.

6.2.1 SONET Electronic Layer Rings

The Unidirectional Path Switched Ring (UPSR) and the Bidirectional Line Switched Ring (BLSR) are the two major types of SONET electronic layer rings that are defined. Correspondingly, there are two approaches to protection switching in SONET rings namely, path protection and shared protection. Path protection has applications beyond physical ring networks as it can be implemented independently of the network architecture [17]. All of the protection schemes to be discussed here are designed to deal with single failures, i.e. a single fiber cut or a single amplifier failure. An exception to this occurs in the 4-fiber ring with span switching, where multiple simultaneous failures can be handled in some cases. The UPSR, the 2-fiber BLSR, the 4-fiber BLSR and the Unidirectional Line Switched Ring (ULSR) constitute the four major SONET rings [18]. The ULSR does not provide for reuse of dropped bandwidth and have not been given as much attention as the other three architectures. It will not be discussed further here; however, considerable detail is given in [18]. Performance monitoring in SONET networks allows for the efficient and timely correction of potential problems that if allowed to go undetected can adversely impact customer service [19]. In SONET there is

a layered set of performance monitoring parameters that allow a degradation to be detected and pinpointed to the exact location of the fault through the monitoring of the section, line and path performance parameters.

6.2.1.1 Unidirectional Path Switched Ring (UPSR)

The UPSR is a 1+1, 2-fiber, unidirectional Path-layer dedicated protection architecture. Diverse routing in opposite directions around the ring is used to ensure that both directions of the signals will not be severed at the same time due to a single failure. The two copies of the signals traversing opposite directions around the ring can either be generated by separate transmitters or can be generated once and split optically, provided the 3 dB reduced power level does not adversely affect the power budget of the ring. Detection of failures is a SONET function and the appropriate alarm indicating signals (AIS) are inserted onto each affected path such that the nodes can switch to the protection fiber to restore the affected paths.

6.2.1.2 Bidirectional Line Switched Ring (BLSR)

The BLSR is a bidirectional, 1:1 line layer shared protection architecture. The 2-fiber and 4-fiber BLSR have been defined. The decision on which architecture to deploy depends on several factors, including: traffic, cost, reliability and network design. A comparison of the cost and reliability issues associated with the 2-fiber and the 4-fiber BLSR is discussed in [20].

6.2.1.2.1 2-Fiber BLSR

In the 2-fiber BLSR, half of the bandwidth (time slots) on each of the two fibers is used for protection of the other fiber's working traffic. In so doing, a logical 4-"channel" bidirectional ring is created from the two physical fibers. Protection switching is coordinated by an automatic protection switching (APS) channel via the K1/K2 bytes of the SONET line overhead, using the protection bandwidth. Protection switching is accomplished by performing limited time slot interchange (TSI). The 2 fiber BLSR is line protected (ring switched) by having each of the add drop multiplexers (ADM) adjacent to the failure bridge its working traffic in the direction of the failure to the protection fiber in the direction away from the failure. At the same time, the ADMs switch to the protection fiber in the direction away from the failure to select the working channels that were coming from the direction of the failure. This switching is always done electronically to ensure the proper alignment of the time slots.

6.2.1.2.2 4-Fiber BLSR

In the 4-fiber BLSR, there are two fibers carrying working traffic and two fibers dedicated to the protection of the working fibers. In addition to ring switching, which is accomplished in a similar manner as explained above for the 2-fiber BLSR, the 4-fiber BLSR can also support span switching in cases where only the working channels between adjacent nodes are affected. Ring switching is used when both working and protection fibers are affected. Inter-nodal communication is required to prevent misconnections, which can occur in rings with bandwidth reuse.

The capacity of the 4-fiber BLSR is twice that of the 2-fiber BLSR since there are two pairs of working and protection fibers (i.e. it can carry twice as much working traffic and twice as much extra low priority traffic). On the other hand, the 4-fiber BLSR, being a 1:1 electrical protection architecture, requires duplicate electronics, and thus will cost approximately twice as much as the 2-fiber BLSR.

6.2.2 SONET Optical Layer Protection

Alternative architectures that involve either all-optical protection switching or a combination of electrical and optical protection switching have been proposed [16]. One such architecture is the 4-fiber passive shared protection ring (4-fiber P/SPRING) BLSR architecture. It uses optical switches in place of duplicate electronics to protect against link failures. All switching is done in the optical domain with only ring switching being supported. The SONET ADM is a conventional 2-fiber BLSR SONET ADM using a slightly modified 2-fiber BLSR protocol to accomplish the ring switching [16],[21].

6.2.3 WDM Ring Architectures

There are two fundamental limitations of self-healing ring (SHR) networks based on single channel SONET ADMs. First, extending the capacity beyond 10 Gbs is very difficult and costly. Furthermore, this capacity has to be shared with all the nodes in the ring. Second, the cost of the 4-fiber BLSR, which uses two SONET ADMs at each node, one for the working path and the other for the protection path, is relatively high. Consequently, multiwavelength survivable ring network architectures using WDM

technology for growth, and optical amplifiers and optical switches for protection are the architectures of choice to meet the increased capacity demand and reliability requirements of future transport networks [1],[22]. Also, WDM creates opportunities for consolidation of switching resources that can result in substantial cost savings [23]. However, the consequences of a fiber cut scales with the number of wavelengths and therefore, protection of traffic in a WDM network is of utmost importance to network operators. The construction and protection concepts used in SONET have close analogies in WDM ring networks. However, WDM rings require more complex components that can render the network less reliable, and therefore make protection even more important. Typically, the nodes in a WDM ring are Wavelength Terminal Multiplexers (WTM), Wavelength Add/Drop Multiplexers (WADM), Wavelength Selective Crossconnects (WSXC), and in-line Erbium-doped Fiber Amplifiers (EDFAs) for multiwavelength amplification. The WTM, WADM and WSXC are constructed from elementary components such as laser arrays, filters, switches and amplifiers that will pose reliability concerns that are generally non-existent or less critical for single wavelength SONET systems. Not all the wavelengths will be dropped and converted to electrical signals at each node and this transparency creates fundamental limitations unique to WDM networks. Transparency complicates the monitoring and management function of the network[24-26]. The impact of transparency on optical protection switching in a WDM network will be discussed in details in Section 6.3.

Both path and shared protection architectures are defined for WDM ring networks. Path protection, with each wavelength channel independently protected (i.e. Optical Channel

Protection (OCHP)) is inherently less complicated than path protection in SONET since each individual connection, which can far out number the number of wavelengths, needs to be protected in the latter. Shared protection can be implemented to protect individual wavelengths, or in the more popular approach, the fiber as a whole (i.e. Optical Multiplexed Section Protection (OMSP)). In the following sections the Unidirectional Self-Healing WDM ring and two flavors of the Bidirectional Self-Healing WDM ring will be discussed.

6.2.3.1 Unidirectional WDM Ring

This 2-fiber ring architecture shown schematically in Fig. 6.1 is similar to a SONET UPSR architecture. In fact, a unidirectional WDM ring network with N wavelengths is logically equivalent to N overlapping SONET ring networks that all subtend the same nodes in a Space Division Multiplexing (SDM) network architecture. However, using N wavelengths instead of N fibers saves on equipment and facilities such as amplifiers and fibers. It also allows for the consolidation of Network Control and Management (NC&M) equipment [27].

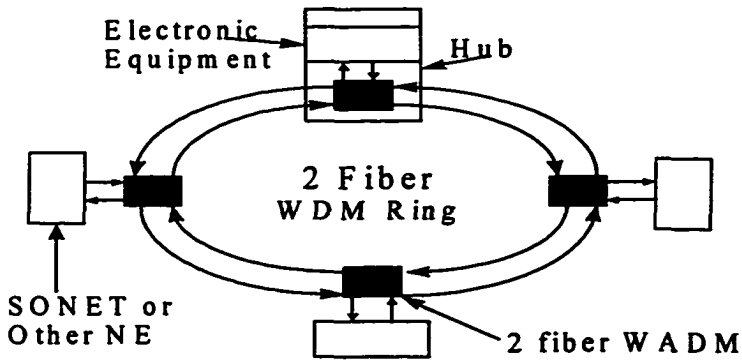

Figure 6.1 2-fiber Unidirectional Path Protection Switch (UPPS) WDM Ring Network

Each optical path is assigned a unique wavelength to satisfy the demand between two nodes. That wavelength cannot be reused on any other path. Therefore, the BW limitation of UPSR in SONET translates to wavelength limitation in the unidirectional path switched WDM ring. There are several approaches to protecting the client equipment and transponders, including: 1) 1+1 OCHP with passive splitters at the source, and per-wavelength optical switching at the destination. 2) 1:1 OCHP with per-wavelength optical switching at both the source and destination of each connection. This architecture avoids the potential reliability problems of loopback switches (LBS) that are generally used in OMSP schemes. LBS may present single point of failure vulnerabilities with large failure group sizes [4].

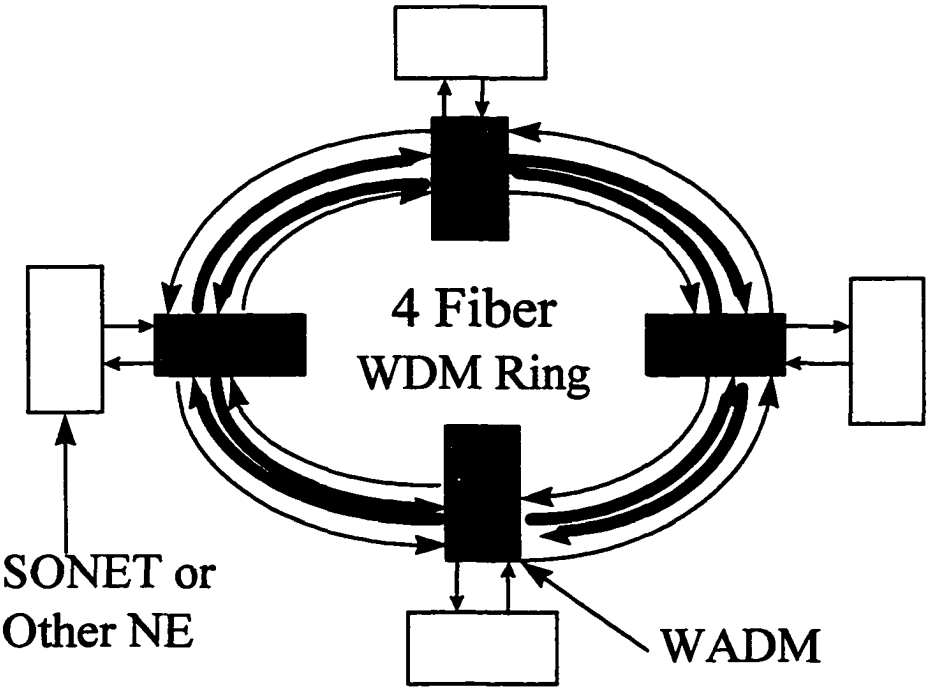

Figure 6.2 Generalized picture of a 4-fiber WDM ring. The darker fibers are the working fibers and the lighter fibers are the protection fibers. The WADMs drop or add any combination of wavelengths from the working fiber.

6.2.3.2 Bidirectional 2-Fiber WDM Ring

The operation of the bidirectional 2-fiber WDM ring is very similar to the more popular 4-fiber design, therefore, its description here will be very brief. Both path and shared protection can be supported. In path protection, each individual wavelength is protected and in shared protection, either the fiber as a whole or the individual wavelengths can be protected. The shared protection design mirrors the 2-fiber BLSR SONET architecture closely, however, there are a few fundamental differences. The path protected design is unique to WDM as there are no bidirectional path switched architectures in SONET. The main reason is the large number of paths that would have to be switched as a result of a single failure. Like the 2-fiber BLSR, each fiber is used to carry both working and protection traffic. Time-slot assignment becomes wavelength assignment in the WDM architecture, as half the wavelengths on each fiber are used for working traffic and half for protection. Protection is accommodated by having complementary subsets carrying the working and likewise the protection traffic in opposite directions on both fibers. However, each of the WDM MUX/DEMUX pairs must be capable of combining/ separating the complete set of wavelengths in the system to ensure recovery from failure conditions.

6.2.3.3 Bidirectional 4-fiber WDM Ring

The bidirectional 4-fiber WDM ring is shown schematically in Fig. 6.2. There are two working and two protection fibers. Both path and shared protection as described above

for the 2-fiber design, can be supported. The path protection architecture is a 1+1 optical

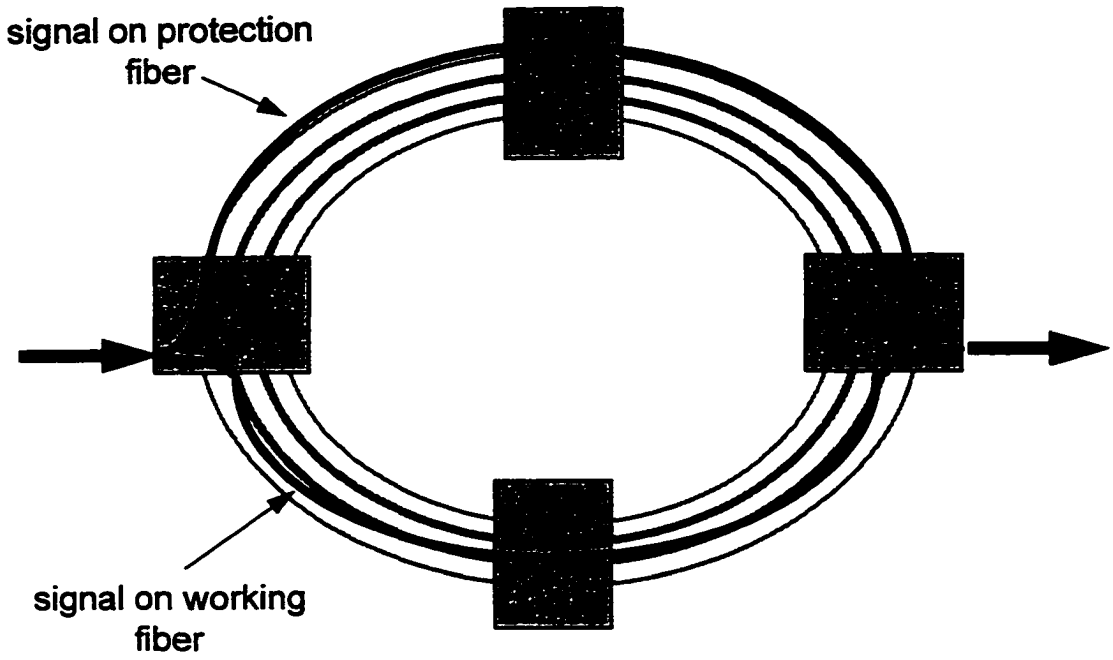

Figure 6.3 The 4-fiber ring with path protection. Path protection is shown for a single wavelength. Duplicate optical paths are established, and a copy of the signal is sent over each path If the working path is interrupted, receiver uses signal from protection path.

facility design as shown in Fig. 6.3. Therefore, the monitoring and protection switching is carried out at the receiving end of each individual path. On the other hand, the shared protection design shown in Fig. 6.4 is a 1:1 optical facility design. The protection fibers carry no traffic when the working fibers are intact as shown in Fig. 6.5, for a signal going from NE1 to NE3. Each working fiber/protection fiber pair shown in Fig. 6.4 will be treated independently but similarly for the purposes of protection switching. When there is a fiber cut between NE4 and NE3 as shown in Fig. 6.6, a LBS at NE4 switches the traffic from the working fiber to the protection fiber and a similar switch at NE3 switches the traffic coming in from the protection fiber to the working fiber as shown in the

Figure. Therefore, the signal takes the longer protection path around the ring to its destination. This ring switching also allows the network to survive certain failures within the network elements and the failure of an in-line amplifier, which is treated in much the same way as a fiber cut. Protection is local as the affected traffic is protected by the two LBSs adjacent to the failure.

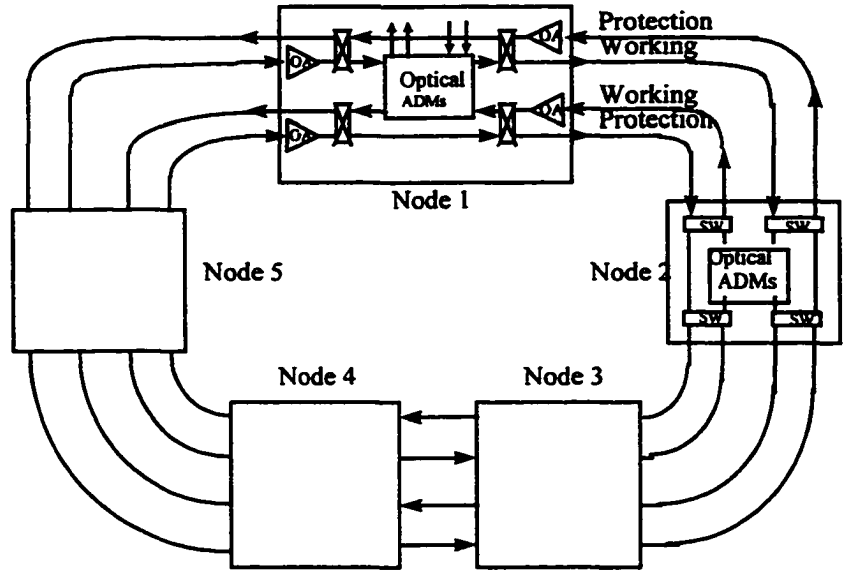

Figure 6.4: 4-Fiber WDM BLSR

6.2.4 Comparing Path and Shared Protection

Table 6.1 makes a preliminary comparison of path and shared protection as it relates to a 4-fiber bidirectional WDM ring. Path protection limits wavelength reuse similar to the

limitations on BW reuse in path protected SONET rings. Shared protection does not

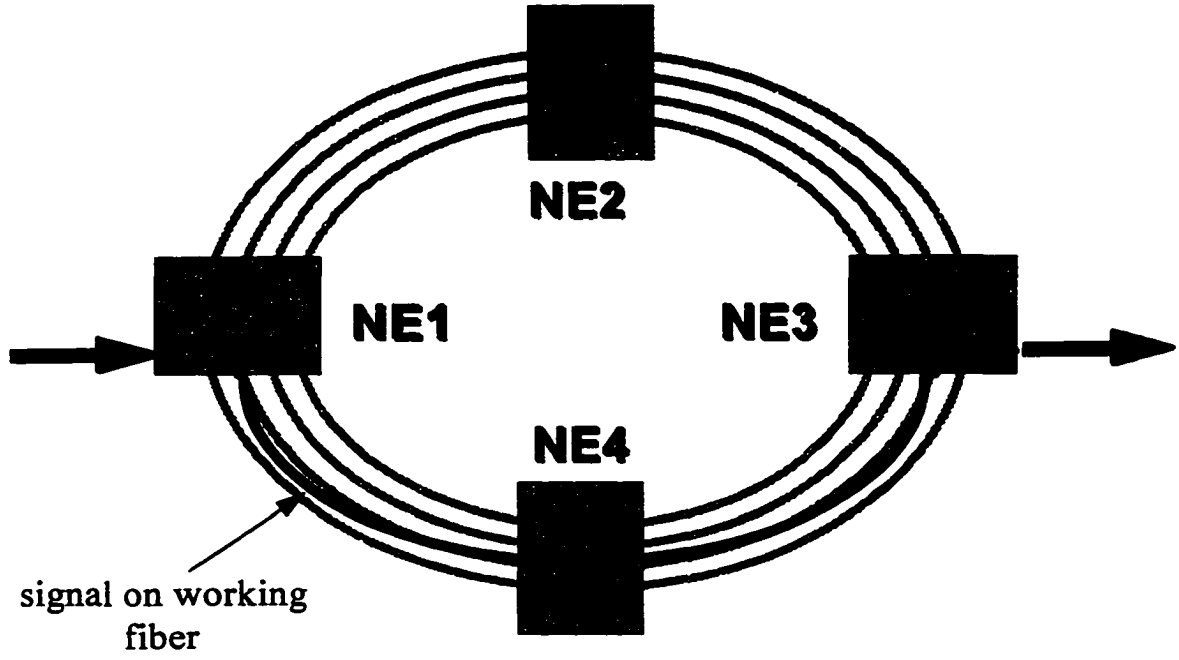

Figure 6.5 When shared protection switching is used, no signals are on the protection fiber when the working fiber is intact.

impose the same limitation on wavelength reuse but as we will see below, the problem of misdirected traffic is further complicated by the wavelength reuse property in WDM networks. Equipment costs are higher in path protection because the nature of the protection requires complete redundancy of the wavelength add/drop multiplexers. On the other hand, shared protection requires only the additional monitors and protection switches. However, path protection does have its merits. Among these, is the ease of detecting failures, since the signal is always sent on both fibers in opposite directions around the ring. Detecting failures in a shared protection environment is complicated by the saturated EDFAs that are indispensable in WDM networks [26]. This issue will be discussed in considerable detail in Section 6.3.

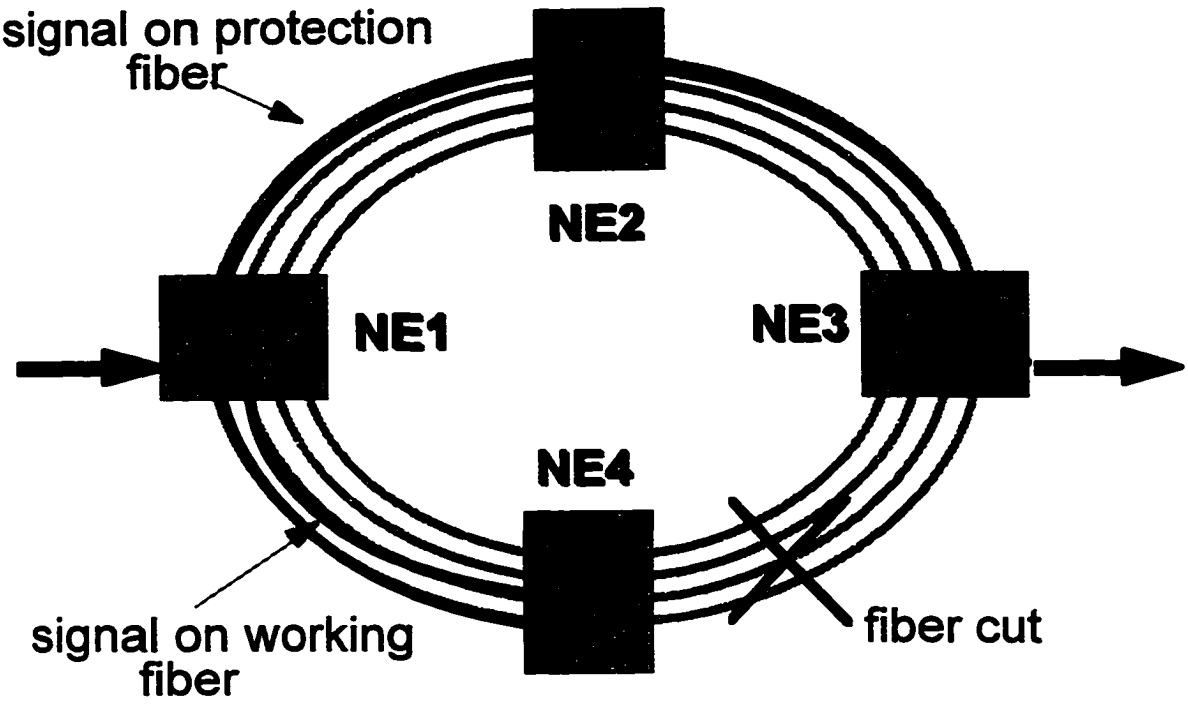

Figure 6.6 In shared protection the cut is isolated by the LBSs in the adjacent network elements.

	Equipment cost	Difficulty of detecting failure	Limitations on wavelength reuse?
Path protection	higher	less	yes
Shared protection	less	greater	no

Table 6.1 Comparison of path and shared protection in a 4-fiber bidirectional WDM ring.

6.2.5 Misdirected Traffic

The traffic that originates at or is destined for a failed node cannot be restored and therefore can become misdirected. The problem of misdirected traffic is of particular importance in WDM networks with shared protection switching. The wavelength reuse property of these networks can lead to violation of the Distinct Channel Allocation (DCA) constraint (channels sharing the same fiber must use separate wavelengths to avoid so called 'color clash'). There is no obvious means of dealing with misdirected traffic and it will be a serious concern for users of the network, as the potential for security violation will not go unnoticed. Some means of 'squelching' this traffic to avoid wrong connections must be implemented in future WDM transport networks.

6.2.6 Types of Failures

The last thing communication network engineers want to be heard talking about is the failure of a system that they designed. For service providers failures are bad for business and such occurrences are kept away from the public domain as much as possible. Furthermore, the Federal Communication Commission (FCC) requires that only major failures lasting more than 30 minutes must be reported. Therefore, it is not difficult to understand how difficult it is to get an objective measure of the extent and distribution of failures in today's telecom networks. As OC-192 rates and higher are deployed the impact of the larger failure group sizes is certain to impact the reliability of the network. In fact, it has been shown that OC-192 system outages would become FCC reportable at only 23% utilization [28]. Some of the failures that are likely in a 4-fiber WDM ring with

shared protection switching are discussed briefly below. A more thorough treatment is given in [26] and [29].

6.2.6.1 Fiber Cuts

Fiber cuts are the most common failures reported to the FCC. This is because of the severe consequences of such outages and not necessarily because it is the most common failure. In a 4-fiber WDM ring with shared protection switching fiber cuts are protected by ring switching as explained above.

6.2.6.2 Amplifier Failures

Pump laser failure accounts for the most common optical amplifier failure. However, breaks in the optical path or a failure in the monitoring which is used to control the amplifier performance can also account for amplifier down time. Line amplifier failures are treated in much the same way as a fiber cut in the 4-fiber WDM ring with shared protection switching. The failure of an amplifier within the network element must be protected by other means.

6.2.6.3 Optical Multiplexers

Many of the filters used to construct optical multiplexers require some kind of temperature control circuitry to prevent the passbands from losing registration with the WDM wavelengths. Fiber breaks within the multiplexer and the optical adhesives that connect the fibers to the device can also raise reliability concerns. A multiplexer failure

can affect a subset of wavelengths or the entire set of wavelengths. Such failures are difficult to deal with in the 4-fiber WDM ring with shared protection switching and can lead to loss of service, as manual intervention may be necessary. Monitoring multiplexer failures and provisioning protection, however limited it may be, is best handled at the SONET electronic layer or at the client layer for non-SONET signals.

6.2.6.4 Optical Switches

In Chapter 2, we saw that there is a wide variety of optical switches based on different technologies, available from suppliers. These switches can be used for adding and dropping of channels, be integrated into optical crossconnects for reconfiguration of the network, or can be the enabler of the protection switching functionality. Interruption of the optical path or malfunction of the switch fabric are likely failures for optical switches. Optical transparency makes such failures difficult to deal with in shared protection switching and relegating protection to the SONET or the client layer is the prudent thing to do.

6.2.6.5 Transmitter/ Receiver

Transmitters and receivers can fail for a number of reasons. The failure can be in the electronics or can be a result of misalignment which causes loss of wavelength registration. Protection is best provided by client layer specific mechanisms, such as SONET APS based on 1:N redundancy.

6.2.6.6 Loss of Electrical Power

Loss of electrical power can result in an in-line amplifier failure or the failure of an entire node. The failure of an in-line amplifier is treated the same way as a fiber cut. In the case of a node failure, the failed node is isolated by the LBS in the adjacent nodes, thus preventing a complete failure. However, traffic associated with the failed node can become misdirected as explained above.

6.2.7 Transparency Related Problems

In a WDM network some wavelengths are dropped at a node and some are passed in their optical form to the other nodes or to the client layer. This transparency complicates the management and identification of faults in the network as the nodes will not have access to the data communication channel (DCC) of the pass through channels [30-31]. Transparency leads to the accumulation of signal impairments such as crosstalk, chromatic dispersion, PMD and amplified spontaneous emission (ASE) noise. Only the last of these is of any consequence for protection switching as explained below.

6.2.7.1 Detecting Fiber Cuts

Detecting fiber cuts in a transparent WDM network is complicated by the same EDFAs that make WDM possible. At the optical layer, the presence or absence of optical power is the simplest means of monitoring failures. However, optical transparency which can lead to ASE noise accumulation in chains of saturated EDFAs can mask real failures, thus causing inconsistent protection switching. In Section 6.3 we will use detailed simulation

to examine the difficulty of detecting a fiber cut, due to transparency and ASE noise accumulation, when varying numbers of EDFAs are present between the cut and the monitor point.

6.2.7.2 Lasing on the Protection Fiber

In the 4-fiber WDM ring with shared protection switching the protection fiber carries no signals when the working fiber is intact. The protection ring is thus a closed path, and since the round-trip gain is greater than the round-trip loss for some wavelengths, a large ring laser can result. This lasing has been observed experimentally in a LEC testbed at Bellcore. The implications of this lasing for protection switching in the 4-fiber WDM ring with shared protection will be examined through detailed simulations in Section 6.3.2.5

6.2.8 Escalation Issues

One benefit of transparency is that it allows heterogeneous traffic to be transported over the same infrastructure with negligible interference. For example, the vision for future networks have ATM, IP, SONET, analog signals, and any future formatted signals, traversing the same fiber in a WDM network. Such flexibility complicates the management of the network. Integral to this complication is the protection strategy that will ensure network survivability. Protection can be offered at the IP, ATM, SONET, or WDM layers. The coordination of the various levels of protection at the different layers is referred to as 'escalation strategies'. Multiple layers of protection in a layered

architecture is attractive since the survivability of the signals is enhanced. This benefit will only be realized if careful coordination of multi-layer survivability is implemented such that contentions and redundancies don't render the network inoperable or inefficient. In order to decide how much protection should be offered, single layer strategies, two layer strategies and three layer strategies were investigated [5]. Two layer strategies were considered the optimum choice to compromise between the reliability and the complication of the network. Escalation strategies are discussed at length in References [5] and [21].

6.2.9 Time Scale to Respond to Failures

SONET declares a loss of signal (LOS) condition if a signal is missing for 2.3-10 μs. The SONET equipment is required to initiate protection switching within 10 ms of detection of a failure and complete it within 50 ms. As we saw in Chapter 2, the switching speed of optical switches vary from the very fast lithium niobate based designs to the much slower optomechanical designs. In a 4-fiber WDM ring with shared protection switching it is impossible to prevent the onset of SONET protection switching regardless of the speed of the optical switches, due either to the propagation delay of the signal around the longer protection path or due to the loss of framing bits [2]. Other architectures, such as those based on path protection may benefit from fast optical switches. Escalation strategies are needed to deal with the 'two layer strategy' based on SONET/WDM protection in the 4-fiber WDM ring. A hold-off time has been suggested for the SONET equipment to allow for the simpler WDM survival mechanism to complete its restoration before SONET

protection switching is invoked, but this would require changes to the widely deployed SONET networks, and is thus less desirable. Alternative solutions are discussed in [5].

6.3 Detecting Fiber Cuts in a WDM Ring with Shared Optical Protection Switching

Optical protection switching cannot be implemented without a fast and unambiguous method for detecting fiber cuts in optically amplified WDM links. As the distance and number of EDFAs between the cut and the monitor point increases, the accumulation of amplified spontaneous emission (ASE) noise complicates the detection of the cut. This section has two objectives. First, some general concepts and constraints of different methods of detecting fiber cuts are presented. Second, these concepts are studied in detail through an original simulation technique of a 3-WADM ring with shared protection

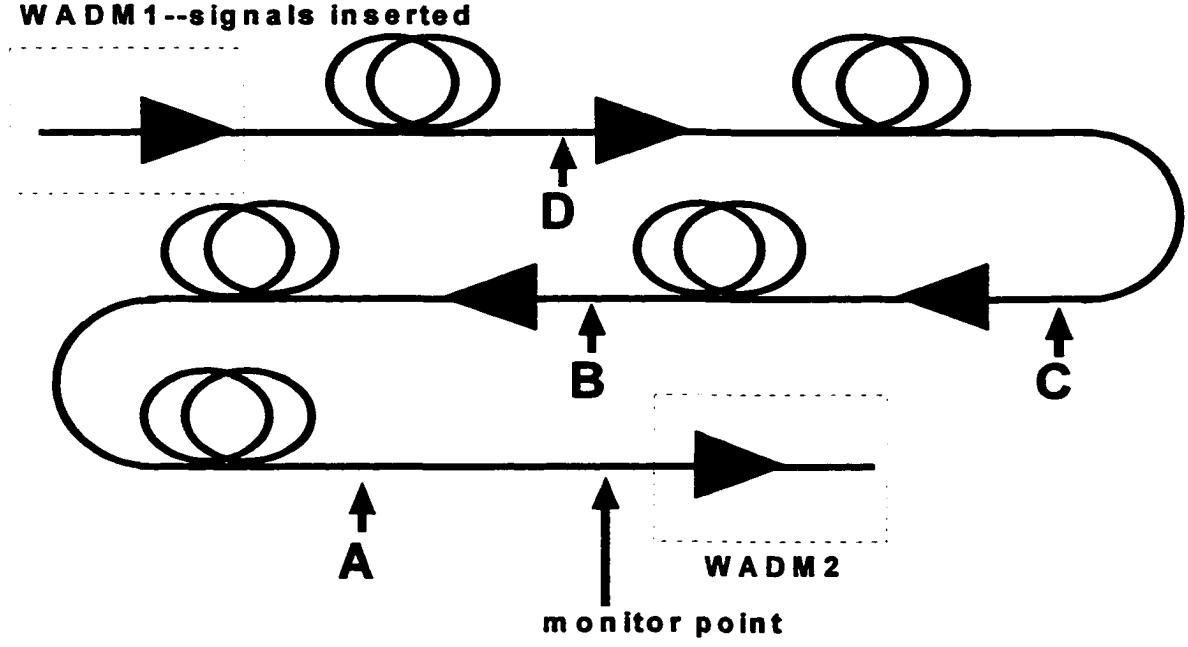

Figure 6.7 In a chain of amplifiers which has been cut at some point, the optical power reaching the monitoring point depends on the location of a cut. For a cut at point A, all optical power is lost, but for cuts at points B-D, ASE from the amplifiers produces significant power at the monitor.

switching [26]. The simulation explores a number of case studies which shed light on the virtues and drawbacks of shared protection switching in a transparent WDM ring network. Unlike 1+1 path protection schemes, the protection fiber normally carries no data except when protection switching is initiated. Due to the transparency of these networks, signal-to-noise ratio (SNR) and bit-error-rate (BER) measurements are not practical 'quality of service' measurements on which to base the need for protection switching. The optical power levels are the simplest and most readily available measurements at the optical layer.

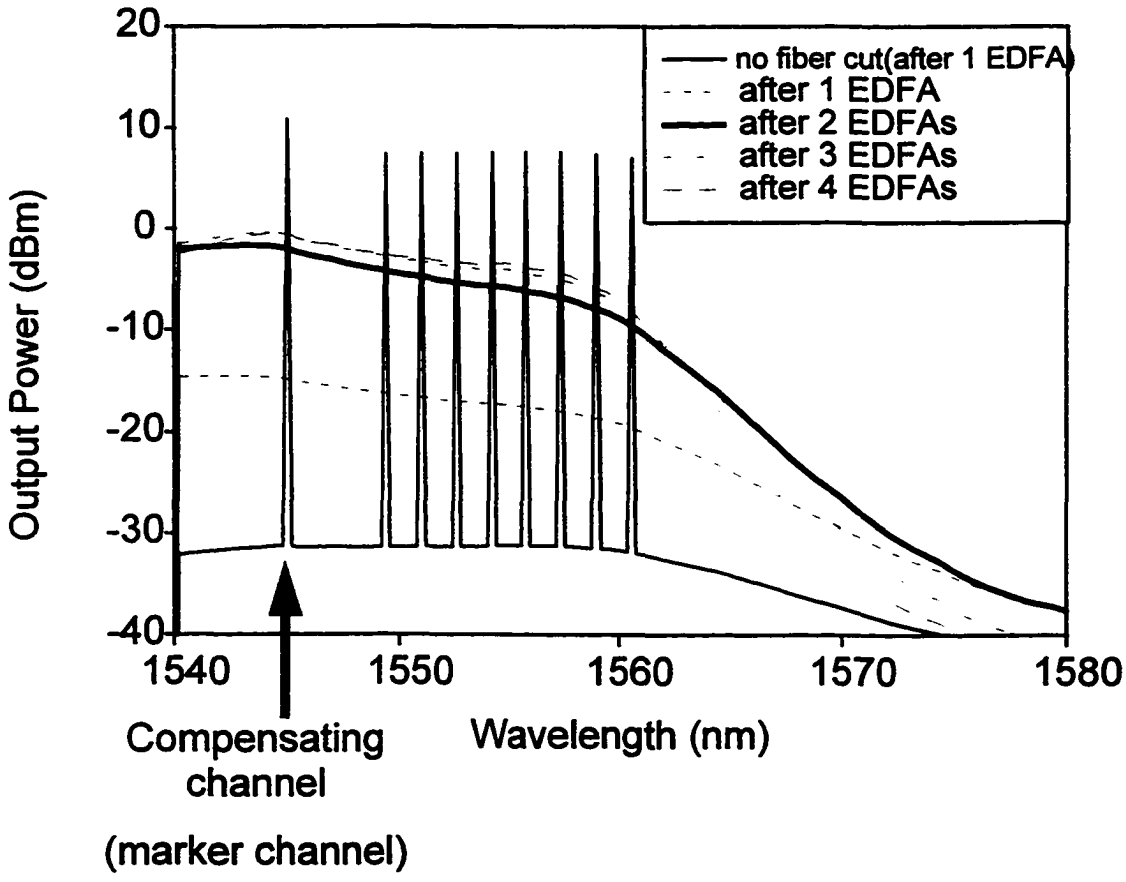

Figure 6.8 Optical spectrum before and after a cut. After more than one EDFA, the ASE from the amplifier effectively replaces the lost signal power.

6.3.1 General Concepts

An effective measurement of a fiber cut or amplifier failure must have high contrast between its value when the fiber is intact and that when there is a failure. We have set the somewhat arbitrary contrast level of 10 dB. Such a high value is necessary for distinguishing a true fiber cut, which demands protection switching, from a degraded power level (the result, for example, of degraded EDFA gain or of increased fiber loss) which may require a different response. The accuracy of fiber cut detection should be independent of the location of the cut, and a technique which gives false alarms is as unacceptable as one which fails to detect actual cuts. Fig. 6.7 shows a simplified diagram of two wavelength add/drop multiplexers (WADMs) with 3 in-line EDFAs between them. A fiber cut can occur at any of the points labeled A-D. Due to ASE noise accumulation, the optical power level at the monitor before WADM2 depends on where the cut occurs and therefore complicates the detection process. For a cut at point A no in-line amplifiers are encountered but for cuts at B, C, and D, 1, 2 and 3 EDFAs respectively, are encountered between the cut and the monitor. Fig. 6.8 shows the steady state optical spectrum before and after a fiber cut for varying numbers of in-line EDFAs between the cut and the monitor point. After 3 or more EDFAs the total power reaches a constant and therefore affects our ability to detect failures if there is not enough contrast relative to before the cut. The Figure also shows the compensating channel that was discussed in Chapters 4 and 5, which as we will see, can also serve as a marker channel for protection switching purposes. The following three sections discuss the virtues and drawbacks of three different means of detecting a fiber cut in the presence of in-line

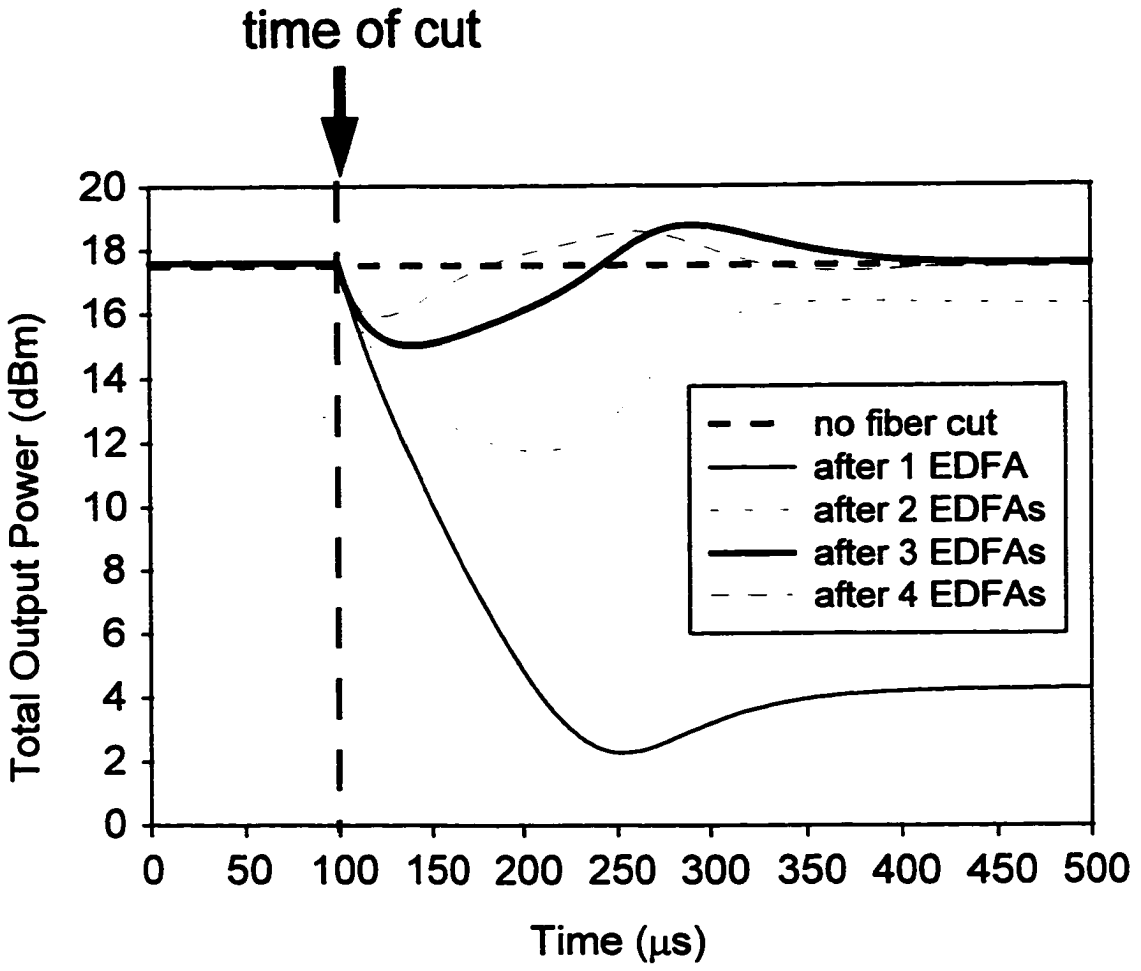

Figure 6.9 Total power after in-line EDFAs for a fiber cut at 100 μs. After more than two EDFAs total power is essentially replaced by ASE. Restoration occurs in < 200 μs.

EDFAs. We focus on time resolved computations as we are also interested in how the dynamics of the EDFAs affect the protection switching mechanism. We also assume that the cut last 100 μs in all three cases.

6.3.1.1 Detecting Total Power

Measuring the total optical power at the input of a network element (NE) appears to be the simplest and most obvious indicator of severe degradations such as fiber cuts and

amplifier failures. However, because of the presence of amplified spontaneous emission (ASE) noise, when there are more than a single EDFA between a cut and a monitor point, the total power recovers in a few hundred microseconds. Therefore, such a measurement cannot be used in systems with two or more in-line EDFAs between network elements (NEs). Fig. 6.9 shows a time resolved simulation of the evolution of the total optical power for a chain of EDFAs. As is clear from the Figure, after two or more in-line EDFAs the total power is almost indistinguishable from that before the cut. An alternative approach that provides enough contrast to ensure consistent protection switching is needed.

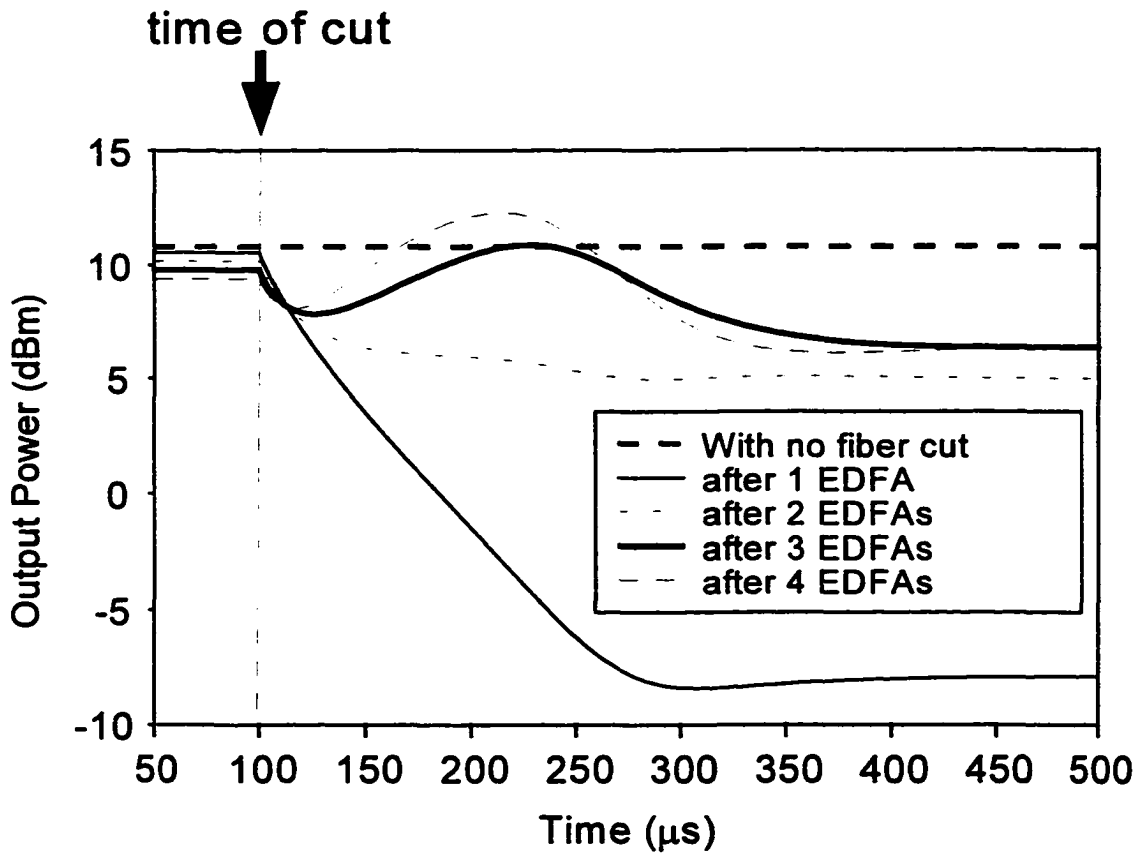

Figure 6.10 Optical power in a 0.8 nm spectral band. Contrast between power levels for uncut and cut fiber is much less than 10 dB for more than 2 in-line EDFAs.

6.3.1.2 Detecting a Narrow-band Signal

Monitoring a narrow-band (marker wavelength) signal rather than the entire spectrum will produce better contrast. If a marker wavelength with high enough power is inserted at each NE there will be sufficient contrast to unambiguously trigger a protection switch when a cut occurs. However, high power in a marker wavelength is less desirable since this will reduce the gain of the information carrying signals. A marker with power equivalent to a single channel will probably be acceptable for practical implementations. For currently available, relatively inexpensive filters with a bandwidth of 0.8-1 nm, the

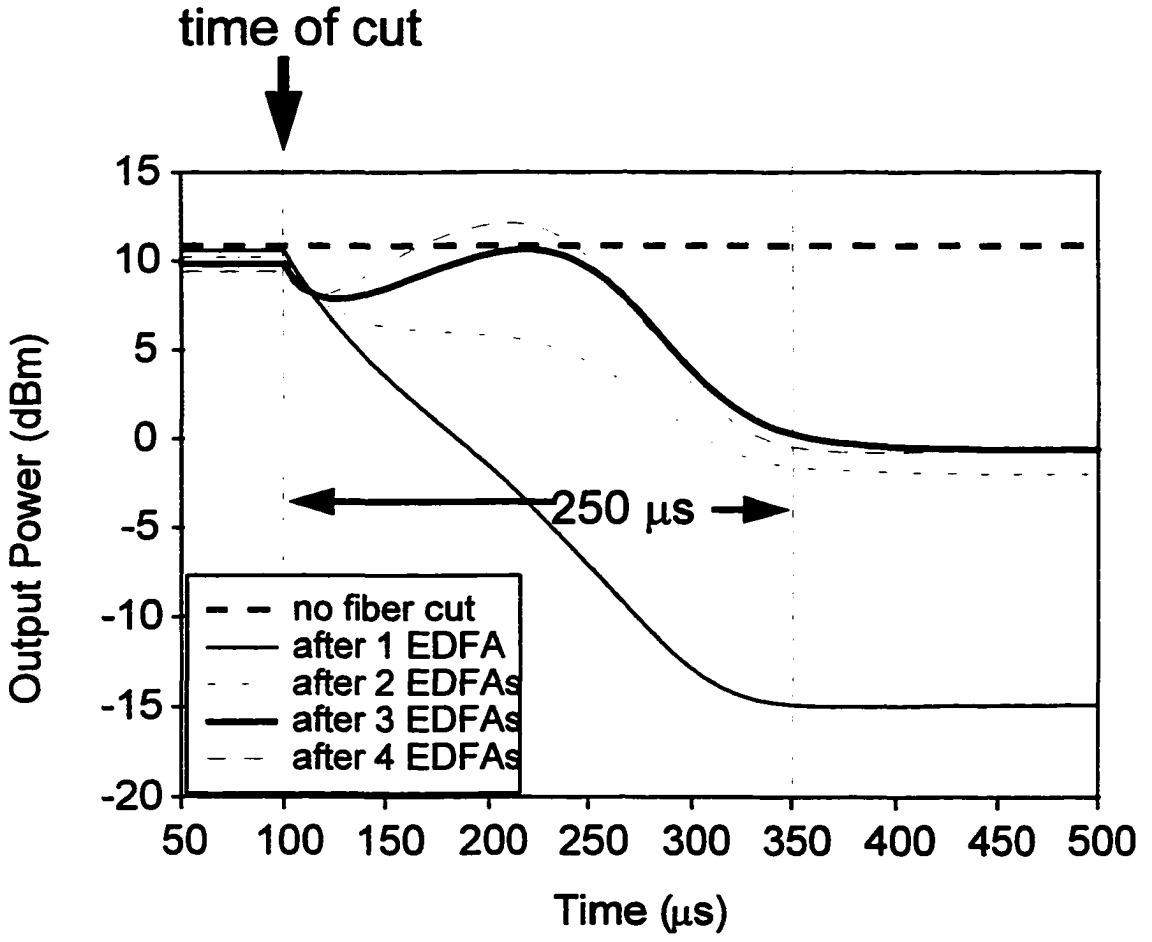

Figure 6.11 Optical power in a 0.2 nm spectral band. Even after 4 EDFAs there is still excellent contrast. (Cut last for 100 µs)

contrast is reduced to much less than 5 dB after 2 or 3 in-line EDFAs as shown in Fig. 6.10. If we make the filter bandpass much smaller, as shown in Fig. 6.11 for a 0.2 nm bandpass, we can achieve the 10 dB contrast requirement for as many as 4 in-line EDFAs. However, this narrow filter bandpass places possibly unrealistic demands on marker wavelength-filter alignment. Therefore, monitoring changes in the power of a marker wavelength improves on the total power detection scheme but is still a very limited solution. Using total power or a single narrow-band signal in the presence of in-line EDFAs will not in general give the 10 dB level of discrimination.

6.3.1.3 Novel Differential Measurement Scheme

To avoid the problems associated with the total power detection scheme and the restrictions on the detection of a single narrow-band signal, we propose using a differential power measurement to compare the power in a marker wavelength spectral band to that in a non-signal wavelength region [33]. This differential measurement scheme is a general solution that works if we have zero, one, or even ten in-line EDFAs between the cut and the monitor point. Fig. 6.12 illustrates the results when there are two in-line EDFAs between the cut and the marker. When the fiber is intact, the ratio of marker wavelength to nearby non-signal wavelength is greater than 30 dB, and reduces to approximately 0 dB after the cut. A similar change in ratio will be seen regardless of the number of EDFAs between the cut and the monitor. The results in Fig. 6.12 assume that the marker and nearby non-signal channel have nearly equal gains (only 3 nm apart). As will be shown below, the power ratios may be different if the two channels have different

gain, but a large difference in power ratios will be observed regardless of the location of the cut.

The marker wavelength that is detected at the monitor is inserted at the preceding network element (NE). Therefore, at most one additional laser source at each WADM will be necessary (two if we consider both protection and working fiber pairs. For economy, it might be possible to use one source plus a 1 × 2 splitter, depending on the relative cost). However, a method that makes use of an automatically generated marker wavelength [34] that does double duty will be described below. At the monitor, the ratio of the two signals is determined and compared with a preset threshold. If the difference is below the threshold, a protection switch is triggered after a hold-off time during which no further threshold passing occurs. The assumption is that for a fiber cut the contrast will be reduced and will remain below the threshold for longer than a certain minimum time. This hold-off time is necessary to eliminate erroneous switching due to short term dynamic perturbations of the network that can result in fluctuations of power levels about the threshold, and to allow the EDFAs to return to a steady state condition after loss of signals; a process which can take hundreds of microseconds to complete. We will examine this issue in more detail in Section 6.3.2.7. The method of detection that is being proposed here will be faster than the time to saturate the EDFA, since the marker channel power will be reduced significantly at the moment of the cut and will then grow simultaneously with the non-signal channel. Therefore, the ratio will be well below the threshold for protection switching, long before the ASE has saturated the EDFAs. This can be observed from Fig. 6.12 where the marker channel first experiences a dip in power

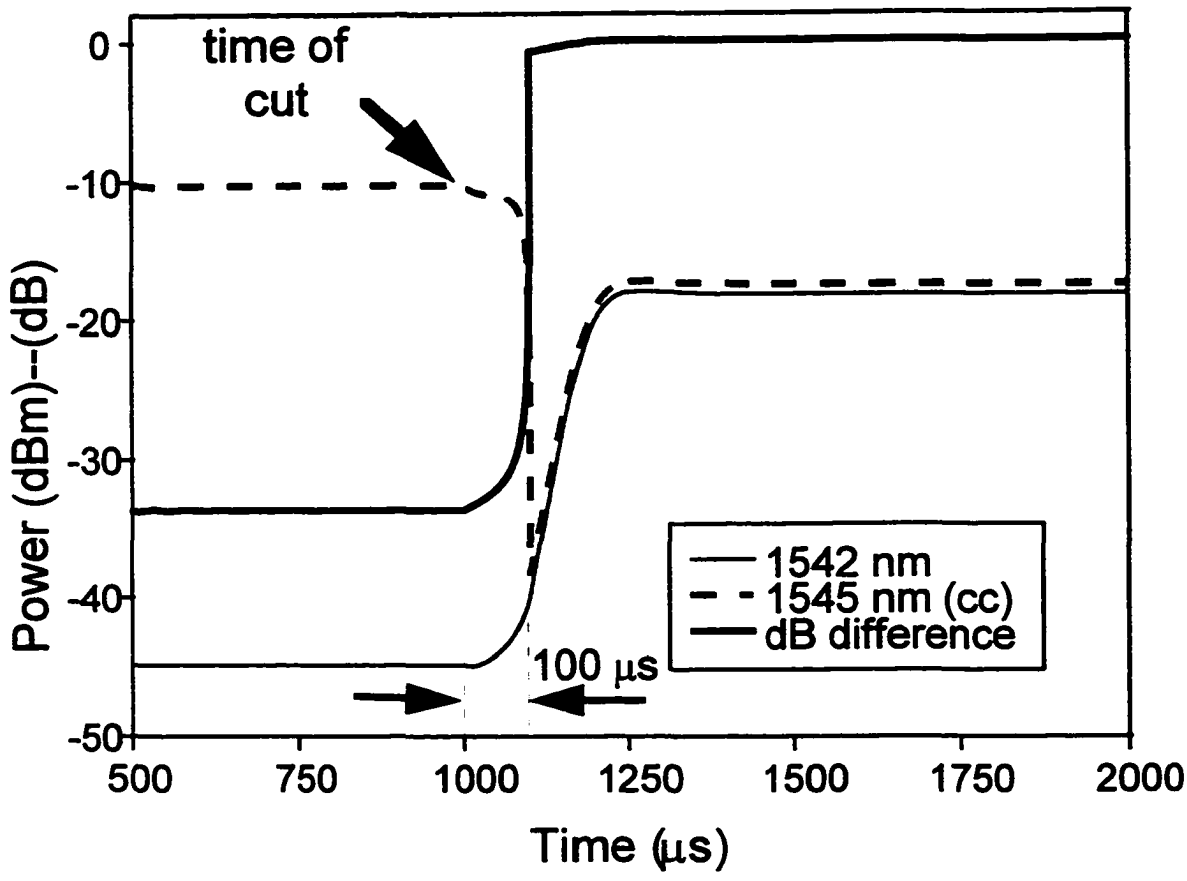

Figure 6.12 Optical power before and after a fiber cut at 1 ms, in the marker channel (1545 nm) and a nearby, non-signal channel (1542 nm), and the ratio of those powers. There are 2 in-line EDFAs between cut and monitor as shown in Fig. (6.7)

followed by a rather slow recovery determined by the dynamics of the EDFA. The response time is approximately 100 μs (cut last 100 μs) which is faster than the approximate 250 μs response time shown in Fig. 6.5 for the single marker wavelength measurement. A specific implementation in a 3 WADM ring with 2 in-line EDFAs between WADM#1 and WADM#3 is described below.

6.3.2 Protection Switching in a 3 WADM Ring: Simulation Results

In this section, we use a simulation tool that we developed at Bellcore [35], to study protection switching in a 3 WADM ring. The approach is very original from a simulation point of view, as we have concentrated on a detailed time-domain analysis. The EDFAs and switching elements are modeled as time dependent elements. That is, we attempt to capture the transient behavior of the components as opposed to the static description which is naturally less detailed. Fiber cuts are also modeled to reflect the finite transition time in which the light goes away. The time-dependent model of the EDFA described in Chapter 3 is the heart of the simulation. The size of the ring is kept small to keep track of very complex interactions and to save on the simulation time.

6.3.2.1 The System Model

The ring is shown in Fig. 6.13. Only a single working fiber / protection fiber pair of the 4-fiber WADM ring is presented. It is understood that a second pair exist that can be treated similarly but independently for protection switching purposes. The system consists of 8 signal wavelengths spaced 1.6 nm apart in the wavelength range 1549.4 - 1560.6-nm. Wavelengths 1, 3, 6 and 8 are added and dropped at WADM#1; wavelengths 4 and 5 are added and dropped at WADM#2; and finally wavelengths 2 and 7 are added and dropped at WADM#3 as shown in the Figure. This is not a practical wavelength assignment scheme but it allows us to study the switching dynamics without worrying about such details. Each WADM consists of several components developed from other elementary components. The main components are two saturated EDFAs (preamplifiers) at the input

of the working and the protection fibers respectively, to compensate for the fiber loss over the previous span, a fixed-gain EDFA at the output on the working fiber, a MUX/DEMUX pair, servo-controlled attenuators, 2 × 2 optical switches for adding and dropping of channels, and 2 × 2 optical protection switches to ensure network survivability. A simplified schematic of the WADM is shown in Fig. 6.8. The fixed-gain amplifier takes care of the losses incurred in the WADM and compensates for the changes in the number of channels as a result of adding and dropping of channels at the WADMs or signal loss due to fiber cuts, as described in Chapters 4 and 5. In so doing, a compensating channel (lasing signal) is generated which can be used as a marker to be propagated to the next NE. This eliminates the need for an additional laser source for protection switching purposes on the working fiber. Under normal operating conditions, the level of this signal is set (by adjusting the level of feedback) for the total number of channels in the network. Except for transient fluctuations this signal will only increase above this set level when channels are lost. Each NE removes the compensating channel from the previous NE via the filters used for the demultiplexers and generates its own, to be propagated with the signals to the next NE (Type 1 in Chapter 4). This ensures that the compensating channel on each link (span) is independent of any other and in effect localizes a failure when used as a marker for protection switching purposes. All the EDFAs in the system were pumped with 90 mW at 980 nm. They were modeled as single-stage forward pumped EDFA with lengths of 50 m. The span losses were 18 dB. The MUX/DEMUXs were modeled as cascades of Multilayer Interference (MI) filters [36]. We will show cuts on either working or protection or on both fibers but in all cases

the location of the cut, if there is one, is consistent. In an effort to keep the simulation as simply as possible, the propagation delay of the signals was not modeled.

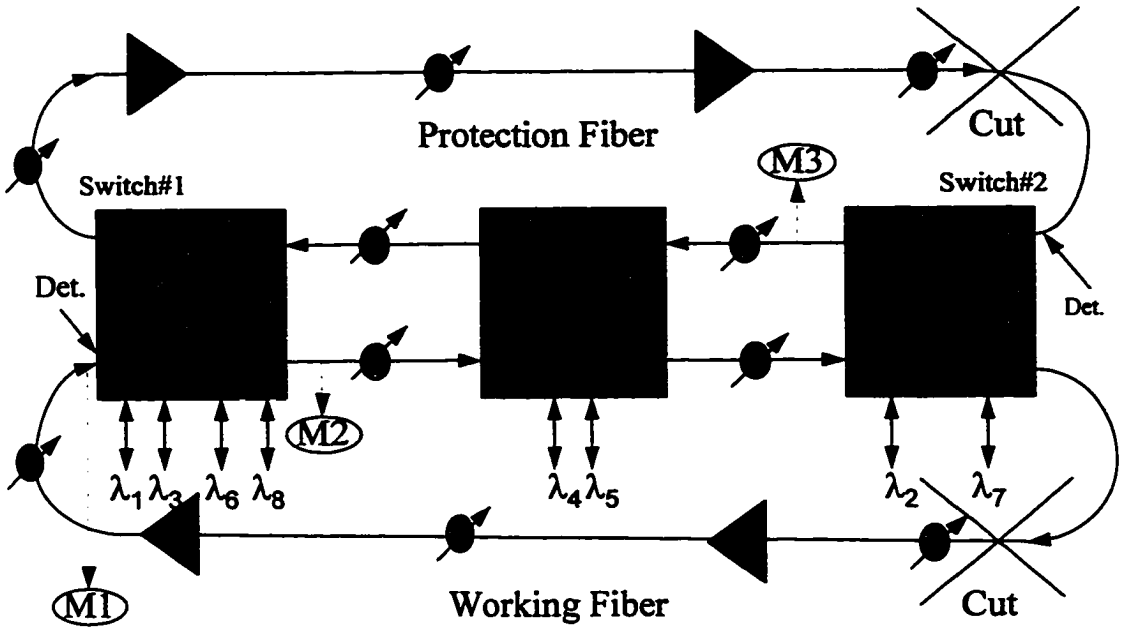

Figure 6.13 3-WADM ring with 2 in-line EDFAs between WADM#1 and WADM#3. The signals were observed at the three observation points shown as M1, M2, and M3. Det represents the location of the relevant monitors to detect failures for the fiber cuts shown.

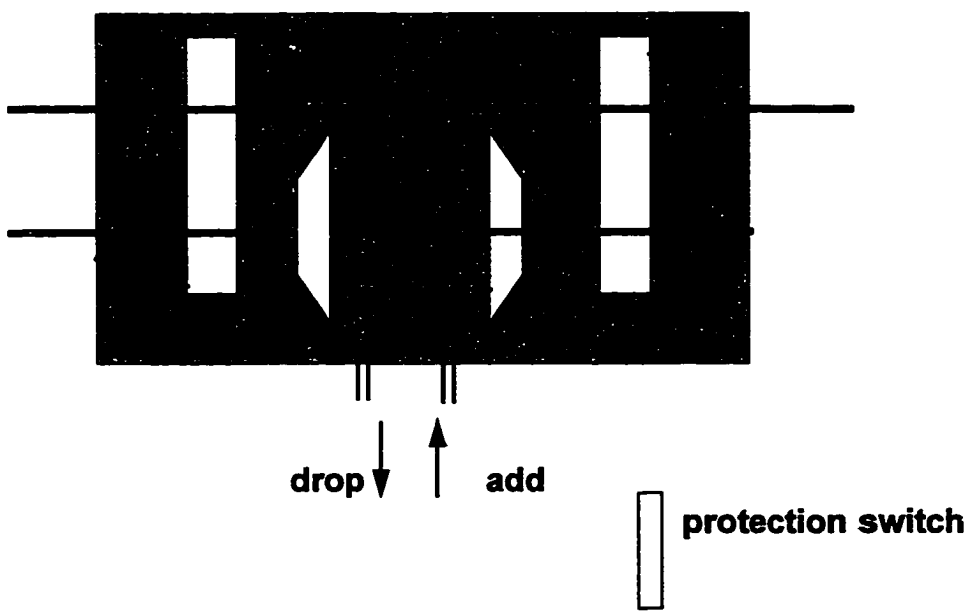

Figure 6.14 Simplified diagram of a generic means of providing shared protection in a WADM for a 4-fiber WADM ring. Protection switches are in the pass-through state indicating normal operation.

6.3.2.2 Protection Switch

The protection switches were implemented as loop back 2 × 2 optical switches [37-38]. Both slow and fast switches were simulated but the speed of the protection switches is of little consequence for the protection switching schemes described in Section 6.2. To save on simulation time, a switching time of 10 μs was arbitrarily assumed. A hold-off time in which the switch remains in its present state after determining that a threshold passing has taken place was also implemented in the controller for the switch. This was set to 200 μs, which is on the order of the time it takes the ASE to recover and saturate the EDFAs after a loss of signals. Switch crosstalk and polarization effects were not taken into account as these effects are not expected to be of any consequence for the protection switching schemes being studied. The switches were assigned an arbitrary insertion loss of 1 dB.

6.3.2.3 Complete Cuts

The likelihood of a complete cut of the fiber (both working and protection fibers cut) occurring is high. Both fibers are likely to be placed in the same housing and therefore possibly be damaged simultaneously. This section examines how survivability can be provided for complete cuts. Except where specifically noted, for all the simulation results shown in the following sections we assume a fiber cut starts at 1 ms and finishes at 1.1 ms.

6.3.2.3.1 Detecting Total Power

Depending on where the cut occurs there may be in-line EDFAs between the cut and the point of detection on both working and protection fiber. A case where no in-line amplifiers are encountered on the protection fiber but 2 are encountered on the working fiber is shown in Fig. 6.13. This difference is inherent to the opposite directions of propagation on the working and protection fiber. For this scenario, wavelengths 4, 5, 2 and 7 will not reach WADM#1 after the cut. If the total power is detected, the detector at WADM#3 on the protection fiber side will see essentially zero power after the cut and will correctly trigger a protection switch. However, as shown in Fig. 6.15, approximately 200 μs after the cut is completed, the total power at the detector on the working fiber at WADM #1, recovers to within 3 dB of what it was before the cut and thus the protection switch was not made, resulting in a complete loss of signals (except for the ASE in the signal bands) as shown in Fig. 6.16. Therefore, detecting the total power will never provide the desired 10 dB contrast after just two in-line EDFAs. Adjusting the threshold in this case would require a less than 3 dB change to trigger a protection switch, which would be unacceptable in practical networks. As we saw in Fig. 6.9, after more than two in-line EDFAs the total power is essentially the same before and after the cut and therefore no threshold can be set for unambiguous detection in such cases. Fig. 6.16 also shows the evolution of the compensating channel (lasing signal) in time at the output of WADM#1. When the cut occurs it oscillates reaching very high levels then slowly settles

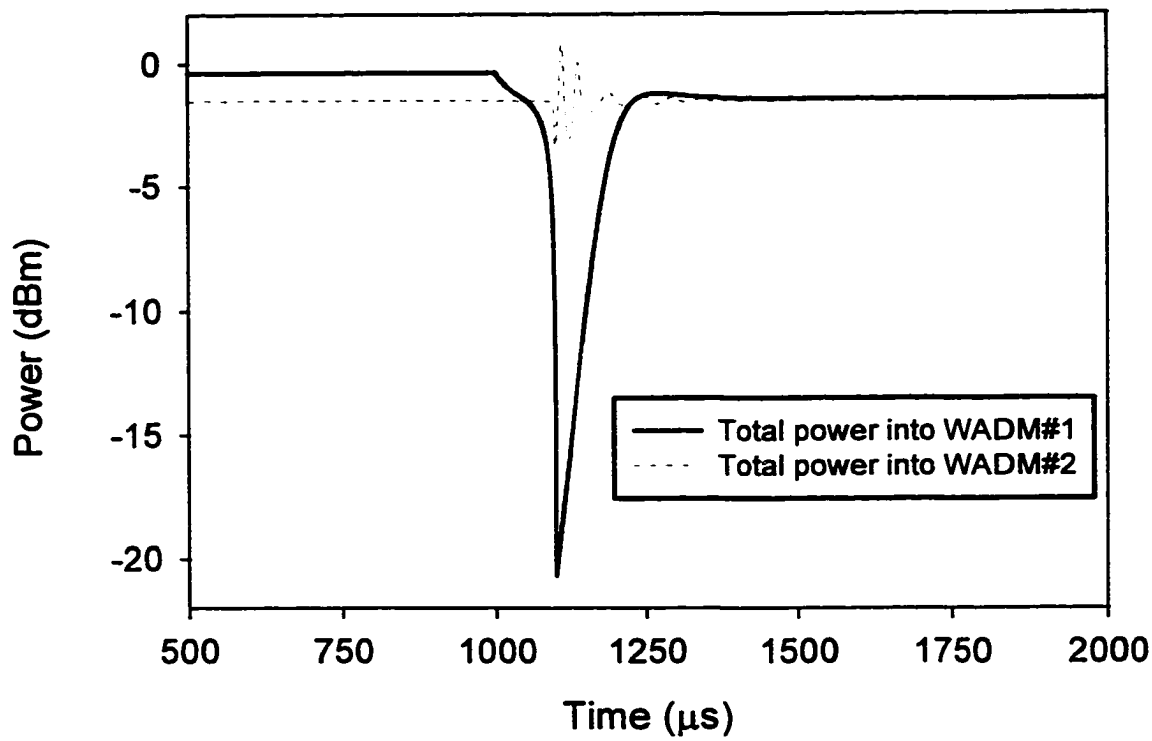

Figure 6.15 Total power at the monitors on the working fiber at the input of WADM#1 (M1) and WADM#2. Cut starts at 1 ms and finishes at 1.1 ms. At WADM#1 the total power is restored to within a few dBs of what it was before the cut. At WADM#2 the total power shows no change except for the transient variations, due the compensating channel from WADM#1. (Note: No propagation delay)

to much smaller power excursions, as along with the ASE at the signal wavelengths it saturates the EDFA back to the level it was before the cut. This ensures that the total power at the monitor of WADM#2 on the working fiber does not experience a prolonged large reduction in total power, thereby falsely causing protection switching at that node. As shown in Fig. 6.15, except for the oscillations caused by the lasing at WADM#1, the monitor at WADM#2 on the working fiber sees essentially the same total power before and after the cut and therefore, no protection switching occurs at that node. For the cut shown in Fig. 6.13, the protection switch that is controlled based on the total power level on the protection fiber at WADM#3 correctly made the protection switch since there are

no in-line amplifiers between the cut and the monitor. However, the protection switch that is controlled based on the total power at the monitor on the working fiber at WADM#1 did not switch because of the two in-line EDFAs between the cut and the monitor. This is an unacceptable implementation and will expose the network to chaotic behavior.

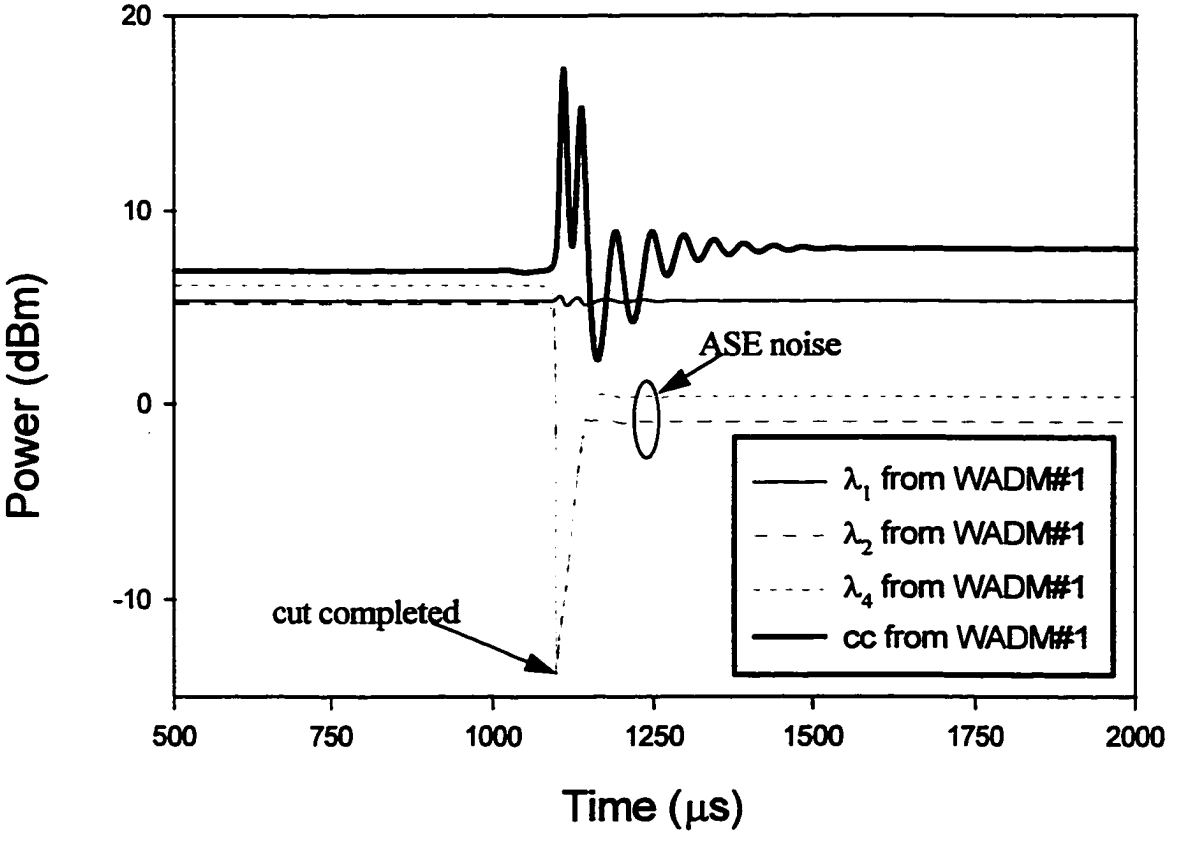

Figure 6.16 Signals at the output of WADM#1 when total power is detected for protection switching purposes. Except for the ASE at the signal wavelengths the signals are lost forever after the cut at 1 ms.

6.3.2.3.2 Detecting a Cut based on a Differential Measurement.

If instead of depending on a 10 dB change in total power at the monitor to determine if a fiber cut has taken place we use a differential measurement of the type described in Section 6.3.1.3, then an unambiguous determination of the cut is made and thus the correct action taken. In the simulation, the compensating channel (lasing signal) at 1545 nm was also used as the marker signal to be compared with a non-signal channel at 1542 nm on the working fiber. The contrast for switching was set at 10 dB as above. Fig. 6.12 shows the evolution of both signals before and after the cut. The Figure also shows the dB difference between the two. A contrast greater than 30 dB was observed before the cut

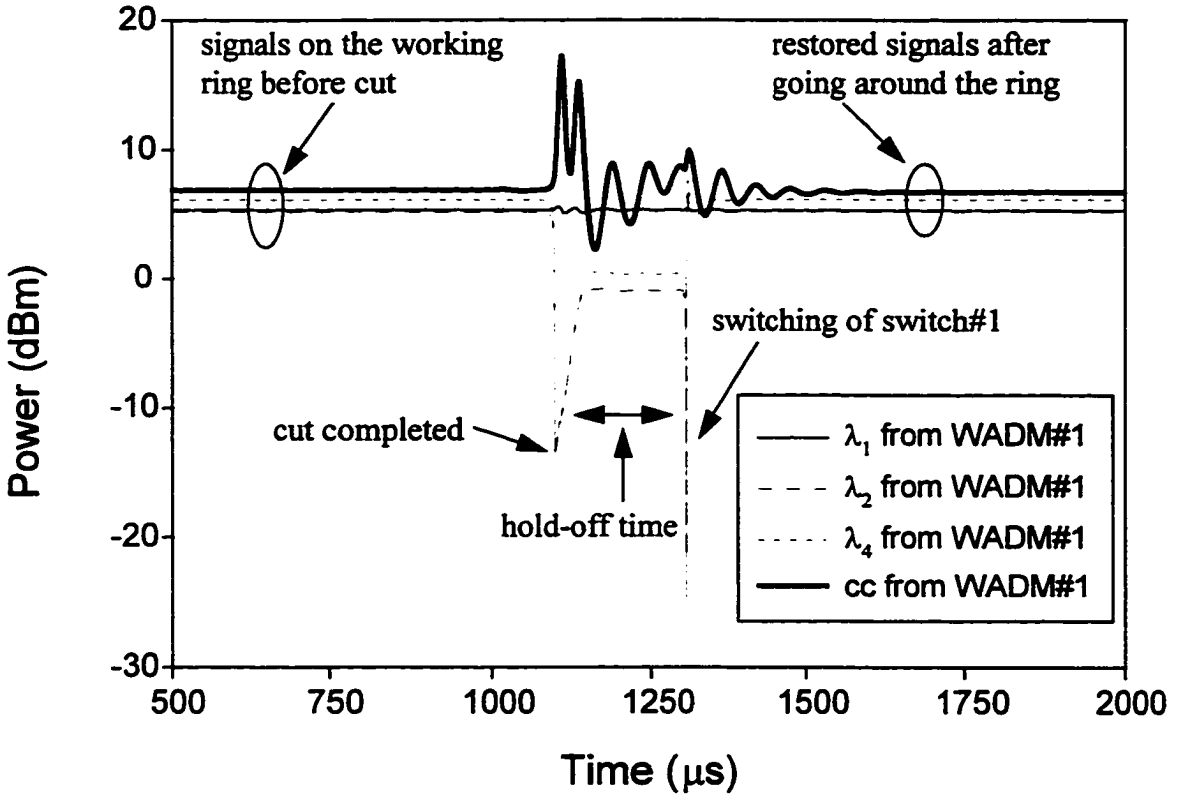

Figure 6.17 Signals at the output of WADM#1 for the case where a differential measurement of the signals, shown in Fig. 6.12, was used to determine when the fiber was cut. Wavelengths 2 and 4 are restored in this case after the hold-off time and the time for the protection switches to switch. Compare with Fig. 6.16.

which reduced to almost 0 dB after the cut.

Fig. 6.17 shows that wavelengths 4, 5, 2 and 7 were restored at WADM#1 (wavelengths 4 and 2 shown in the Figure) after the hold-off time plus the switching time of the protection switches. The hold-off time and switching time of the protection switches were 200 μs and 10 μs respectively, as pointed out before. The Figure also shows the perturbations experienced by the compensating channel for the loss and restoration of the 4 channels. Therefore, it was verified that the differential measurement scheme can be used to correctly determine a fiber cut and thus lead to the correct triggering of the protection switches to restore the network in the presence of in-line amplifiers. Detecting total power or power within a single marker channel will not in general work for more than a few in-line EDFAs, but this differential measurement scheme works for several in-line amplifiers. It therefore allows for graceful network upgrades through a very general means of detecting fiber cuts without the constraints imposed by in-line EDFAs.

6.3.2.4 Partial Cuts

In the previous example it was assumed that both working and protection fibers were cut simultaneously. It is possible for either working or protection fiber to be damaged while the other remains intact. Protection of the data must be provided for such partial fiber cuts but the sequence of events leading to the provisioning of protection depends on which fiber is cut and on the location of the cut. Not only does the sequence of events differ for partial fiber cuts on the working fiber compared to that on the protection fiber, but the sequence for a cut on both fibers is also unique to that situation. To facilitate repair if

both working and protection fibers share a common housing, it is considered prudent to initiate protection switching even if the cut is only on the protection fiber. This section presents simulation results of partial fiber cuts on both the working and protection fibers for the 3-WADM ring shown in Fig. 6.13. The location of the cut is the same as the previous example of a complete cut, but one fiber is intact while the other is damaged. Also, the cut is once again assumed to begin at 1 ms and finish at 1.1 ms. The method of detection is assumed to be based on the differential measurement scheme, as demonstrated above to be an effective means of detecting cuts in the presence of several in-line EDFAs.

6.3.2.4.1 Single Cut on Working Fiber Alone

It is assumed that the cut occurs at the same location on the working fiber as shown in Fig. 6.13 but that the protection fiber is intact. On the protection fiber the marker wavelength (additional laser) was made 1541 nm and to show the robustness of the method the non-signal band was made 1562 nm at the other end of the spectrum. From Fig. 6.8 it is evident that there will be a relatively large difference in power at these wavelengths when there are no signals present and several in-line EDFAs are cascaded. The non-signal (noise) spectrum of the EDFA can be used as a guide to determine the threshold setting in the differential measurement scheme. The sequence of events leading to the provisioning of protection is shown in Fig. 6.19 and an explanation of the process is as follows:

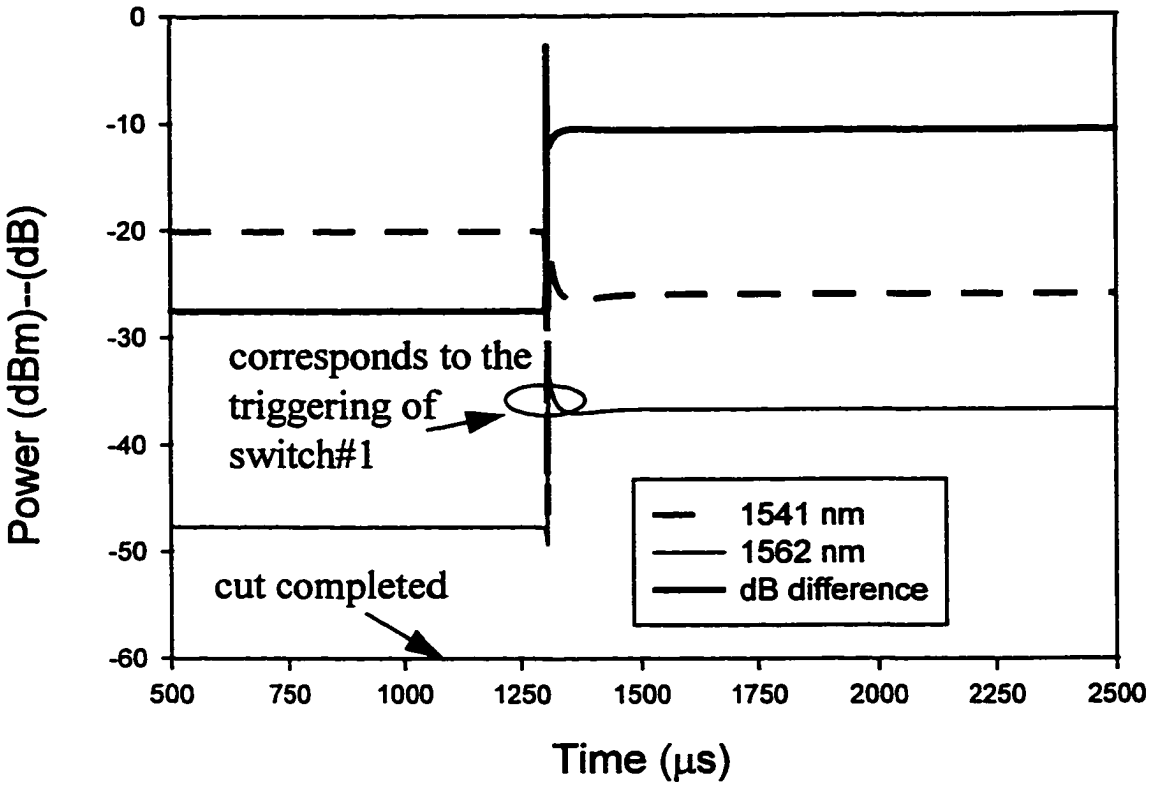

Figure 6.18. Optical power at the monitor on the protection fiber at WADM#3. The marker channel is at 1541 nm and the non-signal channel is at 1562 nm. Switch#1 causes the marker to disappear at the monitor on the protection fiber. There are five in-line EDFAs between the cut and the monitor point.

1) The monitor on the working fiber at WADM#1 determines after 2 in-line EDFAs that the contrast has reduced more than 10 dB (comparing marker and non-signal channel). The relative signal levels at the monitor are the same as those shown in Fig. 6.12.

2) Switch#1 at WADM#1 is switched after the hold-off time. This causes marker wavelength 1541 nm to be switched from the portion of the protection fiber going from WADM#1 to WADM#3.

3) The monitor on the protection fiber at WADM#3 must now determine that the marker wavelength (1541 nm) from WADM#1 is no longer present, based on the

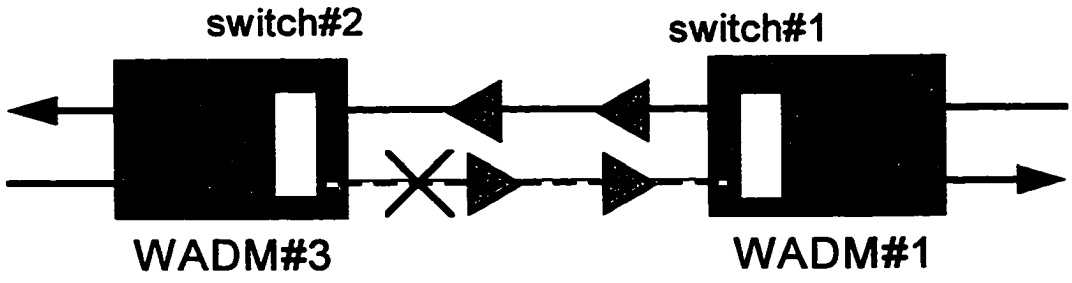

a. Only working fiber cut. Span losses are not shown.

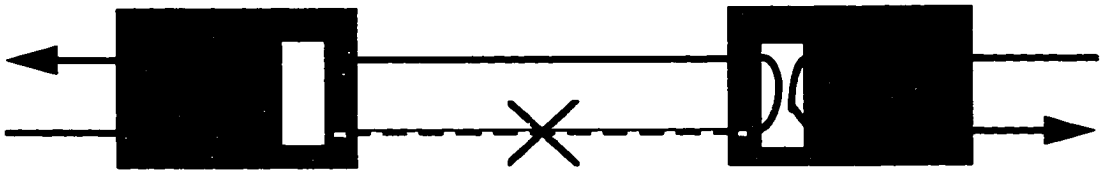

b. Downstream protection switch is triggered and moves to "protect" position.

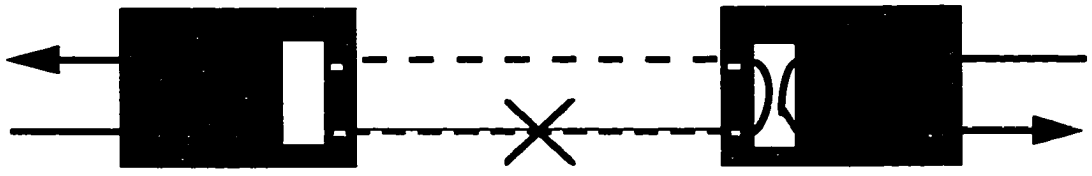

c. Once protection switching occurs, the marker wavelength is lost from the protection fiber. Therefore the contrast is reduced.

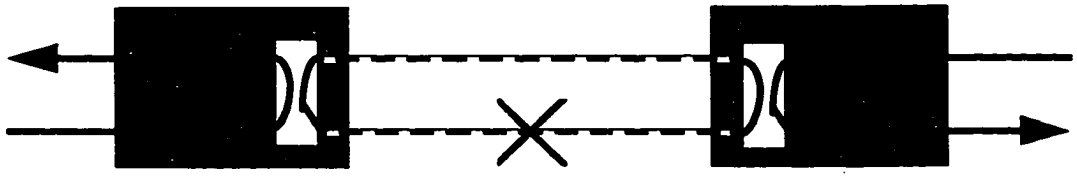

d. Since the contrast is reduced at Switch#2 the upstream protection switch is triggered and moves to "protect" position.

Figure. 6.19 Sequence of events showing how cut on working fiber alone leads to complete protection switching at adjacent network elements. A similar sequence occurs for cuts on the protection fiber only, if all switching decisions are made locally, based on the differential measurement scheme. For simplicity, the in-line EDFAs are not shown in the figures b, c and d.

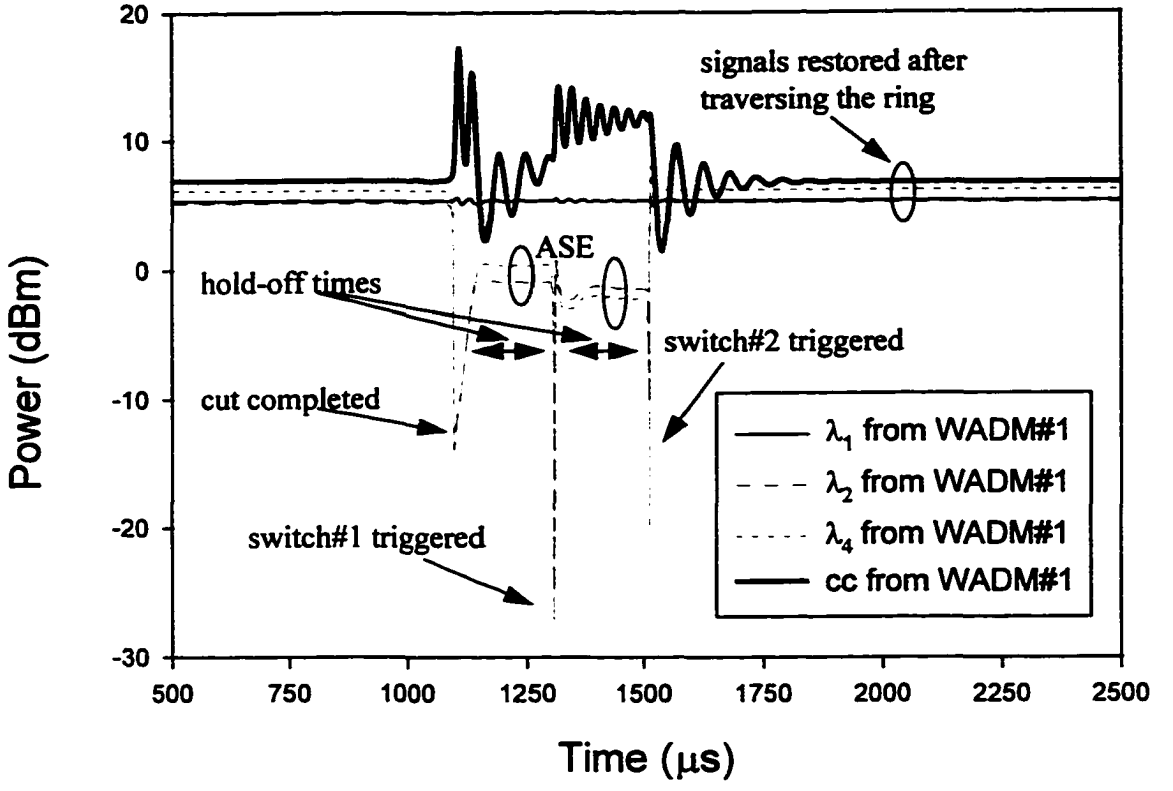

Figure 6.20 Signals at the output of WADM#1 for a cut on the working fiber alone. The dips at approximately 1300 and 1520 μs represent the switching of the protection switches in WADM#1 and WADM#3 respectively.

reduction of contrast between it and the non-signal band at 1562 nm. The relative signal powers at the monitor are shown in Fig. 6.18. Note that there are now 5 in-line EDFAs between the cut and the monitor point at WADM#3 (2 each on both working and protection fiber and the preamplifier in WADM#1).

4) On determining that the contrast has reduced more than 10 dB (decision threshold was set at 15 dB, which represents a change in contrast of more than 10 dB with respect to before and after the cut), Switch#2 at WADM#3 switches to the cross state (protection mode) after the hold-off time. The signals at the outputs of WADM#1 on the working fiber and WADM#3 on the protection fiber are shown in Figs. 6.20 and 6.21 respectively.

In Fig. 6.20 the dips in the signals at approximately 1300 μs and 1520 μs represent the actual switching of the protection switches in WADM#1 and WADM#3 respectively. As was the case for the example with a cut on both fibers, a 10 μs switching time was assumed for the switches. Note that the switching shown in Fig. 6.20 in which the signals appear at the output of WADM#3 corresponds to the second switching shown in Fig. 6.20. In Fig. 6.21 the signals and the compensating channel appear on the protection fiber after the restoration. The natural lasing at 1544.5 nm, shown in Fig. 6.21 disappears as soon as the protection ring is broken by Switch#1. The dynamics of this lasing will be discussed in more details in Section 6.3.2.5.

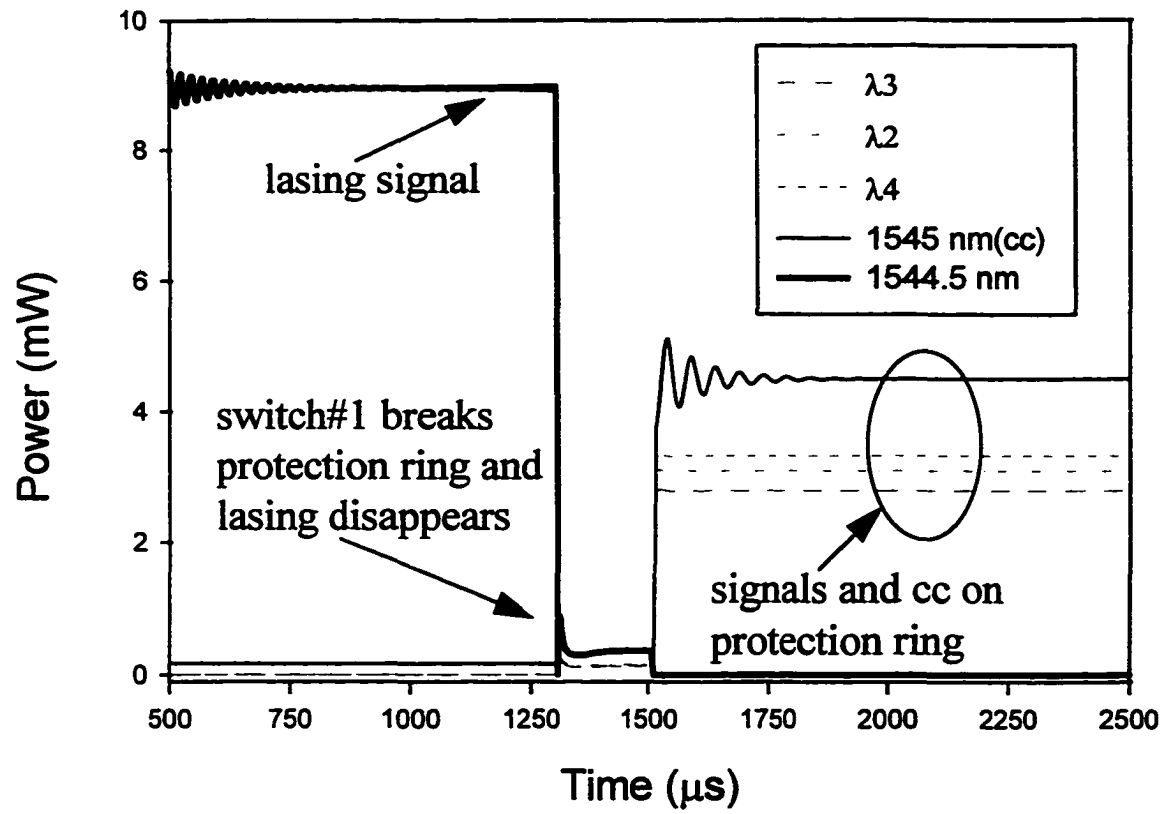

Figure 6.21 Signals at the output of WADM#3 on the protection fiber for a single cut on the working fiber alone.

6.3.2.4.2 Single Cut on Protection Fiber Alone

Once again it is assumed that the cut occurs at the same location on the protection fiber as shown in Fig. 6.13 but that the working fiber is intact. The assumptions for the time of cut, switching time and threshold settings carry over from the previous examples. The sequence of events leading to the provisioning of protection is as follows:

1) The monitor on the protection fiber at WADM#3 detects a reduction of contrast as the power at the marker wavelength and non-signal wavelength are essentially the same since there are no in-line EDFAs in this case.

2) Switch#2 switches to the protection mode in effect switching the signals from the working fiber leaving WADM#3 to the protection fiber going in the opposite direction.

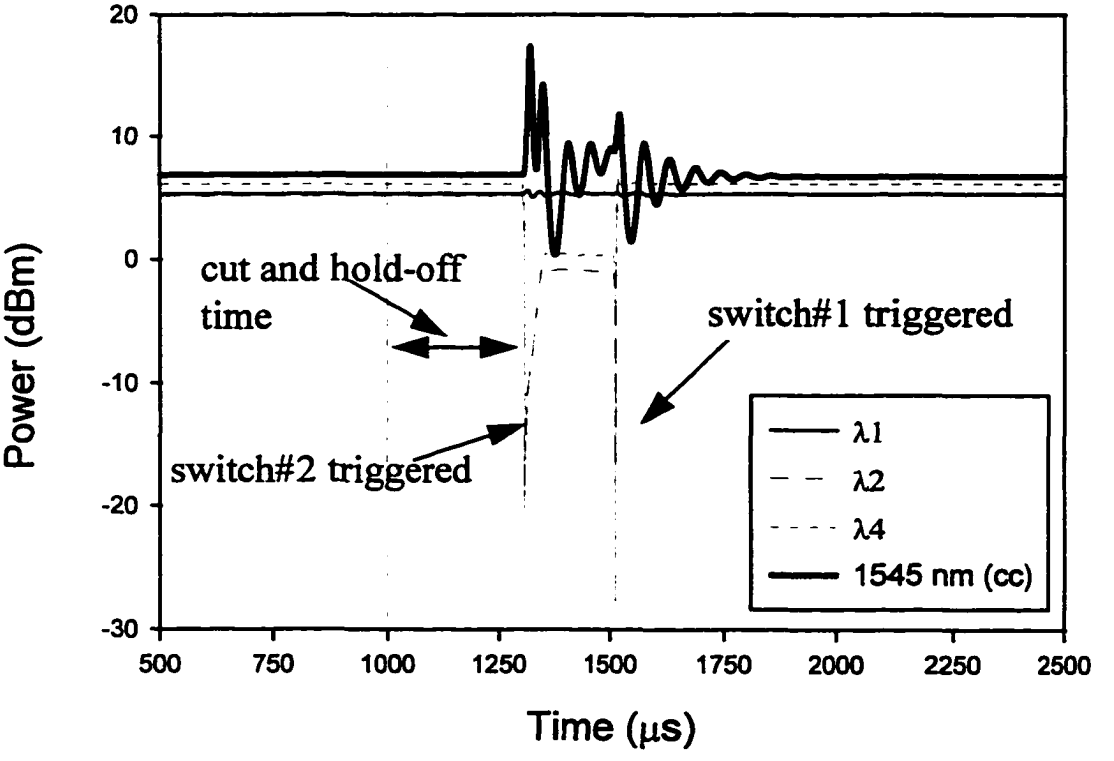

Figure 6.22 Signals at the output of WADM#1 for a single cut on the protection fiber alone. Cut starts at 1000 μs and last for 100 μs. Note that signals are lost after hold-off time and switching time at WADM#3 (i.e. at approximately 1300 μs)

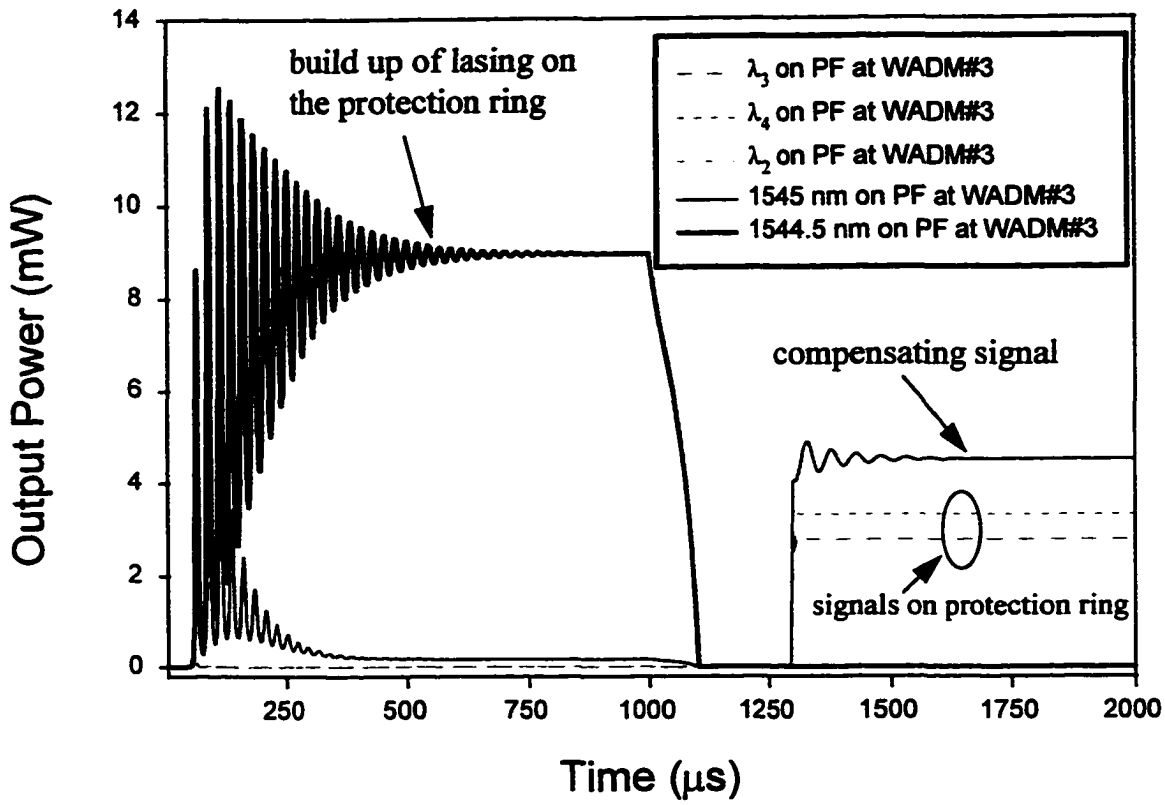

Figure 6.23 Output of WADM#3 on the protection fiber. The favored lasing wavelength (1544.5 nm) disappears when the fiber is cut and thus the signals are unaffected when they are switched. Cut starts at 1 ms and finishes at 1.1 ms.

This occurs after the hold-off time has expired at approximately 1300 μs. Before this time the signals on the working fiber are uninterrupted as seen in Fig. 6.22. Fig. 6.23 shows the signals been switched to the protection fiber at 1300 μs but λ_2, λ_4, λ_5, and λ_7 cannot be restored at the output of WADM#1 until Switch#1 in WADM#1 is switched at approximately 1520 μs (i.e. after the switching time at Switch#2, the hold-off time and the switching time at Switch#1 in WADM#1).

3) Since Switch#2 switched the signal at 1545 nm (cc) to the protection fiber at WADM#3 (step#2), the monitor at WADM#1 will see a reduction in contrast between the marker and the non-signal channel at 1542 nm. The relative powers and the dB difference

are similar to Fig 6.12 and are shown in Fig. 6.24 The minor differences between the figures result from the fact that there are now three in-line EDFAs (one additional amplifier from WADM#3) between the cut and the monitor point, compared to two in the previous case for a cut on both fibers. Also, whereas in Fig. 6.12 the transient behavior is a direct response to the dynamics of the cut, in Fig. 6.24 the transient behavior is in response to the triggering of protection Switch#2 at WADM#3, which takes place some time after the cut (hold-off time). Fig. 6.22 shows the restoration of the signals at the output of WADM#1 when Switch#1 completes its switching at approximately 1520 μs.

Therefore, it was verified that the proper sequence of events resulted for partial fiber cuts on both the working and protection fibers. It was also shown that the differential measurement scheme was able to unambiguously determine a fiber cut with up to 5 in-line EDFAs between the cut and the point of detection. For a cut on both fibers, and on the protection fiber alone the signals are lost for approximately the same amount of time but at different times as is clear from Figs. 6.17 and 6.22. For a cut on the working fiber alone the signals are lost for approximately twice as long and starts at the time of the cut, as in the case for a cut on both fibers, and recovers at the same time as would result for a cut on the protection fiber alone, as shown in Fig 6.20.

6.3.2.5 Lasing on the Protection Ring

When the network is intact (no failures), the protection fiber is an unbroken optical path with ASE noise circulating on the fiber. Some wavelengths will experience gain greater than the round-trip loss and will therefore grow at the expense of the others. This creates

a large ring laser at the wavelength with greatest gain. Changes in polarization via PDL power fluctuations cause the instantaneous peak-gain wavelength to vary. The instability of the lasing wavelength has been observed experimentally at Bellcore. In the simulation, polarization effects were not taken into account and therefore, a well defined lasing wavelength appeared in the simulation on the protection fiber. This lasing wavelength is dependent on the amplifier operating point and design. The favored lasing wavelength on the protection fiber for the parameters used in the system design shown in Fig. 6.13 was 1544.5 nm. Fig. 6.23 shows how this lasing signal builds up to a steady state level on the protection fiber when the protection ring is intact. We ask whether or not the lasing on the protection fiber affects our ability to detect and localize a cut, and whether it affects the real signals when the protection fiber is used to carry signals. Furthermore, we want to know if this lasing signal can be useful for protection switching. Unfortunately, the lasing signal on the protection fiber is not very useful for deciding when and where to protection switch, since it disappears everywhere in the network when the ring is broken. Therefore, the disappearance of the lasing signal can tell us that the protection ring is broken but it gives us no information about the location of the cut. If we were to trigger the protection switches based on the presence or absence of this lasing, all the switches would be triggered as soon as the protection ring is broken. This is certainly undesirable and would lead to turmoil in the network. As Fig 6.23 shows, once the ring is broken the lasing signal ceases to exist and the signals that are switched to the protection fiber are unaffected by it. The squelching of this lasing on the protection fiber is very fast and the hold-off time plus the switching time of the protection switches are more than enough to

ensure that it is totally squelched from the network before the signals are switched to the protection fiber. However, as described in the following section, the squelching of the lasing signal on the protection fiber can create problems of detection because of the saturated behavior of the EDFAs.

6.3.2.6 Broken Protection Ring with No Signals

Although the differential measurement scheme for unambiguous detection of fiber cuts is a simple, relatively inexpensive, and very attractive solution, its implementation details must be carefully engineered. This section points out one potential problem with the

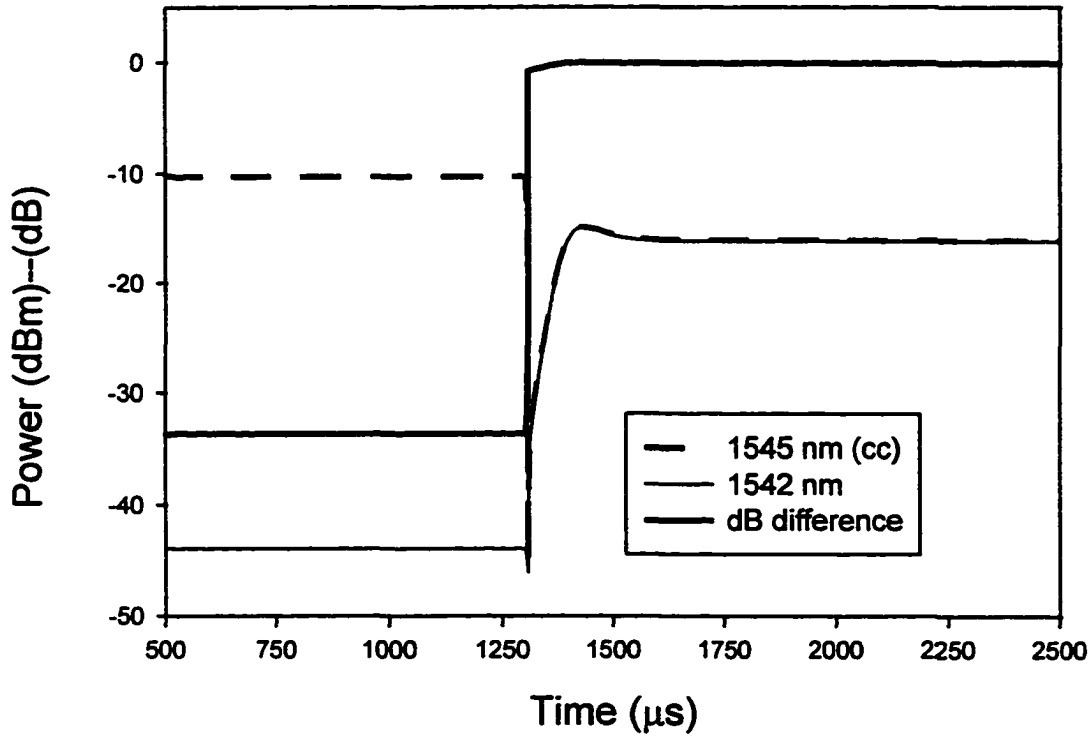

Figure 6.24 Relative optical powers at WADM#1 on working fiber for the marker and non-signal channel. Change in contrast occurs after the switch at WADM#3 is triggered and not after the cut. Note timing difference with respect to Fig. 6.12 in which change in contrast is direct result of the fiber cut.

method and suggest how one could design around the problem. For a network in which there are no in-line amplifiers between NE's the differential method is not strictly necessary and there are cheaper solutions that will work just as well. However, if changes to the network are made that would require the same NE to detect a fiber cut with in-line amplifiers in place, then the cheaper solution might not work. Therefore, as a general solution, it is desirable to have the differential measurement method work independently of whether or not there are in-line amplifiers.

As explained in the previous section, when the protection ring is broken the lasing signal ceases everywhere on the protection ring. The squelching of the lasing from the ring is a rapid process but the EDFAs on the protection fiber will seek to redistribute the energy once associated with the lasing signal. Therefore, the ASE spectrum grows in much the same way as the response to a fiber cut shown in Fig. 6.8. If signals are switched to the protection fiber at the moment the ring is broken, the energy (from the EDFAs) which was depleted by the lasing signal is now available to the new signals traversing the newly formed ring. However, if the lasing ceases and there are no signals switched to the protection fiber, the energy will be distributed over the entire ASE spectrum in amounts proportional to the intrinsic gain at each wavelength bin. In general, there will be some time before signals are switched to the protection fiber after lasing ceases, due either to a hold-off time or the sequence of the switching. During this time, the redistribution of the energy once utilized by the lasing signal is initiated on the protection fiber. The net result is that the contrast between the marker wavelength and the non-signal channel may be reduced on sections of the ring where no protection switching is required. The contrast is

reestablished as soon as signals are switched to the protection fiber. An example of this event is shown in Fig. 6.25 for the signals at the monitor at WADM#2 on the protection fiber. The reduction in contrast results from the fact that there are no in-line EDFAs between WADM#1 and WADM#2 and that the marker wavelength is filtered and added at each WADM while the non-signal channel undergoes no such filtering. A single in-line EDFA between the WADMs could maintain the necessary contrast to prevent false triggering of the protection switches. Fig. 6.25 shows the contrast reduction after the lasing signal disappears and the contrast re-establishment after the signals are switched (λ_2 shown in the figure) to the protection fiber. In the Figure the marker wavelength was located at 1541 nm and the non-signal channel was placed at 1542 nm.

The reduction of contrast can be eliminated if the marker channel has high power but as explained before this has undesirable consequences for the signals. Making the contrast requirement smaller can also eliminate the problem but for reasons explained before this is also undesirable. Another possible method of countering this effect is to measure the non-signal channel at the region of the spectrum that experiences the least growth in ASE when there are no signals present. As seen from Fig. 6.8 this is at the longer wavelengths for the operating point assumed in the simulations. However, the most appealing solution is to filter both marker wavelength and non-signal channel at each WADM to prevent the build up of the ASE at the non-signal channel from propagating from one NE to the other, and thus reducing the contrast. Therefore, we have seen that the ceasing of lasing on the protection fiber can complicate the detection of fiber cuts in the differential measurement scheme. Particularly, it can reduce the contrast thus causing a false triggering of an

upstream protection switch if appropriate measures are not taken to prevent this from happening.

6.3.2.7 Revertive Protection Switches and Hold-off Time

After a fiber cut is repaired the protection switches should return to their normal state so that the signals are exclusively carried by the working fiber and the protection fiber forms a closed ring with no signals. Whether this is done automatically or manually depends on the particular switch implementation. Manual schemes might be required but the answer is not very clear. For an automatic restoration of the network, revertive protection

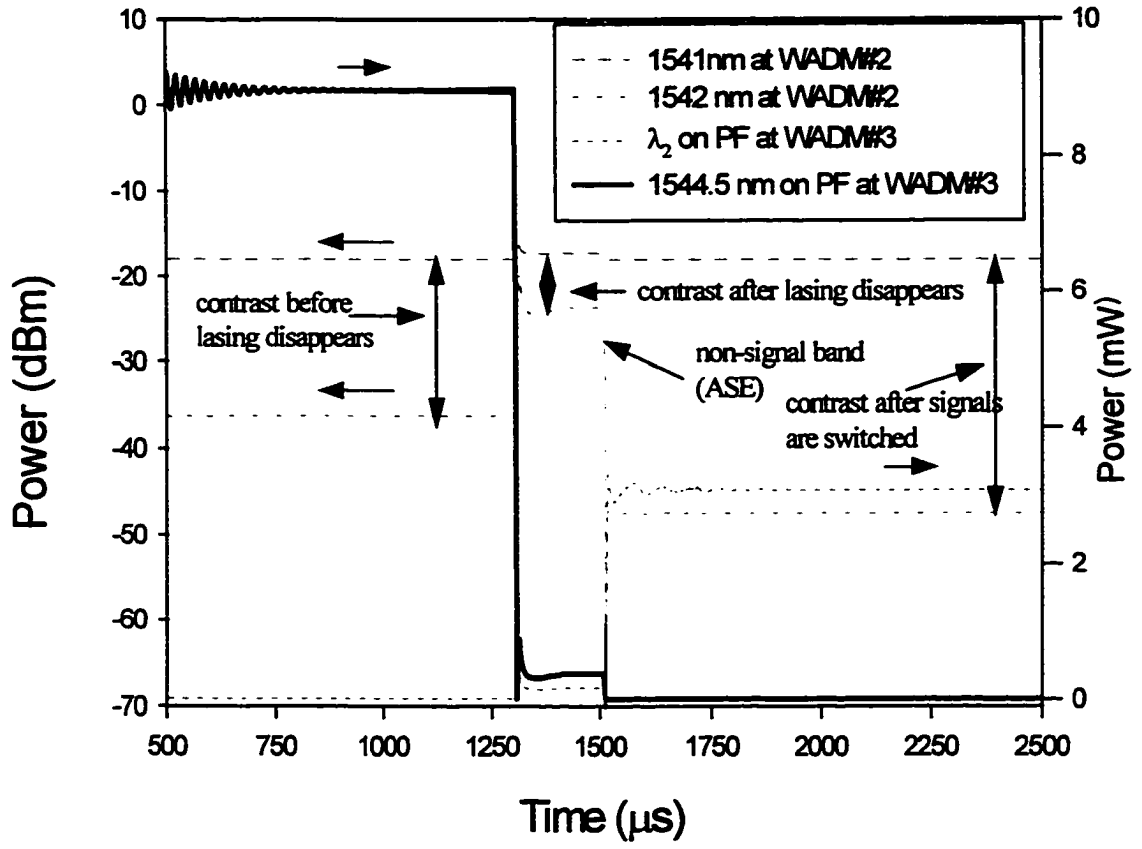

Figure 6.25 Reduction and restoration of contrast for loss of lasing signal and switching of signals on the protection fiber for a cut on the working fiber alone. Arrows on top of plots indicate the reference scales.

switches will be required (i.e. switches that change state to bar or cross depending on some threshold passing and timing criteria). For example; if the protection switches responded to a reduction in contrast in the differential measurement scheme by triggering a protection switch and consequently changing from the bar state to the cross state, when the fiber is repaired the contrast will once again be more than the threshold and the switches will automatically switch back to the bar state. As seen in Fig 6.12, this change in contrast is unidirectional despite the fact that the marker wavelength experiences a dip followed by a slow growth determined by the dynamics of the EDFA. However, if a single wavelength measurement was used to determine the need for a fiber cut then timing effects become more important. In this case the power will experience a dip followed by a recovery as the ASE saturates the in-line EDFAs. The dynamics of this dip and recovery depends on the dynamics of the EDFA, whether there are in-line EDFAs or not, and on how fast the light disappears in the fiber. If the hold-off time for the protection switches is shorter than the time it takes the ASE to saturate the EDFAs then as shown in Fig. 6.26, the switch will first be switched because the power level falls below the threshold but will return to its original state after the ASE saturates the EDFA. Therefore, in such cases a hold-off time that is longer than the time it takes the ASE to saturate the EDFAs (on the order of 200 μs) will prevent this double switching of the protection switches. The hold-off time was only 15 μs in Fig 6.26. On the other hand, one might argue that if the hold-off time is made short enough and manual switches are implemented then the switch would be made regardless of the recovery of the ASE which prevents the high contrast needed for unambiguous switching. However, making

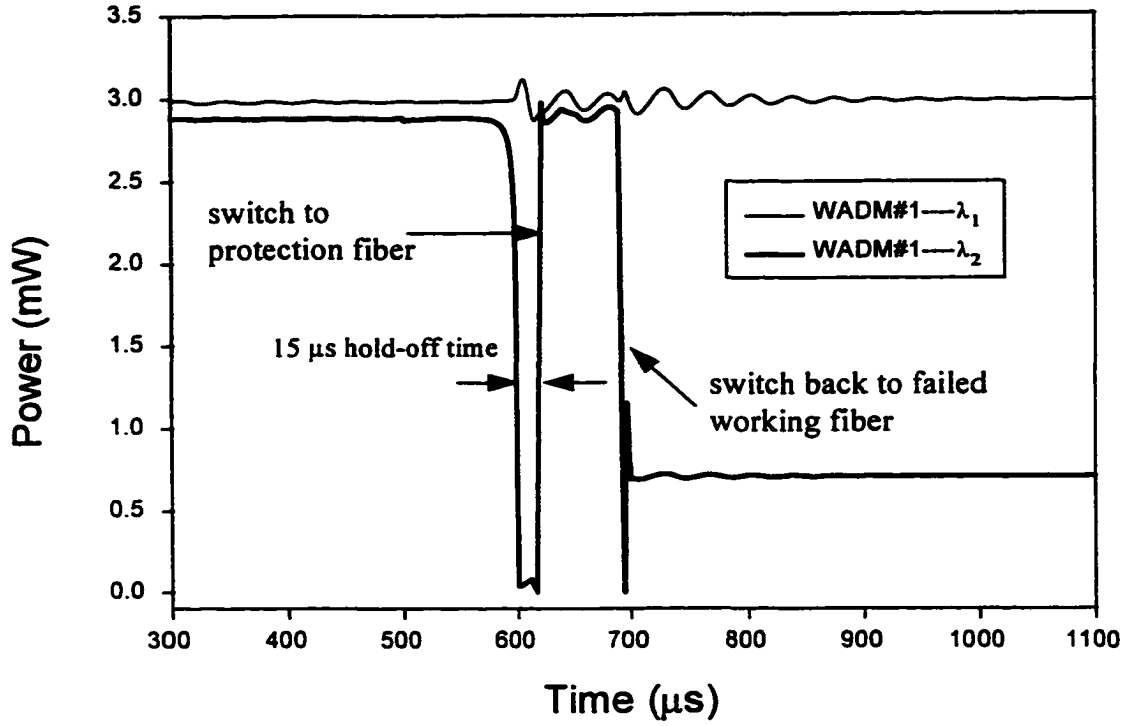

Figure 6.26 Double switching when we detect total power for revertive protection switching with a hold-off time of 15 μs. Cut starts at 500 μs and the fiber is completely cut at 600 μs.

decisions on such transient effects is not thought to be a good practice for reliable consistent operation of a network. Transient degradations wherein power levels can fluctuate about the threshold lasting for a relatively short time can occur in a network under normal operating conditions and triggering a protection switch in such cases is not required and certainly undesirable.

6.3.2.8 Speed of Protection Switches

As discussed in Chapter 2, various switching technologies with different speeds are available. The choice of switching technology depends on economics and application

among other things. For instance, one can obtain very fast switches based on lithium niobate technology, but these switches suffer from polarization dependent switching. On the other hand, much slower switches based on optomechanical technology exist that are basically polarization independent. Fast optical protection switches might seem to imply faster restoration of the network from failures, but as discussed in the Section 6.2.9 this might not be so. In particular, for a network in which optical protection at the optical layer is coexisting with SONET protection switching at the electrical layer an infinitely fast optical switch will not provide an advantage because of the physical constraint imposed by propagation delay in the ring and the loss of critical framing bits [26]. If a hold-off time for the initiation of SONET protection switching is implemented in the future, such that optical protection switching has time to prevent the initiation of protection at the SONET layer, then fast optical switches might become advantageous. From a transient point of view, slower switching ensures smaller power excursions and less oscillation in the network, as described in Chapters 4 and 5. This is related to the relatively slow dynamics of the EDFA and is not inherent to the means of protection switching. A 10 μs switching time for the optical protection switches was assumed for the previous results which is a very fast switch and obtainable with switches based on the electro-optic effect. For comparison, results for a switch that takes a total of 5 ms (similar to a fast optomechanical switch) to complete switching is given in Fig. 6.27. In this figure we also assume that the light takes 1 ms to completely go away (linearly). Note that the oscillations are suppressed as the average inversion of the EDFAs is now better able to follow the changes in power as discussed in Chapter 4.

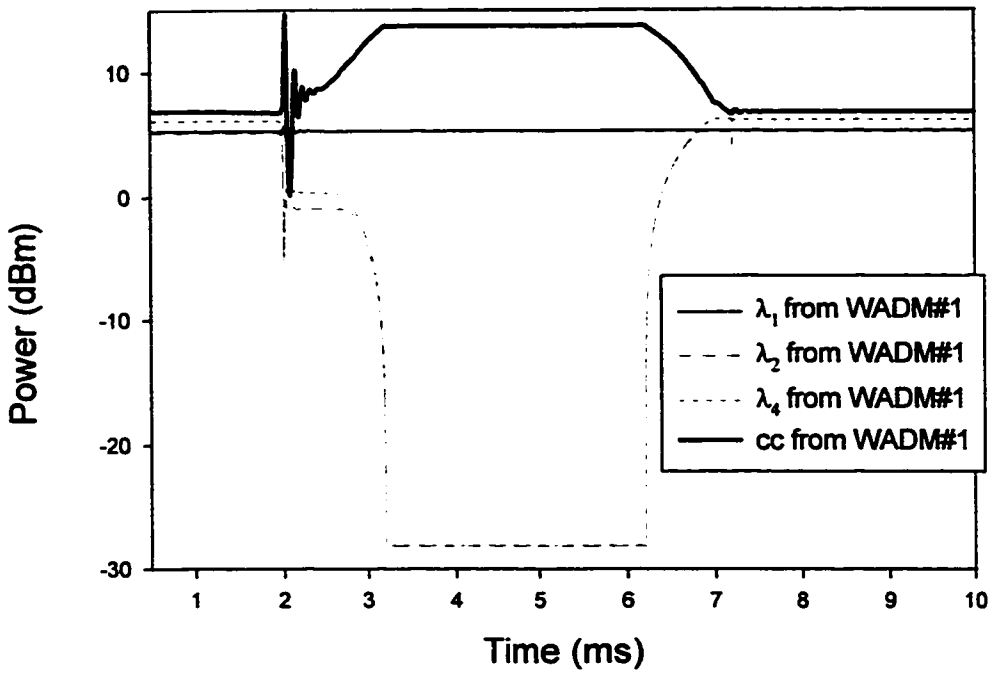

Figure 6.27 Signals at the output of WADM#1 for the slow protection switches (5 ms) and a loss of power that takes 1 ms. During the hold off time (200 μs) only the ASE at the signal wavelengths (i.e. λ_2 and λ_4) is present and during the switching time this reduces linearly to zero and then recovers linearly when the switching is complete with the λ_2 and λ_4 from the new ring.

6.4 Conclusion

The optical layer is responsible for the common resources shared by the higher layer network applications and therefore it can achieve better sharing of recovery resources in a transparent WDM ring network. For applications that do not include protection functions, protection at the optical layer can provide this function. Optical protection switching is

much more efficient than restoration schemes in responding to certain failures, such as fiber cuts. Protection at the optical layer restores the traffic in a simple manner compared to the complex time consuming operations that would be required as multiple higher layer entities attempt the restoration. Optical protection also presents opportunities for substantial equipment cost savings, as some of the protection functions could be off-loaded to the optical layer where protection is inherently simpler and less costly. For example, cost can be reduced by combining 1:N SONET equipment protection at the client layer with 1:1 or 1+1 optical facility protection, instead of depending on conventional SONET protection which requires N-1 SONET ADMs to do the same job [32].

On the other hand, optical protection is limited in what is can accomplish. Due to transparency constraints, it cannot detect bit error rate (BER) degradations, nor select a subset of traffic to protect while leaving the remainder unprotected, unless the subsets are carried on separate wavelengths in a path protection scheme. Also, it cannot handle equipment failures in higher layers, such as transmitter failures. In a ring switched architecture such as the 4-fiber WDM ring with shared protection switching, backup routes are generally much longer than the primary routes and the optical link budget can become a major limiting factor. Coordinating protection across multiple layers is also an issue and revertive optical protection can cause chaos if escalation strategies are not carefully designed.

Detecting fiber cuts in a WDM network is complicated by the same EDFAs that makes WDM possible. Simple monitoring the total optical power or the power in a marker channel do not provide for the detection of fiber cuts at all possible locations. However, modifications that add only moderate cost and complexity can provide sufficient information for rapid and unambiguous identification of cuts. In particular, it was shown how a differential measurement can be used to detect a fiber cut on both the working and protection fibers in the presence of several in-line EDFAs. This method can be implemented in hardware and can therefore be orders of magnitude faster than methods based on the detection of tones, that will necessarily involve some electronics. The differential measurement scheme was tested extensively through an original simulation technique that is reported here for the first time. The simulation used a 'wavelength domain' simulation tool to study protection switching issues at the physical layer through a time-dependent analysis. Detecting total power as a means of determining the need for protection switching was tested experimentally and found not to work in a LEC testbed at Bellcore. Unfortunately, many of the other concepts presented here are yet to be tested experimentally. For the methods that appear to work well this is expected to be done in the near future. However, for others that we have shown not to work in our simulation environment this is a good thing, since experiments are more costly and can be wasteful of limited resources.

6.5 References:

[1] A. F. Elrefaie, "Multiwavelength survivable ring network architectures," International conference on Communications ICC'93, Geneva, May 23-26, 1993, pp. 1245-1251

[2] "Operation of a 4-Fiber Survivable WDM Ring Network," 1997 Deliverable 4.1, Multiwavelength Optical Networking (MONET) Project, Bellcore.

[3] "WDM Alternatives to SONET Multiplexing," Bellcore's HORIZON'98 deliverable 1.2, Optical Networking Initiative, May, 1998.

[4] "WDM Layer Protection and Restoration Strategies for LEC Networks," Bellcore's HORIZON'98 deliverable 1.3, Optical Networking Initiative, July, 1998.

[5] Joseph Sosnosky and Zhi-Wei Lin, "Planning for broadband multilayer survivability," NFOC'98, Sept. 1998.

[6] Rob Batchellor, "Optical Layer Protection: Benefits and Implementation," NFOC'98, Sept. 1998.

[7] Ezhan Karasan, Evan Goldstein, "Optical restoration at the wavelength-multiplex-section level in WDM mesh networks," in Optical Fiber Communication Conference, Vol. 2, 1998, OSA Technical Digest Series (Optical Society of America, Washington DC, 1998), pp. 300-301.

[8] Kris Struyve, Piet Demeester, "Dynamic Routing of Protected Optical Paths in Wavelength Routed and Wavelength Translated Networks," ECOC'97, Edinburgh UK, Sept. 1997.

[9] H. Takeshita, S. Takahashi, T. Kato, S. Kitamura, H. Harano, and N. Henmi, "A demonstration of an optical cross-connect system for a self-healing optical network," in proceeding of ECOC'97, Edinburgh, UK.

[10] Ori Gerstel, "Opportunities for optical protection and restoration," in proceeding of Optical Fiber Communication Conference (OFC'98), paper ThD1, San Jose, CA.

[11] Paul Bonenfant, "Optical layer survivability: a comprehensive approach," in proceeding of Optical Fiber Communication Conference (OFC'98), paper ThD2, San Jose, CA.

[12] Hideaki Tsushima, Hiroshisa Sano, Shigeki Kitajima, Yasushi Sawada, Tatsuo Kakizaki, Yasuyuki Fukashiro, Tsunio Nakata, Shoichi Hanatani, Niall Robinson, Gary B. Davis, John A. Fee, Shoa-Kai liu, "Optical cross-connect systems for restoration of backbone fiber networks," in Proceeding of Optical Fiber Communication Conference, (OFC'98) paper ThD3, San Jose, CA.

[13] J. A. Johnson, P. A. Littlewood, "Survivable SONET/ATM Networks," in Technical Digest, NFOEC'95, Boston, MA, June, 1995.

[14] Ori Gerstel, and Rajiv Ramaswami, "Role of Optical Layer Protection and Restoration in Transport Networks," NFOC'98, Sept. 1998.

[15] Bernard Glance, Christopher Doerr, Ivan Kaminow, and R. Montagne, Optically Restorable WDM ring Network Using Simple Add/Drop Circuitry,", Journal of Lightwave Technol., vol. 14, no. 11. Nov. 1996, pp. 2453-2456.

[16] P. Bonenfant and C. M. C. Davenport, "SONET Optical Layer Protection Switching," Bellcore TM-24609, December 1994.

[17] David Beebe and Mark Barratt, "The hidden power of path-protection switching," Telephony, Oct. 1993. pp. 22-27.

[18] J. Vernon Drake, "A review of the four major SONET/SDH rings," ICC'93, Geneva Switzerland, May 23-26, 1993.

[19] Randy Eisennach, "Performance Monitoring with SONET Networks," NFOC'97, Sept. 1997.

[20] Jonathan Morgan and Samuel Lisle, "A comparative analysis of 2 fiber and 4 fiber bidirectional line switched rings," NFOC'95, Boston, MA, June 1995.

[21] J. Manchester and P. Bonenfant, "Fiber Optic Network Survivability: SONET/Optical Layer Interworking," in Technical Digest, NFOEC'96, Dallas, Sept., 1996.

[22] R. Cadeddu, N. Caponio, M. Cerisola, G. Ferraris, R. Finotti, R. Lano, and A. Mariconda, "Increased capacity of a bidirectional SDH self-healing ring using WDM," in proceedings of ECOC'97, Edinburgh, UK.

[23] Stuart S. Wagner and Thomas E. Chapuran, "Multiwavelength Ring Networks for Switch Consolidation and Interconnection," ICC'92.

[24] A. Fioretti, A. Aguilar, J. Baudron, G. Leroy, F. Masetti, P. Perrier, M. Sexton, C. Sierens, and M. Sotom, "Application of Optical Transparency to the Telecommunications Core Network," ISS'95 April 95, Vol. 1.

[25] Giuseppe Ferraris, and Kimio Oguchi, "Management of Optical Networks," ECOC'98, Madrid, Spain, Sept. 1998.

[26] Bellcore Horizon Deliverable 3.2, "Optical Protection Switching for 4-fiber WDM Rings, Dec. 1997.

[27] "2-Fiber WDM SONET Ring Networks: Reciprocal Impact of WDM Technology and Operations," Bellcore, TM-TSV-023583, April, 1994.

[28] Heena Patel, "A Reliability Analysis of OC-192 and OC-48 SONET Systems," NFOC'95, Boston, MA, 1995.

[29] Thomas R. Del Giorno and Diane M. Pipan, "Reliability of Optically Amplified WDM Transmission Links,", NFOC'97, Sept. 1997

[30] Rajiv Ramaswami and Kumar N. Sivarajan, "Optical Networks: A Practical Perspective," Morgan Kaufmann Publishers, Inc. 1998, Chapter 10.

[31] Chung-Sheng Li, and Rajiv Ramaswami, "Automatic Fault Detection, Isolation, and Recovery in Transparent All-Optical Networks," IEEE Journal of Lightwave Technol. vol. 15, no. 10, pp. 1784-1791.

[32] D. Uehara, K. Asahi, Y. Nakabyashi, M. Yamashita, C. Konishi, and S. Fujita, "Highly Reliable and Economical WDM Ring with Optical Self-Healing and 1:N Wavelength Protection," ECOC'97, Sept. 1997, Edinburg, UK.

[33] D. H. Richards, J. L. Jackel, N. Antoniades, I. Roudas, W. Xin, and M. Ali, "Detecting Fiber Cuts in a WDM Ring with Optical Protection Switching: Simulation and Experiment," ECOC'98, Madrid, Spain, September, 1998.

[34] J. L. Jackel, D. H. Richards, "All-Optical Stabilization of Multiwavelength EDFA Chains: A Network Level Approach," In Proc. LEOS'96, Boston, MA, Nov. 1996, PD 2.2.

[35] I. Roudas, N. Antoniades, R. E. Wagner, S.F. Habiby, T. E. Stern, and A. F. Elrefaie, "Wavelength-Domain Simulation of Linear Multiwavelength Optical Networks," submitted to IEEE Journal of Lightwave Technology.

[36] N. Antoniades, I. Roudas, R. E. Wagner, and S. F. Habiby, "Simulation of ASE Noise Accumulation in a Wavelength Add-Drop Multiplexer," IEEE Photonics Technol. Lett., Vol. 9, No. 9, pp. 1274-1276, 1997.

[37] T.H. Wu, Fiber Network Service Survivability (Artech House 1992)

[38] Steven G. Finn, Muriel Medard, Richard A. Barry, "A new algorithm for bi-directional link self-healing for arbitrary redundant networks." in Optical Fiber Communication Conference, Vol. 2, 1998, OSA Technical Digest Series (Optical Society of America, Washington DC, 1998), pp. 298-299.

CHAPTER 7

CONCLUSION

This thesis presented a detailed dynamic performance analysis and feasibility assessment of emerging optical switching and its impact on the performance of reconfigurable WDM transport networks. Specifically, this thesis compared and examined the potential of both existing and emerging WDM switching technologies and characterized a novel prototype liquid crystal crossconnect. The switching performance of several switching technologies was assessed and compared based on the following criteria:

- Speed of rearrangement
- Insertion loss
- Optical Isolation (crosstalk)
- Polarization dependence

This work examined and identified EDFA dynamic response to different reconfiguration scenarios (switching) and the impacts on the overall network performance. Each network reconfiguration scenario was showed to cause its own network performance degradation, and required a different set of EDFA engineering design rules to mitigate the detrimental effects. The main objective was to maintain a constant per channel output power in case of a network reconfiguration (adding/ dropping of channels) as well as how to identify and recover from failures in the network.

This thesis presented the first experimental study of an all-optical feedback technique for stabilizing the per-channel output both for single amplifier and cascade of amplifiers.

This technique is simple, inexpensive, and robust, requiring neither monitoring of the amplifier output nor any active feedback. One of the great virtues of this technique is that only the first in a chain of amplifiers needs to be modified. Two different all-optical methods of controlling transient power excursions of surviving channels in chains of EDFAs when switching occurred as a result of the adding or dropping of channels were presented and compared. The focus was on the dynamic effects due to the switching of channels. It was shown that both can be used successfully but that each imposed different constraints on the EDFAs and on the network. The compatibility of our novel method of stabilizing chains of EDFAs with another method that adjusts the pump power was examined. This study was then extended to look at dynamic effects in self-healing WDM ring networks where fault recovery is achieved through a protection switching mechanism, and how the interaction between the switching dynamics and the dynamics of the EDFAs affected our ability to detect and recover from failures. It was shown that the ability to detect failures such as fiber cuts is complicated by the amplified spontaneous emission (ASE) noise from the same EDFAs that make WDM possible. We examined the fundamental difficulties that this ASE imposes on some schemes for detecting failures and proposed our novel method that overcomes these difficulties. In this scenario a detailed study of the timing requirements necessary in effecting a protection switch as a result of a real failure in the network, and not as a result of a temporary degradation of the performance due to the dynamic interaction of the components in the network, was specified.

This thesis identified several optical protection schemes for WDM ring networks. The engineering and implementation considerations for WDM optical layer protection architectures was presented. We identied changes to existing SDH Automatic Protection Switching (APS) schemes to WDM optical protection schemes for the 2-fiber uni-directional and 4-fiber bi-directional Self-Healing Rings (SHR). We focused on the WDM optical protection schemes that provide the survivability for the all-optical layer under the SDH/SONET/ATM layer and its potential and limitations.

To model and simulate complex system such as WDM SHR networks with protection switching mechanism to protect the network in case of fiber cuts or equipment failures, a user-friendly application software that uses an input Graphic User Interface (GUI) was developed. Using the developed algorithm, network components were represented by separate modules and thus the simulation program was organized in modular form to satisfy this requirement. Due to the large number of modules, creating the main simulation program using a text editor is impractical and prone to error. An approach that uses an input Graphic User Interface (GUI) was necessary. Each module was thus associated with a graphical object (icon) which was automatically translated to the main program and unambiguously scheduled for execution. The GUI thus allowed for user-friendly simulations requiring little or no programming experience. Signal Processing Workstation (SPW) was found to be most appropriate for this type of modeling. SPW is basically a block diagram based application software where custom coded blocks can be created using the 'C' programming language. These blocks were then used to create complex systems by connecting the custom coded blocks with available standard SPW

blocks provided that the interfaces were compatible. Using SPW, network elements (NE) such as wavelength add drop multiplexers (WADM) were modeled. A WADM is a hierarchical block modeled from lower level blocks. The major sub-blocks are EDFAs, demultiplexers (DMUX), multiplexers (MUX), 2×2 switches for dropping and adding of channels, photodetectors to detect power levels, 2×2 protection switches to protect against failures and attenuator blocks.

These systems were then used to study dynamic effects by simulating the transition of the switches on realistic time scales and examining the effects at various points of the network for adding/dropping of channels and/or protection switching. Failure scenarios were simulated; such as fiber cuts on the working and/or protection fiber, to understand the timing requirements to effect consistent protection switching. The constraint on setting threshold levels in detecting fiber cuts in the case where in-line amplifiers were present between the cut and the point at which the failure was detected was studied. In particular, some schemes depend on a loss of total power to effect a protection switch, but it was shown that because of amplified spontaneous emission (ASE), when in-line amplifiers were present erroneous detection occurred, and thus the wrong action was taken. Different means of detecting fiber cuts on the working and protection path, including our novel method that overcomes the constraint that the ASE noise imposes, were studied. It was shown that because of the transient degradations resulting from switching in these networks, a hold-off time was necessary for the protection switches. It was shown that a protection switch should only take place for degradations that last more than a certain minimum time if these networks are not to display catastrophic behavior,

due to the dynamic degradations caused by the perturbations that the switching actions create in reconfigurable survivable all-optical networks.

The main objective was to investigate and analyze, through experiment and computer simulation, the dynamic effects due to the interaction of switching elements and EDFAs transients in a WDM network. It was shown that the desired properties of optical switches can conflict with the requirements for stable EDFA operation. In particular, a fast switch is required for fast rearrangement of the channels in a WDM network, but this fast switching creates dynamic perturbations which in general are more severe for faster switches because of the slow response of the EDFAs. It was also shown that these degradations accumulate in large networks due to fast power transients in long chains of EDFAs.

Bibliography

Chapter 2

H. Scott Hinton, An Introduction to Photonic Switching Fabrics, Plenum Press: New York, 1993.

P. F. Wysocki, J. Judkins, R. Espindola, M. Andrejco, A. Vensarkar, and K. Walker, "Broad-band erbium-doped fiber amplifier flattened beyond 40 nm using long-period grating," IEEE Photon. Technol. Lett., vol. 9, no. 10, pp. 1343-1345, Oct. 1997.

Y. Sun, J. W. Sulhoff, A. K. Srivastava, J. L. Zyskind, C. Wolf, T. A. Strasser, J. R. Pedrazzani, J. B. Judkins, R. P. Espindola, A. M. Vengsarkar, and J. Zhou, "An 80 nm ultra wide band EDFA with low noise figure and high output power," IEE ECOC'97, Edingburg, Scotland, 1997.

H. Masuda, S. Kawai, K.I. Suzuki, and K. Aida, "Ultrawide 75-nm 3-dB gain-band optical amplification with erbium-doped fluoride fiber amplifiers and distributed raman amplifiers," IEEE Photon. Technol. Lett., vol. 10, no. 4, pp. 516-518, 1998.

A. Mori, Y. Ohishi, M. Yamada, H. Ono, Y. Nishida, K. Oikawa, and S. Sudo, " 1.5 mm broadband amplification by tellurite-based EDFAs," in Proc. Optical Fiber Communication (OFC'97), 1997, postdeadline paper PD1.

A. K. Srivastava, J. L. Zyskind, J. D. Evankow, J. W. Sulhoff, Y. Sun, and M. A. Mills, "Very flat gain erbium-doped fiber amplifier using samarium-doped fiber," IEEE Photon. Technol. Lett., vol. 9, no. 12, pp. 1576-1577, 1997.

Bellcore Technical Reference TR-NWT-001073, *Generic Requirements for Fiber Optic Switches*, Issue 1, January 1994.

J. Zhou, M. J. O'Mohoney, and S. D. Walker, "Analysis of optical crosstalk effects in multi-wavelength switched networks," IEEE Phot. Technol. Lett., vol. 6, pp. 302-305, Feb. 1994.

MONET 2nd quarterly report : Review, Tech Report, Multiwavelength Optical Networking Consortium, Jun. 1995.

Y. D. Jin, Q. Jiang, and M. Kavehrad, "Performance degradation due to crosstalk in multiwavelength optical networks using dynamic wavelength routing," IEEE Phot. Technol. Lett., vol. 7, pp. 1210-1212, Oct. 1995.

D. J. Blumenthal, P. Granestrand, and L. Thylen, "BER floors due to heterodyne coherent crosstalk in space photonic switches for WDM networks," IEEE Phot. Technol. Lett., vol. 8, pp. 284-286, Feb. 1996.

E. L. Goldstein, L. Eskildsen, and A. F. Elrefaie, "Performance implications of component crosstalk in transparent lightwave networks," IEEE Phot. Technol. Lett., vil. 6, pp. 657-660, May 1994.

E. L. Goldstein, L. Eskildsen, and Y. Silberberg, "Polarization statistics of crosstalk-induced noise in transparent lightwave networks," IEEE Phot. Technol. Lett., vol. 7, pp. 1345-1347, Nov. 1995.

N. Antoniades, I. Roudas, R. E. Wagner, J. L. Jackel, and T. E. Stern, "Crosstalk Performance of a wavelength selective cross-connect mesh topology," in Proc. OFC'98, San Jose, CA, 1998.

N. Antoniades, I. Roudas, R. E. Wagner, T. E. Stern, J. L. Jackel, and D. H. Richards, "Study of Performance Degradations due to Crosstalk in a Wavelength Selective Cross-connect Mesh Topology," submitted to IEEE Photonics. Technol. Lett.

T. H. Gilfedder, D. K. Hunter, L. Andonovic, "Crosstalk induced interferometric noise performance degradation of dilated optical TDM switching architectures,", IEE ECOC'97, Edinburg, Scotland, Sept. 1007.

P. J. Legg, D. K. Hunter, I. Andonovic, and P. E. Barnsley, "Inter-Channel crosstalk phenomena in optical time division multiplexed switching networks," IEEE Photon. Technol. Lett., vol. 6, no. 5, pp. 661-663, 1994.

P. J. Legg, M. Tur, and I. Andonovic, "Solution paths to limit interferometric noise induced performance degradation in ASK/Direct detection lightwave networks," J. Lightwave Technol., vol. 14, no. 9, pp. 1943-1954, 1996.

Y. D. Jin, M. Kavehrad, "An optical cross-connect system as a high-speed switching core and its performance analysis," J. Lightwave Technol., vol. 14, no. 6, pp. 1183-1197, 1996.

C. P. Larsen, L. Gillner, M. Gustavsson, "Linear crosstalk properties of large WDM cross-connects," IEE ECOC'97, Edingburg, Scotland, Sept. 1997.

Krishnan Padmanabhan and Arun N. Netravali, "Dilated Networks for Photonic Switching," IEEE Trans. on Comms. vol. com-35, no. 12, pp. 1357-1365, 1987.

G. Hugh Song, "Asymmetric dilation of multiwavelength cross-connect switches for low-crosstalk WDM optical networks," J. Lightwave Technol. vol. 15, no. 3, p. 430-436, 1997.

B. E. A. Saleh, M. C. Teich, Fundamentals of Photonics, New York: John Wiley and Sons, Inc., 1991.

R. A. Spanke, "Architectures for guided-wave optical space switching systems," IEEE Comm. Mag. vol. 25, no. 5, May 1987, pp. 42-48.

Ron. A. Spanke, "Architectures for large nonblocking optical space switches,", IEEE J. Quantum Electronics, vol. QE-22, no. 6, pp. 964-967, 1986.

R. Ramaswami and K. N. Sivaranan, " Optical Networks: A practical perspective," Morgan Kaufmann Publishers, Inc. San Francisco, California, 1998.

R. A. Spanke, and V. E. Benes, "An n-stage planar optical permutation network," Applied Optics, 26, April 1987.

C. Clos, "A study of non-blocking switching networks," Bell Syst. Tech. J. 32, pp. 406-424, 1953.

L. Thylen, G. Karlsson, O. Nilsson, "Switching technologies for future guided wave optical networks: potential and limitations of photonics and electronics," IEEE Comm. Mag. Feb. 1996, pp. 106-113.

J. L. Spencer, "Reliability of Optoelectronic Components and Its Network Implications," Proc. Opt. Fiber Commun. Conf., OSA Tech. Dig. Series, vol. 8, 1995, pp. 100 - 101.

H. N. Rourke, S. R. Baker, V. Baker, R. S. Baulcomb, K. C. Byron, S. J. Clements, T. J. Cullen, S. Davis, A. Fielding, D. Goodchild, "A low loss 4-channel wavelength demultiplexer based on fiber Bragg gratings," IEE ECOC'96, Oslo, paper Wed. 1.7.

Neil A. Jackman, "Multilayer optical filters with random errors," Bell Labs Technical Journal, Jan- March 1998, pp. 112-121.

Katsunari Okamoto, "Fundamentals, Technology and Application of AWGs," ECOC'98, Madrid, Spain, Sept. 1998.

A. d'Alessandro, D. A. Smith, and J. E. Baran, "Multichannel operation of an integrated acousto-optic wavelength routing switch for WDM systems," IEEE Photon. Technol. Lett., vol. 6, no. 3, pp. 390-393, 1994.

L. Y. Lin, E.L. Goldstein, J. M. Simmons, and R. W. Tkach, "High-density Connection-symmetric Free-space Micromachined Polygon Optical Crossconnects with Low Loss for WDM Networks," Optical Fiber Communication Conference 98, San Jose, California, Paper PD 24.

Joseph Ford, James A. Walker, Vladmir Aksyuk, and David J. Bishop, "Wavelength-Selectable Add/Drop with Tilting Micromirror," LEOS'97, paper PD 2.3.

C. Randy Giles, "Lightwave Micromachines," ECOC'98, Madrid, Spain, Sept. 1998.

L. Y. Lin, E. L. Goldstein, and R. W. Tkach, "Free-Space Micromachined Optical Switches with Submillisecond Switching Time for Large-Scale Optical Crossconnects," IEEE Photonics Technol. Lett., Vol. 10, no. 4, pp. 525-527.

J. E. Ford, J. A. Walker, K. W. Goossen, and C. C. Chang, "Passband-Free Dynamic WDM Equalization," ECOC'98, Madrid, Spain, Sept. 1998.

B. Barber, C. R. Giles, V. Askyuk, R. Ruel, L. Stulz, and D. Bishop, "A Fiber connectorized MEMS Variable Optical Attenuator," IEEE Photonics Technol. Lett. Vol. 10, no. 9, pp. 1262-1264.

Joseph E. Ford, James A. Walker, Dennis S. Greywall, and Keith W. Goossen, "Micromechanical Fiber-Optic Attenuator with 3 μs Response," Journal of Lightwave Technol. Vol. 16, no. 9, pp. 1663-1670.

T. A. Tumolillo, Jr. , M. Donckers, and W. H. G. Horsthuis, "Solid state optical space switches for network cross-connect and protection applications," IEEE comm. mag. Feb. 1997, pp. 124-130.

MONET 14th quarterly report: Review, Tech. Report, Multiwavelength Optical Networking Consortium, June 1998.

D. A. Smith, R. S. Chakravarthy, Z. Bao, J. E. Baran, J. L. Jackel, A. d'Alesandro, D. J. Fritz, S. H. Huang, X. Y. Zou, S. M. Hwang, A. E. Willner, and K. D. Li, "Evolution of the acousto-optic wavelength routing switch," J. Lightwave Technol., vol. 14, no. 6, pp. 1005-1019, 1996.

D. A. Smith, A. d'Alessandro, J. E. Baran, D. J. Fritz, J. L. Jackel, and R. S. Chakravarthy, "Multiwavelength performance of an apodized acousto-optic switch," J. Lightwave Technol., vol. 14, no. 9, pp. 2044-2051, 1996.

J. L. Jackel, M. S. Goodman, J. E. Baran, W. J. Tomlinson, G. K. Chang, M. Z. Iqbal, G. H. Song, K. Bala, C. A. Brackett, D. A. Smith, R. S. Chakravarthy, R. H. Hobbs, D. J. Fritz, R. W. Ase, and K. M. Kissa, "Acousto-optic tunable filters (AOTF's) for multiwavelength optical cross-connects: crosstalk considerations," J. Lightwave Technol., vol. 14, no. 6, pp. 1056-1066, 1996.

G. Hugh Song, "Time-Dependent analysis of acousto-optic tunable filters for multichannel optical switching," J. Lightwave Technol., vol. 15, no. 3, pp. 519-528, 1997.

D. A. Smith and J. J. Johnson, "Sidelobe suppression in an acousto-optic filter with a raised cosine interaction strength," Appl. Phys. Lett., vol. 61, pp. 1025-1027, 1992.

D. A. Smith, J. J. Johnson, B. L. Heffner, K. W. Cheung, and J. E. Baran, "Two-stage integrated-optic acoustically tunable optical filter with enhanced sidelobe suppression,", IEEE Electronics Lett., vol. 25, no. 6, pp. 398-399, 1989.

J. S. Patel, and Y. Silberberg, "Liquid crystal and grating-based multiple-wavelength cross-connect switch," IEEE Photonics Technol. Lett., vol. 7, no. 5, pp. 514-516, 1995.

Kuang-Yi Wu, and Jian-Yu Liu, "Liquid-crystal space and wavelength routing switches," IEE ECOC'97, Edingburgh, Scotland, Sept. 1997, paper MC4.

F. Pain, R. Coquille, B. Vinouze, N. Wolffer, and P. Garvey, "High contrast nematic liquid crystal polarization controllers: application to a 4 × 4 free space optical switch at 1.5 μm,", ECOC'97, Edinburg, UK, Sept. 1997.

P. G. de Gennes, "The Physics of Liquid Crystals," Oxford University Press, 1974.

Chapter 3

J. S. Patel, and Y. Silberberg, "Liquid crystal and grating-based multiple-wavelength cross-connect switch," IEEE Photonics Technol. Lett., vol. 7, no. 5, pp. 514-516, 1995.

Kuang-Yi Wu, and Jian-Yu Liu, "Liquid-crystal space and wavelength routing switches," IEE ECOC'97, Edingburg, Scotland, Sept. 1997, paper MC4.

F. Pain, R. Coquille, B. Vinouze, N. Wolffer, and P. Garvey, "High contrast nematic liquid crystal polarization controllers: application to a 4 × 4 free space optical switch at 1.5 μm,", ECOC'97, Edinburgh, UK, Sept. 1997.

R. E. Wagner, R. C. Alferness, A. A. M. Saleh, and M. S. Goodman, "MONET: Multiwavelength optical networking," IEEE Journal of Lightwave Technol. June 1996. pp. 1349-1355.

P. G. de Gennes, "The Physics of Liquid Crystals," Oxford University Press, 1974.

Chapter 4

E. Desurvire, C. R. Giles, and J. R. Simpson, "Gain dynamics of erbium-doped fiber amplifiers," SPIE Vol. 1171 Fiber Laser Sources and Amplifiers (1989).

C. R. Giles, and E. Desurvire, "Transient gain and cross talk in erbium-doped fiber amplifiers," Optics Letters, vol. 14, no. 16 Aug. 1989, pp. 880-882.

R. J. Mears, L. Reekie, I. M. Jauncey, and D. N. Payne, "Low-noise Erbium-doped fiber amplifiers operating at 1.54 μm," Electron. Lett. vol. 23 pp. 1026-1028. Sept. 1987.
E. Desurvire, J. R. Simpson, and P. C. Becker, "High-gain Erbium-doped traveling-wave fiber amplifier," Opt. Lett., vol. 12, pp. 888-890, Nov. 1987.

E. Snitzer et al., "Erbium fiber laser amplifier at 1.55 μm with pump at 1.49 μm and Yb sensitized Er oscillator," postdeadline papers, in OFC '88, OSA, Washington, DC 1988, paper PD2.

B. J. Ainsle, "A review of the fabrication and properties of Erbium-doped fiber for optical amplifiers," J. Lightwave Tech., vol. 9, no. 2, pp. 220-227, 1991.

R. I. Laming et al., "Efficient pump wavelengths of Erbium doped fiber optical amplifiers," Electron. Lett., vol. 25, pp. 12-14, 1989.

H. V. Pommer et al., "Noise and gain performance for Erbium-doped fiber amplifier pumped at 980 or 1480 nm," Fiber Laser Amplifiers II, M. J. F. Digornet, ED., Proc. SPIE, vol. 1373, pp. 254-265, 1990.

W. J. Miniscalco, "Erbium-doped glasses for fiber amplifiers at 1500 nm," J. Lightwave Tech., vol. 9, no. 2, pp. 234-250, 1991.

E. Desurvire, Erbium-Doped Fiber Amplifiers: Principles and Applications, (John Wiley & Sons, NY, 1994)

C. R. Giles et al., "Noise performance of Erbium-doped fiber amplifiers pumped at 1.49 mm, and application of signal preamplification at 1.8 Gbits/s," IEEE Photonics Tech. Lett., vol. 1, pp. 367-369, 1989.

Randy Giles, Tingye Li, "Optical amplifiers transform long-distance lightwave telecommunications," Proceedings of the IEEE, vol. 84, no. 6. June 1996, pp. 870-883.

M. Zirngibl, "Gain Control in Erbium-Doped Fiber Amplifier by an all-optical feedback loop," Electron. Lett., 27, 560-561 (1991).

Haruo Okamura, "Automatic Optical Loss Compensation with Erbium-Doped Fiber Amplifiers," J. Lightwave Technology, 10, 1110-1116 (1992).

J. F. Massicott, S. D. Willson, R. Wyatt, J. R. Armitage, R. Kashyap, D. Williams, and R. A. Lobbett, "1480 nm pumped erbium doped fiber amplifier with all optical automatic gain control." Electron. Lett.,. 30 962-964 (1994).

M. Fake, J. Simmons, J. Massicott, R. Wyatt, "Optically stabilized EDFA for in-band WDM system," in proc. of OFC'95, paper TuP3.
Seung Hee Lee and Seong Ha Kim, "Performance of all optical gain-clamped EDFA in 8 channel × 10 Gbps WDM using stimulated brillouin scattering," ECOC'98, Madrid, Spain, Sept. 1998.

Seung Hee Lee, and Seong Ha Kim, "All-optical gain-clamped erbium-doped fiber amplifier for wavelength-division multiplexed networking using stimulated Brillouin scattering," in proc. of OFC'98 San Jose, CA. paper WM52.

A. K. Srivastava, Y. Sun, J. L. Zyskind, J. W. Sulhoff, C. Wolf, R. W. Tkach, "Fast Gain Control in Erbium-Doped Fiber Amplifier," in Optical Amplifier and Their Applications, Vol. V of 1996 Trends in Optics and Photonic Series (Optical Society of America, Washington, D. C., 1996) p. 24.

A. K. Srivastava, Y. Sun, J. L. Zyskind, and J. W. Sulhoff, "EDFA Transient Response to Channel Loss in WDM Transmission System," IEEE Photonics Technol. Lett., vol. 9, no. 3, pp. 386-388, 1997.

Seo Yeon Park, Hyang Kyun Kim, Gap Yeol Lyu, Sun Mo Kang, and Sang-Yung Shim, "Dynamic Gain and Output Power Control in a Gain-Flattened Erbium-Doped Fiber Amplifier," IEEE Photonics Technology Lett. vol. 10, no. 6, pp. 787-789, 1998.

F. Shehadeh, R. S. Vodhanel, C. Gibbons, and M. Ali, "Comparison of gain control techniques to stabilize EDFAs for WDM networks," in Technical Digest of Optical Fiber Communications (Optical Society of America, San Jose, CA, 1996) paper WM8.

E. Desurvire, M. Zirngibl, H. M. Presby, and D. DiGiovanni, "Dynamic Gain Compensation in Saturated Erbium-Doped Fiber Amplifiers," IEEE Photonics Technol. Lett. Vol. 3, no. 5, pp. 453-455, 1991.

B. Clesca, V. Harvard, S. Gauchard, V. Rodriques, E. Lantoine, D. Cravec, and F. X. Ollivier, "Upper limit and control scheme for power channel in optically-amplified WDM systems", in Proceedings of European Conference on Optical Communications (Oslo, 1996) paper WeP.31.

J. L. Zyskind, A. K. Srivastava, Y. Sun, J. C. Ellison, G. W. Newsome, R. W. Tkach, A. R. Chraplyvy, J. W. Sulhoff, T. A. Strasser, J. R. Pedrazzani and C. Wolf, " Fast link control protection for surviving channels in multiwavelength optical networks," in Proceedings of European Conference on Optical Communications (Oslo, 1996) postdeadline paper.

A. K. Srivastava, J. L. Zyskind, Y. Sun, J. Ellson, G. Newsome, R. W. Tkach, A. R. Chraplyvy, J. W. Sulhoff, T. A. Strasser, C. Wolf, and J. R. Pedrazzani, "Fast-Link Control Protection of Surviving Channels in Multiwavelength Optical Networks," IEEE Photonics Technol. Lett. vol. 9, no. 12, pp. 1667-1669, 1997.

J. L. Jackel and D. Richards, "All-optical stabilization of multi-wavelength EDFA chains: a network-level approach," in Proceedings of LEOS'96 (IEEE Laser and Electro-Optics Society) postdeadline paper.

J. L. Zyskind, Y. Sun, A. K. Srivastava, J. W. Sulhoff, A. J. Lucero, C. Wolf, and R. W. Tkach, "Fast Power Transients in Optically Amplified Optical Networks," Optical Fiber Communication Conference (Optical Society of America) postdeadline paper PD31.

A Yu and M. J. O'Mahony, "Modeling of laser-controlled erbium-doped fiber amplifiers," in Technical Digest of Optical Fiber Communication (Optical Society of America, San Jose, CA, 1996) paper WK14.

Y. Takushima and K. Kikuchi, "Gain stabilization of all-optical gain-clamped amplifier by using Faraday rotator mirrors," Electronics Lett. vol. 34, No. 5, March, 1998, pp. 458-459.

J. C. van der Plaats, F. W. Willems, and A. M. J. Koonen, "Dynamic pump-loss controlled gain-locking system for erbium-doped fiber amplifiers in multi-wavelength networks," ECOC'97, Edinburgh, UK, Sept. 1997.

M. Karasek, and J. C. van der Plaats, "Analysis of Dynamic Pump-Loss Controlled Gain Locking System for Erbium-Doped Fiber Amplifiers," IEEE Photonics Technol. Lett. vol. 10, no. 8, pp. 1171-1173, 1998.

H. Suzuki, N. Takachio, O. Ishida, and M. Koga, Dynamic gain control by maximum signal power channel in optical linear repeaters for WDM photonic transport networks," IEEE Photonics Technol. Lett. vol. 10, no. 5, pp. 734-736.

M. Karasek and F. W. Willems, "Suppression of Dynamic Cross Saturation in Cascades of Overpumped Erbium-Doped Fiber Amplifiers," IEEE Photonics Technol. Lett. vol. 10, no. 7, pp. 1036-1038, 1998.

Janet Lehr Jackel, and Dwight Richards, "All-optical stabilization of cascaded multichannel EDFAs with changing number of channels," in proc. of OFC'97, Dallas, TX. Feb. 1997, paper TuP4.

Chapter 5

Multiwavelength Optical Networking (MONET) Consortium, 15th Quarterly Report, September, 1998.

J. L. Jackel and D. Richards, "All-optical stabilization of multi-wavelength EDFA chains: a network-level approach," in Proceedings of LEOS'96 (IEEE Laser and Electro-Optics Society) postdeadline paper.

C. R. Giles and E. Desurvire, "Modeling Erbium-Doped Fiber Amplifiers", J. Lightwave Technology, vol. 9, no. 2, pp. 271-283, 1991.

A.A Saleh, R. M. Jopson, J. D. Evankow, and J. Aspell, "Modeling of gain in erbium-doped fiber amplifiers," IEEE Photon. Tech. Lett., Oct. 1990

C. R. Giles and D. DiGiovanni, "Spectral dependence of gain and noise in erbium-doped fiber amplifiers," Photon. Tech. Lett., vol.2, no. 11, pp. 797-800, 1990.

R. W. Hamming, Numerical Methods for Scientist and Engineers. New York: Dover Publications, 1973.

C. R. Giles, E. Desurvire, and J. R. Simpson, "Transient gain and cross talk in erbium-doped fiber amplifiers," Opt. Lett., Vol. 14, pp. 880-882,1989.

R. I. Laming, L. Reekie, P. R. Morkel, and D. N. Payne, "Multichannel crosstalk and pump noise characterization of Er^{3+} -doped fiber amplifier pumped at 980 nm," Electron. Lett., vol. 25, pp. 455-456, 1989.

M. A. Ali, A. F. Elrefaie, R. E. Wagner and S. A. Ahmed, " A Detailed Comparison of the Overall Performance of 980 and 1480 nm Pumped EDFA Cascades in WDM Multiple-Access Lightwave Networks", J. Lightwave Technology, vol. 14, pp. 1436-1448, 1996.

Janet L. Jackel and Dwight H. Richards, "All-Optical Stabilization of Multi-wavelength Erbium-doped Fiber Amplifiers with Changing Number of Channels," OSA Trends in Optics and Photonics, Vol. 12, System Technologies (Optical Society of America, Washington, DC, 1997).

Dwight H. Richards, Janet L. Jackel, and Mohamed Ali, "A Theoretical Investigation of Dynamic All-Optical Automatic Gain Control in Multichannel EDFAs and EDFA Cascades," IEEE Journal of Selected Topics in Quantum Electronics, vol. 3, no. 4, pp. 1027-1036, August, 1997.

D. H. Richards, J. L. Jackel, and M. A. Ali, "Multichannel EDFA Chain Control: A Comparison of Two All-optical Approaches," IEEE Photonics Technol. Lett., vol. 10, no. 1, pp. 156-158, 1998.

D. H. Richards, M. A. Ali, J. L. Jackel, "EDFA Chain Control: A Comparison of Two Approaches," In Proc. LEOS'97, Montreal, Quebec, Aug. 1997, Paper FB2.

D. H. Richards, M. A. Ali, and J. L. Jackel, "A Theoretical Investigation of Dynamic Automatic Gain Control in Multi-channel EDFA Cascades," ECOC'97, Edinburgh, UK, September, 1997.

G. Luo, J. L. Zyskind, Y. Sun, A. K. Srivastava, J.W. Sulhoff and M.A. Ali, "Relaxation Oscillations and spectral hole burning in laser automatic gain control of EDFAs", in Technical Digest of Optical Fiber Communication Conference (Optical Society of America, Dallas, TX, 1997) paper WF4.

G. Luo, J. L Zyskind, J. A. Nagel, and Mohamed Ali, "Experimental and Theoretical Analysis of Relaxation-Oscillations and Spectral Hole Burning Effects in All-Optical Gain-Clamped EDFAs for WDM Networks," Journal of Lightwave Technol. vo. 16, no.4, pp. 527-533, 1998.

B. Landousies, T. Georges, E. Delevaque, R. Lebref and M. Monerie, "Low power transients in multichannel equalized and stabilized gain amplifier using passive gain control.", Electron. Lett., 32, 1912-1913, 1996.

E. Desurvire, "Erbium-doped Fiber Amplifiers", New York: Wiley, 1994.

A Yu and M. J. O'Mahony, "Modeling of laser-controlled erbium-doped fiber amplifiers," in Technical Digest of Optical Fiber Communication (Optical Society of America, San Jose, CA, 1996) paper WK14.

Janet Lehr Jackel, and Dwight Richards, "All-optical stabilization of cascaded multi-channel EDFAs with changing number of channels," in proc. of OFC'97, San Jose, CA, Feb. 1997.

A. K. Srivastava, Y. Sun, J. L. Zyskind, J. W. Sulhoff, C. Wolf, R. W. Tkach, "Fast Gain Control in Erbium-Doped Fiber Amplifier," in Optical Amplifier and Their Applications, Vol. V of 1996 Trends in Optics and Photonic Series (Optical Society of America, Washington, D. C., 1996) p. 24.

A. K. Srivastava, Y. Sun, J. L. Zyskind, and J. W. Sulhoff, "EDFA Transient Response to Channel Loss in WDM Transmission System," IEEE Photonics Technol. Lett., vol. 9, no. 3, pp. 386-388, 1997.

Chapter 6

A. F. Elrefaie, "Multiwavelength survivable ring network architectures," International conference on Communications ICC'93, Geneva, May 23-26, 1993, pp. 1245-1251

"Operation of a 4-Fiber Survivable WDM Ring Network," 1997 Deliverable 4.1, Multiwavelength Optical Networking (MONET) Project, Bellcore.

"WDM Alternatives to SONET Multiplexing," Bellcore's HORIZON'98 deliverable 1.2, Optical Networking Initiative, May, 1998.

"WDM Layer Protection and Restoration Strategies for LEC Networks," Bellcore's HORIZON'98 deliverable 1.3, Optical Networking Initiative, July, 1998.

Joseph Sosnosky and Zhi-Wei Lin, "Planning for broadband multilayer survivability," NFOC'98, Sept. 1998.

Rob Batchellor, "Optical Layer Protection: Benefits and Implementation," NFOC'98, Sept. 1998.

Ezhan Karasan, Evan Goldstein, "Optical restoration at the wavelength-multiplex-section level in WDM mesh networks," in Optical Fiber Communication Conference, Vol. 2, 1998, OSA Technical Digest Series (Optical Society of America, Washington DC, 1998), pp. 300-301.

Kris Struyve, Piet Demeester, "Dynamic Routing of Protected Optical Paths in Wavelength Routed and Wavelength Translated Networks," ECOC'97, Edinburgh UK, Sept. 1997.

H. Takeshita, S. Takahashi, T. Kato, S. Kitamura, H. Harano, and N. Henmi, "A demonstration of an optical cross-connect system for a self-healing optical network," in proceeding of ECOC'97, Edinburgh, UK.

Ori Gerstel, "Opportunities for optical protection and restoration," in proceeding of Optical Fiber Communication Conference (OFC'98), paper ThD1, San Jose, CA.

Paul Bonenfant, "Optical layer survivability: a comprehensive approach," in proceeding of Optical Fiber Communication Conference (OFC'98), paper ThD2, San Jose, CA.

Hideaki Tsushima, Hiroshisa Sano, Shigeki Kitajima, Yasushi Sawada, Tatsuo Kakizaki, Yasuyuki Fukashiro, Tsunio Nakata, Shoichi Hanatani, Niall Robinson, Gary B. Davis, John A. Fee, Shoa-Kai liu, "Optical cross-connect systems for restoration of backbone fiber networks," in Proceeding of Optical Fiber Communication Conference, (OFC'98) paper ThD3, San Jose, CA.

J. A. Johnson, P. A. Littlewood, "Survivable SONET/ATM Networks," in Technical Digest, NFOEC'95, Boston, MA, June, 1995.

Ori Gerstel, and Rajiv Ramaswami, "Role of Optical Layer Protection and Restoration in Transport Networks," NFOC'98, Sept. 1998.

Bernard Glance, Christopher Doerr, Ivan Kaminow, and R. Montagne, Optically Restorable WDM ring Network Using Simple Add/Drop Circuitry,", Journal of Lightwave Technol., vol. 14, no. 11. Nov. 1996, pp. 2453-2456.

P. Bonenfant and C. M. C. Davenport, "SONET Optical Layer Protection Switching," Bellcore TM-24609, December 1994.

David Beebe and Mark Barratt, "The hidden power of path-protection switching," Telephony, Oct. 1993. pp. 22-27.

J. Vernon Drake, "A review of the four major SONET/SDH rings," ICC'93, Geneva Switzerland, May 23-26, 1993.

Randy Eisennach, "Performance Monitoring with SONET Networks," NFOC'97, Sept. 1997.

Jonathan Morgan and Samuel Lisle, "A comparative analysis of 2 fiber and 4 fiber bidirectional line switched rings," NFOC'95, Boston, MA, June 1995.

J. Manchester and P. Bonenfant, "Fiber Optic Network Survivability: SONET/Optical Layer Interworking," in Technical Digest, NFOEC'96, Dallas, Sept., 1996.

R. Cadeddu, N. Caponio, M. Cerisola, G. Ferraris, R. Finotti, R. Lano, and A. Mariconda, "Increased capacity of a bidirectional SDH self-healing ring using WDM," in proceedings of ECOC'97, Edinburgh, UK.

Stuart S. Wagner and Thomas E. Chapuran, "Multiwavelength Ring Networks for Switch Consolidation and Interconnection," ICC'92.

A. Fioretti, A. Aguilar, J. Baudron, G. Leroy, F. Masetti, P. Perrier, M. Sexton, C. Sierens, and M. Sotom, "Application of Optical Transparency to the Telecommunications Core Network," ISS'95 April 95, Vol. 1.

Giuseppe Ferraris, and Kimio Oguchi, "Management of Optical Networks," ECOC'98, Madrid, Spain, Sept. 1998.

Bellcore Horizon Deliverable 3.2, "Optical Protection Switching for 4-fiber WDM Rings, Dec. 1997.

"2-Fiber WDM SONET Ring Networks: Reciprocal Impact of WDM Technology and Operations," Bellcore, TM-TSV-023583, April, 1994.

Heena Patel, "A Reliability Analysis of OC-192 and OC-48 SONET Systems," NFOC'95, Boston, MA, 1995.

Thomas R. Del Giorno and Diane M. Pipan, "Reliability of Optically Amplified WDM Transmission Links,", NFOC'97, Sept. 1997

Rajiv Ramaswami and Kumar N. Sivarajan, "Optical Networks: A Practical Perspective," Morgan Kaufmann Publishers, Inc. 1998, Chapter 10.

Chung-Sheng Li, and Rajiv Ramaswami, "Automatic Fault Detection, Isolation, and Recovery in Transparent All-Optical Networks," IEEE Journal of Lightwave Technol. vol. 15, no. 10, pp. 1784-1791.

D. Uehara, K. Asahi, Y. Nakabyashi, M. Yamashita, C. Konishi, and S. Fujita, "Highly Reliable and Economical WDM Ring with Optical Self-Healing and 1:N Wavelength Protection," ECOC'97, Sept. 1997, Edinburg, UK.

D. H. Richards, J. L. Jackel, N. Antoniades, I. Roudas, W. Xin, and M. Ali, "Detecting Fiber Cuts in a WDM Ring with Optical Protection Switching: Simulation and Experiment," ECOC'98, Madrid, Spain, September, 1998.

J. L. Jackel, D. H. Richards, "All-Optical Stabilization of Multiwavelength EDFA Chains: A Network Level Approach," In Proc. LEOS'96, Boston, MA, Nov. 1996, PD 2.2.

I. Roudas, N. Antoniades, R. E. Wagner, S.F. Habiby, T. E. Stern, and A. F. Elrefaie, "Wavelength-Domain Simulation of Linear Multiwavelength Optical Networks," submitted to IEEE Journal of Lightwave Technology.

N. Antoniades, I. Roudas, R. E. Wagner, and S. F. Habiby, "Simulation of ASE Noise Accumulation in a Wavelength Add-Drop Multiplexer," IEEE Photonics Technol. Lett., Vol. 9, No. 9, pp. 1274-1276, 1997.

T.H. Wu, Fiber Network Service Survivability (Artech House 1992).

Steven G. Finn, Muriel Medard, Richard A. Barry, "A new algorithm for bi-directional link self-healing for arbitrary redundant networks." in Optical Fiber Communication Conference, Vol. 2, 1998, OSA Technical Digest Series (Optical Society of America, Washington DC, 1998), pp. 298-299.

IMAGE EVALUATION
TEST TARGET (QA-3)

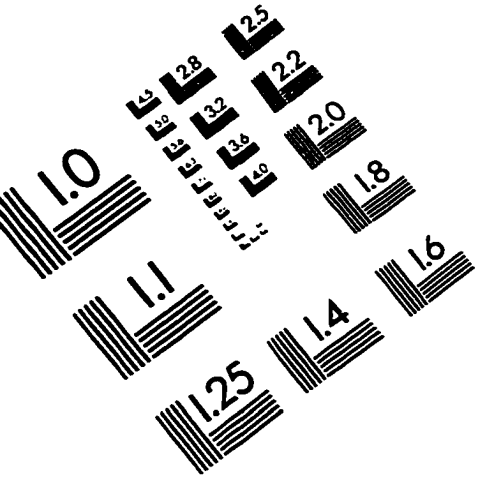

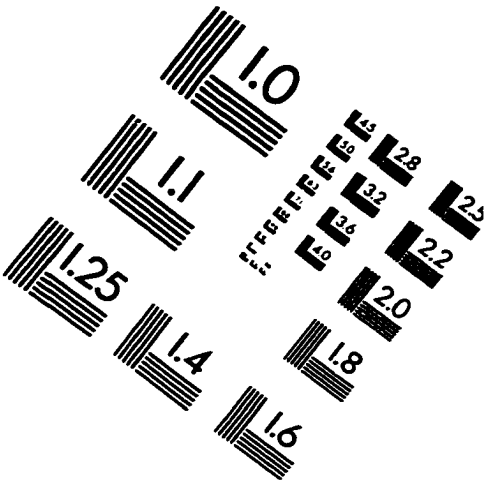

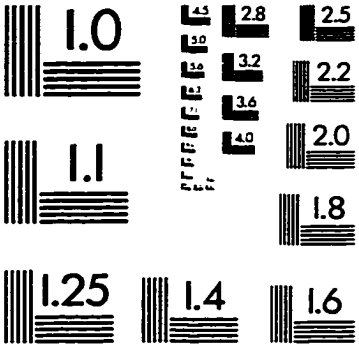

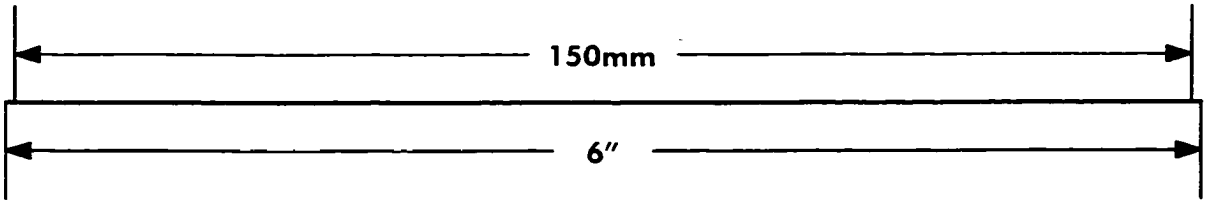

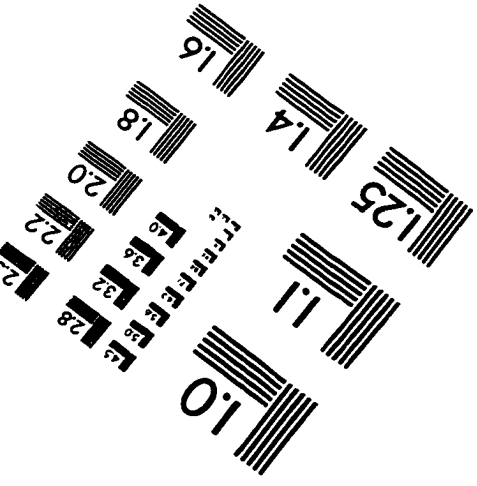

APPLIED IMAGE, Inc
1653 East Main Street
Rochester, NY 14609 USA
Phone: 716/482-0300
Fax: 716/288-5989